Improving the spatial and temporal variability of ammonia emissions from agriculture in Western Europe

Xinrui Ge

Propositions

1. Detailed local information on crop and livestock distributions increases the accuracy of spatial variations in ammonia emissions and concentrations.
(this thesis)

2. Considering local meteorology and related fertilizer and manure application practices improves the modeled temporal variation of ammonia emissions and concentrations.
(this thesis)

3. Data sets concerning environmental issues should be made freely available for non-commercial use.

4. Using remote sensing and machine learning to obtain business information like crop maps and livestock housing locations does not invade privacy and confidentiality.

5. We are not doing the environment a favor by only stating the negative effects of agriculture on the environment without willingness to invest in a healthier diet.

6. Modern technologies, including GPT and machine learning, make the contribution of science to societal debates less convincing.

Propositions belonging to the thesis, entitled

Improving the spatial and temporal variability of ammonia emissions from agriculture in Western Europe

Xinrui Ge
Wageningen,
10/10/2023

Improving the spatial and temporal variability of ammonia emissions from agriculture in Western Europe

Xinrui Ge

Thesis committee

Promotor
Prof. Dr. Wim de Vries
Professor, Integrated Nutrient Impact Modelling, Environmental Systems Analysis
Wageningen University, the Netherlands

Co-promotor
Prof. Dr. Martijn Schaap
Professor, Atmospheric Chemistry
Free University of Berlin, Berlin, Germany

Other members
Prof. Dr. Jordi Vila-Guerau de Arellano, Wageningen University, the Netherlands
Prof. Dr. Jan Willem Erisman, Leiden University, the Netherlands
Prof. Dr. Guus Velders, Utrecht University, the Netherlands
Prof. Dr. Carsten Ambelas Skjøth, Aarhus University, Denmark

Improving the spatial and temporal variability of ammonia emissions from agriculture in Western Europe

Xinrui Ge

Summary

The alteration of the global nitrogen cycle by human activities has increased reactive nitrogen losses to the environment, surpassing numerous thresholds for human and ecosystem health. Reactive nitrogen deposition to natural ecosystems may trigger soil acidification, eutrophication, and subsequent biodiversity loss. Additionally, nitrogen deposition may magnify the effects of climate change by influencing vegetation growth and carbon exchange during droughts. However, as the main drivers of reactive nitrogen deposition, ammonia emissions are challenging to estimate, resulting in significant uncertainties in regional budgets and distributions of NH_3 (and its deposition) in space and time. This Ph.D. thesis aims to refine agricultural ammonia emission estimates for use in chemistry transport models (CTMs) like LOTOS-EUROS by combining and refining existing models (INTEGRATOR, TIMELINES, and ALFAM2) and assimilating remote sensing together with various datasets on agricultural activities, emission factors, and meteorology. Special attention is focused on the integration of land use derived from satellite observations into the emission model and on the application of novel satellite data on atmospheric ammonia concentrations from the Infrared Atmospheric Sounding Interferometer (IASI) and the Cross-track Infrared Sounder (CrIS) to evaluate the modeling results. The rationale behind the approach is the assumption that combining models and measurements decreases the uncertainties in the atmospheric budget and distribution of NH_3 and allows us to trace back the sources of uncertainties in the model.

In **Chapter 1**, the thesis's central ambition is laid out: "The central aim of this thesis is to stepwise improve the spatial-temporal variability in ammonia emissions by accounting for variations in agricultural practices, livestock (housing) distributions, crop distributions, and meteorology" The overall goal was translated into four research questions, being evaluated in four chapters:

- What are the impacts of different agricultural practices and their timing based on meteorology (chapter 2)?
- What are the impacts of detailed crop and livestock distributions and emission fractions based on country-specific information (chapter 3)?
- What are the impacts of detailed livestock housing information and remote sensed crop distributions (chapter 4)?
- What are the impacts of varying emission factors based on manure characteristics, meteorology, and application techniques (chapter 5)?

In **Chapter 2** of this thesis (Ge et al., 2020), I present a method for increasing the spatial detail of ammonia emissions by replacing the ammonia emissions in the MACC emission inventory with the more detailed emissions from INTEGRATOR. Furthermore, the temporal

allocation was improved by the implementation of the TIMELINES module, which correlates the timing of manure and fertilizer application with meteorology. The method produced an annual emission map and spatially explicit time profiles for Germany and the Benelux for 2010. The newly derived emission information was imported into LOTOS-EUROS to model the ammonia surface concentration and total column distributions. The validation with in situ measurements showed that the model performance improves significantly with respect to the temporal variation of ammonia concentrations in comparison to the simulation with static emission profiles. The comparison with satellite observations confirmed these results and identified an overestimation of ammonia concentrations in Southern Germany and an underestimation in Northern Germany. The conclusion was that the spatial details on the data input needed to be refined further, including crop and livestock distributions, excretion rates, emissions fractions, and the locations of animal houses.

Chapter 3 builds on the work described in Chapter 2 and assesses how the spatial allocation in the ammonia emission modeling can be improved by using publicly available crop maps with higher spatial resolution and livestock number data from national registries for the Netherlands, Denmark, and Portugal. Livestock distributions affect the spatial distribution of excreted N and thus ammonia emission, while detailing the crop distribution affects both the spatial and temporal distributions of application emissions. Emission fractions were also updated using the results of local experiments. The differences in the spatial distribution of ammonia emissions are more evident in the animal housing and manure sectors than in the manure and fertilizer application sectors because the changes in animal number data were greater than that in crop distribution. At the same time, the adapted emission distributions show more spatial details because emissions from manure and fertilizer application to crops are only allocated to where the respective crops are grown. The emissions from the standard INTEGRATOR model and the adapted approaches were validated by comparing surface concentrations predicted with LOTOS-EUROS with in situ observations. The validation was made for springtime and wintertime separately to investigate the improvements brought by crop maps and livestock information. The results show that the inclusion of such data has improved both the spatial and temporal distribution of ammonia emissions. However, uncertainties in the spatial and temporal distribution of ammonia emissions remain, which are caused by not accounting for the exact locations of animal houses and the spatial variation in meteorological conditions, application techniques, manure composition, and soil properties. Moreover, the lack of in situ measurement data only allowed model validation for the Netherlands. Last, it has to be noted that crop maps are not always publicly available for other countries, which means that crop mapping is needed to increase the applicability of this method.

Chapter 4 (Ge et al., 2023b) presents the method of using a high-resolution crop map generated with machine learning of multispectral multitemporal Sentinel-2 data as well as information on livestock housing locations to improve the spatial and temporal variation of ammonia emissions in the Netherlands. The derived ammonia concentrations thus compare better with satellite observations and in situ measurements than the ones obtained using the original crop and animal house information inputs. Using Sentinel-2 data and machine learning to derive a crop map enables our emission model to be applied to other regions that do not publish or regularly update crop maps. The improvements are more significant at locations where animal housing dominates ammonia emissions than those where manure and fertilizer application dominates. It indicates that the accessibility of animal house locations is essential to reduce the uncertainties in ammonia emission estimates. The smaller improvements at application-dominated locations could be caused by the miscategorization of crops, uncertainties in fertilization day predictions, and the constant country-dependent emission fractions, which do not consider the spatial variation in emission fractions within a country.

Chapter 5 (Ge et al., 2023a) describes a method for creating high-resolution spatially explicit distributions of emission fractions by utilizing the ALFAM2 model (for manure application) and a temperature-dependent scaling approach (for animal housing). Unlike the previous country-dependent constant emission fractions, the emission fractions in this chapter are predicted with data on local meteorological conditions, application methods, incorporation time, and manure characteristics. The meteorological conditions used in deriving the emission fraction represent the conditions when each crop is fertilized. The emission fractions for livestock housing were made variable through a temperature-dependent scaling. The interannual sensitivity of surface concentrations and total columns to temperature was calculated for early spring, late spring, and summer between 2014 and 2018. Compared to a national generic time allocation of emission within the year, the spatially explicit time profile largely improved the ability to reproduce the interannual sensitivity of surface concentrations and total columns to temperature. The updated weather-dependent emission fractions brought the improvement further. The improvement was more pronounced in early spring fertilization, followed by late spring fertilization. However, the summer period did not show a noticeable change because animal housing and manure storage dominated ammonia emission at this time. The study indicates that spatially explicit emission fractions can significantly improve ammonia emission modeling and are of great importance for studying the temporal variability between years.

In the last **Chapter 6** (Synthesis), the thesis findings are put into the context of the overall research question. First, the main results are summarized, focusing on the improvements of the ammonia emission distribution in space and time when accounting for temporal

variation in agricultural practices, livestock (housing) distributions, crop distributions, and in meteorology. In short, the developed spatially explicit time profiles improved the temporal allocation of ammonia emissions, detailed crop maps and livestock distributions contributed to both the improvement in spatial and temporal distribution, and the spatial explicit emission fractions added inter- and intra-annual emission variability. The chapter also presents an outlook of methods to improve ammonia emission distribution in space and time and make the model applicable to much bigger regions. This includes refining the prediction of fertilization day by improving the thermal sum approach and accounting for trafficability on various soil types, using remote sensing and machine learning to detect livestock housing systems automatically, and more accurate estimates of the timing of (multiple) fertilization.

Table of Content

1

Introduction

In this introduction, I first present the reactive nitrogen cycle and its impacts on air quality, human health, and ecosystems, with a specific focus on the role of agriculture (Section 1.1). This is followed by an overview of measurements and modeling approaches to assess the concentrations and deposition of atmospheric ammonia, including a list of available emission models and chemical transport models for Europe (Section 1.2). Then an overview is given of the factors that affect the temporal and spatial variability of agricultural ammonia emissions, including crop and livestock distributions, manure characteristics, application techniques, and meteorological conditions. A summary of how these factors are included in currently available emission models is given (Section 1.3). Finally, knowledge gaps are introduced, followed by my research aims and approaches to tackle part of these knowledge gaps (Section 1.4).

1.1 Reactive nitrogen emissions and their impacts

1.1.1 Mankind largely altered the global nitrogen cycle

Nitrogen (N) is essential for all life forms on Earth. Humans, animals, and plants need nitrogen to produce proteins, carbohydrates, and fibers (Erisman et al., 2011). Nature and its biodiversity only exist because of the nitrogen availability in the system. The atmosphere consists of a large part (78%) of nitrogen compounds, which is fundamental to the atmosphere's chemical and radiative properties (Richardson et al., 2009). Nitrogen in the atmosphere is present in various chemical forms. Although the dominant form, dinitrogen (N_2), accounts for nearly 100% of all the nitrogen in the atmosphere, it cannot be directly used to support life (Masero et al., 2021). Instead, its nitrogen component can only be utilized after atmospheric dinitrogen, which has a strong triple covalent bond, is converted into reactive nitrogen (N_r).

Reactive nitrogen is defined as the container of all nitrogen compounds except for N_2 (Erisman et al., 2011). Hence, reactive nitrogen includes inorganic reduced nitrogen compounds (e.g. ammonia (NH_3) and ammonium (NH_4^+)), inorganic oxidized nitrogen compounds (e.g., nitrogen oxides (NO_x), nitrous oxide (N_2O), nitric acid (HNO_3), nitrites (NO_2^-) and nitrates (NO_3^-)), as well as N-containing organic compounds (e.g., urea, amines, proteins, and nucleic acids). The most dominant N_r species in terms of annual emissions to the atmosphere are ammonia (NH_3) and nitrogen oxides (NO_x).

Reactive nitrogen can come from nitrogen fixation, the chemical process of converting atmospheric dinitrogen into reactive nitrogen (Galloway, 2003). Under natural conditions, the occurrence of nitrogen fixation to support life is limited. Lightning is one of the natural processes during which the high energy (and thus temperature) is able to break the strong bonds between the two nitrogen in N_2 and the two oxygen atoms in O_2, after

which the N atoms bind to oxygen atoms to form nitrogen oxides (Galloway et al., 2004). Also, microorganisms termed diazotrophs in the soil can convert N_2 into N_r. This biological nitrogen fixation (BNF) also occurs in the oceans primarily by cyanobacteria, commonly known as blue-green algae (Ladha et al., 2022; Vitousek et al., 2013). In addition to fixation, wildlife contributes to the emission of reactive nitrogen through excretion, e.g. bird colonies or fallow deer (Galloway et al., 2003). Besides, soil organisms can set reactive nitrogen free through the decomposition or hydrolyzation of dead organic matter to NH_3 or NH_4^+. Reactive nitrogen is also emitted through burning processes, including natural fires of forests, savannahs, and peatlands, primarily as NO_x and NH_3 compounds (Fowler et al., 2013). Finally, active volcanoes contribute to N_r in the atmosphere as diverse species are emitted in their plumes (Martin et al., 2012). In general, oxidized nitrogen compound production prevails in high-temperature burning processes, and reduced nitrogen is produced by evaporation processes at lower temperatures (Sapek, 2013).

Since the Industrial Revolution began in the mid-18th century, human activities have contributed substantially to reactive nitrogen emissions. According to the inventory Emissions Database for Global Atmospheric Research (EDGAR), global emissions of NO_x were about 120 Tg in 2018 (Global Air Pollutant Emissions, 2023). Transport is the largest source of NO_x with 53 Tg a^{-1}, whereas fossil fuel combustion for energy production alone contributes to about 30 Tg each year (Paustian et al., 2006; Buendia et al., 2019; Skiba et al., 2021). The remaining emissions come from the combustion of fossil fuels for industrial or domestic usage, biomass, and biofuel burning. Wildfires also cause NO_x emissions and may globally affect the atmosphere's composition.

In pre-industrial times, humans mainly relied on animal feces and urine for agricultural production, but their low availability limited the scale of agriculture and, thus, the population. The discovery of a procedure to synthesize ammonia from nitrogen and hydrogen gas was made by Fritz Haber in 1908, after which further development and upscaling by Carl Bosch enabled large-scale industrial production of inorganic fertilizers (Paull, 2009; Erisman et al., 2008). The discovery led to a rapidly growing population during the twentieth century since it secured food and feed supply. Because of Artificial N fertilizer use, food, feed, and livestock production have increased substantially, but it has simultaneously increased the losses of N compounds to air and water. With respect to emissions into the air, ammonia is the major N confound, although agricultural activities also cause the emission of nitrogen oxides and nitrous oxide. According to the inventory Emissions Database for Global Atmospheric Research (EDGAR), NH_3 global emissions were about 58 Tg as NH_3 (48 TG NH_3-N) in 2018 (Global Air Pollutant Emissions, 2023), thus being higher than the NO_x-N emissions.

Human activities in 2020 were estimated to produce 226 Tg N_r, about five times more than in 1961 (Galloway et al., 2021). It is also an increase of ~61% and ~7% relative to 1990 (140 Tg Nr) and 2010 (210 Tg), respectively (Galloway and Cowling, 2002; Fowler et al., 2013). Human ingestion in food and food production contributes to the majority of reactive nitrogen (about 70%), while the rest is from fuel combustion and other uses by the Haber-Bosch process. As a result of enhanced energy use and N-induced agricultural production, the global emissions of NH_3 and NO_x increased almost linearly and nearly doubled between 1970 and 2018 (Global Air Pollutant Emissions, 2023). For the first decade of the 21st century alone, the EDGAR inventory already indicates approximately 20% and 18% increase in the global NH_3 and NO_x emissions, but with significant spatial variations at regional and national scales (Reis et al., 2009; Van Damme et al., 2021). Overall total reactive nitrogen emissions from human activities are now seven times greater than those from natural sources (Vitousek et al., 2013; Fowler et al., 2013)

Figure 1-1 shows the estimated global distribution of ammonia emissions in 2018 from the EDGAR-v6.1 inventory (Global Air Pollutant Emissions, 2023). As one can see, the largest ammonia emissions occur in the world's agricultural regions. These include Eastern China, Northern India, North-western Europe, the mid-west of the United States, and Central Canada. The emissions in the tropical regions mainly originate from biomass burning and are found in the sub-Sahel region, parts of Brazil, Indonesia, etc. Although the contribution of non-agriculture sources remains low, it has increasingly become more visible as industries develop. For example, global NH_3 emissions from the power industry and on-road vehicles increased by 57% and 50% from 2000 to 2015, respectively (Global Air Pollutant Emissions, 2023). Besides, vehicles installed with three-way catalysts (TWC) and NO_x controls are more likely to release more ammonia than the ones without (Wu et al., 2020).
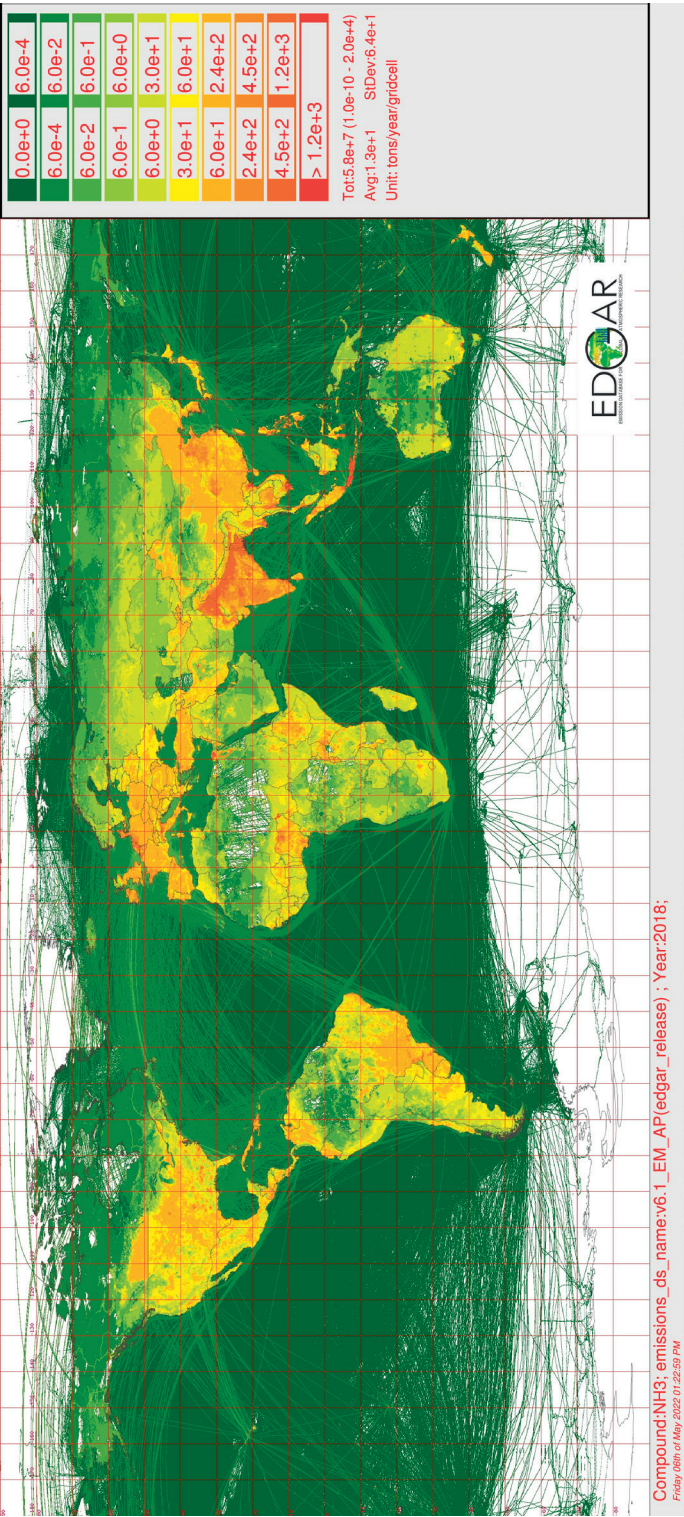
Figure 1-1 Annual emission map of ammonia in 2018 from the EDGAR v6.1 inventory (source: Global Air Pollutant Emissions (2023)).

1.1.2 Shift of N deposition towards ammonium-dominance in Europe

Paulot et al. (2018) used future International Panel on Climate Change (IPCC) Representative Concentration Pathways (RCPs) scenarios for 2010–2050. They showed that future decreases in reactive nitrogen deposition due to NO_x emission controls will be offset by the expected increases in ammonia emissions from agriculture over North America. This is in alignment with information for Europe.

Countries in Europe have committed to significant reductions in NO_x emissions but only to modest reductions of NH_3 emissions in the framework of the convention on Long-Range Transboundary Air Pollution (LRTAP) and the National Emissions Ceilings (NEC) Directive. Overall, agricultural activities account for 85–98% of the atmospheric NH_3 emissions in Western countries (Anderson et al., 2003; Gyldenkærne et al., 2005), with energy emissions from traffic and road transport, biomass burning, and fossil fuel combustion making up the remainder, and reductions in NH_3 emissions from agriculture were limited in the last decades. Even though the annual European Union emission inventory report 1990-2015 shows that NH_3 emissions of EU-28 countries fell by 23% between 1990 and 2015, the decreasing trend started to flatten in recent years (EEA, 2017). European emissions even rose for the fourth year between 2014 and 2017, with an overall 2.5% increase, according to the annual EEA briefing 'National Emission Ceilings (NEC) Directive reporting status 2019' (European Environment Agency, 2019c). These increases may be because of increased livestock animal numbers and the lack of emission reduction measures.

In comparison, significant reductions in NO_x emissions have been achieved in Europe. In Europe, total NO_x emissions fell by 55% between 1990 and 2017. Especially the traffic sector has contributed to the decline of NO_x emissions. The agricultural sector witnessed more modest declines of 7.8% from 20 Eastern European countries and 19.1% from 22 Western European countries (Skiba et al., 2021). The future projection confirms the continuation of these trends. Schmitz et al. (2019) estimated the area-averaged deposition of NO_x, NH_3, and total N between 1900 and 2050 to the EU28, Norway, and Switzerland according to EMEP model results. It is illustrated that from 2000 to 2040, the total N deposition is expected to continue to decline. The stagnating reduction in NH_3 depositions leads to an NH_x-dominant deposition situation, with the deposition of reduced nitrogen about three times that of NO_y. Future decreases are expected to be minor, and inorganic N deposition is likely to converge to a level approximately twice as high compared to 1900.

1
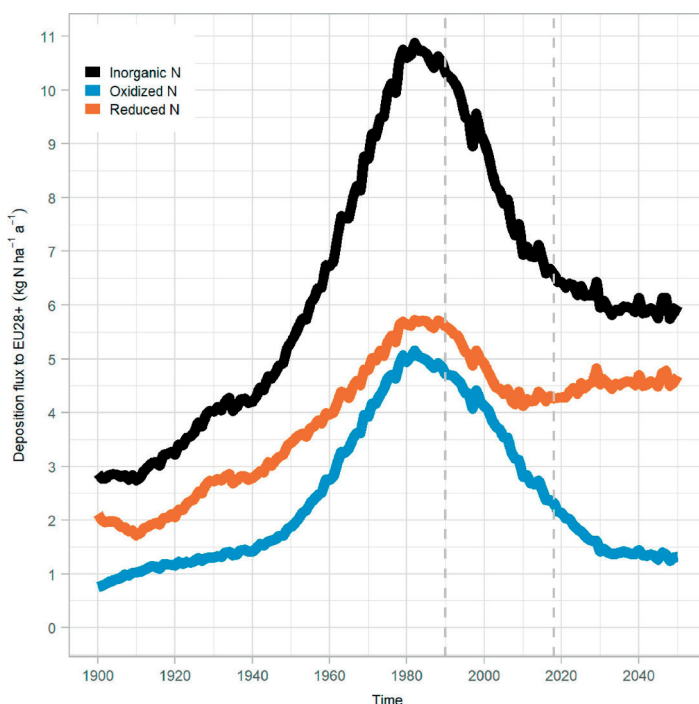
Figure 1-2 Average depositions of oxidized, reduced, and total N between 1900 and 2050 to the EU28, Norway, and Switzerland according to EMEP model results (source: Schmitz et al. (2019)**). Vertical dashed lines indicate the years 1990 and 2018.**

It can be concluded that the deposition of reactive nitrogen is becoming much more NH_3-dominated than before. Given the (increasing relative) importance of NH_3 in total deposition, there is a growing need to understand and quantify the emission of ammonia, considering that 1) ammonia emissions and concentrations are very variable in space and time, 2) there is a lack of observations in comparison to other species (e.g., OMI, TROPOMI for NO_2), 3) there is a lack of monitoring across large parts of Europe for ammonia. Recognition of this shift is critical to formulating effective future policies to protect ecosystems from excess nitrogen deposition.

1.1.3 Impacts of ammonia on human health and ecosystems

Humans have benefited significantly from large-scale fertilizer use in agriculture. Half of the world's population is fed because of Habor & Bosch's discovery. Furthermore, the world economy depends on the combustion of fossil fuels, which also results in an overwhelming emission of reactive nitrogen into the atmosphere. This reactive nitrogen emission, however, also alters our living environment, negatively impacting our habitat, health, and society, which we cannot afford to overlook. The main impacts are adverse human health impacts through poor air quality and biodiversity loss through eutrophication and

acidification. The latter occurs after the emitted nitrogen compounds are deposited from the atmosphere on terrestrial ecosystems, while it also affects aquatic ecosystems.

Human health impacts due to reactive nitrogen (NH_3 and NO_x) emissions can be categorized as (i) direct impacts of elevated NO_x concentrations, (ii) NO_x-induced O_3 exposure impacts, and (iii) NH_3- and NO_x-induced particulate matter (PM) exposure impacts, while impacts on terrestrial and aquatic ecosystems include impacts of (iv) direct above-ground exposure and of (v) soil-mediated N deposition impacts by eutrophication and acidification. (see de Vries (2021) for a short overview of those effects). A summary of those effects, limited to NH_3, is given below, while soil-mediated N deposition impacts and critical N loads also include NO_x deposition as this can not be distinguished from NH_3.

1.1.3.1 Impacts on human health

NH_3 plays a key role in the formation of particulate matter (PM) (Lovarelli et al., 2020). Exposure to particulate matter and health risks are significantly correlated. The size ranges of the relevant particles are directly associated with their ability to damage human health because the size of the particles determines the site in the respiratory tract where they will deposit. PM_{10} deposits mainly in the upper respiratory tract and can irritate a person's eyes, nose, and throat. In contrast, $PM_{2.5}$ can reach lung alveoli, posing the most significant risk (Wyer et al., 2022). Its health effects may include cardiovascular effects such as cardiac arrhythmias and heart attacks and respiratory effects such as asthma attacks and bronchitis. Exposure to particle pollution can especially harm those with pre-existing heart or lung disease, older people, and children. It can even cause premature death. Wyer et al. (2022) estimated that NH_3 contributed 50% and 30% of $PM_{2.5}$ air pollution in the EU and the US, respectively. De Leeuw (2002) estimated that 640 kg of PM_{10} can be formed per ton of NH_3 emitted. For $PM_{2.5}$ in the Netherlands, Weijers et al. (2011) indicated that the secondary inorganic aerosol, including ammonium sulfate and ammonium nitrate, is the most dominant (42–48%) source. Global premature mortality from PM exposure has been projected to increase from over 3.3 million in 2010 to 6.6 million in 2050, with most deaths occurring in China and India (Lelieveld et al., 2015). In Europe, about 400,000 premature deaths yearly are attributable to $PM_{2.5}$ concentrations long-term exposure (European Environment Agency, 2019a). A recent study showed that a 50% reduction in agricultural ammonia emissions would reduce the annual mean $PM_{2.5}$ concentrations and the related mortality attributable to PM pollution by 19% in Europe (de Vries, 2021).

1.1.3.2 Impacts on terrestrial ecosystems

NH_3 emissions to the atmosphere impact terrestrial ecosystems via direct above-ground exposure and soil-mediated N deposition, including eutrophication and acidification (see de Vries (2021) for a summarizing overview).

Adverse effects of direct exposure to elevated NH_3 concentrations on higher plants include damage to the epicuticular wax layer, increased susceptibility to drought stress, and an enhanced risk for fungal infection and pest attacks caused by increased nitrogen levels in plant tissue (de Vries, 2021). Direct adverse effects on vegetation occur when the foliar uptake rate of NH_3 is higher than the detoxification rate of the plants. The most sensitive species to gas-phase effects of NH_3 (in combination with SO_2, NO_2) are epiphytic lichens.

Regarding soil-mediated N deposition, it is relevant to distinguish between forests and other ecosystems (Bouwman et al., 2002). In forests, N deposition may first enhance growth and productivity through enhanced N availability. But at higher deposition levels (above $10 - 15$ kg N ha^{-1} yr^{-1}), N leaching starts to increase as the forest approaches 'nitrogen saturation', associated with soil acidification and elevated leaching of base cations (Aber et al., 1998; de Vries, 2021). Inputs of acidifying compounds may lead in the long term to losses of soil buffer capacity by loss of cations, lower pH, increased leaching of nitrate accompanied by base cations, increased concentrations of toxic metals, and changes in the balance between nitrogen species (Reuss and Johnson, 1986). Acidification makes forests more vulnerable to other stress factors such as frost, drought, and pests.

In other ecosystems, plant species in many habitats are adapted to nutrient-poor conditions and can only compete successfully on soils with low N levels. Inputs of N to ecosystems may increase the availability of N, which can lead to shifts in plant species composition towards nitrophilic species and, subsequently, a decrease in plant species diversity (Bobbink et al., 1998). As a consequence, the complete foodchain supported by the original vegetation is affected. This process is referred to as eutrophication.

1.1.3.3 Impacts on aquatic ecosystems

Elevated N concentrations in surface waters and coastal/marine waters contribute to eutrophication with related impacts on phytoplankton, benthic algae, zooplankton, water plant communities (macrophytes), and fishes, which can lead to many negative effects (de Vries, 2021). For example, N_r leads to increased biomass of phytoplankton, microalgae, and macroalgae (seaweed). Excessive phytoplankton and algae growth blocks sunlight and interferes with aquatic plant and animal productivity, water temperature, and current flow, eventually leading to ecosystem collapse. However, eutrophication effects in aquatic ecosystems are dominated by runoff from agricultural ecosystems and much less by N deposition induced runoff from terrestrial ecosystems or direct N deposition. Unlike eutrophication, N deposition is a dominant cause of surface water acidification, caused by Aluminum (Al) release from nonagricultural acidic soils that leaches from watersheds into lakes and streams (de Vries, 2021). Surface water acidification has led to fish population deaths by inducing fish kills and other biological effects linked to low pH and high Al concentrations (Schofield, 1976; Baker and Schofield, 1982).

1.1.3.4 Critical load of ecosystems

To define the deposition level above which natural ecosystems can be negatively affected, the concept of a critical load was introduced as the "quantitative estimate of ecosystem exposure to one or more pollutants below which significant harmful effects on specified sensitive elements of the environment do not occur, according to present knowledge" (Nilsson, 1988; Williams and Tonnessen, 2000). In Germany and Europe, nitrogen deposition critical loads for eutrophication exceeded by about 71% and 58% of the area of ecosystems in 2020, compared to 81% and 67% in 2005 (Hettelingh et al., 2017). Meanwhile, critical loads for acidification were exceeded by about 35% and 4% for Germany and Europe in 2020, compared to 65% and 11% in 2005. One can see that even though a considerable reduction in NO_x deposition, and to a less extent in NH_3 deposition (Figure 1-2), has been achieved, there still exists significant exceedance in critical loads for eutrophication and acidification in ecosystems.

1.2 Measuring and modeling the fate of atmospheric ammonia

1.2.1 Fate of ammonia in the atmosphere

The atmospheric ammonia budget is studied as a mass balance between the atmospheric molar fraction ("storage"), sources, and sinks. Given the significant uncertainties in the ammonia budget, ammonia's relevance in the formation of air pollution, and the negative impact of ammonia, it is of great significance to improve ammonia budgets (emissions) of agricultural systems, which helps to assess the effects of N inputs on the environment and identify levers for action. A better understanding of the insight of ammonia emission and its fate afterward at both continental and regional scales gives indications of areas where N depositions exceed critical loads in terrestrial and aquatic ecosystems, which causes adverse effects on human health and biodiversity (as discussed previously).

An overview of the fate of NH_3 in the atmosphere is shown in Figure 1-3 (Effects of air pollution on natural ecosystems, 2023). After NH_3 is emitted mainly from agricultural sources, it has a typical atmospheric lifetime of several hours (Van Damme et al., 2021). After chemical reactions, NH_3 can be transformed into an ammonium aerosol (e.g., ammonium sulfate or ammonium nitrate), which enables long-range transport in the atmosphere. In addition, NH_3 is removed from the atmosphere by dry and wet deposition, while NH_3 exchange fluxes between the surface (soil and vegetation) and the atmosphere are bi-directional (Asman, 2001; Erisman et al., 1998).
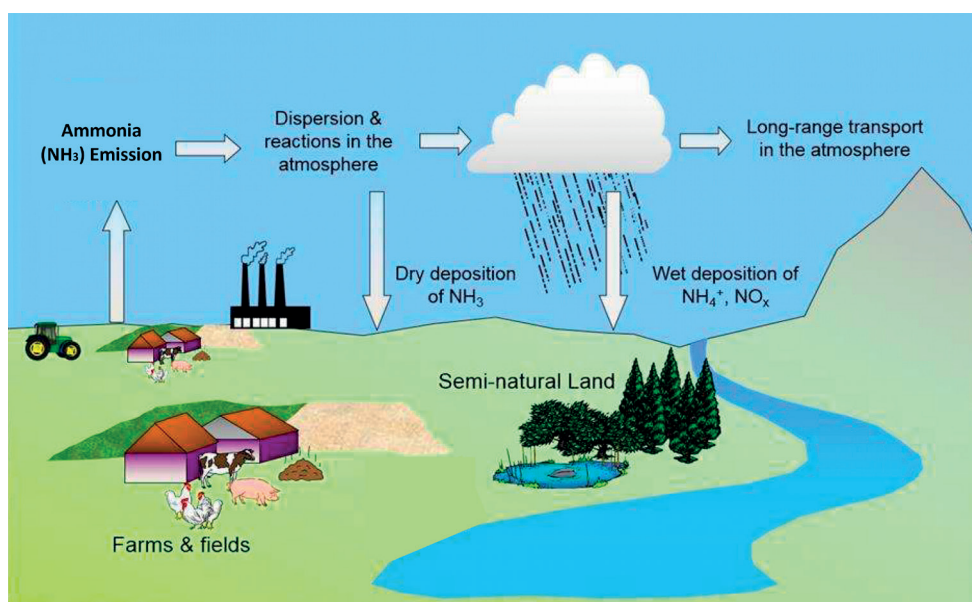
Figure 1-3 A sketch demonstrates the fate of ammonia in the atmosphere (adapted from Effects of air pollution on natural ecosystems (2023)**).**

1.2.1.1 Emission

In an agricultural system, emission from manure management starts with domestic animal houses where N is excreted in the form of urea (in mammals) or uric acid (in birds) through urine discharge of livestock and poultry, and in the form of urea, NH_3 and organic N in animal feces. In animal houses, slurry channels on slatted floors collect the excreted slurry, during which ammonia volatilization in these barns occurs. Manure from animal houses is typically put in manure storage facilities to mineralize, during which ammonia emission also occurs. Outside animal houses and manure storage, additional ammonia is emitted from the excretion of grazing animals. Moreover, when manure, mineral fertilizer, compost, and crop residue are applied to arable crops and grassland, ammonia volatilization also leads to atmospheric emissions.

1.2.1.2 Dry deposition

Dry deposition is a mass transfer process where ammonia is first transported to the surface by turbulent and molecular diffusion and then removed by adsorption or absorption by vegetation, soil, or other surfaces (Swart et al., 2023; van der Graaf et al., 2018). The process is governed by 1) the concentration in air, 2) turbulent transport processes in the boundary layer, 3) the chemical and physical nature of the depositing species, and 4) the efficiency of the surface to capture or absorb gases and particles (Chamberlain and Spence, 1997). Dry deposition may comprise a large part of the total deposition (Zhang

et al., 2009). Earlier modeling studies showed that dry deposition of NH_x constitutes over 60 % of the total N deposition in Western Europe (van der Graaf et al., 2018).

Dry deposition NH_3 fluxes between the surface (soil and vegetation) and the atmosphere are bi-directional (Asman, 2001; Erisman et al., 1998). The underlying reason is that an ammonia solution has a vapor pressure above it. The apoplast pH, NH_4^+ concentration, and temperature drive the gaseous equilibrium concentration. Depending on whether the ambient air NH_3 concentration is above or below the equilibrium NH_3 concentration, NH_3 can be released or taken up by the plant (Massad et al., 2010). The equilibrium concentration is also called the compensation point.

Over unfertilized vegetation, deposition fluxes typically prevail and dominate the local NH_3 budget (Flechard et al., 2011). For forests and other rough surfaces, dry deposition is fast. It has been confirmed surface roughness can increase dry deposition effectiveness in the particle diffusion and diffusion–impaction regime, despite at very small values. In general, the topography of a rough surface distorts the airflow characteristics and the boundary layer itself, resulting in a shorter stopping distance for the deposited particles (Hussein et al., 2012). On agricultural vegetation, NH_3 exchange is often characterized by deposition fluxes interrupted by the NH_3 emissions directly associated with slurry application, which strongly dominate the NH_3 budget of fertilized fields (Flechard et al., 2010).

1.2.1.3 Wet deposition

NH_3 and NH_4^+ are also removed from the atmosphere by the wet deposition process. Wet deposition is the process where atmospheric pollutants are delivered to the earth's surface by precipitation (rain, hail, or snow) (Fowler, 1980). Wet deposition depends on the amount of rain and the location relative to the sources of the pollutant (Erisman and Draaijers, 1995). Orography plays an essential role in wet deposition patterns. Temperature is also crucial in the wet deposition process since it influences the chemistry of clouds (Hicks, 2005). Unlike dry deposition, wet deposition is not largely influenced by the characteristics of the surface but rather by the processes within the cloud.

During wet deposition, atmospheric pollutants are dissolved in clouds and precipitation droplets or attached to hail or snow. Two main processes are involved in wet deposition – in-cloud scavenging and below-cloud scavenging (van der Swaluw et al., 2010). In-cloud scavenging includes the process of forming cloud droplets due to humid air condensation. When the air contains particles (e.g., ammonium salts), droplets will form more rapidly because the particles act as condensation nuclei. In addition, water-soluble gases like ammonia may dissolve into the cloud water from the air masses drawn into a (convective) cloud. Below-cloud scavenging or wash-out is the process where the uptake of gases and/ or particles can occur during the downward transport of the droplet to the earth's surface

(Shimshock and De Pena, 1989). It is a very efficient removal mechanism for soluble gases like NH_3. Wet deposition also occurs under conditions with fog and early morning dew, although this is usually described as a separate process called occult deposition (Unsworth and Wilshaw, 1989). Occult deposition is usually considered unimportant. In the Netherlands, it contributes almost nothing (<1-2%) to the total deposition of N compounds from the atmosphere (Bobbink et al., 2013). However, it may be the dominant nitrogen flux to the surface at high altitudes in mountainous areas (Walker et al., 2019). Occult deposition was found to exceed deposition by precipitation and dry deposition in high elevation settings from North Carolina to Maine.

1.2.1.4 Chemistry

Ammonia also plays a crucial role in atmospheric chemistry. Eventually, much of NH_3 is either deposited or transformed into an ammonium aerosol. Gaseous NH_3 reacts with acids like sulphuric acid (H_2SO_4), nitric acid (HNO_3), and hydrochloric acid (HCl), forming ammonium salts in the particulate phase. The loss rate of ammonia towards PM formation depends on the production of the relevant acids, humidity, and temperature (Behera and Sharma, 2012). Hence, the loss rates for ammonia show temporal and spatial variations and may systematically change over time as a function of mitigation efforts for SO_2 and NO_x (Banzhaf et al., 2015).

In the atmosphere, NH_3 effectively combines with sulphuric acid to form ammonium sulfate ($(NH_4)_2SO_4$) (Schobesberger et al., 2015). As a strong acid, sulphuric acid is formed from sulfur dioxide by gas phase reactions (with the OH radical) and through wet chemical reactions in clouds. The sulphuric acid formed has a very low vapor pressure, meaning it will all be present as small droplets. The reaction is irreversible under common atmospheric conditions due to the low vapor pressure of sulphuric acid.

$$2NH_3(g) + H_2SO_4(g) \rightarrow (NH_4)_2SO_4(s)$$
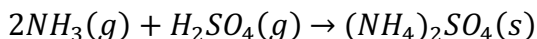
In addition, ammonium salts with a semi-volatile nature can also be formed, i.e., ammonium nitrate and ammonium chloride (NH_4NO_3 and NH_4Cl). Both reactions are reversible, and the partitioning between the gas and aerosol phases strongly depends on atmospheric conditions such as temperature and relative humidity (Bassett and Seinfeld, 1983).

$$NH_3(g) + HCl(g) \leftrightarrow NH_4Cl(s)$$

$$NH_3(g) + HNO_3(g) \leftrightarrow NH_4NO_3(s)$$

1
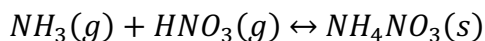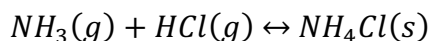
In practice, ammonium nitrate is a main contributor to particulate matter (Schaap et al., 2002, 2004b), but the much more volatile ammonium chloride has hardly been observed in practice. The typical atmospheric lifetime of ammonium aerosols is in the order of several days, thus providing the means for long-range transport of reactive nitrogen to more remote regions.

Conversion rates for NH_3 to its NH_4^+ aerosols are dependent on the molecular ratio of the ionic species (NH_4^+, NO_3^-, H^+, and SO_4^{2-}) and the relative humidity and thus vary both in space and time (Behera and Sharma, 2012; Renard et al., 2004). The ratio of the ionic species determines the chemical entities present, and the relative humidity influences in which phase they will be mainly present. As long as the high partial pressure of gas-phase ammonia persists, ammonium nitrate or ammonium chloride will not volatilize. When the cloud of ammonia dissipates, the ammonium nitrate will decompose into NH_3 and HNO_3 until the concentration of the two gases reaches its equilibrium value for the prevailing temperature and relative humidity (Renard et al., 2004).

Gaseous NH_3 has a relatively short atmospheric lifetime of hours because of its high deposition velocity and reactivity (Evangeliou et al., 2021). On the contrary, NH_4^+ has a longer atmospheric lifetime of 1–15 days as the main deposition route is via wet deposition. Therefore, close to the source, NH_x (NH_3 and NH_4^+) is mainly removed from the atmosphere in the form of dry deposition of NH_3; whereas away from the source areas, NH_x is removed primarily in the form of wet deposition of NH_4^+, which deposits slower than NH_3 and has a more extensive spatial sphere of influence (Bleeker, 2018).

In summary, ammonia's short lifetime, deposition dynamics, reaction with other compounds, and emission sources prone to high spatial and temporal variability make monitoring and modeling challenging.

1.2.2 Monitoring and measurements
Due to the severe side effects of ammonia and the urgency to estimate the regional and global budget, it is essential to study the fate of ammonia after it is emitted into the atmosphere. Several measurement methods and approaches have been developed to monitor ammonia levels.

1.2.2.1 Ground-based observations of concentration
Nowadays, the most common and accurate way to monitor surface ammonia distributions is by measuring concentrations directly (Liu et al., 2022). The most widely used instruments to measure NH_3 concentrations are passive samplers, denuders, and filter packs (Ferm, 1979).

The passive samplers are based on the slow diffusion of NH_3 onto a medium, commonly filters coated with an acidic substance that binds the NH_3 to the surface. The samplers are then removed, rinsed, and analyzed inside a lab. Adopting this system at a large scale is relatively cheap but has a low temporal resolution of a week to a month. Moreover, the preparation and analysis are labor intensive. There are several passive sampler networks in Europe. The Measuring Ammonia in Nature (MAN) network monitors atmospheric ammonia concentrations in nature reserve areas in the Netherlands (http://man.rivm.nl) (Ge et al., 2020). The Umweltbundesamt (UBA) from Germany also sets up monitoring stations, providing governments and the public with information on the concentration of air pollutants, including ammonia. The UBA also collects data from the network of the 16 German federal states.

Denuders use the airflow that passes through a tube with NH_3 diffusing onto a tube, wetted with an acidic substance, while particles pass through the tube. Often a filter pack is placed behind the denuder to sample the aerosols. The gas-denuder removes gases, while these otherwise would be collected in the filter pack and counted as aerosols. In this way, the denuder can effectively differentiate the gas and aerosol phases and simultaneously measure aerosol and gas components (Trebs et al., 2004). Denuders are commonly applied to measure daily means, but a rotating denuder (for example, the Monitor for AeRosols and Gases in ambient Air (MARGA) systems) can conduct hourly measurements (ten Brink et al., 2009).

In the active filter pack approach, the filters collect both the aerosol and gas phase of the air that is sucked through a series of filters which generally consist of Teflon filters for aerosol collection, followed by NaCl-impregnated filters for collection of gaseous HNO_3 and by citric acid for NH_3. After a specific time (commonly a day), the filters are exchanged and analyzed to derive the daily mean concentration. However, the impregnated backup filter can collect the evaporation of NH_4^+ salts as NH_3 from the front filter. Therefore, the NH_3 concentration measured from the backup filter should be interpreted as a maximum value. Such artifacts can be significant, especially at temperatures above 20 degrees Celsius when all ammonium nitrate may evaporate (Schaap et al., 2004a).

Each of the instruments described above uses airflows or diffusion to measure NH_3 that sticks to either a tube or a filter after the air passes through. Recently, spectroscopy instruments with mini-DOAS systems have been developed to determine the amount of NH_3 through open path measurements without using inlets (Volten et al., 2012; Sintermann et al., 2016). In a mini-DOAS system, a UV light source sends out a focused light beam, which is reflected by a retro reflector at the end of the measurement path. The reflected light is then measured by a charge-coupled device (CCD) that maps the UV light for a specific spectral window. The concentration is calculated using the Lambert-Beer

law. One example is the Dutch Monitoring Air Quality Network (LML; Landelijk Meetnet Luchtkwaliteit), the previously used denuder ammonia monitor system in the network was gradually replaced by mini-DOAS after 2014 (Berkhout et al., 2017).

Another technique is open-path FTIR (Dammers et al., 2017). FTIR instruments use the absorption of infrared light at specific wavelengths. The absorption strength depends on the vibrational and rotational absorption modes of the molecule of interest. Open-path FTIR measurements have been used to measure NH_3 from large agricultural fields with path lengths up to a km (Galle et al., 2000; Todd et al., 2001). The FTIR system can also be used to measure the vertical profile and column of NH_3 utilizing the sun as the infrared source. For the retrieval strategy of NH_3 from ground-based FTIR solar spectra, I refer to Dammers et al. (2015). The main advantages of the FTIR and DOAS techniques are that the instruments are free from inlet and sampling artifacts while retaining high precision. The main drawbacks are the high instrument costs in the case of the FTIR and the novelty of mini-DOAS.

Ground-based stations measure NH_3 surface concentration consistently at fixed locations, and some of them have relatively high temporal resolutions (hourly or daily), which offers the possibility of studying the behavior of NH_3 emission. However, the networks lack vertical information as most instruments only measure surface concentrations (Van Damme et al., 2015). Horizontally, the setup of station networks is coarse because a denser setup of networks means even higher costs. As a result, representativeness is an issue since local and regional agricultural activities and other local sources will influence all monitoring sites' measurements. Therefore, performing reliable measurements of NH_3 concentrations and fluxes is challenging to get a complete picture.

1.2.2.2 Ground-based observations of deposition

Ammonia can also be monitored by direct deposition measurements. However, because of the requirements for expensive instrumentation and the technical difficulties of measuring highly reactive gases, the availability of dry deposition monitoring networks across Europe is minimal (Erisman et al., 1998). Consequently, large-scale assessment of NH_3 dry deposition is hindered by the extremely limited number of deposition observation sites (van der Graaf et al., 2018). Measurements of NH_3 dry deposition fluxes largely remain experimental and are limited to campaigns of short durations (Zöll et al., 2016). These measurements are typically conducted for a specific ecosystem. Less expensive and simpler methods for dry deposition measurements are in need to achieve an extensive network. One of the most successful methods has been the Conditional Time Averaged Gradient method (CoTAG) (Famulari et al., 2010). The CoTAG instrument determines dry deposition after ammonia concentrations are measured at two heights, accounting for wind velocity friction measurements and atmospheric stability parameters for heat and

momentum. CoTAG measurements were also found to be in good agreement with the MAN concentration measurements obtained in Bargerveen in the Netherlands, while the differences may be due to a difference in measurement height, a difference in location, and not exactly identical measurement periods (Stolk et al., 2014).

In contrast to dry deposition, large data sets are available for wet deposition in Europe and European countries such as Germany and the Netherlands. Germany has an extensive countrywide wet deposition measurement network maintained by various national and regional monitoring programs. The national UBA network consists of 11 sites, and the various regional networks add 249 stations to the database (Schaap et al., 2017b). Two types of samplers are used at the available stations: wet-only and bulk deposition samplers. Bulk samplers collect precipitation in a bucket, which is always open, leading to a slight tendency to cause an overestimation of the wet deposition because it is susceptible to dry deposition during dry conditions. In contrast, wet-only samplers collect the precipitation in a funnel, the lid of which is automatically opened at the beginning of a rain event and closed at the end. Forty out of the 260 stations use wet-only samplers. The number of wet deposition measurement stations is smaller outside Germany in Northwestern Europe. For instance, in the Netherlands, there have been only 10 locations that continuously measure the wet deposition of ammonium (NH_4^+) by the LML network between 1985 and 2014, even though the Netherlands is among the countries with the highest reactive nitrogen deposition level (van Zanten et al., 2017).

1.2.2.3 Satellite measurements of total columns

Unlike ground-based measurements, satellite remote sensing products traditionally have much higher spatial coverage since satellites regularly orbit around the Earth or stay stationary above a certain location. Recently, remote sensing products with a higher spatial and temporal resolution (such as IASI and CrIS) have become available for better NH_3 concentration monitoring in the lower troposphere (Clarisse et al., 2009; Van Damme et al., 2015). The instruments take advantage of the unique infrared spectrum, which makes NH_3 distinguishable from other chemical species and background noise. Therefore, infrared spectrometers in orbit around the Earth can offer the possibility of continuous, real-time, global measurements of NH_3, capable of capturing spatiotemporal variations in NH_3 columns (Shephard et al., 2020; Shephard and Cady-Pereira, 2015; Warner et al., 2016; Someya et al., 2020). Table 1-1 (Dammers, 2017) summarizes the satellite instruments used for NH_3 retrievals, showing the overpass times, footprints, and overall instrument detection limit.

Table 1-1 Summary of satellite infrared spectrometers used to measure ammonia (Dammers, 2017)**.**

Instrument	Satellite	Agency	Period	Overpass	Field-of-View	Data Access
AIRS	Aqua	NASA	2002–2016	13:30	13.5 km	https://dx.doi.org/10.5067/06YIT7GX74FN
CrIS	Suomi-NPP	NOAA	2012–2017	13:30	14 km	https://hpfx.collab.science.gc.ca/~mas001/satellite_ext/cris/snpp/nh3/v1_5/
IASI	MetOp-A/B/C	ESA	2006–2020	09:30	12–39 km	https://iasi.aeris-data.fr/nh3/
MIPAS	Envisat	ESA	2002–2012	N/A *	420 km	http://share.lsdf.kit.edu/imk/asf/sat/mipas-export/
TANSO-FTS	GOSAT	JAXA	2009–2020	13:00	10.5 km	https://doi.org/10.5194/amt-13-309-2020
TES	Aura	NASA	2004-2018	13:30	5–8 km	https://dx.doi.org/10.5067/AURA/TES/TL2NH3N.008

The first attempt was made using infrared radiances measured by the Tropospheric Emission Spectrometer (TES) to infer NH_3 from the spectral residual differences in the 960–972 cm^{-1} region (Beer et al., 2008). Onboard the EOS Aura satellite, TES is in a sun-synchronous orbit with a daytime ascending orbit that provides favorable conditions for high thermal contrast and, thus, increased sensitivity to boundary layer NH_3 and a nighttime descending orbit (Clarisse et al., 2010). Even though it has small geographic coverage and consequent inability to provide daily coverage, the smaller satellite footprint of TES (5 km×8 km) allows for the potential to detect more localized NH_3 sources. The TES instrument has good signal-to-noise ratio (SNR) and relative radiometric calibration that is stable over time (Shephard et al., 2011). The combination of the high spectral resolution and good SNR of the TES instrument in the NH_3 region provides increased sensitivity to NH_3 mixing ratios near the surface from satellite observations and the selection of spectral regions that reduce the impact of interfering species and, consequently, systematic errors in the retrievals.

Infrared Atmospheric Sounding Interferometer (IASI) onboard the MetOp-A satellite was then used as an improved alternative (Dammers, 2017). IASI is a Fourier transform infrared (FTIR) spectrometer that circles in a polar Sun-synchronous orbit. IASI measures the thermal infrared (TIR) radiation in the spectral range from 645–2760 cm^{-1} with a spectral resolution of 0.5 cm^{-1} with overpass times of 09:30 and 21:30 mean local time. It has a wide swath width of 2×1100 km, corresponding to 2×15 mirror positions. Its spatial resolution is 50 km×50 km, composed of 2 circular pixels×2 circular pixels. Each circular pixel is a 12 km diameter footprint on the ground at the nadir (Clerbaux et al., 2009). Under elevated ammonia and favorable thermal contrast conditions, IASI has peak sensitivity to atmospheric ammonia in the boundary layer (Clarisse et al., 2010). Van Damme et al. (2014) presented an improved NH_3 retrieval scheme for IASI spectra, which relies on calculating a dimensionless Hyperspectral Range Index (HRI). Whitburn et al. (2016) continued with HRI and introduced a neural network-based algorithm to obtain NH_3 total columns. Van Damme et al. (2017) further improved the algorithm by training separate neural networks

for land and sea observations, enhancing thermal contrast, introducing a bias correction over land and sea, and treating satellite zenith angle.

The Crosstrack Infrared Sounder (CrIS) instrument is an FTS operated by the USA NOAA/NASA/DoD Joint Polar Satellite System (JPSS) program on Suomi National Polar-orbiting Partnership (NPP) satellite, which was launched on 28 October 2011 (Cao et al., 2022; Shephard et al., 2020; Cao et al., 2020). CrIS is an across-track scanning instrument in a sun-synchronous orbit with a mean local daytime overpass time of 13:30 in the ascending node and a mean local nighttime overpass time of 01:30 in the descending node. CrIS has a 2200 km swath width with the total angular field of view (±50º) consisting of 3×3 circular pixels of 14 km diameter each (nadir spatial resolution). CrIS provides soundings of the atmosphere over three wavelength bands in the infrared with good radiometric calibration and instrument SNR (Shephard and Cady-Pereira, 2015; Dammers et al., 2019). For NH_3 retrievals, the 9.14–15.38 µm (650–1095 cm^{-1}) range is selected as the main NH_3 infrared absorbing spectral region is between 960 and 970 cm^{-1}. Its spectral resolution in this spectral region is 0.625 cm^{-1}. While the spectral and spatial resolution of CrIS is lower than that of TES, its across-track scanning swath provides a greater spatial coverage which is more similar to IASI. CrIS has a similar spectral resolution as IASI and around four times decrease in spectral noise (~0.04 K at 280 K) in the ammonia spectral region, making it a potential candidate to detect smaller NH_3 concentrations than what is currently possible with IASI (Zavyalov et al., 2013).

Despite the improvements from the newer instruments and retrieval algorithms, recent studies have shown the limitation of satellite measurement (Dammers, 2017). The revisit time of several days and the requirement for clear-sky conditions lead to discontinuous temporal measurements, which is unideal for real-time monitoring to study NH_3 with such a short lifetime. The requirement of a strong thermal contrast means more considerable uncertainty in nighttime measurements. Furthermore, a priori assumptions on the NH_3 profile and shape for conversion of radiances into a concentration also result in uncertainties. Last but not least, regardless of the improvement of NH_3 column retrievals from satellite observations, there is still substantial variability in measurement uncertainty, varying from 5 % to over 1000 % (Van Damme et al., 2017). However, satellite remote sensing still has been used widely, given the advantage of having global coverage, making it possible to identify prominent features of ammonia levels on Earth. It also helps to study the long-term temporal variability of a larger region. Dammers et al. (2019) validated the CrIS fast physical NH_3 retrieval (CFPR) column and profile measurements using ground-based Fourier transform infrared observations. The total column comparison shows that both retrievals have a correlation of R = 0.77 and almost no bias. It illustrates that satellite observations are an essential complementary use to ground-based measurements for locations with stations.

1.2.3 Models

Because of the lack of spatial coverage of in situ measurement and coarse temporal resolution of satellite observations (revisit time of a few days), models are used to derive complete ammonia spatial and temporal distribution. Despite the challenges to modeling the spatial and temporal variability of ammonia emission and resulting deposition and concentration, there are various reasons for developing models, including large size of scale, mapping, source apportionment, and mitigation strategy development. An overview of the reasons is described below:

First of all, models provide a framework for assimilating current knowledge, and they enable the calculation of different processes' contributions to deposition (e.g., in-cloud, below-cloud scavenging), which cannot otherwise be separated. This capability is essential in pinpointing the most crucial processes for deposition. In addition, models can be used for detailing the causal relationships between source and effect. The connections can be defined in a scheme that is amenable to future refinement and corrections. Moreover, models allow for calculating nitrogen deposition across extensive geographical areas. This is especially useful in the case of NH_3, where the high spatial and temporal variability makes it very difficult to estimate national distributions of NH_3 concentrations and deposition from measurements alone. It is also worth mentioning that continental-scale models allow the assessment of contributions from different countries and sectors to the deposition levels within a specific country. Furthermore, models can also be used to predict future concentration and deposition for different scenarios. This is important if the aim is to reduce the deposition in particular areas and investigate the effectiveness of various emission reduction measures. Hence, models are of great value for policymaking. Lastly, models are instrumental in designing strategies for field measurements and monitoring. They can offer insights into potential locations with the most significant concentration gradients. With this knowledge, measuring sites can be chosen to gather the maximum amount of information with the available resources.

1.2.3.1 Emission inventories

The NEC Directive specifies that countries shall prepare and annually update national emission totals for SO_2, NO_x, NMVOCs, $PM_{2.5}$, NH_3, and other pollutants for which the European Union is obliged or requested to report to the LRTAP Convention, as well as emission projections, gridded data, and large point source (LPS) data. To help ensure harmonized and consistent emission information is reported, the NEC Directive requires all Member States to establish emission inventories using the methodologies agreed upon under the LRTAP Convention. An emission inventory usually produces the total emissions and distributions for greenhouse gases or air pollutants originating from all source categories in a particular geographical area and within a specified period (usually a specific year). They have been developed on global, regional, or even local scales to

inform on the most important emission sources, the impact of potential measures, and for further use in chemistry transport models (CTMs). Global NH_3 emission inventories include the Community Emissions Data System (CEDS) (McDuffie et al., 2020) and the Emissions Database for Global Atmospheric Research (EDGAR) (Crippa et al., 2018).

Emission inventories usually use the standard bottom-up approach to estimate the spatial distribution of NH_3 emissions from agriculture with a nitrogen (N) flow approach. In such an approach, starting from animal excreta, the NH_3 emission is calculated by multiplication of N excretion rates (housing systems) or N manure application and grazing rates with NH_3 emission factors from each particular source type. An example of an N flow model is the INTEGRATOR model, which uses a bottom-up approach to provide the spatial distribution of land system budgets at the EU-27 level (de Vries et al., 2021, 2022). Its output includes N uptake, N emissions (in the forms of NH_3, N_2O, NO_x, and N_2) from housing and manure storage systems, N accumulation in or release from the soil (due to manure and mineral fertilizer application), and N losses to water by leaching and runoff, using empirical linear relationships between the different N fluxes. The results are aggregated for all agricultural land (crops + grassland), different crop groups (C3 cereals, maize, other crops, grassland + fodder crops), and major soil types (sand, clay, and peat). The emissions of NH_3 and other gases to the atmosphere are estimated by multiplying N inputs by emission factors (de Vries et al., 2021, 2022). A schematic overview of the NH_3 emission module of the INTEGRATOR model is presented in Figure 1-4 (de Vries et al., 2022).

The INTEGRATOR model starts with the calculation of N excretion by multiplying the number of animals with the N excretion rate per animal for eight animal categories (dairy cows, other cows, pigs, laying hens, other poultry, horses, sheep and goats, and fur animals). A major distinction is made between grazing animals and other animals. Dairy cows, other cattle, sheep, and goats are assumed to depend highly on local land resources for grazing or feed production. Pigs and poultry are assumed to be held in more land-independent systems. The N excreted in housing systems is the multiplication of N manure excretion and the housing fraction (f_{hous} in Figure 1-4), while the N excreted from grazing on land is obtained by subtracting N excreted in housing systems from total N manure excretion. The gaseous emission from housing and manure storage is calculated by multiplying N excretion with the emission fraction per housing and manure storage system ($f_{NH3em,hous}$) NH_3 emission fractions for housing and manure storage are distinguished per animal type and manure type. The total manure production is derived by subtracting gaseous emissions and leaching in housing and manure storage systems from the N excretion. The emissions of NH_3 from agricultural land are calculated by multiplying the N input by grazing, manure application and fertilizer application with NH_3 emission fractions for grazing ($f_{NH3em,graz}$), manure application ($f_{NH3em,ma}$) and fertilizer application ($f_{NH3em,fe}$), respectively.

1

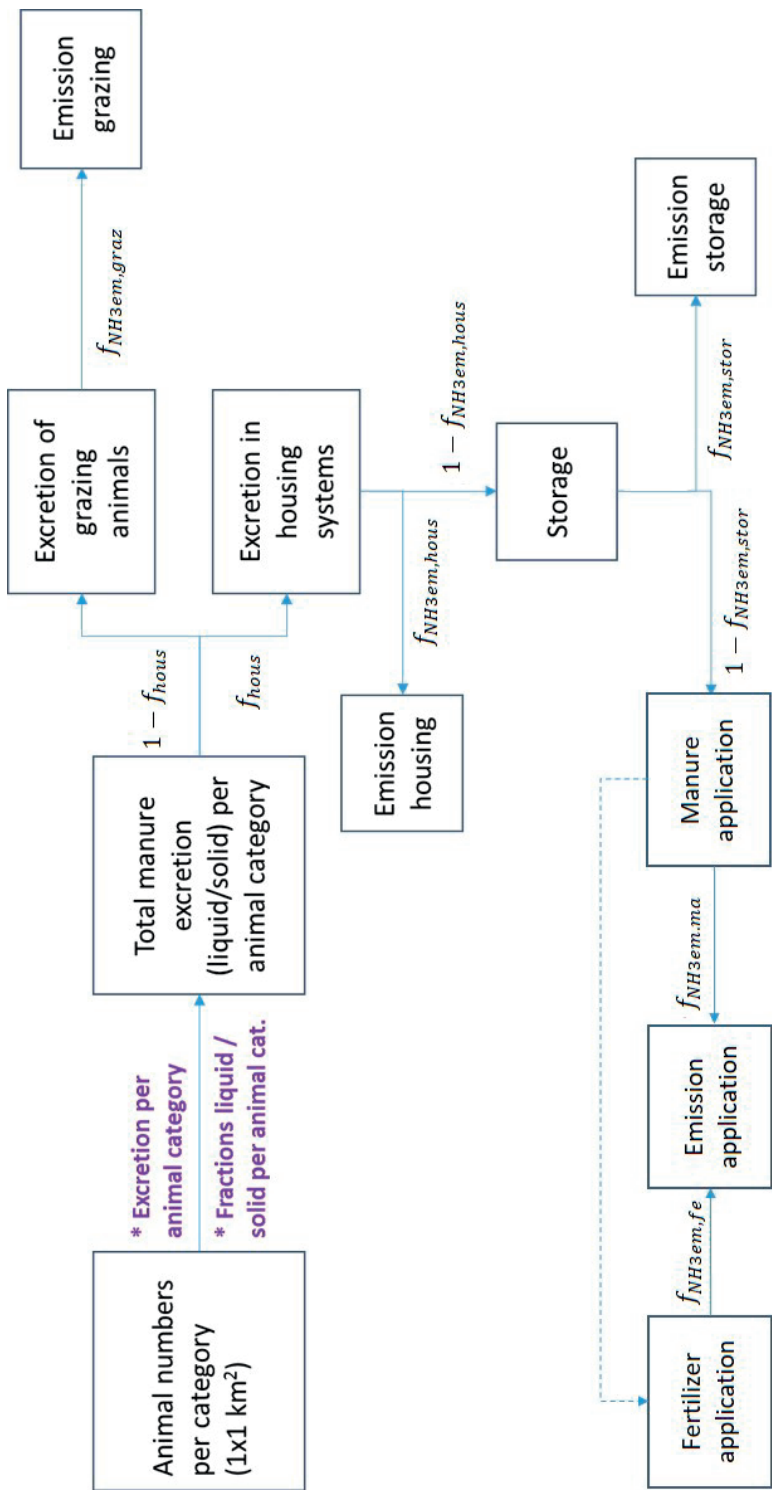**Figure 1-4 A schematic workflow of the NH$_3$ emission module in INTEGRATOR (de Vries et al., 2022). f_{hous} is the fraction of total manure excretion going to housing systems. $f_{NH3em,graz}$, $f_{NH3em,hous}$, $f_{NH3em,stor}$, $f_{NH3em,ma}$ and $f_{NH3em,fe}$ represent emission fractions of grazing, animal housing, manure storage, manure application, and fertilizer application, respectively.**

Emission fractions for manure application ($f_{NH3em,ma}$) are distinguished for three animal types, i.e., cattle (including dairy cows, other cows, sheep and goats, horses and fur animals), pigs and poultry (laying hens, other poultry) and manure type (liquid vs. solid for cattle and pigs). Emission fractions for fertilizer application ($f_{NH3em,fe}$) are differentiated between urea-based fertilizers and nitrate-based fertilizers. Details on the various fractions and the procedure to allocate manure over grassland and different crop groups are given in de Vries et al. (2022).

One of the main issues of developing reliable NH_3 emissions inventories using the N flow method is that it requires comprehensive information on activity input data and emission factors. The spatial resolution and quality of activity input data will impact the uncertainties of emission products. Emission factors indicate the potential emissions for specific locations from individual source types, such as animal housing, manure storage, and fertilizer application. This requires detailed and comprehensive emission measurements to capture the complex spatial variability of emissions across source types considering variations in meteorology, application technique, soil properties, manure characteristics, housing type, etc. Currently, the emission factors used in the previously European studies by (de Vries et al., 2021, 2022) hardly account for those spatial variations. Only in a limited way manure type and housing type were taken into account, based on local measurements conducted in various studies. However, the climate and soil conditions during different measurements did not represent the variations in larger regions. Moreover, one constant emission factor, calculated from the measurements, is generally used for each emission sector for each country, leading to inaccurate annual emissions and the failure to identify spatial and inter-annual variability in ammonia emissions.

1.2.3.2 Chemistry transport model

Once an emission distribution is obtained, one common way of validation is to simulate concentrations, depositions, or total columns with atmospheric chemistry transport models (CTMs), so that they can be compared with measurements. CTMs simulate the transport, chemical conversion, and deposition of various atmospheric species. They are used to investigate the distribution and evolution of tracers in the atmosphere.

The first case of using CTM to model global distributions of NH_3 was Dentener and Crutzen (1994), who used a climatological three-dimensional global tropospheric transport model MOGUNTIA (Zimmermann et al., 1989) with the help of a 10°×10° emission inventory. Subsequently, several CTMs have been developed. Due to the environmental policies in Europe, there are several implementations for the region, including TM5 (Huijnen et al., 2010), the EMEP model (Simpson et al., 2012), the DAMOS/Danish Eulerian Hemispheric Model (DEHM) (Geels et al., 2012), CHIMERE (Menut et al., 2021), and LOTOS-EUROS (Manders et al., 2017).

1

The CTM used in this study is LOTOS-EUROS, a state-of-the-art 3D model that simulates air pollution in the lower troposphere (Manders et al., 2017; Schaap et al., 2008a). The model is of intermediate complexity, which means that relevant processes are parameterized for modest computational demands, enabling hour-by-hour calculations over extended periods of several years within acceptable CPU time. The model has been used in a large number of other studies for the assessment of primary air pollutants and trace gases (e.g., secondary inorganic aerosol (Banzhaf et al., 2015), PM (Timmermans et al., 2022), and ammonia (van der Graaf et al., 2022)). The model projection is normal longitude-latitude, and the standard grid resolution is 0.125° longitude × 0.0625° latitude, approximately 7 × 7 km. In the vertical direction, the model consists of a static surface layer of 25 m, a dynamic layer extending from 25 m to the top of the mixing layer, and three dynamic reservoir layers, filling the vertical between the top of the mixing layer to 5 km altitude.

CTMs, including LOTOS-EUROS, use emission distribution inputs derived from emission inventories. Emission inventories provide gridded annual total emissions per category, but CTMs require a methodology to obtain hourly gridded emissions. CTMs usually use fixed time profiles to allocate gridded agricultural emissions into hourly resolution (Hutchings et al., 2001; Hendriks et al., 2016). They are relatively simple and static hourly, weekly, and monthly time profiles and do not account for the temporal and spatial variability in human activity and meteorology. There is sometimes a seasonal cycle in NH_3, which is dominantly caused by agriculture. The application of manure for agriculture, especially in the spring, as well as animal housing and manure storage in warm months, contributes to the peaks in ammonia emissions. It means that the NH_3 emission peaks at a specific location are highly correlated to the local agricultural activities and meteorology, which is not taken into account in most CTMs.

New improvements in time profiles have been introduced in recent years. Some were achieved using measurements, for example, manure transport data (Hendriks et al., 2016; Lonsdale et al., 2017). Skjøth et al. (2004) implemented a simplified model based on the dynamic parameterization in the Atmospheric Chemistry and Deposition model (ACDEP). They correlated temperature with emission functions for 15 agricultural subsectors for Denmark. The method takes into account physical processes like volatilization and agricultural production activities. Based on the work of Skjøth et al. (2004), Gyldenkærne et al. (2005) developed a parameterization of the temporal variation of ammonia emission, which describes emission from animal housing and manure storage, manure application, and emission from grown crops, which reflects the differences in farming practices and meteorological conditions. The parameterization was applied to northwestern Europe. The proposed parameterization is a considerable improvement compared to previous simpler models. However, the method also has flaws that lead to uncertainties and make it not easily applicable to regions outside northwestern Europe. They only distinguished

one generic spring crop type and one generic winter crop type to incorporate the impact of crops' different growing seasons on the temporal variability of ammonia emission. Besides the uncertainty from the generalization of various crops into two groups, the growing seasons of spring and winter crops differ from region to region, which is related to the local climate and topography.

In summary, given the shortcomings of the current ammonia emission estimates, one would have to improve the emission fractions, use more realistic time profiles and update activity input data accordingly. To achieve that, one needs to account for the factors that impact ammonia emission, both quantitively and temporally.

1.3 Research gaps for ammonia emission modeling

When it comes to ammonia emission (and deposition) modeling, it is essential to focus on agricultural sources, and then especially on livestock. Most agricultural emissions occur from livestock management (animal housing and manure storage), grazing, and manure and mineral fertilizer application to fields. A smaller and less significant amount of ammonia formed during mineralization may also be emitted. Ammonia emissions from some agricultural activities are short-term and spatially highly variable, such as those from manure and fertilizer application. In contrast, animal housing and manure storage represent a long-term, less variable emission source.

Depending on the emission sources, many factors influence the variability of agricultural NH_3 emissions (Battye et al., 2003; Dennis et al., 2010; Hutchings et al., 2012; Pinder et al., 2004, 2006). Agricultural NH_3 emissions are related to farm buildings, manure and fertilizer application, and grazing animals (Werner et al., 2015a). In summary, impact factors include:

- Livestock and animal house distributions (animal numbers and animal house locations affecting the spatial variation in N excretion) and type of animal houses and manure storage (affecting the spatial variation in NH_3 emission factors
- Arable crop and grassland distributions (affecting the amount and timing of manure and mineral fertilizer applied to fields)
- Manure characteristics (including total ammoniacal N (TAN) concentration, dry matter content, and pH)
- Manure application techniques and their timing
- Meteorological conditions (air temperature, wind speed, precipitation)

In order to make adequate predictions of ammonia concentration and deposition, the factors mentioned above should be appropriately accounted for in emission estimates.

Most factors are either not included or oversimplified in the current ammonia emission inventories, which inevitably leads to uncertainties. This section gives an overview of the relevance of the various factors and how they are included in current emission-deposition models with the related knowledge gaps.

1.3.1 Livestock and animal house distributions and type of animal housing and manure storage

Livestock and animal house distributions (animal numbers and housing locations) largely affect the spatial distribution of NH_3, as emission models usually calculate excretion by multiplying the number of animals with the N excretion rate per animal type. Velthof et al. (2015) reviewed that the N excretion rate of dairy cattle can be twice that of non-dairy cattle. While pigs and sheep have similar N excretion rates, the NH_3 volatilization loss of pig waste is three times higher than that of sheep due to manure characteristics (discussed in Section 1.3.3) (Bouwman, 1997). Therefore, knowing the exact numbers and types of animals in animal houses is important.

The type of animal housing and manure storage systems affects the ammonia emission fractions from the excreted manure. Animal feces mainly contain organic N that mineralizes very slowly to produce NH_3, suggesting that the NH_3 volatilization potential of fresh feces is relatively low in buildings (Bussink and Oenema, 1998; Arogo et al., 2002). The volatilization of NH_3 inside the animal housing and manure storage system is related to the NH_4^+ concentration, pH, and surface area of the slurry and to the temperature and ventilation in the housing system (Monteny, 2000). Consequently, the type of animal houses will affect the potential for ammonia emission.

There is a variety of housing categories in Europe, and emission from livestock housing is much affected by floor design, manure removal, cleaning, etc. (Sommer et al., 2019). Cattle are commonly housed in tie-stall barns, free-stall barns, and open feedlots. In practice, there are several different housing systems concerning the use of bedding and the storage of cattle excretions. Bussink and Oenema (1998) mentioned that NH_3 losses per housed cow increase in the order: cubicle houses < free stall with straw yard < open housing with solid or slatted floors. Pigs are commonly housed in either a deep-litter or slatted housing system. In a deep-litter system, bedding such as straw or sawdust is used to absorb and cover urine and feces. In a slatted housing facility, a slatted floor allows fecal and urine excretions to drop into a pit below the floor for removal. In a common poultry housing system, laying hens are kept in high-rise battery cage systems, where manure is collected either on a conveyor belt or dropped into a storage pit or pile below the cages. The excreted manure is often removed annually, resulting in long-term storage in the housing system and causing more NH_3 emissions (Arogo et al., 2002).

NH_3 emission from manure storage depends on storage type, type of waste, duration, and time of the waste storage (Rotz, 2004a; Hristov et al., 2011). During long-term storage for buildings with under-floor storage, organic N compounds are degraded anaerobically, increasing NH_4^+ concentration in the manure (Arogo et al., 2002). In contrast, covering slurry stores (e.g. with straw) significantly decreases NH_3 loss. A high frequency of manure scraping and removal from animal buildings can reduce gas emissions from the buildings (Starmans and van der Hoek, 2007; Nimmermark et al., 2009). Frequent manure removal from animal buildings should reduce indoor emissions by limiting the exposure of manure over time. In addition, external storage of manure at lower outdoor temperatures, compared to the usually higher indoor temperatures, further limits emissions since emissions increase along with temperature (Nimmermark and Gustafsson, 2005). The impact of meteorology on animal houses is presented in Section 1.3.5.

In short, detailed information on livestock and animal house distributions that differentiate animal type, manure type, and housing type is crucial for assessing high spatial resolution ammonia emissions. In countries with detailed housing information, models have been developed that include local information on animal numbers and housing systems (e.g., the INITIATOR model for the Netherlands (de Vries et al., 2023). However, in large-scale air quality models, the current practice is that averaged ammonia emission fractions are given for high-, intermediate-, and low-emission housing systems. Also, livestock distribution is usually resampled from corser data (at the provincial or municipal level). This reduces the quality of the predicted spatial distribution of ammonia emissions.

1.3.2 Arable crop and grassland distributions

Arable crop and grassland distributions (referred to as crop distribution for simplification) impact both the spatial and temporal distribution of ammonia emission since crops have different N demands (allocation of N excretion) and are fertilized in different times. Here, the spatial impact is discussed, and the temporal impact (timing of fertilization) is discussed in Section 1.3.4.

Crop type influences the amount of manure and fertilizer applied to fields. Even when manure is considered to have a high N fertilizer value, this may not translate into high crop yields unless the plant-available N is released from manure in synchrony with crop N demands (Crews and Peoples, 2005). When the N input from manure exceeds crop N demands, there is a risk of N loss to the environment (Qian and Schoenau, 2002; Whalen et al., 2019). The plant-available N losses increased exponentially when the manure application rates exceeded this limit. However, low application rates of manure may not sustain crop production, requiring the application of supplemental N sources (e.g., legume residues, inorganic N fertilizer) to support crop N needs. Models typically simulate the

most optimal scenario where nitrogen is applied at rates that meet agronomic nutrient requirements.

Current practice in the EU is generally using CORINE database as the crop distribution input for models (Sanz-Cobena et al., 2014; Morán et al., 2016; Skjøth and Geels, 2013). However, CORINE land use data has relatively low spatial resolution and is only updated every few years. Consequently, when calculating annual emissions, these emission models do not update crop information for each year. Moreover, the spatial resolution of the crop information is relatively coarse, illustrated by crop area in each grid or spatial unit, which makes it challenging to increase spatial resolution. Considering the impact of crop type on the amount of manure and fertilizer applied on fields and thereby on the spatial and temporal resolution of ammonia emission, detailed crop maps in air quality models are currently limited to include those impacts.

1.3.3 Manure characteristics

The volatilization of ammonia from any manure management operation can be highly variable depending on manure characteristics, including total ammoniacal N (TAN) concentration, dry matter content and pH. The difference in manure characteristics/ composition is related to the species and breed of farm animals, the housing system, and the diet composition (Nicholson et al., 2004; Hristov et al., 2011).

Regarding manure, if used without diluting, the TAN content of manure depends primarily on the N content of the feed intake and on the metabolic activity of the animal, which varies according to animal species, sex, breed, age, and the production system and climatic conditions. Ammonia emission from manure will depend on how much NH_3-N in the solution reacts to form ammonia versus ionized ammonium (NH_4^+), which is nonvolatile. The NH_4^+ concentration in the manure is decreased by diluting the manure with soil or water, resulting in less emission of NH_3. Besides, if there is more water content in the manure, the manure will percolate to the ground, resulting in less evaporation of NH_4^+. A high dry matter content decreases manure infiltration into the soil, which leads to more evaporation of NH_4^+ (Rotz, 2004b). Moreover, a high pH favors a higher concentration of ammonia and, thus, greater emissions. The pH of manures handled as solids can range from 7.5 to 8.5, which results in fairly rapid ammonia volatilization. Manure handled as liquids or semi-solids tends to have lower pH. However, there may be little difference in annual ammonia emissions between solid and liquid manure handling systems if liquid manure is stored over extended periods before land application.

Considering the impact of manure characteristics on ammonia emission, limited use is made of the information on those characteristics, combined with approaches to account for them on ammonia emissions in air quality models. There are undoubtedly

simplifications in the calculation of total N excretion. For example, emission fractions of manure application in inventories are typically given per manure type (animal, liquid/solid) at the country level based on local experiments and expert expertise. However, these numbers do not take into account the spatial variability in manure characteristics, which require more detailed (e.g., farm-level) data on the quality and composition of food fed to animals.

1.3.4 Technique and timing of manure and fertilizer application

Agricultural practices, including the technique and timing of manure and fertilizer application, depend on the crops grown, soil properties on the farm, the legislation, and weather conditions. The volatilization rate depends on the application technique.

Application technique has been known as a significant factor that affects ammonia loss from manure applied to fields. The application of animal manure to soil induces a sequence of reactions. The ammonia volatilization rate from broadcast manure is not linear with time but peaks during the first hours after spreading. Later on, the rate of NH_3 volatilization is very low after a few days (Huijsmans et al., 2001). Hence, incorporating manure into the soil is the most effective way of decreasing NH_3 volatilization. There are various application techniques, such as deep injection, shallow injection, incorporating manure by plowing or rotary harrow, and manure application with trailing hoses. Generally, the most significant reduction in NH_3 emission is obtained when the manure is immediately deeply incorporated (Webb et al., 2010). Therefore, considering the spatial variability of manure application technique can improve the spatial distribution of ammonia emission from manure application.

Mannheim et al. (1995) reported the following losses (N as % TAN) in experiments on cattle slurry applied to grassland/arable land: broadcast (grassland) 38 - 74%, shallow injection on grassland 7 - 23%, shallow injection on arable land 0 - 6%. NH_3 emission when slurry was applied by band spread, trailing shoe, and shallow injection techniques was reduced by 39%, 43%, and 57%, respectively, compared to the emission from the surface broadcast application (Smith et al., 2000). Burying manure with the mouldboard plow gave a 90% reduction compared to surface spreading. Huijsmans and Hol (1995) observed that the interval between spreading and incorporation affects the overall ammonia volatilization when manure is spread and incorporated on a farm field scale. Sommer and Hutchings (2001) found that incorporating pig slurry one hour after application would have reduced losses by 80%, whereas if incorporation were delayed until six hours after application, the reduction would only be 45%.

The timing of manure application varies from crop type to crop type. The optimum time for manure application is usually in spring and summer when crops take up nutrients. As

crop rotation regains its popularity due to its lower environmental impacts (Section 1.3.2), the temporal distribution of ammonia emissions from manure application becomes more variable between years. In addition, the timing of manure application is also affected by legislation and extreme weather. Most EU countries have a regulation prescribing a blocking period during which spreading manure is prohibited, affecting almost all composts and digestate products. Farmers and contractors also choose the implements that fulfill the weather and soil requirements. Excessive rainfall and wet soils result in unfavorable working conditions for farmers and vehicles and decreased trafficability, defined as a vehicle's capability to move across a field without causing undue damage to the crops or soil while effectively applying fertilizers.

In summary, having a good insight into the technique and timing of manure application, coupled with a refinement that accounts for legislation and extreme weather, is essential to the spatial and temporal distribution of NH_3 emissions from manure application. In countries with detailed information on those techniques, models have been developed that included differences in those practices (e.g., the INITIATOR model for the Netherlands (de Vries et al., 2023)). However, in large-scale air quality models, the current practice generally uses averaged ammonia emission fractions for high, intermediate, and low emission application techniques.

1.3.5 Meteorological impacts

Agricultural emissions are highly influenced by climate and weather (Skjøth and Geels, 2013). NH_3 emission from manure application varies primarily with temperature and air velocity during and shortly after fertilization (Sommer and Olesen, 1991). Temperature was found to be the most significant meteorological parameter after Robarge et al. (2002) examined the meteorological factors, including air temperature, relative humidity, and wind speed and direction. Gyldenkærne et al. (2005) found that the volatilization potential nearly doubles for every 5 °C increase in temperature and varies significantly through the day and season. Sutton et al. (2013) showed a factor of nine increase in emission rates between 5 °C and 25 °C, with additional effects from humidity and precipitation (Riddick et al., 2017). The observations by the experiments of Sommer et al. (1991) found that NH_3 emissions after six hours were exponentially related to temperature, but the correlation weakened with time after slurry application. Regarding wind, there is also a positive correlation with ammonia emissions. When surface applied, cattle slurry was found to emit more ammonia when wind speeds increased up to 2.5 m/s, but no consistent increase in ammonia volatilization was found when the wind speed increased from 2.5 to 4 m/s (Sommer et al., 1991). In addition to temperature and wind speed, precipitation plays a role in ammonia loss from manure application. Schjoerring and Mattsson (2001) demonstrated that a light shower in dry soil could accelerate the dissolution of the fertilizer granules and increase the NH_3 volatilization from the soil. However, heavy rain

will reduce the volatilization of NH_3 from the soil. Bouwmeester et al. (1985) reported that 20 mm of rain is sufficient to reduce NH_3 volatilization significantly.

Many climate-related factors have been identified to affect NH_3 emissions from animal buildings (Starmans and van der Hoek, 2007). When the temperature rises, so do NH_3 emissions from animal houses (Poteko et al., 2019; Sanchis et al., 2019; Hempel et al., 2016). Dairy cow buildings are usually naturally ventilated, implying that the outdoor climate can directly affect the indoor microclimate (Snell et al., 2003). For dairy housing with perforated or solid floors and housing systems with open lots, there is a correlation between outside temperature and NH_3 emissions and a significant effect of season on the NH_3 emissions (Bougouin et al., 2016).

It is clear that meteorological parameters, in terms of wind speed, temperature, and rainfall, strongly affect the spatial and temporal resolution of ammonia emissions from field-applied manure and animal houses. The uncertainties brought by meteorology in emission modeling are primarily a result of model simplification. Emission inventories usually use static emission fractions to derive the spatial distribution of ammonia emission without accounting for the impact of meteorology on the spatial variability of emission fractions. Nevertheless, limited use is currently made of detailed meteorological data sets combined with approaches to account for the impacts of these meteorological parameters on ammonia emissions in air quality models.

1.4 Research aims, approach and thesis outline

1.4.1 Research aims
The central aim of this thesis is to stepwise improve the quantification of the spatial-temporal variability in agricultural ammonia emissions in Western Europe by by accounting for variations in agricultural practices, livestock (housing) distributions, crop distributions, and meteorology. More specifically, it aims to answer the knowledge gaps mentioned in Section 1.3 related to limited information on the spatial variation in (i) livestock and animal house distributions, including animal numbers, animal house locations, and type of housing; ii) crop distribution, affecting the amount and timing of manure and mineral fertilizer applied to fields, (iii) meteorology, including temperature, wind speed and precipitation, and iv) agricultural practices, including application technique, incorporation, legislation, and extreme weather. These aspects are illustrated in the center of Figure 1-5, with a picture of a typical farm showing where the factors come from in an agricultural system.

1

What are the impacts of detailed crop and livestock distributions and emission fractions based on country-specific information? (Chapter 3)

What are the impacts of varying emission factors based on manure characteristics, meteorology and application techniques? (Chapter 5)

Meteorology

Crop distribution

Livestock and animal house distributions

Agricultural practices

Meteorology

Crop distribution

Livestock and animal house distributions

Agricultural practices

What are the impacts of different agricultural practices and their timing based on meteorology? (Chapter 2)

What are the impacts of detailed livestock housing information and remote sensed crop distributions? (Chapter 4)

Figure 1-5 A schematic overview of the thesis with research questions.

1.4.2 Research questions and approaches

To achieve the central aim of this thesis, remote sensing and ground-based observations, models, and statistics from national surveys are used to increase insight into the spatial variability and temporal dynamics of ammonia emissions with higher spatial and temporal resolution. The inherent spatial and temporal details of the variables are reflected in the derived emission distributions. The novel emission products are verified using ammonia total column data from IASI and CrIS observations as well as surface concentrations from in-situ measurements.

This Ph.D. aims to answer the following: What are the improvements in the ammonia emission distribution in space and time if we account for variations in meteorology, agricultural practices, crop distributions, and livestock and animal house distributions? It is divided into four research questions (also shown in Figure 1-5). Each research question is designed to answer a combination of the aspects, which will be answered in the corresponding chapter in the thesis. The research questions, which all relate to the spatial-temporal variability in ammonia emissions, are given below.

- **What are the impacts of different agricultural practices and their timing based on meteorology?**

Objective: Develop methodologies and parameterizations to detail agricultural emission distribution in time, taking into account temperature, rainfall, wind speed, land use, and legislative constraints.

The temporal variability of ammonia emissions is largely related to farming activities. This holds specifically for ammonia emissions from manure and fertilizer application, which depend on the fertilization time of different crops. Fertilization time can be influenced by crop type, manure and fertilizer type, and meteorology. In addition, legislative constraints of each country (blocking period) limit fertilization to a shorter period, and extreme weather impacts the trafficability for fertilization machinery. Moreover, animal housing types also contribute to different temporal allocations of ammonia emissions. I used a combination of INTEGRATOR and MACC-III and an adapted TIMELINES model to answer Research Question 1 in Chapter 2.

- **What are the impacts of detailed crop and livestock distributions and emission fractions based on country-specific information?**

Objective: Adapt the developed emission model locally for different EU countries by accounting for local activity data, land use, and geospatial data for better spatial details.

The standard INTEGRATOR model calculates ammonia emissions at the European scale, using reported input data at relatively low resolutions that are updated every few years. However, some countries update their statistics (e.g., animal and crop distributions) at higher resolution (e.g., at the farm or municipality level) and more frequently. In addition, local experiments have been performed to improve model parameters like emission fractions. Moreover, the geospatial vector used in INTEGRATOR is sometimes larger than the municipal boundaries. Therefore, the standard INTEGRATOR should be adapted locally with improved spatial resolution, more up-to-date crop and livestock distributions, and updated emission fractions based on local information. I used the Netherlands, Portugal, and Denmark as study cases to answer Research Question 2 in Chapter 3.

- **What are the impacts of detailed livestock housing information and remote sensed crop distributions?**

Objective: Derive high-resolution spatial and temporal allocation of ammonia emissions using a crop map obtained from Sentinel-2 and animal house locations.

In ammonia emission modeling, livestock houses should be regarded as point sources. Thus, their location data is essential for deriving accurate spatial details. In addition, crop distribution not only impacts the amount of manure and fertilizer needed due to the different N demands of crops, but also influences the temporal distribution of ammonia emissions because different crops are fertilized at different times. Unlike the Netherlands, many countries do not have available public data on crop distribution that is updated yearly. To obtain high-resolution crop maps for any country, crop classification can be conducted using machine learning of the multispectral multitemporal surface reflectance observations and calculated vegetation indices from Sentinel-2. The obtained crop map can then be used to update crop area information in INTEGRATOR. I used the Netherlands as a case study to answer Research Question 3 in Chapter 4.

- **What are the impacts of varying emission factors based on manure characteristics, meteorology, and application techniques?**

Objective: Create spatially explicit emission fractions to replace the constant country-dependent emission fractions after considering meteorology, manure characteristics, and application techniques.

The emission fractions used in emission inventories are usually country-dependent constants that only distinguish manure types (manure properties like dry matter and TAN concentration). However, emission fractions are affected by meteorology during fertilization (temperature, wind speed, and precipitation), and application techniques.

Since different crops are fertilized at different times, meteorological conditions during fertilization can contribute significantly to the spatial and inter-annual variability of emission fractions. I used the ALFAM2 model, which estimates emission fractions based on manure properties (dry matter, TAN, acidity), meteorology (temperature, wind speed, precipitation), application technique, and incorporation time to derive spatially explicit emission fractions of slurry application. Emission fractions of animal housing were updated using temperature-dependent scaling. The method was applied to Germany between 2014 and 2018 as a study case to answer Research Question 4 in Chapter 5.

1.4.3 Thesis outline

In Chapter 2, I explore how a more detailed categorization of ammonia emissions and spatially explicit time profiles of ammonia emissions from manure and fertilizer application and animal housing can improve NH_3 emission modeling, which is validated through the comparison with IASI and in situ measurements (Ge et al., 2020). In Chapter 3, I study how detailed information on livestock and crop distributions and emission fractions based on local information can improve regional emission estimates by locally adapting the standard EU-scale INTEGRATOR model to the Netherlands, Denmark, and Portugal. In Chapter 4, I present crop classification using multitemporal multispectral surface reflectance observations and calculated vegetation indices from Sentinel-2. The high-resolution crop map and detailed information on animal house locations are used to better estimate ammonia in space and time (Ge et al., 2023b). In Chapter 5, I create spatially explicit emission fractions of slurry application (using ALFAM2) and animal housing (using temperature-dependent scaling) by accounting for meteorology, manure properties, application technique, and incorporation time. The emission fractions are used to reproduce the inter-annual variability of ammonia emissions, concentrations, and total columns for Germany between 2015 and 2018 (Ge et al., 2023a). In Chapter 6, a synthesis is given, including the main results of the research questions formulated above, followed by a description of the remaining uncertainties brought by the model inputs, model methodologies, and measurements, as well as suggestions for further research directions.

CHAPTER 2

Modeling atmospheric ammonia using agricultural emissions with improved spatial variability and temporal dynamics

Ammonia emissions to the atmosphere have increased substantially in Europe since 1960, primarily due to the intensification of agriculture as illustrated by enhanced livestock and the use of fertilizers. These associated emissions of reactive nitrogen, particulate matter, and acid deposition have contributed to negative societal impacts on human health and terrestrial ecosystems. Due to the limited availability of reliable measurements, emission inventories are used to assess large-scale ammonia emissions from agriculture by creating gridded annual emission maps and emission time profiles globally and regionally. The modeled emissions are subsequently utilized in chemistry transport models to obtain ammonia concentrations and depositions. However, current emission inventories usually have relatively low spatial resolutions and coarse categorizations that do not distinguish between fertilization on various crops, grazing, animal housing, and manure storage in its spatial allocation. Furthermore, in assessing the seasonal variation of ammonia emissions, they do not consider local climatology and agricultural management, which limits the capability to reproduce observed spatial and seasonal variations in the ammonia concentrations.

This paper describes a novel ammonia emission model that quantifies agricultural emissions with improved spatial details and temporal dynamics in 2010 in Germany and Benelux. The spatial allocation was achieved by embedding the agricultural emission model Integrated Nitrogen Tool across Europe for Greenhouse gases and Ammonia Targeted to Operational Responses (INTEGRATOR) into the air pollution inventory Monitoring Atmospheric Composition and Climate -III (MACC-III), thus accounting for differentiation in ammonia emissions from manure and fertilizer application, grazing, animal houses and manure storage systems. The more detailed temporal distribution came from the integration of TIMELINES which provided predictions of the timing of key agricultural operations, including the day of fertilization across Europe. The emission maps and time profiles were imported into LOTOS-EUROS to obtain surface concentrations and total columns for validation. The comparison of surface concentration between modeled output and in situ measurements illustrated that the updated model had been improved significantly with respect to the temporal variation of ammonia emission, and its performance was more stable and robust. The comparison of total columns between remote sensing observations and model simulations showed that some spatial characteristics were smoothened. Also, there was an overestimation in Southern Germany and underestimation in Northern Germany. The results suggested that updating ammonia emission fractions and accounting for manure transport are the direction for further improvement, and detailed land use is needed to increase the spatial resolution of spatial allocation in ammonia emission modeling.

Abstract

2.1 Introduction

Ammonia (NH_3) emission to the atmosphere has risen substantially on a global scale during the twentieth century following the demand for food of a rapidly growing population (Erisman et al., 2008). Increases are especially large in areas with intense agricultural activities, such as Europe, the US, and China. The annual European Union emission inventory report 1990-2015 shows that even though NH_3 emission of EU-28 countries fell by 23% between 1990 and 2015, Germany, Spain, Sweden, and the EU as a whole exceeded their NH_3 emission ceilings in 2015 (EEA, 2017). The main source of NH_3 emission is agriculture, contributing to more than 90% of the total emissions in EU-28 (Monteny and Hartung, 2007). NH_3 from agriculture is emitted to the atmosphere during the application of manure and inorganic mineral fertilizers, as well as from animal houses and manure storage systems (Velthof et al., 2012). Meanwhile, emission from traffic and road transport occupies less than 2% (EEA, 2017). Additional minor sources include food processing, biomass burning, and fossil fuel combustion, making up about 4% of the NH_3 emissions (Galloway et al., 2003; Krupa, 2003; Erisman et al., 2008).

NH_3 concentrations are highly variable in space and time because of its short atmospheric residence time as it is effectively removed by dry and wet deposition several hours after emission (Fangmeier et al., 1994). In addition, NH_3 reacts with sulfuric (H_2SO_4) and nitric acid (HNO_3) in the atmosphere, leading to the transformation from NH_3 to fine ammonium salts (($NH_4)_2SO_4$, NH_4HSO_4, NH_4NO_3) (Schaap et al., 2004b). The ammonium salts account for a large fraction of particulate matter which has a longer lifetime in the atmosphere and is subject to long-range atmospheric transport (Fowler et al., 2009). Particulate matter has various negative societal impacts. It is a major contributor to smog and is associated with severely harmful effects on human health (Brunekreef and Holgate, 2002; Pope et al., 2009). Furthermore, it influences the scattering of sunlight and alters the properties of cloud condensation nuclei, which causes visibility impairment and disturbing the radiance balance of the Earth (Charlson et al., 1991; Erisman et al., 2007). After deposition, the nitrogen components can lead to the acidification and eutrophication of ecosystems, as well as the loss of biodiversity (Krupa, 2003; Vitousek et al., 2008; Bobbink et al., 2010).

Although NH_3 emissions contribute to a range of threats to the environment and human health, there are large uncertainties (more than 50%) in NH_3 budget and distribution regionally and globally (Erisman et al., 2007; Sutton et al., 2014). NH_3 emissions from agricultural activities are prone to considerable spatial and temporal variability (Battye et al., 2003; Sutton et al., 2003). Emissions from some activities are short-term and highly variable, such as manure and fertilizer application. In contrast, some other activities contribute to long-term and less variable emissions, such as animal housing and manure

storage. Many factors influence the variability of agricultural NH_3 emissions (Battye et al., 2003; Dennis et al., 2010; Hutchings et al., 2012; Pinder et al., 2004, 2006), including:

- Local agricultural practices
    - Type and amount of manure and inorganic fertilizer applied to land
    - Method of manure and fertilizer application
    - Animal type, housing type, manure storage type
- Meteorological conditions (air temperature, wind speed, humidity, precipitation)
- Soil conditions (soil temperature, texture)
- Regulation of agricultural practice

Several emission inventories have been developed to improve the spatial details of NH_3 emission in different countries. Hutchings et al. (2001) introduced a nitrogen flow approach to model annually averaged NH_3 emission for Denmark, taking into account animal types or different amount of fertilizers applied on various regions. In their study, NH_3 emissions are calculated as a percentage of the total N in manure, which means that the model will be valid as long as the chemical and physical characteristics of the manure remain the same. It also indicates that the model can be easily adapted as long as the only parameters that change are the number of animals or their distribution between the manure handling systems. Similar methodology has been adopted by Gac et al. (2007) in France, Webb and Misselbrook (2004) in the UK, and Hyde et al. (2003) in Ireland. In the air pollution model Monitoring Atmospheric Composition and Climate -III (MACC-III), emission factors and proxy maps are utilized to obtain the spatial distribution of annual emissions from emission totals officially reported by countries (Kuenen et al., 2014a; Velthof et al., 2012).

Subsequently, temporal distribution profiles are used to obtain temporally resolved emissions. Skjøth et al. (2004) implemented a simplified version of the dynamic parameterization in the Atmospheric Chemistry and Deposition model (ACDEP). They correlated temperature with emission functions for 15 agricultural subsectors for Denmark. The method takes into account physical processes like volatilization and agricultural production activities, such as the timing of fertilization. Based on the work of Skjøth et al. (2004), Gyldenkærne et al. (2005) improved the parameterization by including the effect of ventilation rates inside buildings, ambient wind speeds, and a more realistic description of temperatures inside animal houses.

Current emission inventories used in European chemistry transport models (CTMs) usually distinguish sectors defined by EMEP SNAP Level 1 Category which has a single sector for agriculture. They do not indicate crop types and fertilizer types that are important for interpreting the results and future applications such as policymaking. Furthermore, in

most European regional scale CTMs, such as LOTOS-EUROS (Hendriks et al., 2016; Schaap et al., 2008a), the accompanying time profiles that allocate gridded emission in time are mostly generated by simplified and static seasonal functions, without taking into account local climatology and agricultural practices. However, it is a challenge to improve this situation for European scale applications as NH_3 emission modeling requires detailed information on land use, number of different livestock, and the spatial distribution of farmhouses and storages (Skjøth et al., 2004; Gyldenkærne et al., 2005).

Given the above shortcomings, we developed a novel NH_3 emission model that quantifies agricultural emissions with better spatial details and gives insight into the temporal dynamics. Integrated Nitrogen Tool across Europe for Greenhouse gases and Ammonia Targeted to Operational Responses (INTEGRATOR) assesses greenhouse gases and nitrogen fluxes from agricultural sectors at high spatial resolution and accounts for differences in crop types, fertilizer types, animal housing, and manure storage (de Vries et al., 2011; Kros et al., 2018). The improvement of the spatial emission allocation was realized by embedding the INTEGRATOR model results in MACC-III. The more detailed temporal distribution came from the emission functions in the work of Gyldenkærne et al. (2005) and Skjøth et al. (2004) with the integration of the TIMELINES model. TIMELINES provides predictions of key agricultural operations' timing across Europe (Hutchings et al., 2012). These new emission products were then used in LOTOS-EUROS for validation by comparing modeled outputs with measurements. In this work, the improvements in NH_3 emission estimates were made for Germany and Benelux in the year of 2010 as a first test case.

In this paper, we first describe the methodology of 1) the new emission model which generates spatially and temporally resolved emission products; 2) the chemistry transport model LOTOS-EUROS that translates emission into concentrations and total columns; 3) data processing of the available measurements. Then we assess the model by comparing the simulated total columns and surface concentrations with remote sensing and ground-based observations, respectively. Finally, we evaluate the model performance in terms of improvements and shortcomings of the modeled results for this work's future perspectives.

2.2 Methodology and data

A schematic overview of the methodology and workflow is presented in Figure 2-1. The new emission model is composed of two parts, a spatial allocator which produces gridded maps of NH_3 annual emissions from various categories and a temporal allocator that disaggregates the annual emission within a grid cell over a year, creating emission distributions in space and time. The spatial allocator integrates the detailed agricultural emission information from INTEGRATOR into MACC-III. With the help of the agricultural management model TIMELINES, the temporal allocator characterizes the temporal variation as hourly time series according to land use, agricultural practice, and climate. The emission estimates were then imported into the CTM LOTOS-EUROS to derive NH_3 concentrations which were subsequently compared with Infrared Atmospheric Sounding Interferometer (IASI) observations on NH_3 total columns and in situ measurements of surface concentrations for verification. Normalized root mean square error (NRMSE), normalized mean absolute error (NMAE), model efficiency (EF), and index of agreement between modeled output and measurements were calculated to determine the performance of the models (see supplementary material Section S2.1).
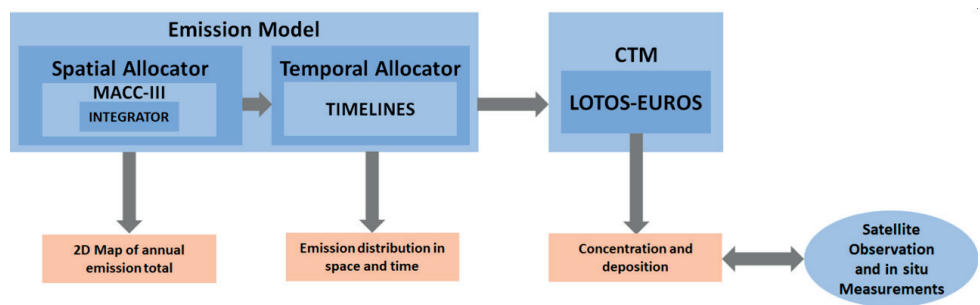
Figure 2-1 A simplified scheme of the workflow in this project, involving the development of spatial and temporal allocators of the emission model and the verification with measurement data.

2.2.1 Model parameters

In this study, the spatial domain of the area of interest was 2ºE–16ºE in longitude with a step of 0.125º and 47ºN–55ºN in latitude with a step of 0.0625º, which corresponds to a spatial resolution of approximately 7km × 7km. Two model runs were conducted to identify the influence brought by the new method. In the first simulation, the original MACC-III annual emission distribution and LOTOS-EUROS time profiles were used. The second model run utilized the improved spatial distribution and the dynamic time profiles obtained with

Modeling atmospheric ammonia using agricultural emissions with improved
spatial variability and temporal dynamics | **55**

2

the updated model. It has to be noted that a European scale run was conducted priorly to ensure the same boundary conditions for the two model runs.

2.2.2 Spatial allocator

2.2.2.1 Emission inventories

MACC-III is a spatially explicit emission inventory with a resolution of 0.125º × 0.0625º longitude-latitude (approximately 7km × 7km), providing Europe-wide annual emission inputs for NO_x, SO_2, NMVOC, CH_4, NH_3, CO, PM_{10} and $PM_{2.5}$ for air quality models (Kuenen et al., 2014a). The inventory is based on national emission total per sector officially reported by the countries themselves. In case emission data for a sector/country are unavailable for a particular year, estimates from GAINS are used to ensure that the emission inventory is complete and applicable for every country in Europe (Kuenen et al., 2011). Emission totals are spatially disaggregated across the countries as point or area sources, using point source locations and proxy maps (e.g., population density, traffic intensity), respectively (Kuenen et al., 2014a). MACC-III provides the spatial distribution of annual NH_3 emissions from agriculture and non-agricultural sectors including traffic and industry. However, due to the top-down nature of the inventory, it does not distinguish agricultural NH_3 emission sources between animal housing, manure storage, and fertilization on crop lands. Instead, it differentiates emissions by animal types, which includes the application and storage of certain animal manure, housing of this animal.

The aim is to improve the inventory towards a more detailed categorization to provide more in-depth information on the impact of various agricultural activities on emission. Besides, the inventory's information does not fulfill the TIMELINES model's requirements for temporal allocation. The disadvantages are the reason why we introduced the INTEGRATOR model in this study.

2.2.2.2 The INTEGRATOR model

The INTEGRATOR model is a static N cycling model and an adapted, more detailed version of the former MITERRA-Europe model (Velthof et al., 2009). It calculates land system budgets at EU-27 level, including N uptake, N emissions (in the forms of NH_3, N_2O, NO_x and N_2) from housing and manure storage systems, N accumulation in or release from the soil (due to manure and mineral fertilizer application) and N losses by leaching and runoff (de Vries et al., 2011). The emissions of NH_3 and other gases (N_2O, NO_x and N_2) to the atmosphere are estimated by multiplying N inputs with emission factors (de Vries et al., 2011). In this study, we focus on the modules of the model that estimate NH_3 emissions from animal housing, manure storage and manure/fertilizer application to arable land and grassland.

Unlike the MACC-III inventory, which provides emission distributions on longitude-latitude grids in the reference system World Geodetic System 1984 (WGS84), INTEGRATOR estimates emissions in NitroEurope Classification Units (NCUs). These NCUs are multi-part polygons composed of several 1 km × 1 km grid cells in ETRS89/LAEA Europe coordinate system. The polygons sharing one NCU number have the same administrative unit (Nomenclature of Territorial Units for Statistics (NUTS)), soil type (Soil Geographic Database (SGDB) classification), similar slopes (Catchment Characterisation and Modeling Digital Elevation Model (CCM DEM) 250 in five classes), and altitude (with differences less than 200m) (de Vries et al., 2011). Therefore, the area of one NCU varies from several square kilometers (mostly in Western and Southern Europe) to hundreds of square kilometers (in Northern Europe).

A schematic overview of the NH_3 emission module of the INTEGRATOR model is presented in Figure 2-2. The emission model starts with the calculation of N excretion by multiplying the number of animals at NCU level with N excretion rate per animal per country for eight animal categories (dairy cows, other cows, pigs, laying hens, other poultry, horses, sheep and goats, and fur animals) (Kros et al., 2012). The livestock data were obtained from the FAO database at country level, using Common Agricultural Policy Regionalised Impact analysis (CAPRI) data for distribution at NUTS 2 level. The data on livestock numbers of various animal categories at NUTS2 level were downscaled to a 1km × 1km resolution using expert-based judgment with spatial data sources on land use, slope, altitude, and soil characteristics influencing the livestock carrying (Neumann et al., 2009). A major distinction was made between grazing animals and other animals. Dairy cows, other cattle, and sheep and goats were assumed to be highly dependent on local land resources for grazing or feed production. Pigs and poultry were assumed to be held in more land independent systems. We refer to Neumann et al. (2009) for more detailed information on livestock's downscaling. The N excreted in housing systems is the multiplication of N manure excretion and the housing fraction (f_{hous}) in Figure 2-2), while the N excreted from grazing on land is obtained by subtracting N excreted in housing systems from total N manure excretion. The total manure production is derived by subtracting gaseous emissions and leaching in housing and manure storage systems from the N excretion, while the gaseous emission from housing is calculated by multiplying N excretion with the emission fraction per housing system ($f_{NH3em,hous}$). Ammonia emission fractions for housing and manure storage are distinguished per animal type and manure type. The emissions of ammonia from agricultural land are calculated by multiplying the N input by grazing, manure application and fertilizer application with ammonia emission fractions for grazing ($f_{NH3em,graz}$), manure application ($f_{NH3em,ma}$) and fertilizer application ($f_{NH3em,fe}$), respectively (Kros et al., 2012; De Vries et al., 2020b). The procedure to allocate manure over grassland and different crop groups is given in Section S2.2. Emission fractions for manure application ($f_{NH3em,ma}$) are distinguished for three animal types,

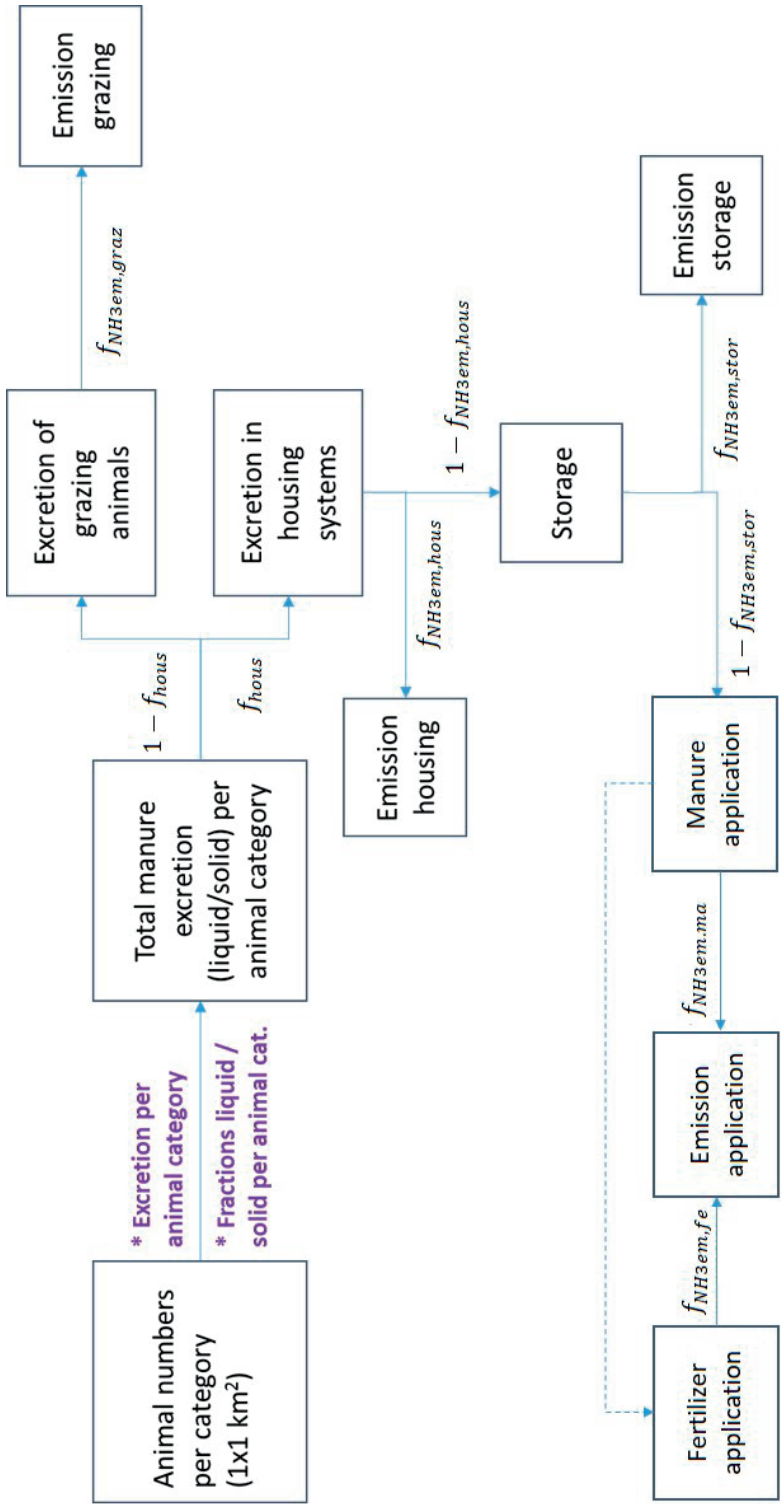**Figure 2-2 A schematic workflow of the NH_3 emission module in INTEGRATOR (de Vries et al., 2022). f_{hous} is the fraction of total manure excretion going to housing systems. $f_{NH3em,graz}$, $f_{NH3em,hous}$, $f_{NH3em,stor}$, $f_{NH3em,ma}$ and $f_{NH3em,fe}$ represent emission fractions of grazing, animal housing, manure storage, manure application, and fertilizer application, respectively.**

i.e., cattle (including dairy cows, other cows, sheep and goats, horses and fur animals), pigs and poultry (laying hens, other poultry) and manure type (liquid vs. solid for cattle and pigs) (De Vries et al., 2020b). Emission fractions for fertilizer application ($f_{NH3em,fe}$) are differentiated between urea-based fertilizers and nitrate-based fertilizers. Details on the various fractions are given in De Vries et al. (2020).

Finally, NH_3 emissions in each NCU are available for fertilization on 32 croplands (31 CAPRI arable crop types and grassland) with 5 types of manure (poultry, cattle liquid/solid, pig liquid/solid) and mineral fertilizer, as well as for grazing, housing of three animal types and manure storage of 5 manure types, in total 201 categories.

2.2.2.3 The MACC-INTEGRATOR combined inventory
We replaced the agricultural emissions in the original MACC-III inventory with the INTEGRATOR emissions, which significantly increases the level of details. For simplification, the 31 CAPRI crop types in INTEGRATOR were aggregated into cereals, root crops, industrial crops, vegetables, grass and fodder using the Indicative Crop Classification (ICC). Consequently, there were 36 categories regarding emissions from fertilization on croplands. Grazing, animal housing, and manure storage were kept as they were, resulting in 45 categories in total in the combined emission inventory (see Figure S2.1 in the supplementary material Section S2.3).

Since the two inventories use different coordinate systems, coordinate transformation was performed to resample INTEGRATOR emissions onto the grid utilized in MACC-III. The resampling was conducted by 1) averaging the emission in one NCU evenly over the whole polygon; 2) dividing each square kilometer grid cell into 25 subpixels and calculating the coordinate of the center of each subpixel in latitude/longitude; 3) locating the calculated coordinate of each subpixel of NCU in MACC-III grid and assigning emission to the corresponding MACC-III grid.

It has to be pointed out that the NH_3 emission estimates from INTEGRATOR differ from the officially reported national emission totals used in the MACC-III inventory. This is because each country uses its own emission inventory methodology, whereas INTEGRATOR uses a uniform method for all countries. To assess the impact of the different spatial (and temporal) allocation and be in line with officially reported emissions, we scaled the NH_3 emissions from INTEGRATOR with the country totals of 2010 officially reported in 2018. The scalar is computed per country per animal type, namely the division of INTEGRATOR emission and officially reported emission to EMEP.

2.2.3 Temporal allocator

The usual approach to characterizing the temporal variability in NH_3 emissions is to use time profiles that distribute the annual emission total in a grid cell over a year. Fixed and oversimplified temporal profiles (monthly, daily, or hourly resolved) are often used (Van Pul et al., 2009). In this section, we explicitly described the temporal allocation of NH_3 emissions from manure and fertilizer application based on the concepts of Skjøth et al. (2004), Gyldenkærne et al. (2005), and Hutchings et al. (2012). The temporal distribution functions of ammonia emission from grazing, animal housing and manure storage were taken from Gyldenkærne et al. (2005), which are presented in Section S2.4.

The temporal distribution of NH_3 emission from fertilization is dependent on the timing of manure and fertilizer application on arable lands and grassland, weather conditions, as well as legislative constraints. We first followed the methodology as outlined by Gyldenkærne et al. (2005) to characterize the temporal variation of the emission strength as a function of time, temperature, and wind speed. The emission function used may be described as Eq. (2.1):

$$E_{i,j,k}(t,T,W) = \epsilon_{i,j,k} e^{0.0223T(t)} e^{0.0419W(t)} \frac{1}{\sigma\sqrt{2\pi}} e^{\left(\frac{(t-\mu)^2}{-2\sigma^2}\right)} \tag{2.1}$$

where $E_{i,j,k}$ is the emission strength after application of fertilizer k on crop j in NCU i, $\epsilon_{i,j,k}$ is the annual total emission (kg/ha), T(t) and W(t) are the air temperature (Celsius) and wind speed (m/s) for the applied time step (t), μ is the day with peak emissions, and σ is the standard deviation to represent spread and uncertainty in the application activities and emission timing.

2.2.3.1 The improvement of fertilization day

The first challenge was to update the estimated central day μ (the day with peak emissions) for manure and fertilizer applications. The timing of these field operations was obtained by the TIMELINES model's methodology that was developed to assess the timing of field operations, including the Julian day of fertilization on a wide range of crops (Hutchings et al., 2012). It was calculated at the 50 km $\times$ 50 km MARS meteorological grid level in Europe (Goot, 1998). Hutchings et al. (2012) took the weather conditions over a year into account when simulating crop calendars by introducing a thermal time approach. Thermal time is the sum of the positive differences between daily mean air temperature and a base temperature and is written as Eq. (2.2):

$$\tau_t = \sum_{k=t_0}^{t} \max\left((\theta_k - \theta_b), 0\right) \tag{2.2}$$

where τ_t is the thermal time (in Celsius) over time t (day), θ_k is the daily mean air temperature at 2 meters, θ_b is the base temperature (0 degree Celsius), τ_0 is the starting

time of calculation 1 January. As soon as thermal time on Julian day t reaches the reference thermal time for sowing (or harvesting), it is considered that sowing (or harvesting) occurs on this day. All other field operations, including plowing and manure and mineral fertilizer applications, are related to it.

We back-calculated the reference thermal times $\tau_{ref,sow(harv)}$ for various crops based on the sowing and harvesting dates provided by Hutchings et al. (2012). ECMWF meteorological data for the years between 1985 and 1995 and the respective days $t_{sow(harv)}$ were inserted into Eq. (2.3):

$$\tau_{ref,sow(harv)} = \sum_{k=t_0}^{t_{sow(harv)}} \max\left((\theta_k - \theta_b), 0\right) \tag{2.3}$$

The period between 1985 and 1995 was selected as Hutchings et al. (2012) followed a similar proceeding based on the Crop Growth Monitoring System (CGMS) dataset and used obtained reference thermal times to calculate sowing and harvesting days for 1995 onwards. The sowing and harvesting dates derived in this paper are in good alignment with the work of Hutchings et al. (2012), as shown in Figure S2.2 in Section S2.5. The sowing day estimates of winter wheat and spring wheat in 2010 are shown in Figure S2.3 in Section S2.6. The timing of manure application is based on sowing dates and varies from one manure type to another. Mineral fertilizer is applied in two applications, with the first application (20% of the annual amount) conducted five days prior to sowing for spring crops and at the start of the growing season for winter crops. The second application is made after 20% of the growing season has elapsed (Hutchings et al., 2012).

We assumed that the peak of emission after application occurs at noon on the second day after the estimated central fertilization day. This is based on field experiments that show the emission from mineral fertilizers has its maximum in the first days after application (Loubet et al., 2009; Schjoerring and Mattsson, 2001; Whitehead and Raistrick, 1993). Søgaard et al. (2002) observed that half of the NH_3 emission takes place within the first 30 hours. Plöchl (2001) looked into 227 experimental trials and found that 80% of the emission was reached within two days. However, in some cases (e.g., urea applied in dry conditions resulting in slow hydrolysis), fertilizer emission may proceed for over a month after application, which is unlikely in our study area (Sutton et al., 1995). We assumed that the peak of emission after application occurs at noon on the second day after the estimated central fertilization day.

Even though the TIMELINES model indicates a single day of fertilization in an NCU, in practice, farmers certainly would not operate precisely at the same time. The central estimate of fertilization day is uncertain due to other influencing parameters such as soil conditions and the availability of machinery and labor. Also, Gyldenkærne et al. (2005)

argued that there would still be variation in the timing of fertilization because it would take time for farmers to complete these operations. As a consequence, normal distribution around the central estimate was used here to characterize it.

The standard deviation around the central value is given in a fixed number of days, since it is determined by farmers' agricultural practice (independent of the thermal sum approach) and includes a random uncertainty. Gyldenkærne et al. (2005) assumed there are four times of manure application in a year: early spring, late spring, spring-summer, summer-autumn. The standard deviation of the spring-summer application is 16 days, while that of the remaining applications was nine days. The standard deviation of the timing of the mineral fertilization applications in early spring and summer were 9 and 16 days, respectively. We made a similar assumption in this paper: for fertilizations that lie between mid-May and mid-August, the standard deviation of the corresponding emission function is 16 days. For the remainder, the standard deviation is considered to be nine days.

2.2.3.2 The inclusion of legislative conditions

The next step is to implement legislative constraints on manure and fertilizer application. In Germany, manure application is not allowed from 1 November to 31 January on arable land and from 15 November to 31 January on grassland (Kuhn, 2017). In Flanders of Belgium, manure spreading is not allowed in the winter period from 15 October till 15 February (Uitrijregeling volgens type meststof). We expanded this period to Belgium and Luxemburg due to a lack of knowledge in these regions. As for the Netherlands, solid manure is prohibited from 1 September to 31 January, while other manures are banned between 16 September and 15 February on arable land and between 1 September and 15 February on grassland. Mineral fertilizer is prohibited from 16 September to 31 January on both grassland and arable land (Wanneer mest uitrijden). Furthermore, Vlaamse Landmaatschappij (2016a) pointed out that it is not allowed to fertilize on Sundays, nor when the soil is frozen or covered by snow in Flanders. Usually, frozen soil and snow cover appear outside permitted dates. The ban on fertilization outside permitted dates and on Sundays is the most significant constraint and was applied to all regions in the area of interest by setting the emission strength to zero in Eq. (2.1).

2.2.3.3 The impact of excessive precipitation

The occurrence of excessive precipitation was also accounted for since the soil can become water-saturated, negatively impacting the infiltration rate of liquid manures and the risk of strongly enhanced surface runoff. Furthermore, trafficking the wet soil surface with heavy machinery is likely impossible. We used the weekly De Martonne-Index to capture the characteristics related to precipitation or soil water content. The index describes the ratio between precipitation sums and average 2-meter temperature (Croitoru et al., 2012).

Here, the index is computed on a weekly basis to represent more real-time humidity. For weekly values, it is written as Eq. (2.4):

$$I_W = \frac{52.143 P_W}{T_W + C} \qquad\qquad (2.4)$$

where P_w is weekly total precipitation in millimeter, T_w is weekly mean temperature in Celsius, and C is a constant (10) that assures that negative mean temperatures do not result in negative indices. The introduction of temperature parameterizes the impact that higher temperatures will lead to faster evaporation and more effective infiltration. Baltas (2007) defined that when the annual De Martonne-Index exceeds 55 (namely 55/52.143≈1.055 in the weekly index), the air is considered extremely humid. One example of the weekly De Martonne-Index time series is given in Figure S2.4 in Section S2.7. Kranenburg et al. (2016) used visual inspection to set up a threshold of 1.7, above which precipitation and soil water content are not suitable for fertilization, and farmers will have to postpone application. Therefore, whichever day the threshold is violated, ammonia emission is set to zero, and the remaining part of the function is moved forward by a day.

2.2.3.4 The finalization of the emission time profile

Moreover, a baseline in the time profile was introduced. Due to some application techniques, especially injection, manure and fertilizer stay underneath the soil for a much more extended period before ventilation. Thus, 5% of annual emission is allocated throughout the year as a baseline to represent background emission. Since the emission time profile needed by LOTOS-EUROS has an hourly temporal resolution and a mean of 1, the temporal distribution of emission strength for fertilization was normalized to derive the final emission time profiles. Compared with the original time profiles used in LOTOS-EUROS, the newly developed ones are spatially and dynamically explicit based on land type, amounts of emission and local climatology. Examples of NH_3 emission time profiles during construction at location (47.41º, 10.98º) in latitude/longitude in 2010 are presented in Figure S2.5 Section S2.8.

2.2.4 The LOTOS-EUROS model

The annual emission distribution and gridded hourly time profile were then imported into LOTOS-EUROS to obtain modeled surface concentrations and total columns. They were compared with satellite observations and in situ measurements for model evaluation. LOTOS-EUROS is a 3-dimensional regional CTM that uses a description of the bidirectional surface-atmosphere exchange of NH_3 (Wichink Kruit et al., 2010; Manders et al., 2017). In the previous studies, the model showed a good agreement with yearly averaged NH_3 measured concentrations, except that there is slight underestimation in agricultural source areas and slight overestimation in nature areas (Wichink Kruit et al., 2012). The version of LOTOS-EUROS in this study includes the labeling module by Kranenburg et al.

(2016), which tracks the contribution of emission sources from specific categories to the final simulated products. The categories that we wanted to label, namely all agricultural sectors, were defined accordingly before the model runs. As a result, besides the regular outputs, the fractional contribution of each labeled category was also calculated.

2.2.5 Available measurements

Among the outputs of LOTOS-EUROS, surface concentration and 3-d concentration were compared with in situ measurement and satellite observations for verification. Both in situ and satellite observations have their advantages and disadvantages. Since the transport of NH_3 in the atmosphere and the reaction with other atmospheric components are rapid, its emission and deposition dynamics affect concentrations on the scale of hours to days. Ground-based stations measure NH_3 surface concentration consistently at fixed locations, and some of them have relatively high temporal resolutions (hourly or daily), which offers the possibility to study the behavior of NH_3 emission. However, the measurements lack vertical information as most instruments only measure surface concentrations (Van Damme et al., 2015; Erisman et al., 2007). Horizontally, the setup of station networks is coarse. Representativeness is an issue since all monitoring sites' measurements will be influenced by local and regional agricultural activities and other local sources. Consequently, we need to carefully consider the stations' locations when comparing in situ measurements with simulated results. Airborne measurements have been carried out, but only occasionally with limited spatial coverage during campaigns (Dammers et al., 2016; Leen et al., 2013; Nowak et al., 2010). Satellite observations have the advantage of global coverage and the possibility of calculating area-averaged observations, which are in much better correspondence with the size of the grid cells in regional/global models (Flechard et al., 2013). Recently, remote sensing products with a higher spatial and temporal resolution have become available for better NH_3 concentration monitoring in the lower troposphere (Clarisse et al., 2009; Van Damme et al., 2015).

2.2.5.1 In situ measurements

The Umweltbundesamt (UBA) research foundation sets up monitoring stations, providing governments and the public with information on air pollutants (Schleyer et al., 2013). It measures species, including NH_3, that are essential for the improvement of knowledge about air quality and climate change. The UBA also collects the data from the network of the German federal states. In addition to the German networks, the Measuring Ammonia in Nature (MAN) network monitors monthly mean values of NH_3 concentrations in Natura2000 areas in the Netherlands to detect the spatial pattern in concentration or to assess the influence of local sources (agriculture activities but also traffic) (https://man.rivm.nl/) (Lolkema et al., 2015; Noordijk et al., 2020). The network aims to be representative of different habitat types, NH_3 concentration levels, area size and shape, as well as the geographical distribution (Lolkema et al., 2015). When illustrating the comparison

of concentrations time series, we selected several stations that are not close to local agricultural sources (as shown in Table S2.1 in Section S2.9) so that the local influences on measurements could be minimized. Besides, by comparing all individual measurements at all available stations, the overall performance of the updated model can be determined.

2.2.5.2 Satellite observation

Infrared Atmospheric Sounding Interferometer (IASI) is a Fourier transform infrared (FTIR) spectrometer that measures the thermal infrared (TIR) radiation emitted by the Earth's surface and the atmosphere. It circles in a polar Sun-synchronous orbit and operates in nadir mode. It has a wide swath width of 2 x 1100 km, which corresponds to 2x15 mirror positions, while the spatial resolution is 50 km x 50 km, composed of 2 x 2 circular pixels. Each circular pixel is a 12 km diameter footprint on the ground at nadir (Clerbaux et al., 2009).

Van Damme et al. (2014) presented an improved NH_3 retrieval scheme for IASI spectra, which relies on the calculation of a dimensionless Hyperspectral Range Index (HRI). Whitburn et al. (2016) continued with HRI and introduced a neural-network-based algorithm to obtain NH_3 total columns. Van Damme et al. (2017) made some improvements by training separate neural networks for land and sea observations, enhancing thermal contrast, and introducing a bias correction over land and sea and the treatment of satellite zenith angle, which resulted in the latest product Artificial Neural Network for IASI ANNI-NH3-v2.1. As is pointed out by Van Damme et al. (2017), weighted averaging is no longer recommended in ANNI-NH3-v2.1, arithmetic mean or median is suggested if averaging has to be performed.

Regardless of the improvement of NH_3 column retrieval from satellite observations, there is still substantial variability in measurement uncertainty, varying from 5% to over 1000 % (Van Damme et al., 2017). Measurements with small magnitude tend to have larger relative uncertainties. Due to considerable uncertainties and the requirement of clear-sky conditions, IASI data is insufficient for real-time monitoring but sufficient if used to calculate monthly or yearly average distributions. In this study, the annual mean was compared with LOTOS-EUROS output for verification. The monthly mean was calculated to investigate the feasibility of being used for validation of temporal variability. For each IASI observations, the modeled results that are closest in space and time were selected.

In this paper, we used ANNI-NH3-v2.2R-I IASI dataset which was obtained with ECMWF ERA-Interim meteorological data and surface temperature data retrieved from a dedicated network. After the dataset was downloaded from the AERIS portal (https://iasi.aeris-data.fr/NH3R-I_IASI_A_data/), we only selected satellite observations with daytime overpass because daytime is the better time to measure NH_3 Van Damme et al., 2017).

Area-weighted annual mean was derived by resampling the circular footprints of IASI onto the grid used in LOTOS-EUROS. Area averaging was also applied to the calculation of the mean relative error of each grid cell. Finally, post-filtering was carried out to obtain more reliable distributions: all grid cells with less than ten measurements were rejected.

2.3 Results

2.3.1 Comparison between MACC-III and MACC-INTEGRATOR annual emission

Because of the less detailed EMEP SNAP Level 1 categorization in the MACC-III inventory, comparisons were made at country level for cattle, pig, poultry related emissions (the sum of housing, manure storage, and application), as well as mineral fertilizer emissions. Table 2-1 shows that country emission totals from the updated inventory MACC-INTEGRATOR are all larger than those from the original MACC-III inventory because it uses a different version of reported emission totals. Germany witnesses the largest positive difference in absolute value, while Luxemburg shows the most significant relative change. Compared to MACC-III, MACC-INTEGRATOR estimates more emissions from cattle and mineral fertilizer in all countries except for the Netherlands. Pig emissions in Germany and the Netherlands rise by 24.7% and 36.4%, respectively, while that in Belgium slightly decreases. Poultry emission drops by more than 20% in Germany, whereas the amount increases in other countries. It implies that the scaling we applied per country based on animal types and mineral fertilizer plays an essential role. For example, INTEGRATOR estimates less agricultural emission in Germany than MACC-III, but after scaling, the combined inventory reveals the opposite trend, indicating 14% more emission in Germany than MACC-III.

Table 2-1 *NH$_3$* emission country totals (Gg/yr) for all agricultural categories and cattle, pig, poultry, and mineral fertilizer in 2010.

	Germany		Netherlands		Belgium		Luxemburg	
	Original	Updated	Original	Updated	Original	Updated	Original	Updated
Cattle	290.02	333.22	59.36	53.60	29.48	30.02	3.30	4.49
Pig	105.86	131.96	23.57	32.15	22.34	21.73	0.52	0.41
Poultry	46.62	37.11	14.11	19.58	4.41	5.30	0.04	0.08
Fertilizer	69.48	82.60	9.62	9.69	7.25	8.70	0.39	0.77
Total	513.05	584.89 (+14%)	106.70	115.03 (+7.8%)	63.97	65.76 (+2.8%)	4.26	5.72 (34.3%)

The spatial distributions of NH_3 emissions from the two inventories are presented in Figure 2-3(a) and Figure 2-3(b) are the maps of annual total agricultural emissions. In Germany, the new spatial allocator assigns more emissions in the southeast near the border with Austria. The two hot spots in Bremen and Ruhr in the original inventory merge into one located in the Ostwestfalen-Lippe region. In Schleswig-Holstein in Northern Germany, the original model indicates that most of the emissions are located in the state's center. Meanwhile, the updated one tells emissions are situated along the eastern coastline in the state. In the southeast of the Netherlands, the updated inventory allocates more emissions and smoothens the spatial details into larger blocks. After looking into NCU polygons, we found out the sizes of polygons at this location are much larger than the others. Because we evenly allocated emission within an NCU polygon over the polygon, it is possible to lose spatial characteristics, especially when a polygon has a larger size. Figure 2-3(c) and Figure 2-3(d) show that cattle emission remains a similar pattern in the updated inventory, except that it is generally lower in Northwestern Germany and the Netherlands. The hot spots in Overijssel and Gelderland in the east of the Netherlands disappear. On the contrary, there is a much higher level of cattle emission in Southern Germany bordering Switzerland and Austria. Figure 2-3(e) and Figure 2-3(f) illustrate that in the updated inventory, pig emission increases in the southeast of the Netherlands and is more spread out in Nordrhein-Westfalen and Niedersachsen of Germany. Figure 2-3(g) and Figure 2-3(h) demonstrate that the updated poultry emission estimate is higher in the southeast of the Netherlands, while it is lower in Niedersachsen of Germany, but to a lesser extent. It can be seen from Figure 2-3(i) and Figure 2-3(j) that emission from mineral fertilizer application only occupies a small portion of the annual totals. The patterns are quite similar, except that the emission from MACC-III sometimes shows higher values at country borders, which is not seen in MACC-INTEGRATOR. This is because they use different allocation methods: the original inventory uses proxy maps, while the updated one utilizes a balanced N fertilization approach at NCU level.

(a) Total NH_3 emission map in 2010 (original)

(b) Total NH_3 emission map in 2010 (updated)

(c) Cattle NH_3 emission map in 2010 (original)

(d) Cattle NH_3 emission map in 2010 (updated)

(e) Pig NH_3 emission map in 2010 (original)

(f) Pig NH_3 emission map in 2010 (updated)

(g) Poultry NH_3 emission map in 2010 (original)

(h) Poultry NH_3 emission map in 2010 (updated)

(i) Mineral fertilizer NH_3 emission map in 2010 (original)

(j) Mineral fertilizer NH_3 emission map in 2010 (updated)

Figure 2-3 Maps of annual emission total (Gg/yr) for all agricultural categories and cattle, pig, poultry, and mineral fertilizer in 2010. The left panel indicates the original MACC-III inventory results, while the right panel represents the output of the updated inventory. (a, b) emission from all agricultural sectors; (c, d) emission from cattle; (e, f) emission from pig; (g, h) emission from poultry; (i, j) emission from mineral fertilizer.

2.3.2 Observed and modeled NH_3 total columns

After filtering IASI measurements, the number of valid daytime overpass measurements in each month is illustrated in Figure S2.6(a) in Section S2.10. The month in which the most valid observations (more than 7500) occurred is April, followed by July and June in which there were nearly 6100 and 5600 measurements, respectively. The measurements in these three months occupy more than half of the daytime measurements in the whole year. Figure S2.6(b) shows the spatial distribution of measurement counts over the area of interest. NH_3 is measured most frequently in Western Germany, Southern Germany bordering Austria, the Netherlands, Belgium and Northern France. The influence of satellite footprint on the availability of data leads to the strips which are more visible in Germany and France.

The spatial characteristics of area-averaged relative error are shown in Figure 2-4(a). The regions with fewer measurements tend to have a higher relative error, while low errors (less than 80%) appear in the Netherlands, Belgium, and Western Germany, where many observations are available. Figure 2-4(b) represents annual area-averaged NH_3 total columns after post-filtering which excludes gird cells that have less than ten measurements. One can see that NH_3 level is considerably high in the Netherlands, Belgium, and Western Germany.

The modeled annual averaged total columns from LOTOS-EUROS simulations are shown in Figure 2-5. Overall, the updated result (Figure 2-5(b)) obtained with the updated annual emission distribution and time profiles gives a higher magnitude of NH_3 columns than the original one (Figure 2-5(a)). Large relative differences that are more than 100% occur mostly over Germany and the Eastern Netherlands. The hot spots in the Eastern Netherlands, Nordrhein-Westfalen, and Niedersachsen in the original simulations expand prominently to a much more extensive domain in the new simulation. Moreover, new hot spots are witnessed in other regions in Germany, such as Bayern and Baden-Württemberg, close to Austria and Switzerland's border.
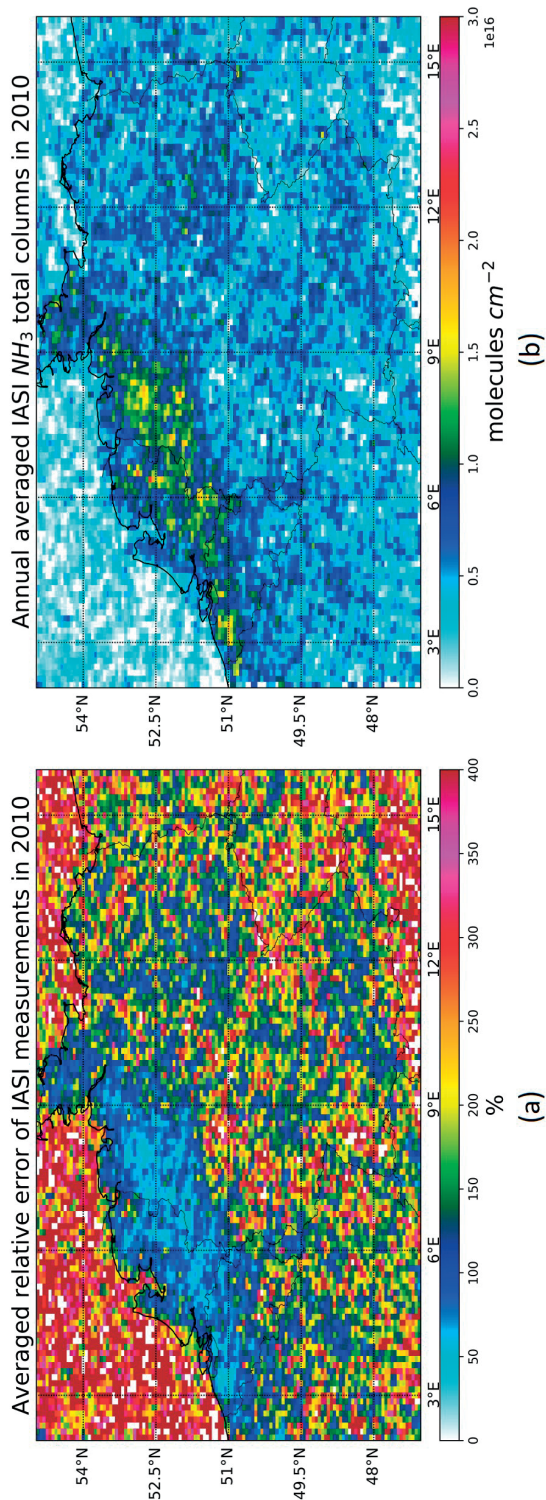
Figure 2-4 The map of area-averaged relative error of IASI daytime measurements in 2010 (a). The map of area-averaged total columns after filtering out grid cells with less than ten valid measurements and an averaged relative error larger than 75% (b).
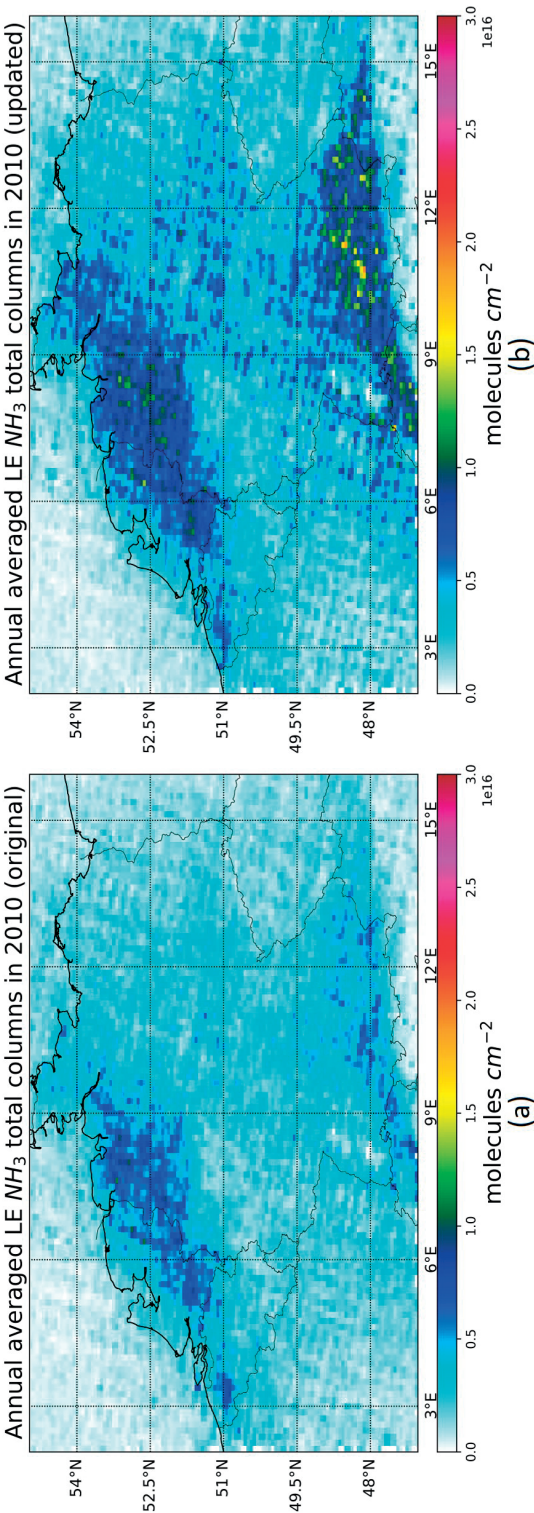
2

Figure 2-5 Simulated annual averaged total columns from LOTOS-EUROS using the original MACC-III annual emission distribution and static time profile (a) and using MACC-INTEGRATOR emission totals and updated time profiles (b).

Figure 2-6 shows scatter plots comparing IASI observations and LOTOS-EUROS estimates, with the left and right panel comparing the measurements with the original modeled result and the updated output, respectively. Figure 2-6(a) and Figure 2-6(b) include all grid cells in Germany and Benelux. The simulated total columns from the original model are mostly underestimated. Meanwhile, there exist both overestimation and underestimation in the updated output. Two clusters appear in Figure 2-6(b), with one lying on the upper side of y=x and the other lying on the lower side. For a more straightforward illustration, comparisons were made in Figure 2-6(c) and Figure 2-6(d) for grid cells at lower latitudes (smaller than 49°N) in Germany. The former shows underestimation in the south in the original model, while the latter indicates a considerable overestimation in the updated model. Moreover, Figure 2-6(e) and Figure 2-6(f) focus on the rest of the grid cells at higher latitudes and tell that both models underestimate ammonia at these locations. Weighted linear regression was performed, with weight being inversely proportional to the square of the averaged relative error. The outcomes obtained by the new model have been improved, but both performed relatively poorly.

The performances of the original and updated model comparing with IASI observations were investigated for all grid cells within Germany and Benelux, as well as separately in each country (Table 2-2). Every indicator has improved for the new modeled results. Both NRMSE and NMAE have dropped, with the largest deductions from Luxemburg. Regarding model efficiency, even though the new modeled output gives values closer to one, they are still negative. In addition, the index of agreement witnessed the largest increase in Germany and the Netherlands.

The feasibility of verifying emission estimates by comparing weekly or monthly time series derived from IASI measurements and simulations was also investigated. However, the majority of valid data are in April, June, and July (Figure S2.6(a) in Section S2.10). The number of valid measurements per month is insufficient for most grid cells to obtain reliable continuous time series. Consequently, two alternatives could be considered to resolve this issue. First, multiple years averaging is required for a better trend analysis within a year. It is also possible to look at a longer time frame with coarser temporal resolution.
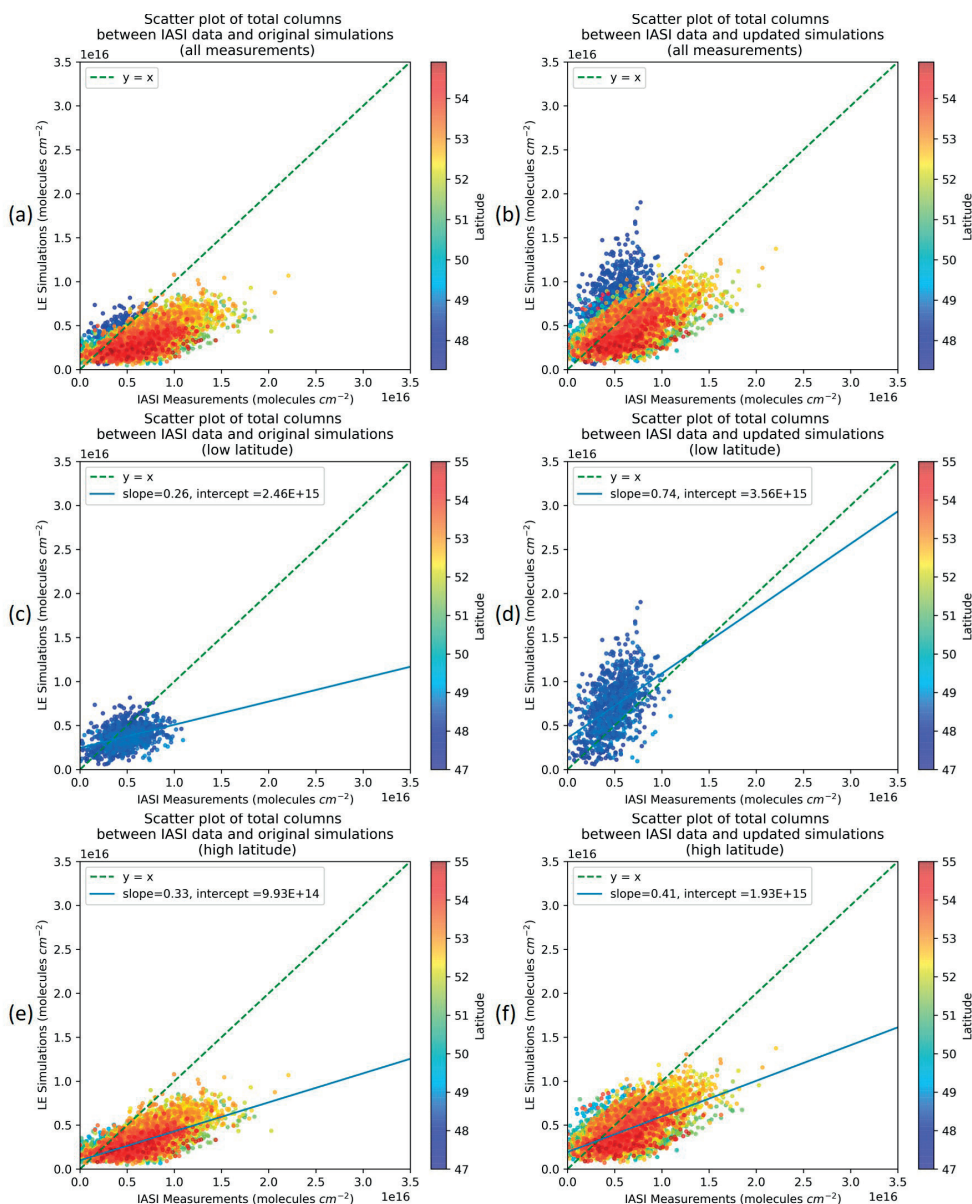
Figure 2-6 Scatter plots comparing NH_3 annual averaged total column from IASI measurements and LOTOS-EUROS. The color of the points indicates latitude. The left panels and right panels use original and updated modeled results, respectively. (a) and (b) include all valid grid cells. (c) and (d) show grid cell with lower latitude (< 49°N) while (e) and (f) focus on points with latitudes larger than 49°N.

Table 2-2 Performance assessment of the original and the updated model by comparing annual averaged total columns. NRMSE, NMAE, EF, and d are calculated using in situ measurements and modeled results.

	NRMSE		NMAE		EF		d	
	Original	Updated	Original	Updated	Original	Updated	Original	Updated
All	14.49	11.82	51.22	40.13	-0.67	-0.11	0.55	0.63
Germany	14.46	11.81	50.29	39.43	-0.66	-0.11	0.55	0.65
Netherlands	22.56	17.25	50.75	37.13	-1.21	-0.30	0.56	0.66
Belgium	24.65	21.53	59.29	50.16	-1.60	-0.98	0.51	0.54
Luxemburg	52.77	39.75	64.73	47.56	-3.98	-1.83	0.43	0.52

Table 2-3 Performance assessment of the original and the updated model by comparing NH_3 weekly (monthly) surface concentration. Correlation, NRMSE, NMAE, EF and d are calculated using in situ measurements and modeled results.

	Correlation		NRMSE		NMAE		EF		d	
	Original	Updated	Original	Updated	Original	Updated	Original	Updated	Original	Updated
All	0.46	0.59	7.47	6.29	57.62	48.25	0.00	0.29	0.65	0.75
Netherlands	0.41	0.57	12.39	9.96	56.10	45.60	-0.16	0.25	0.63	0.74
Germany	0.44	0.48	6.85	6.73	67.61	65.62	0.16	0.18	0.57	0.63

Modeling atmospheric ammonia using agricultural emissions with improved
spatial variability and temporal dynamics | **75**

2

2.3.3 Observed and modeled *NH₃* surface concentrations

Figure 2-7 provides the scatter plots between paired in situ measurements and LOTOS-EUROS simulations, showing all weekly or monthly averaged measurements (the temporal resolution depends on the measuring interval of the ground station). The updated linear regression result is better than the original one, with a slope closer to 1 and higher R-squared value. It appears that using the updated emission model yields a more coherent estimate with reality than the original model. The mid-day of the sampling period is indicated through the coloring of scatter points. In Figure 2-7(a), most of the blue points lie on the upper side of the fitted line and y=x, which indicates that the original model usually overestimates surface concentrations (emissions) in the first three months of the year. In the meantime, the points in Figure 2-7(b) are more evenly distributed with a narrower spreading. If the scatter points in the first three months are excluded, as is shown in Figure 2-7(c) and Figure 2-7(d), the linear regression result is worsened dramatically. On the contrary, filtering out measurements in the beginning months does not impact on the comparison between the new modeled results and measurements. Both slope and R-squared almost remain the same, which implies that the updated model's performance is more robust and stable.

Once again, the four indicators and correlation coefficient were calculated to determine the performance of the original and updated model (Table 2-3). All indices illustrate that the updated model has improved surface concentration estimates. The improvement in the Netherlands is much larger than that in Germany. The reason might be that the setup of ground stations is more consistent in the Netherlands. The locations of the Dutch stations are in the nature areas, making them more representative of the overall emission temporal variation of a grid cell.
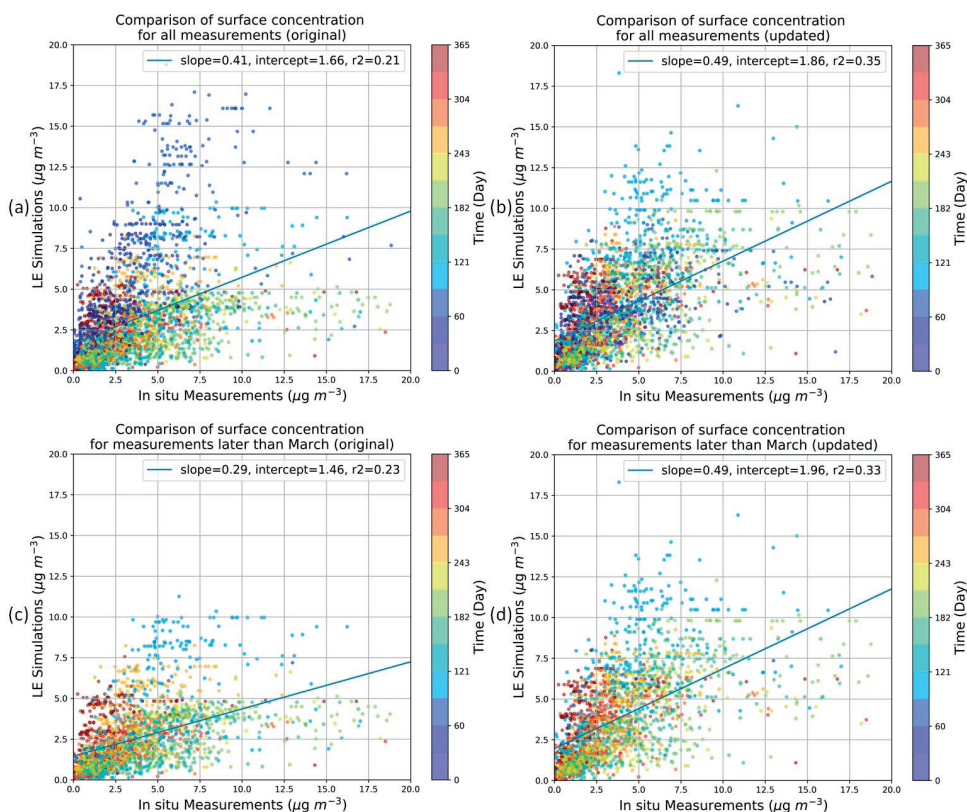
Figure 2-7 Scatter plots comparing NH_3 weekly or monthly averaged surface concentrations from in situ measurements and the LOTOS-EUROS model. The color of the points indicates the time (day of a year). The left panels and right panels use original and new modeled results, respectively. (a) and (b) include all measurements and correspondent simulation results, while (c) and (d) exclude the data from the first three months of the year.

Figure 2-8(a) and Figure 2-8(b) show the change in modeled surface concentration time series for Station DEUB028 in Zingst, Mecklenburg-Vorpommern, Germany. The station is located in an agriculturally active region with cereals, industrial crops, and animal housing. As can be seen in Figure 2-8(a), the original model does not correspond with the measurements well. There is almost no NH_3 measured before Julian Day 64, but the original model estimates that there are two peaks on Day 38 and 59. Besides, the first two peaks in the measurement on Julian Day 80 and 110 are not captured by the original model. On the contrary, the updated model manages to simulate these two peaks, even though they are slightly delayed by ten days. The first and larger peak of the two in spring is mainly explained by cattle manure application, followed by pig and poultry manure application, and mineral fertilizer contributes to a lesser extent. In the summer between Day 150 and 275, the new modeled result also does a good job distributing NH_3 emission temporally, with animal houses, cattle storage and mineral fertilizer application dominating NH_3 emission.

A similar situation applies to station DEUB005 in Lüder-Langenbrügge, as shown in Figure 2-8(c) and Figure 2-8(d). We can see from Figure 2-8(c) that the original model again allocates substantial emissions at the beginning of the year. The updated model improves the estimates a lot, even merged peaks from spring mineral fertilizer and manure application are detected. However, there still exist two issues. One is that the peaks in spring between Day 64 and 140 are overestimated. The other one is that the whole time series is delayed by five days. A possible reason for the delay of fertilization emission is that the reference temperature sum in TIMELINES to estimate fertilization day is too large at this location. Another cause could be that the threshold of De Martonne-Index (1.7) is too low at this location. Some days in February are considered to have excessive rain, so the whole curve is shifted to the right direction of the x-axis.

Time series of Ammonia Surface Concentration
DEUB028 (54.44, 12.72) (Original)

(a)

Time series of Ammonia Surface Concentration
DEUB028 (54.44, 12.72) (Updated)

(b)

Time series of Ammonia Surface Concentration
DEUB005 (52.8, 10.76) (Original)

(c)

Time series of Ammonia Surface Concentration
DEUB005 (52.8, 10.76) (Updated)

(d)
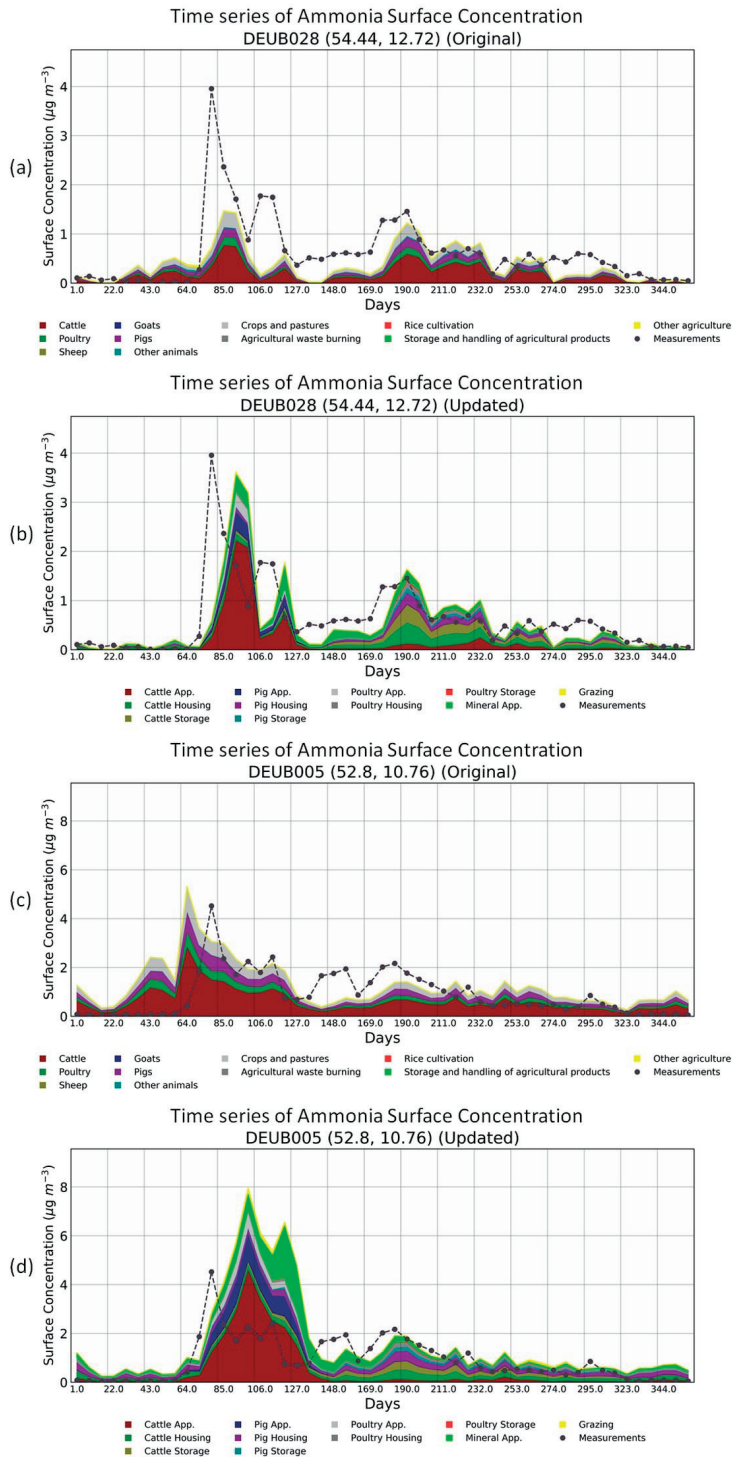
<<
Figure 2-8 Comparison of surface concentration measurements within EMEP network and simulated surface concentrations from original and updated modeled annual emission and time profiles: (a) in situ measurements vs. the original modeled output at station DEUB028; (b) in situ measurements vs. the updated modeled output at station DEUB028; (c) in situ measurements vs. the original modeled output at station DEUB005; (d) in situ measurements vs. the updated modeled output at station DEUB005.

Another station in the region of Hanover, Lower Saxony, is demonstrated in Figure 2-9. The measurements at this station only have a monthly temporal resolution. The updated model has shown much better correspondence with measurements than the original one, except that the average surface concentration in May is almost 50 percent higher. Figure 2-9(b) is able to point out that most of the agricultural activity at this location is related to fertilization, among which cattle and pig manure applications have dominance. Thus, the overestimation in spring is probably linked to cattle or pig manure application. There are two possible contributions to this behavior. One is the emission fractions used in INTEGRATOR. The INTEGRATOR model uses country dependent emission fractions, which have been updated and detailed through others' studies. However, they do not account for differences in manure characteristics, climatology, and soil properties. Another reason is the way of resampling emission from NCU polygons to the grids in LOTOS-EUROS, which leads to misallocation of emission to places without any sources. Last but not least, Lower Saxony is one of the states in Germany which has the highest density of livestock in the country. INTEGRATOR model calculates NH_3 emission based on proxy maps of animal number and excretion input, without considering the fact that manure from this high production region could be transported to other areas where manure is in demand. This will also lead to an overestimation in regions with excessive livestock excretion.
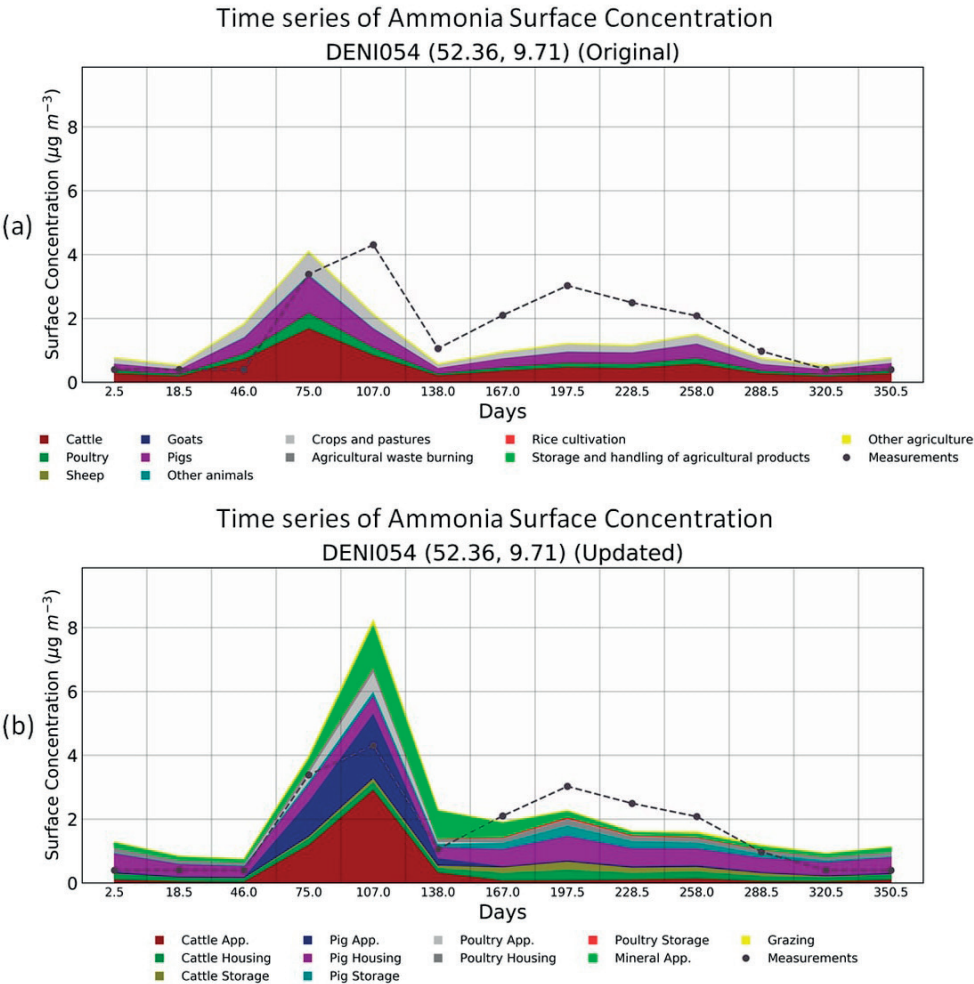
Figure 2-9 Comparison of surface concentration measurements within EMEP network and simulated surface concentrations from original and updated modeled annual emission and time profiles at station DENI054. (a) in situ measurements vs. the original modeled output; (b) in situ measurements vs. the updated modeled output.

2.4 Discussion and conclusions

The comparison with in situ surface concentration measurements
The comparison of surface concentration mainly casts light on the quality of the temporal allocator. Regarding the newly developed temporal allocator, we made modifications to the parameterization proposed by Skjøth (2004, 2011) and Gyldenkærne (2005), which accounts for the agricultural activities and their differences, based on meteorological variables as well as the ventilation and heating inside stables. The first modification is that subsectors of manure/fertilizer application emission were created to adapt to INTEGRATOR's categorization. Secondly, emission peak μ in Eq. (2.1) was updated by the estimated fertilization day from TIMELINES. Last, legislative constraints and the impact of excessive precipitation were also implemented.

The time series of surface concentrations from the updated model show better alignment with in situ measurements than those from the original model, making it possible to detect the NH_3 temporal variability brought by various agricultural activities. This is achieved by making adjustments to the method in Gyldenkærne et al. (2005) using TIMELINES, implementing legislative constraints, and including the impact of excessive precipitation. Nevertheless, there are occurrences of inconsistency.

First, the modeled time series could be delayed with respect to in situ measurements. A possible reason is that the reference temperature sum in TIMELINES to estimate fertilization day needs correction. Agricultural models, including TIMELINES, usually work from the perspective of maximizing the efficiency of nitrogen use. However, farmers are likely to choose to apply manure and mineral fertilizer when labor and machinery are both available and are unlikely to finish manure application in one day on the farmlands. This leads to the inaccuracy between the fertilization day estimate and reality and an extended manure application period. Moreover, the TIMELINES model heavily depends on the empirical data on sowing and harvesting dates currently used within CGMS to calculate the thermal time thresholds. The data need updates and are limited regarding the variety of crops, making it capable of simulating the timing of field operations for some but not all arable crops at different locations across Europe. Consequently, a more thorough analysis is needed to refine the relationships between various field operations (Hutchings et al., 2012). There are other factors related to the timing of fertilization. For example, soil moisture, workability, and trafficability were neglected in TIMELINES, but they might affect the prediction of plowing and sowing. In addition, solid manure applications for spring crops could be made in autumn of the previous year. Another reason for the delay could be the threshold of De Martonne-Index (1.7) which was decided with a visual inspection for Flanders by Kranenburg et al. (2016) and expanded to the whole area of interest. When the threshold is too small, the time profile will be delayed because precipitation is too

often considered to be excessive for fertilization operations. Further improvement of the De Martonne-Index algorithm is in need to account for regional differences. More studies about De Martonne-Index should be done to correlate excessive precipitation and its impact on agricultural practices.

Furthermore, sometimes the magnitude of surface concentration is not in accordance with measurement, or the time series completely mismatches measurements. This could be caused by emission reallocation from NCU to the LOTOS-EUROS grid as well as the restricted spatial representativity of measurement locations. During the resampling of emissions from NCU level to the LOTOS-EUROS grid, emission estimates within an NCU from INTEGRATOR are evenly distributed all over the polygon, regardless of the actual locations of crops, animal houses, and manure storage facilities. In addition, some NCUs are composed of multiple disconnected polygons, within only some of which a particular crop, animal house, or manure storage is present. Hence, emissions are wrongly allocated to areas without any sources. Besides, spatial characteristics such as hot spots will be smoothened out for NCU polygons of larger sizes. Therefore, high-resolution crop maps can help allocate emission from fertilization inside polygons onto where arable land and grassland appear, and detailed information on animal housing locations can transform housing emissions into point emissions. What's more, in situ measurements represent the NH_3 emission characteristics of a point source, but the spatial resolution of the updated model is around 7km × 7km which is relatively coarse. A station next to animal houses or manure storage facilities will result in a constant high level of NH_3 over the year, while a station next to farmlands will be highly affected by agricultural operations on the farmlands. Therefore, stations in remote areas are more representative of a broader region. This is why the updated model performs better at Dutch stations than at German stations (Table 2-3). MAN stations are set up to measure nature emission of ammonia, so their measurements represent better the emission variability in the grid cells. However, there are always stations next to sources given the size of the country. Ideally, in order to accurately verify the temporal allocation of emission from fertilization and housing, the spatial resolution should be increased with the help of a detailed crop map and animal housing information so that grid cell can represent local agricultural activity more.

As a result, a detailed crop map is a key to the improvement of ammonia emission estimates. Inglada et al. (2015) assessed the state-of-the-art supervised classification methods and produced more accurate crop type maps with high resolution multi-temporal optical imagery from SPOT4 (Take5) and Landsat 8. Surface reflectance, the normalized difference vegetation index (NDVI), the normalized difference water index (NDWI) and brightness were chosen as features, random forest and support vector machine (SVM) were selected as classifiers. Belgiu and Csillik (2018) proposed a time-weighted dynamic time warping (TWDTW) method that uses NDVI time series obtained by Sentinel-2 data

for classification. It was proved to be more efficient in terms of computational time and less sensitive concerning the training samples, which is essential for regions where inputs for training samples are limited. Besides Sentinel-2 optical images, Giordano et al. (2018) also included Sentinel-1 radar measurements for crop classification using the complementarity between the multi-modal images, because Sentinel-1 radar images allow getting more information where Sentinel-2 suffers from cloud cover. We will make use of the above methods to obtain crop maps with high spatial resolution. The maps will be used to update manure distribution according to N demand of different crops and subsequent ammonia emissions. They are helpful in allocating emission from manure and fertilizer application in a more precise way.

The comparison with IASI total column data

The quality of the modeled annual averaged total column relies on the assumption that the spatial distribution of the NH_3 emission in LOTOS-EUROS closely represents reality. The temporal distribution is also of great importance because only modeled columns at overpass time were selected for averaging.

There are large inconsistencies in the comparison between IASI observations and the modeled results from both the original and updated model. One reason for the inaccurate emission allocation could be that land use data and local agricultural activity inputs such as animal numbers and N excretion in INTEGRATOR are inaccurate. Local agricultural activity data are more accessible in countries like the Netherlands, Denmark, and Portugal. And land use data can be updated with a detailed crop map as discussed previously to achieve more accurate N demand estimates, manure and fertilizer distribution, and subsequent ammonia emission. Another factor that could cause spatial inconsistencies is the emission fractions used in INTEGRATOR. Emission fractions are nation-wide averages that describe the linear relation between emission and N input (excretion in animal housing and manure storage, applied manure and fertilizer). But in reality, they could vary from region to region due to application methods, manure properties, soil properties, and weather conditions. Huijsmans has studied those impacts for both arable land and grassland (Huijsmans et al., 2001; Huijsmans, 2003). He defined the formula to describe the relationship between NH_3 volatilization rate and the method of application and incorporation, total ammoniacal nitrogen (TAN) content of the manure, manure application rate, wind speed and ambient temperature. Additionally, the empirical modeling of the emission process is carried out by RIVM and WUR using Volt'air approach (Huijsmans et al., 2014). Preliminary results show that the variations of weather conditions over the past 20 years lead to different emission fractions per month, and soil and manure characteristics also influence emission fraction. As a result, emission fraction differs at farm scale, contributing to inhomogeneous emission fraction on a regional or national scale. Therefore, there are two steps for improvement in terms of land use, local agricultural activity data and emission fraction. In the short term,

we will implement detailed land use and local activity data for the Netherlands, Denmark, and Portugal, and investigate the difference brought by the refinement of the input. Next, a meta-analysis will be performed for the parameterization of spatially and temporally explicit emission fractions, taking into account local climatology, soil properties, fertilizer characteristics and application method.

A possible source of overestimation in lower latitudes and underestimation in higher latitudes in Germany is the neglect of possible manure transport. INTEGRATOR assumes that the emissions from a certain animal, including housing, storage and manure application, occur where the animal is located, ignoring manure transport from regions with excessive manure to those with shortages. The role of manure transport is more significant when there is a lot of animal livestock. Hendriks et al. (2016) looked into manure transport data in Flanders and found that the manure transport data account for roughly one-third of the amount of manure used in Flanders each year, while the remaining two-thirds consists of manure that farmers apply on their own land. Hansen-Kuhn et al. (2014) showed that southern Germany is one of the areas in the country which has the highest density of cattle and pig livestock. It is likely that the neglect of manure transport contributes to the overestimation in the lower latitudes. Therefore, manure transport data can be used as a proxy to improve the spatial distribution, and the pattern of manure transport can additionally help construct the temporal pattern of NH_3 emissions from manure application, under the assumption that manure is applied to the fields on the day of transport.

Moreover, the uncertainty in IASI measurements also has an impact on the comparison. Dammers et al. (2016) found that the validity of the IASI product is quite limited because the satellite retrievals are biased. The retrieval of NH_3 columns from IASI is still an on-going process, with a few studies having examined the quality of the products. Further development and validation of the IASI retrieval are very much in need for the understanding of the satellite's product. It remains poorly validated with only a few dedicated campaigns performed with limited spatial, vertical or temporal coverage. The key finding of the previous studies on the retrieval is that vertical profiles of NH_3 distribution has lots of uncertainties and need to be improved. Dammers et al. (2016) suggested that tower measurement campaigns are crucial for a better understanding of the vertical profile. Li et al. (2017) showed that there is an apparent seasonal variation in the vertical distribution of NH_3 and that the slope of the NH_3 concentration gradient varies throughout the year, with relatively high NH_3 ground concentrations during winter. His reasoning was that boundary layer is shallower in winter, which will potentially trap NH_3 emissions and reduce NH_3 concentrations higher up the column. As a result, IASI could miss high NH_3 ground concentrations in winter because of the lack of sensitivity to the lower parts of the boundary layer. On the contrary, most of the measurements used

in this paper to calculate annual average are in April, June and July in which weather is relatively warmer and the boundary layer is thicker, especially during clear-sky daytime condition. Recently, new products become available, making it possible to cross-check results among satellites. Cross-track Infrared Sounder (CrIS) is one of the new products that deserve attention, having the advantage of acquiring more explicit information on the sensitivity of the satellite (averaging kernel).

Conclusions

In summary, this paper is an attempt to build a new NH_3 emission model which is composed of a spatial allocator and a temporal allocator. The spatial allocator provides more spatial details and can distinguish various agricultural sectors, including crop types, fertilizer types, animal houses and manure storages. The distribution of annual emission obtained from MACC-INTEGRATOR demonstrates more emissions overall, with country totals 14% higher in Germany, and 6.6% higher in Benelux. Extra new hot spots appear in southeastern Germany, while the spatial characteristics in the east of the Netherlands are smoothened due to the allocation algorithm. The temporal allocator is spatially explicit and dynamic based on land use, local climatology, and legislative constraints. The labeling module of LOTOS-EUROS helps to trackback the emission sector of the modeled NH_3 surface concentration and total columns for better interpretation and future improvement. Despite the limitations in modeling and data for validation, LOTOS-EUROS performed better with the updated emission products, especially in the representation of the temporal behavior of NH_3 concentrations. Comparison between updated modeled results and observed NH_3 levels show much better correspondence and more robust performance, especially the temporal variability is captured better as the new methodology successfully differentiates regional variability in seasonality in NH_3 emissions. When reliable and detailed input datasets are available, and the methodology is further improved as described, we can expect to extend this approach to Europe.

CHAPTER 3

A comparison of agricultural ammonia emissions for the Netherlands, Denmark, and Portugal using a Europe-wide and locally adapted approaches

Ammonia is one of the most relevant pollutants emitted from agricultural activities, harming human health and contributing to biodiversity loss. Crop and animal distribution strongly impact the spatial and temporal distribution of simulated ammonia emissions. Animal distributions, including the type of animal houses and the number of animals in these houses, determine the amount of nitrogen (N) excretion. Through the nitrogen flow calculation, these numbers determine the emissions from animal housing and manure storage on the farm, and manure application on arable- and grassland. Crop distributions influence the locations of manure application and the amount of manure applied to the different crops. Current large-scale ammonia emission models, including INTEGRATOR, do not use high-resolution information on animal and crop distribution as this is lacking at a European scale, where information usually is given at the NUTS3 level. In addition, average ammonia emission factors, averaging out the variation that exists due to differences in e.g. manure composition, meteorology, and soil properties. As a result of all these factors, the absolute estimated values and spatial and temporal details of the model results contain significant uncertainties.

Here we used high-resolution information on crop and animal distributions and locally derived emission fractions for the Netherlands, Denmark, and Portugal, in the INTEGRATOR model to assess the impact on the spatial and temporal variability in agricultural ammonia emissions. The comparison of modeled surface concentrations with in situ measurements for the Netherlands showed improvements in both spatial and temporal distributions, being most evident in spatial distribution. As with the Netherlands, the modeled results for Denmark and Portugal showed much more spatial detail than the original model, but the results could not be validated due to the lack of measurements. Nevertheless, our study shows that detailed crop and livestock distributions are crucial for a more detailed spatial distribution of ammonia emissions.

Abstract

3.1 Introduction

The enhanced N input by livestock manure and mineral fertilizers in global agriculture, specifically since 1960, has strongly increased the emission of ammonia (NH_3), being the most dominant reactive nitrogen species in the atmosphere (Amann et al., 2013). Between 1970 and 2005, global agricultural NH_3 emissions increased by 90%. Excessive levels of ammonia lead to significant adverse effects on human health, the environment, and biodiversity (de Vries, 2021). High emissions with related high concentration and deposition levels of ammonia lead to significant adverse effects on soil quality, biodiversity, and human health (de Vries, 2021). First, excessive ammonia deposition on the soil can contribute to eutrophication and acidification, leading to imbalances in nutrient availability. This in turn, reduces soil biodiversity and plant biodiversity by promoting the growth of certain plant species over others, particularly nitrogen-sensitive species (Bobbink et al., 2010; Pitcairn et al., 2009), which in turn, affects the entire ecosystem, including the organisms, such as butterflies and birds that depend on these plants for food or habitat. Additionally, ammonia can react with atmospheric acids to form harmful particulate matter ($PM_{2.5}$) (Sutton et al., 2013; Krupa, 2003), worsening air quality. Exposure to high concentrations of particulate matter may lead to severe health issues, including respiratory, skin, and eye irritation, chronic lung disease, burns, and even death (Kim et al., 2015; Khaniabadi et al., 2017; Boldo et al., 2006). At lower levels, exposure may lead to nose and throat irritation.

To define a deposition threshold above which natural ecosystems can be negatively affected, a concept of critical loads was introduced to quantitatively estimate the ecosystem exposure to one or more pollutants below which significant harmful effects on specified sensitive elements of the environment do not occur (Williams and Tonnessen, 2000). In Germany and Europe, critical loads for eutrophication were estimated to be exceeded by about 71% and 58% of the area of ecosystems in 2020, compared to 81% and 67% in 2005 (Hettelingh et al., 2017). Meanwhile, critical loads for acidification were exceeded by about 35% and 4% for Germany and Europe in 2020, respectively. Despite the reductions, the exceedances are still significant for both eutrophication and acidification.

Properly assessing the spatial variation in ammonia emission, concentration, deposition, and related impacts requires a very dense monitoring network (Erisman et al., 2005). Since this is not practically feasible (especially in the long run), emission and deposition models are typically utilized (Hertel et al., 2007). However, emission and atmospheric deposition of N, especially of NH_3-N, is highly spatially variable, implying that estimated areas exceeding critical N loads using spatially low-resolution model results may be over- or underestimated. It has been shown that current regional chemistry transport models (CTMs) with a resolution of 50 km to 10 km tend to poorly represent observed NH_3 levels

3

across Europe (Simpson et al., 2011). Several studies have shown that a higher spatial resolution in NH$_3$ emission data leads to significant changes in modeled N depositions (Duyzer et al., 2001; Pul et al., 2004). A few national-scale models with resolutions from 5 km to 1 km have shown better agreement with observations (Dore et al., 2012; Theobald et al., 2004). Note that coarse resolution deposition mapping combined with critical load limits generally leads to underestimation of the exceedances of critical loads (Spranger et al., 2001). For example, Dragosits et al. (2002) concluded that N critical load exceedances were underestimated in a UK national assessment at the 5 km grid level since the variability of NH$_3$ in agricultural landscapes was not included. High-resolution and high-quality emission information is thus required to properly account for the impact of spatial variability on critical N load exceedance.

Emission inventories have been developed to improve the spatial details of NH$_3$ emissions in different countries by Gac et al. (2007) in France, Webb and Misselbrook (2004) in the UK, and Hyde et al. (2003) in Ireland. At the European (EU) scale, the Integrated Nitrogen Tool across Europe for Greenhouse gases and Ammonia Targeted to Operational Responses (INTEGRATOR) assesses greenhouse gases and nitrogen fluxes from agricultural sectors at relatively high spatial resolution and accounts for differences in crop types, fertilizer types, animal housing, and manure storage (de Vries et al., 2021). INTEGRATOR, however, does not include detailed animal and crop distribution information for all the countries included. In addition, ammonia emissions from different sectors are assessed with average empirical emission fractions derived from field experiments and expert knowledge, averaging out the regional variation that exists due to differences in e.g. manure composition, meteorology, and soil properties. As a result of all those factors, the absolute estimated values and spatial and temporal details of the model results contain significant uncertainties. Therefore, updating emission models with detailed inputs on the distribution of crops and livestock and ammonia emission factors is essential to obtain high-quality, high-resolution ammonia emission estimates (Kryza et al., 2011).

Ge et al. (2020) presented a method for increasing the spatial details of ammonia emissions using INTEGRATOR and improving the temporal allocation by correlating the timing of manure and fertilizer application with meteorology. Based on the work of Ge et al. (2020), this study aims to develop a framework that improves the spatial resolution of ammonia emissions by including national inputs on crop maps, livestock number distribution, and emission fractions. This showcases the method that can be used for other countries in INTEGRATOR if sufficient data are available. We chose the Netherlands, Denmark, and Portugal as case studies due to their distinct geographic locations (from north to south). Besides, the three countries reflect a range from highly intensive (the Netherlands) towards intermediate (Denmark) and low intensive (Portugal) livestock areas, with many sensible natural and semi-natural ecosystems closely surrounded by agricultural areas. The

Netherlands is the second-largest exporter of food and agricultural products globally and has a very intensive agricultural system (Dollmann et al., 2021). As a result, the Netherlands has Europe's highest ammonia emission density, with an average of about 3180 kg NH_3-N per square kilometer (Wever et al., 2019). Denmark started following several mandatory regulations and measures through a series of national environmental action plans in the mid-1980s, which were implemented nationwide after 2016. However, the overall effects of the efforts have been challenging to determine due to spatial and temporal variations in climate and differences in agricultural practices. The Portuguese ecosystems belong to the most nitrogen sensitive in the world and are being threatened by N deposition, but current research and policy support capacity is lacking.

The aim of this paper is to assess the impact of using high-resolution data of crop and livestock distributions and locally derived emission fractions on the spatial variability in agricultural ammonia emissions by comparing results from locally adapted approaches for the Netherlands, Denmark, and Portugal with those from the standard Europe-wide approach. We start by introducing the EU-scale emission model INTEGRATOR and then describe how we embedded more detailed input data of crop and livestock distributions and emission fractions in the locally adapted INTEGRATOR models for each of the three countries. We then compare emission results and the surface concentrations simulated by the CTM LOTOS-EUROS, using the original EU-scale emission model and the locally adapted models, with in situ ammonia measurements. Finally, we evaluate the model performance in terms of improvements and describe the shortcomings of the modeled results for future improvement.

3.2 Methodology

In this section, first, the EU-scale emission model INTEGRATOR is described (Section 3.2.1). Then we illustrate how the model is adapted for the case studies of the Netherlands, Denmark, and Portugal for 2018 (Section 3.2.2). The Dutch and Danish models referred to as INTEGRATOR-NL and INTEGRATOR-DK, respectively, were previously developed. The Portuguese model was newly developed as INTEGRATOR-PT. INTEGRATOR-DK and INTEGRATOR-PT were updated using officially reported municipality-level livestock numbers and officially published parcel-level crop maps for 2018 and locally derived emission fractions. Subsequently, we describe LOTOS-EUROS, a chemistry transport model (CTM) that was used to model ammonia surface concentrations from the emission distributions of INTEGRATOR, INTEGRATOR-NL, INTEGRATOR-DK, and INTEGRATOR-PT for validation with in situ measurements (Section 3.2.3).

3.2.1 The EU-scale emission model INTEGRATOR

The INTEGRATOR model is a nitrogen (N) flow model that includes a complete N balance for agricultural land (housing systems, grassland, and cropland) for the European Union using relatively simple and transparent model calculations based on existing model approaches combined with relatively high-resolution spatially explicit input data. It includes sub-models for the prediction of ammonia (NH_3), nitrous oxide (N_2O), other oxides of N (NO_x) and dinitrogen (N_2) emissions, crop N uptake, N leaching from the root zone to groundwater (principally nitrate, NO_3^-) and N runoff to surface water from animal housing systems, manure storage systems, and agricultural soils (de Vries et al., 2011, 2022). Below we describe the approach to assess the ammonia emissions.

3.2.1.1 Animal distribution, N excretion, and manure N application

INTEGRATOR calculates the total manure production for the so-called NitroEurope Classification Units (NCUs), being polygons composed of several 1 km × 1 km grid cells with the same administrative unit (NUTS3 regions), soil type, slope, and altitude (de Vries et al., 2011). To do so, livestock numbers of various animal categories obtained from the FAO database at the country level, combined with Common Agricultural Policy Regionalised Impact analysis (CAPRI) data for distribution at the NUTS2 level are downscaled to a 1 km × 1 km resolution (Ge et al., 2020). The total manure N production is calculated by multiplying those livestock numbers with national values for N excretion rates per animal type from the CAPRI model (Gocht and Britz, 2011). A division is made between the excretion of animals in housing systems and grazing animals on pastures based on data at the country level derived from the GAINS model (Klimont and Brink, 2004). In agricultural areas, the maximum amount of manure N applied to agricultural land is set to 170 kg N ha^{-1} year^{-1} specified in the EU Nitrates Directive, except for grassland and other roughage crops in Belgium, Denmark, Germany, UK, Ireland, Italy, and the Netherlands. Here, values of 230 or 250 kg N ha^{-1} year^{-1} are used, depending on the derogation received from the EU. The actual manure application rates, which is the N excreted minus N emissions in housing systems and by grazing, depend on the crop and grassland type-specific weighing factors described in more detail by Ge et al. (2020).

3.2.1.2 Crop distribution and fertilizer N application

The N crop offtake is calculated as the product of the crop yield (in terms of harvest) and the N content in harvested crops, which is a function of the N input. The total demand in a NUTS3 region is calculated by multiplying the N removal of each crop by the total area of the crops in each NUTS3 region. The areas of crops in NUTS3 regions are derived from CAPRI. The yields of arable crops for each country are derived from FAOSTAT (de Vries et al., 2022). The N contents of harvested crop products, the amount of crop residues, and the relation with N input are based on literature (Fink et al., 1999; Velthof and Kuikman, 2000). The N in crop residues is calculated by dividing the N removed in the harvest

with an N index. The N fertilizer application at the NCU level is based on the total N crop offtake, the available non-N fertilizer inputs (N inputs by animal manure, crop residues, N mineralization, N deposition, and N fixation), and the N use efficiency (NUE) of the effective N input. The results thus obtained are corrected, where needed, using national fertilizer consumption rates (de Vries et al., 2022).

3.2.1.3 NH$_3$ emission fractions

The emissions of NH$_3$ accounted for in the model include emissions (i) from feces and urine during storage in housing and manure storage systems, (ii) by grazing animals, (iii) after application of manure and fertilizers to agricultural land, and (iv) due to atmospheric deposition, N fixation and crop residue input (not included for NH$_3$). NH$_3$ emissions from animal housing, manure storage systems, and grazing are calculated by multiplying N excreted in these sectors by the corresponding animal and country-specific emission factors, with more details in Ge et al. (2020). NH$_3$ emissions from fertilizer and animal manure applications are calculated by multiplying the application rates of different animal manures and fertilizers by country-specific emission factors that also distinguish manure and fertilizer types, with values given in de Vries et al. (2022), based on the GAINS model (Klimont and Brink, 2004).

3.2.2 The adapted emission models for the Netherlands, Denmark, and Portugal

A summary of adaptations to INTEGRATOR made for the various countries is given in Table 3-1. Apart from using adapted ammonia emissions fractions (see Table 3-2), the adaptations refer explicitly to improvements in 1) the spatial variation in animal housing and manure storage emissions by the inclusion of the officially reported animal numbers at the municipality or farm level in a given year and 2) the spatial variation in manure and fertilizer application emissions based on more detailed information of crop and livestock distributions, which affects the distribution of manure excretion and fertilizer. Then the adaptions are described below for the different countries compared to the standard INTEGRATOR approach regarding spatial resolution (Section 3.2.2.1), livestock distribution (Section 3.2.2.2), crop distribution (Section 3.2.2.3), and emission fractions (Section 3.2.2.4).

3.2.2.1 Spatial resolution of emission output

The Netherlands (INTEGRATOR-NL)

For the application of INTEGRATOR with high spatial resolution national data for the Netherlands, we used datasets and calculation procedures used in the model INITIATOR (de Vries et al., 2023). Ammonia emissions from animal housing and manure storage systems were derived for unique housing locations, while emissions from grazing animals and the application of manure and fertilizer to soil were derived for unique combinations of soil and crop types. More specifically, the inputs by fertilizer and manure and related

ammonia emissions from the field were calculated at the parcel level (BRP, 2017). Parcels from one farm with similar crop type and soil type (sand, loess, clay, peat) and located in the same agricultural region were combined into one spatial unit.

Denmark (INTEGRATOR-DK)

During the development of INTEGRATOR-DK, Kros et al. (2018) made the following changes to INTEGRATOR to derive high spatial resolution ammonia emissions for Denmark: (i) adaptation of the boundaries of the NCU; (ii) adaptation of the manure distribution module; and (iii) translation/aggregation of the more detailed codes used for animal types, manure and crop types in the Danish data to the more aggregated codes used in INTEGRATOR. Based on the boundaries of the municipalities, firstly, the NCUs were stretched such that they exactly fill the municipal boundaries, which is only a cosmetic adaptation and does not influence the results. Secondly, NCUs that crossed a municipal boundary were split so that the municipality borders bind all NCUs. The overlay with 99 municipalities resulted in 610 NCUs for Denmark, an increase of 497 NCUs compared to INTEGRATOR. We refer readers to Kros et al. (2018) for more detailed information regarding INTEGRATOR-DK.

Portugal (INTEGRATOR-PT)

Similar to INTEGRATOR-DK, we adapted the boundaries of the NCUs for Portugal (INTEGRATOR-PT). We used the intersection of municipalities' boundaries and the original NCU polygons as geospatial data for INTEGRATOR-PT. The polygons sharing the same NCU number and municipality name were assigned the same new polygon (NCU-PT) ID. The geospatial data of Portuguese municipalities was downloaded from GADM (https://gadm.org/). This was done for the deviation of the updated livestock distribution using reported municipality data. The more detailed codes used for animal types, manure, and crop types in the Portuguese data were translated to the more aggregated codes used in INTEGRATOR. As a result, compared to the original 961 NCU polygons, there are 4320 polygons in the adapted model (see Figure 3-1).

Table 3-1 Updates in the assessment of the spatial variation in manure and fertilizer application and ammonia emissions estimates.

Input	INTEGRATOR	INTEGRATOR-NL	INTEGRATOR-DK	INTEGRATOR-PT
Animal Number	Downscaled from CAPRI at NUTS2 level	RVO/CBS/GIAB census data: at point level	Statistics Denmark: at the municipality level	Statistics Portugal: at the municipality level
Crop area	CAPRI at the NUTS3 level	Official crop map at the parce level	Official crop map at the parce level	Official crop map at the parce level
Emission fractions from animal housing and manure storage	Country-specific data from GAINS model	From NEMA model (Velthof et al., 2012)	Weighted emission fractions (Kros et al., 2018)	Updated local data
Emissions from manure and fertilizer application	Evenly over NCU	On crops	On crops	On crops
Emissions from animal housing and manure storage	Evenly over NCU	As point sources at animal house locations	Evenly over NCU	Evenly over NCU

3

Figure 3-1 The geospatial data for Portugal used in the original INTEGRATOR (left) and the updated INTEGRATOR-PT (right). There are 961 unique NCU IDs in the original INTEGRATOR and 4320 unique NCU-PT IDs in INTEGRATOR-PT.

3.2.2.2 Livestock and manure distributions

The models start with the calculation of N excretion by multiplying the number of animals with the N excretion rate per animal per country for animal type (Kros et al., 2012). It indicates that the animal number affects the following computation of N excretion from grazing animals, housing systems, manure storage, and total manure production, which undoubtedly impacts ammonia emissions from these sectors.

The Netherlands (INTEGRATOR-NL)

The distributions of Dutch livestock (animal numbers) were derived at the farm level from CBS data (Statistics Netherlands), combined with information on the housing locations that are known through the GIAB database (van Os et al., 2016). The emissions from animal housing were then calculated for all individual farms based on geo-referenced animal number information for each housing system (GIAB) (van Os et al., 2016). The manure produced on farms is redistributed across the region, dependent on the manure production and the allowed nitrogen and phosphorus dose. This dose is regulated by the *Dutch Manure and Fertilizers Act*, which implements the Nitrates Directive, and determines how much N may be applied on grassland and arable land. In more detail, the Nitrates

Directive sets a strict maximum threshold for animal manure of 170 kg N ha^{-1}. Farms with grazing livestock and the option of derogation are allowed to apply up to 250 kg N ha^{-1}. The redistribution of manure is calculated in five steps (details in Kros et al. (2019) and de Vries et al. (2023)): (i) estimate N excretion, (ii) estimate N that can potentially be applied, (iii) estimate the maximum N doses that are allowed to be applied, (iv) redistribute the manure over the fields owned by the farm and (v) export the manure excess of livestock farms to farms with a demand for manure. Suppose an excess exists on the regional level. In that case, this excess is distributed over those surrounding regions with a demand for manure while accounting for distance, given the type of manure distributed. Suppose there is more manure than the amount that legally can be applied nationally (implying a violation of the legal N application limits). In that case, this final volume of excess manure is redistributed over maize fields in areas with a manure excess. The redistribution over those fields is proportional to the excretion rate per region.

Denmark (INTEGRATOR-DK) and Portugal (INTEGRATOR-PT)
Animal numbers at the municipality level in 2018 were retrieved from Statistics Denmark (https://www.dst.dk/) and Statistics Portugal (https://www.ine.pt/) for Denmark and Portugal, respectively. Statistics Denmark and Statistics Portugal are the central authorities responsible for collecting, compiling, and disseminating statistical information on various aspects of Danish and Portuguese societies, including agriculture and livestock. The livestock number data is divided into several categories, reflecting the diverse range of animals raised for various purposes. The more detailed categorization of animal types was translated to the more aggregated animal types codes used in INTEGRATOR, with the translation method by Kros et al. (2018). Subsequently, using a scaling method, the municipality-level reported data were utilized to update the livestock distribution input in INTEGRATOR-DK and INTEGRATOR-PT. Firstly, animal numbers were obtained at the new NCU level (area-based disaggregation was used for INTEGRATOR-PT). Secondly, municipal-level animal numbers were derived from the new NCU-level data. Thirdly, scalars were calculated as the division of the officially reported number of one animal in one municipality and the municipal-level animal numbers from the INTEGRATOR-DK and INTEGRATOR-PT. Lastly, the scalar of a municipality was applied to all NCUs located in that municipality per animal type. In this way, we ensured that the animal numbers used in the model were the same as the reported values.

Figure 3-2 demonstrates the area-averaged density in Portugal (head per squared meter) of cattle, pig, and poultry (from left to right) in the standard INTEGRATOR (the upper row) and INTEGRATOR-PT (the lower row). One can see that even though the areas with higher densities remain similar. The cattle population is mostly distributed in the southeast of the country, with one hotspot in the northwest. The pig population is highly concentrated in the region of Leiria. Poultry is more populous in Viseu, Coimbra, and Leiria. However,

the absolute values of the distributions are quite different. The updated distributions generally show high values in the high-density areas and less homogeneity with more hot spots due to the more detailed input data.

Like INTEGRATOR-DK by Kros et al. (2018), INTEGRATOR-PT also used the INTEGRATOR-EU manure distribution module to calculate the manure distribution. This was done to ensure that all N flows through the manure management system from excretion to application were included. The manure produced was distributed over the available agricultural land within an NCU while considering the maximum permissible manure application rates, according to the Nitrates Directive. We refer to Kros et al. (2018) for detailed information on the calculation process.

### 3.2.2.3 Crop distributions

INTEGRATOR-NL calculates ammonia emissions at the farm level, which requires a parcel-level crop map as input. In INTEGRATOR-DK and INTEGRATOR-PT, emissions are computed at the NCU level, with the areas of crops within each NCU as input. The intersections of the crop parcels in crop maps and the NCU polygons were obtained using QGIS. The areas of crops in each NCU were calculated using the intersected crop parcels sharing the same NCU number. After the emissions from manure and fertilizer application of a crop type in an NCU were calculated, they were allocated to where the crop is located in the NCU using the high-resolution crop maps taken from available data sets in each country.

The Netherlands (INTEGRATOR-NL)

The Dutch crop distribution in 2018 was obtained from Basisregistratie GewasPercelen (BRP) (https://www.pdok.nl/datasets). The BRP contains the geographical boundaries of each individual parcel in the Netherlands, coupled with the crop that is grown on it. It contains over 780,000 individual agricultural parcels in the Netherlands. The boundaries of the agricultural plots are based on the Agricultural Area of the Netherlands (AAN). The user of the plot must annually register his crop plots and indicate which crop is grown on the relevant plot. The crop map is generated for each year.

Denmark (INTEGRATOR-DK)

The Danish crop map in 2018 was based on Marker, a geospatial tool designed to monitor and map agricultural land use and crop types across Denmark developed by the Danish Agency for Agriculture. Each field contains attributes indicating the field number, geometric area of the field, crop code, crop name, and field block number. The crop map Marker uses up-to-date satellite imagery to map agricultural areas and identify different crop types accurately, which enables real-time monitoring of crop growth and development patterns. It uses machine learning algorithms to recognize and classify various crop types, such as wheat, barley, potatoes, and other vegetables.
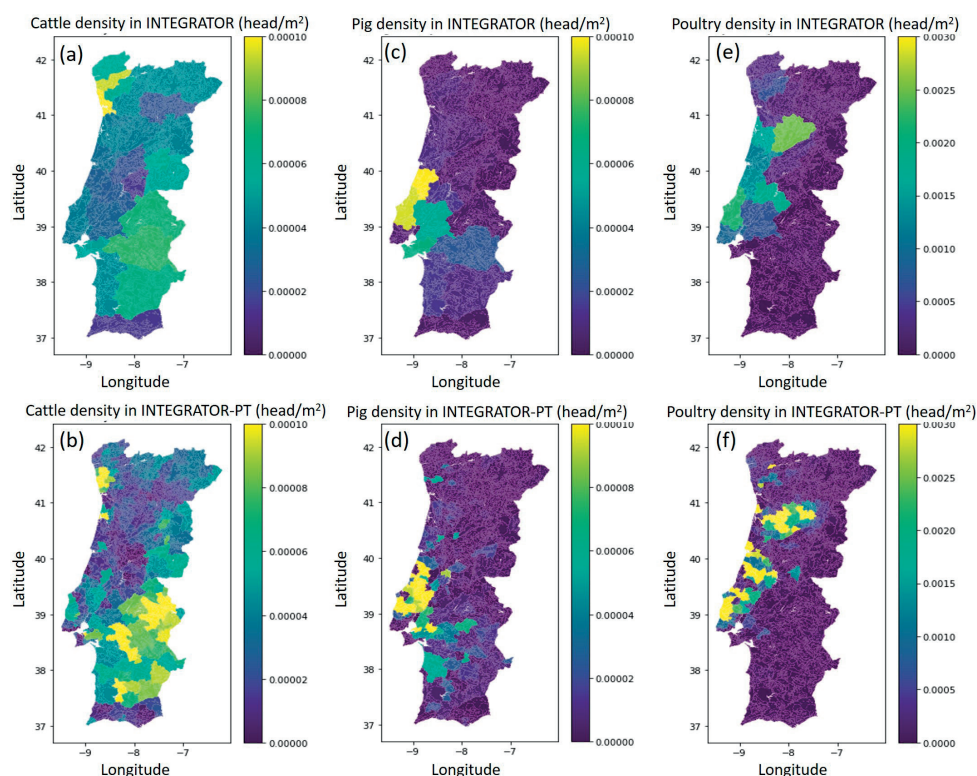
Figure 3-2 Area-averaged density at the NCU level (head per square meter) of cattle (a, b), pig (c, d) and poultry (e, f) in the standard INTEGRATOR (a, c, e) and the locally adapted models (b, d, f).

Portugal (INTEGRATOR-PT)

The Portuguese crop map in 2018 was obtained from IFAP (Instituto de Financiamento da Agricultura e Pescas) (https://www.ifap.pt/isip/ows/). This map was created using data from the Integrated Administration and Control System (IACS), which is a part of the Common Agricultural Policy (CAP) of the European Union. The Portuguese crop map from IFAP contains information on various crop types, such as cereals, fruits, vegetables, and more. The data is collected through farmer declarations, field inspections, and remote sensing techniques, such as satellite imagery and aerial photography. Each year, farmers in Portugal are required to submit declarations about their agricultural activities, including the crop types they cultivate, to IFAP. To verify the accuracy of farmer declarations, IFAP conducts field inspections. Satellite imagery and aerial photography are used to supplement the information gathered from farmer declarations and field inspections.

3.2.2.4 Ammonia emission fractions

The ammonia emission fractions used in INTEGRATOR are country-specific fractions from the GAINS model for animal housing and manure storage and for applied manure distinguishing various combinations of animal types and manure types (solid and slurry), also accounting for the percentage implementation of emission-reducing techniques related to either housing systems or application techniques. Specific values are given in de Vries et al. (2023) with average numbers for the three countries (see Table 3-2).

Several factors other than emission-reducing techniques related to housing systems or application techniques also affect ammonia emissions, including meteorology, manure characteristics, and soil properties. Temperature, humidity, wind speed, and precipitation can all influence the rate of ammonia volatilization (the process of ammonia changing from a liquid or solid state into a gas). For example, higher temperatures increase the rate of ammonia volatilization, and larger wind speeds can disperse ammonia more quickly, leading to greater ammonia emissions. In addition, the method used to apply manure to agricultural fields can significantly affect ammonia emissions. Spreading manure directly onto the soil surface leads to high ammonia emission fractions due to the large surface area exposed to the atmosphere. On the contrary, injecting manure directly into the soil minimizes ammonia emission fractions by reducing the surface area exposed to the atmosphere and ensuring immediate contact with the soil.

The locally adapted models took into account some or more of these factors. In INTEGRATOR-NL, emission fractions for housing systems were based on commercial farms or experimental station measurements (Velthof et al., 2012). The information on manure application techniques was derived from statistics, and the emission fractions for manure application techniques were based on field experiments (Velthof et al., 2012). The emission fractions for the different fertilizer types were the same as the standard INTEGRATOR. The emission fraction for grazing by cattle was based on the results of studies by Bussink (1992, 1994). In INTEGRATOR-DK (Kros et al., 2018), the emission fractions for housing and storage emissions were based on the national average yearly housing type fractions for 1990–2010 and a time-independent emission fraction per housing type. The annual (weighted) mean emission fraction was derived for 2010 and was used in this study. Similarly, a yearly weighted mean emission fraction for manure application was calculated using yearly information at the national level on the used application technique (for liquid manure: injection, trailing hose, broadcast spreading, for solid manure: broadcast spreading) and the related emission fraction for the period 1985–2011. The emission fractions for the different fertilizer types were also used as in the standard INTEGRATOR. For INTEGRATOR-PT, the emission fractions were the weighted mean of the ones from European Environment Agency (2019), after tracking manure N flows and associated NH_3 emissions of all animal categories and manure types.

Table 3-2 Default values for national mean emission fractions (as % of the total N applied or produced) for housing and storage emission and application of livestock manure for the year 2010 as used in INTEGRATOR, the Netherlands *(de Vries et al., 2022),* **Denmark** *(Kros et al., 2018)* **and Portugal.**

Emission source	NH$_3$-N emission fractions (% of N flow)					
	Netherlands		Denmark		Portugal	
	INTEGRATOR	INTEGRATOR-NL	INTEGRATOR	INTEGRATOR-DK	INTEGRATOR	INTEGRATOR-PT
Housing manure						
Dairy cattle manure liquid	8.4	9.8	7.9	6.9	12.0	14.4
Dairy cattle manure solid	14.0	9.8	7.0	6.0	12.0	4.8
Other cattle manure liquid	14.0	9.8	7.8	10.1	12.0	14.4
Other cattle manure solid	9.6	9.8	7.0	6.0	12.0	4.8
Pig manure liquid	13.3	13.8	15.1	14.0	16.0	20.5
Pig manure solid	17.9	13.8	18.0	25.0	17.0	16.2
Sheep and Goat manure	10.0	9.8	15.0	/	10.0	11
Laying hens manure	9.3	16.0	19.0	13.5	13.7	14
Other poultry manure	10.5	16.0	12.6	20.0	16.5	16.5
Application manure						
cattle manure liquid	12.9	12.5	18.4	18.4	30.0	28.0
cattle manure solid	12.9	12.5	4.9	4.9	15.5	20.1
Pig manure liquid	3.4	8.2	9.1	9.1	13.5	21.1
Pig manure solid	11.6	8.2	4.4	4.4	13.6	13.8
Poultry manure	6.2	8.5	6.2	6.2	15.6	19.3
Grazing	7.0	2.1	6.7	6.7	10.0	8.3
Fertilizer						
• Urea (NH$_4$-based)	15.0	15.0	15.0	15.0	15.0	11.8
• Other fertilizers (NO$_3$ based)	2.3	2.3	2.1	2.1	3.1	3.0

3

3.2.3 Model validation

The CTM LOTOS-EUROS was used to assess the improvement in the emission products brought by the local adaptations. LOTOS-EUROS is a 3-dimensional regional CTM (Manders et al., 2017, 2009; Schaap et al., 2008b) that uses a description of the bidirectional surface-atmosphere exchange of ammonia (Wichink Kruit et al., 2017). The derived annual emission distributions from the standard and the locally adapted models were imported into LOTOS-EUROS to obtain modeled surface concentrations, which were then compared with measurements. The LOTOS-EUROS uses a set of temporal factors to break down annual total emissions into hourly emissions. The model is regularly used to address reactive nitrogen budgets (Banzhaf et al., 2015; Hendriks et al., 2016; van der Graaf et al., 2020, 2018), and we refer to these publications for a detailed model description.

For each of the three countries, two model runs were performed, focusing on the year 2018. Two model runs were performed for each country (a summary is given in Table 3-3). One used the annual emission distribution from the standard INTEGRATOR model, and the other used the emission result from the locally adapted models. Both runs used the spatially explicit time profiles from Ge et al. (2020), which accounts for meteorology and the timing of fertilization. The outputs of the model runs were total columns and surface concentrations, which were compared with satellite observation and in situ measurements, respectively, for validation. However, after investigation, comparisons with satellite observations from CrIS (Shephard and Cady-Pereira, 2015; Shephard et al., 2020) and IASI (Clerbaux et al., 2009) were not presented here since the spatial resolution of the total column observation was too coarse to detect the changes in spatial details in such small countries.

Table 3-3 The setup of the six simulations in this study. Two model runs, using the standard and locally adapted modeled emissions, were performed for each country.

Region	Spatial domain	Spatial resolution	Emission input
NL	longitude (2.0, 9.0)	0.03125 degrees in longitude	INTEGRATOR output for 2018
	latitude (50.0, 54.0)	0.015625 degrees in latitude	INTEGRATOR-NL output for 2018
DK	longitude (6.0, 17.0)	0.0625 degrees in longitude	INTEGRATOR output for 2018
	longitude (53.0, 59.0)	0.03125 degrees in latitude	INTEGRATOR-DK output for 2018
PT	latitude (-10.0, -6.0)	0.0625 degrees in longitude	INTEGRATOR output for 2018
	latitude (36.0, 43.0)	0.03125 degrees in latitude	INTEGRATOR-PT output for 2018

We used in situ measurements of surface concentrations to validate the improvement in the emission products brought by the local adaptions. In the Netherlands, measurements from the Measuring Ammonia in Nature (MAN) network were used, including monthly mean values of ammonia concentrations at 255 sites in 60 Natura2000 to detect the spatial and temporal patterns in concentration to assess the influence of local sources on different habitat types and geographical distribution (https://man.rivm.nl/) (Lolkema et al., 2015; Noordijk et al., 2020). For Denmark, data from the Danish Background Air Quality Monitoring Program were used. Currently, the levels of various nitrogen gases are tracked at five stations. These stations are strategically situated in areas not influenced by local emissions to represent the ambient air quality of specific regions accurately. Unfortunately, there are very limited available measurements on surface concentration for Portugal, even completely lacking for 2018.

3.3 Results

3.3.1 Comparison of emissions from INTEGRATOR and locally adapted models

The emission totals for the three countries were calculated for 2018 with the original INTEGRATOR and the three updated models using local information. The estimates are compared to each other and the nationally reported data to EMEP in Table 3-4 (NL), Table 3-5 (DK), and Table 3-6 (PT). Note that the animal management emissions equal the sum of animal housing and manure storage emissions. The corresponding emission maps for annual totals and each sector are also visualized to illustrate how the spatial distributions have been changed by using updated crop and livestock distributions and emission fractions.

The Netherlands
Table 3-4 compares emission totals per sector from the original INTEGRATOR, updated INTEGRATOR-NL, and reported values. One can see that the modeled annual emission totals from INTEGRATOR-NL are closer to the reported values with a 2.1% offset and 6.8% higher than the annual total from the original INTEGRATOR.

In total, 46.9%, 46.8%, and 42.6% of the emissions in the INTEGRATOR, INTEGRATOR-NL, and reported numbers are from cropland and grassland (manure and mineral fertilizer application and grazing). The original and updated annual emission maps (Figure 3-3(a) and Figure 3-3(b)) demonstrate that the two maps follow a similar pattern, but the updated map shows much more spatial details that are smoothened out in the original map. It is caused by the fact that INTEGRATOR-NL calculated emissions at the parcel level, whereas INTEGRATOR evenly allocates the emissions in an NCU all over the NCU. Through the even

allocation across an NCU, even large urban areas and forests receive ammonia emissions from agriculture. Besides that, the distributions from INTEGRATOR-NL (Figure 3-3(d)) display new hot spots (e.g. in the center (Flevoland) and southeast (North Brabant) and Zeeland). In addition, we observe a trend in which the emissions from manure application and grazing are shifting from the west to the east of the Netherlands. The reason lies in the crop distributions showing larger coverage of fodder, temporary grassland, wheat, and maize in these areas, which results in a larger allocation of manure there.

Table 3-4 Annual agricultural ammonia emission totals per sector from the original INTEGRATOR, the updated INTEGRATOR-NL, and the national reporting to EMEP for 2018 (unit: Gg NH$_3$).

	Netherlands		
	Original	Updated	Reported
Cattle management	33.5	32.4	34.9
Pig management	13.0	13.5	15.3
Poultry management	8.9	13.4	12.3
Manure application and grazing	39.2	43.1	37.4
Mineral fertilizer application	9.8	9.1	9.2
Total	104.4	111.5	109.2

For animal management, the modeled emission totals from cattle and pig management are similar and closer to the reported values. However, poultry management emissions in INTEGRATOR-NL are approximately 50% larger than in the original, which is in line with the relative increase in the updated emission fraction (see Table 3-2). Moreover, because the INTEGRATO-NL sees animal houses and manure storage as point sources, the updated maps (Figure 3-4(b) (d) (f) (h)) only show emissions at the locations where animal houses are. In contrast, the original maps (Figure 3-4(a) (c) (e) (g)) demonstrate homogeneity in agricultural areas.
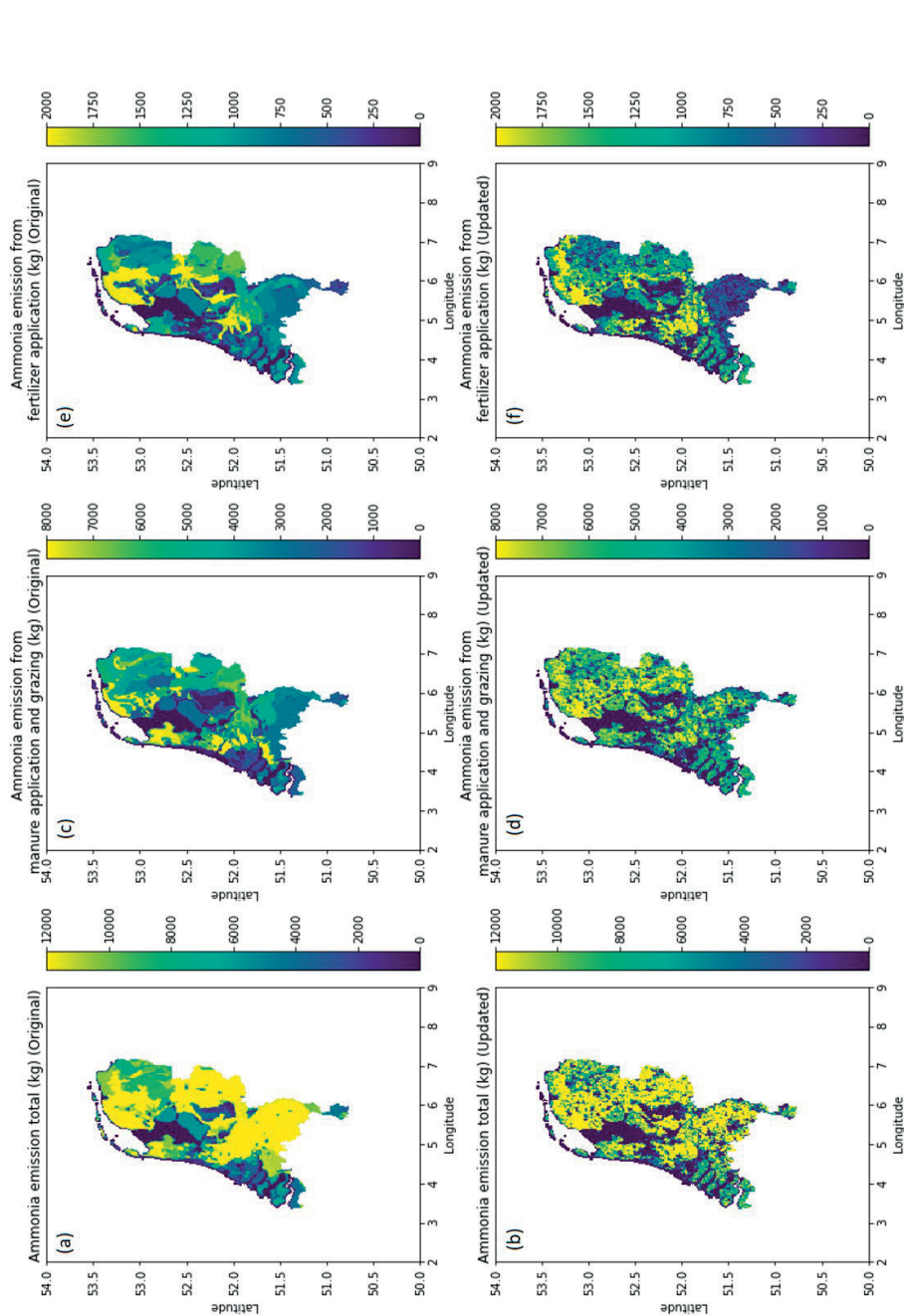
Figure 3-3 Maps of annual total emission (a, b), emission from manure application and grazing (c, d), and emission from mineral fertilizer application (e, f), derived from the standard INTEGRATOR (a, c, e) and INTEGRATOR-NL (b, d, f). The unit is in kg NH$_3$.
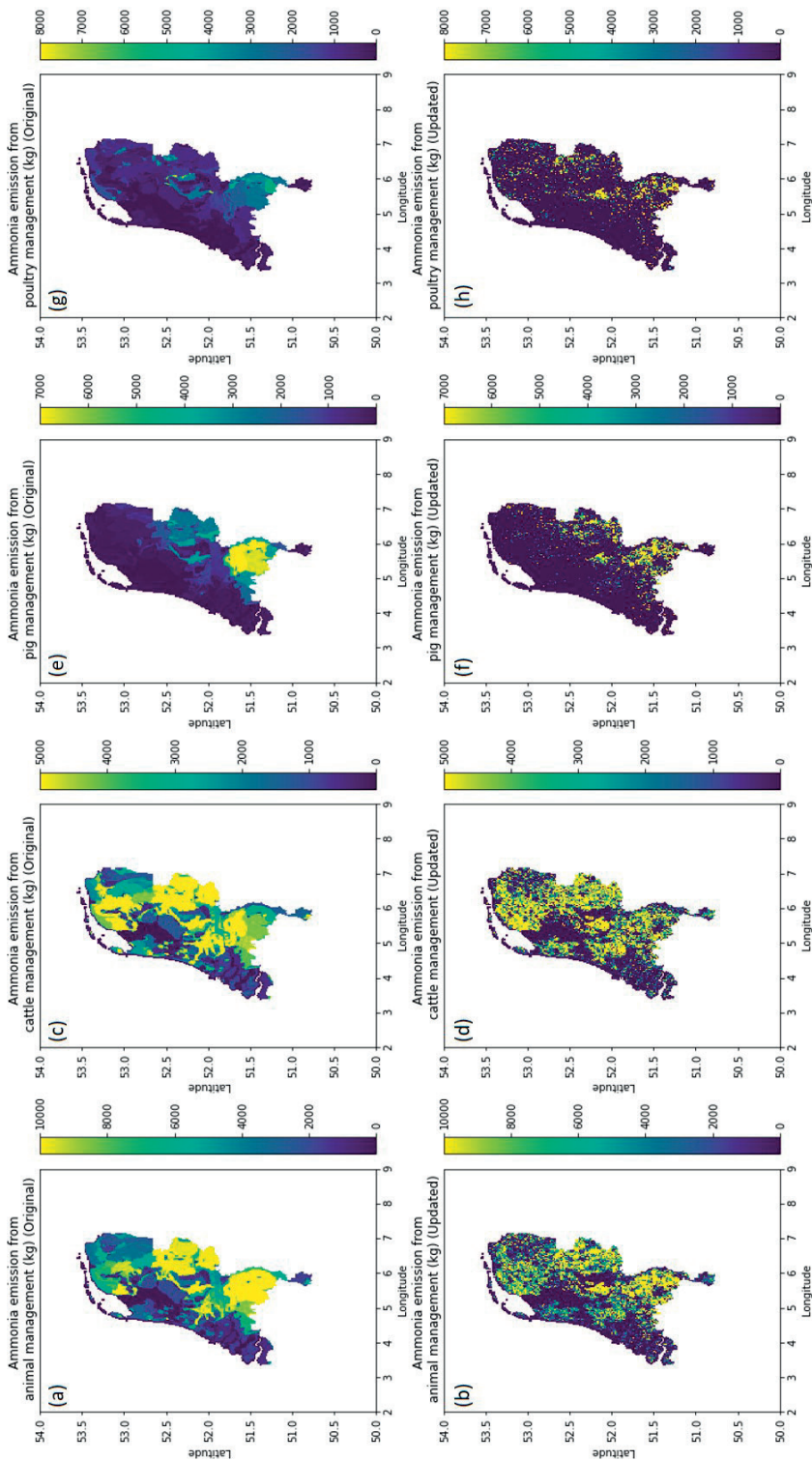
3

Figure 3-4 Maps of total animal management emission (a, b), cattle management emission (c, d), pig management emission (e, f) and poultry management emission (g, h), derived from the standard INTEGRATOR (a, c, e, g) and INTEGRATOR-NL (b, d, f, h). The unit is in kg NH$_3$.

Denmark

The comparison of emission total per sector for Denmark is listed in Table 3-5. The annual emission totals from INTEGRATOR and INTEGRATOR-DK are 4.6% lower and 12 % higher than the reported value, respectively. The sector allocations in the emissions show differences. The emission from cattle management in INTEGRATOR-DK is 42% larger than that in the European model version and closer to the reported emission because Statistics Denmark reports more cattle in the country. The modeled pig management emission totals are comparable, but they are 58.3% (original) and 43.6% (updated) larger than the national reported value. The grazing emission totals derived from both models are very different from each other and from the reported value (2.7 Gg), with the original total being 81.4% lower (0.5 Gg) and the updated one (4.4 Gg) being 63% larger than the reported one. Both modeled emission totals from manure application are larger than the reported numbers due to larger animal numbers and associated excretion, which are also reflected in the animal management emissions. As a result, both modeled emission totals from mineral fertilizer application are smaller than the reported number, with the updated total being 45% lower than the original one. This is due to the fact that INTEGRATOR uses an N-balance approach in which less mineral fertilizer is needed in case the N-demand can be fulfilled by a larger N excretion from livestock.

It can be seen that the maps from INTEGRATOR (Figure 3-5(a) (c) (e) (g) and Figure 3-6(a) (c) (e) (g)) show a high level of homogeneity because the model allocated emissions almost all over NCUs that are rather large in size. The results from INTEGRATOR-DK are more spatially variable. The differences in the spatial distributions of emissions from manure application (Figure 3-5(c) (d)) are quite significant. There is very low emission in the midwestern part of Denmark in the updated maps, which is attributed to the cultivation of vegetables in this region. Vegetables are regarded as arable with no manure application, so there is no emission from manure application. Emissions from livestock management also show more spatial variations thanks to the more detailed animal number data used. At the same time, there are almost no animal management emissions in the Midwest, which is another reason why manure application emissions are low (lack of manure).

Table 3-5 Emission totals per sector from the standard INTEGRATOR and INTEGRATOR-DK, compared with officially reported emission totals from EMEP for 2018 (unit: Gg NH$_3$).

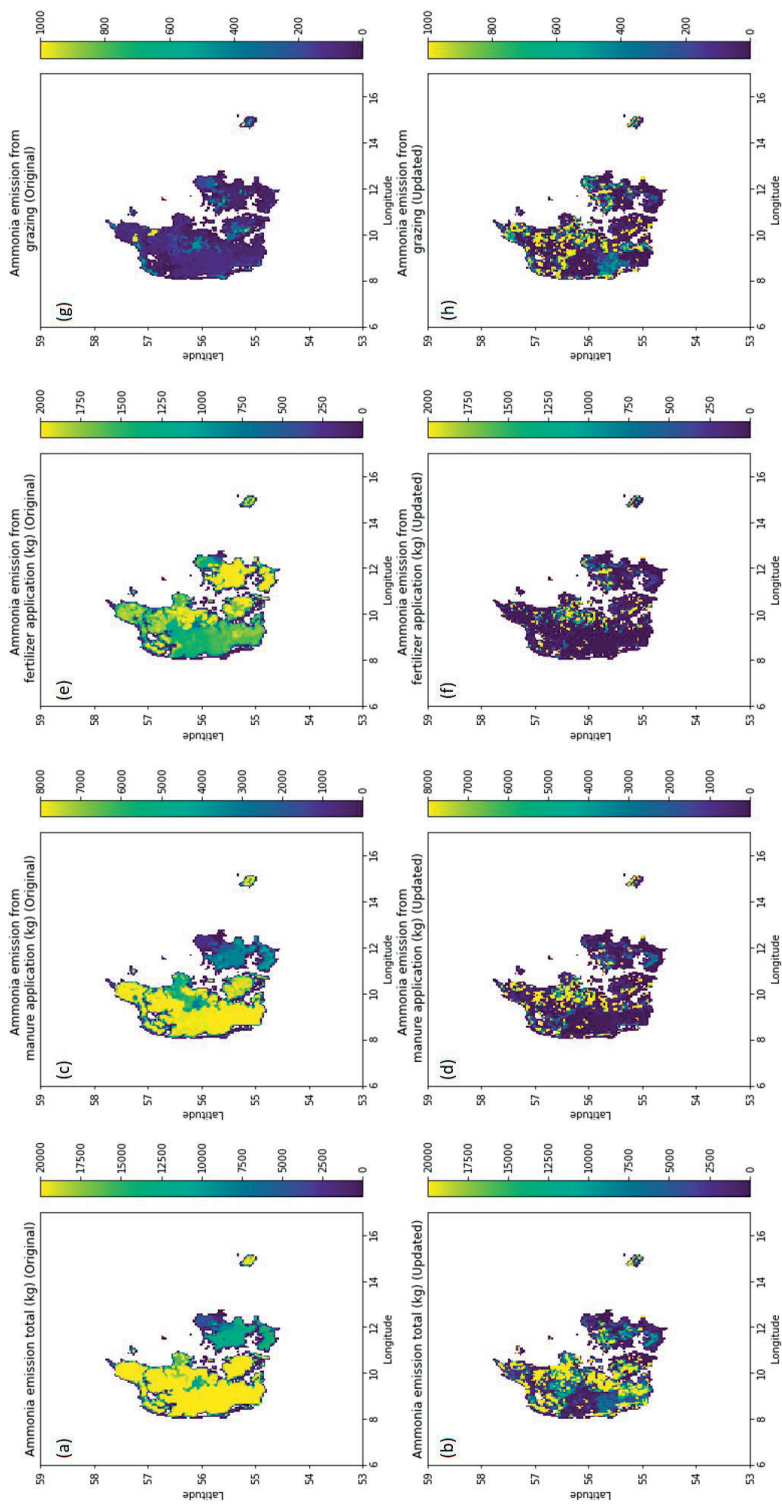|	Denmark		
	Original	**Updated**	**Reported**
Cattle management	13.1	18.6	17.6
Pig management	23.6	21.4	14.9
Poultry management	3.0	4.0	2.5
Manure application	20.9	26.6	18.9
Mineral fertilizer application	5.1	2.8	12.8
Grazing	0.5	4.4	2.7
Total	66.1	77.9	69.3

Figure 3-5 Maps of annual total emission (a, b), emission from manure application (c, d), emission from mineral fertilizer application (e, f), and emission from grazing (g, h), derived from the standard INTEGRATOR (a, c, e, g) and INTEGRATOR-DK (b, d, f, h). The unit is in kg NH$_3$.
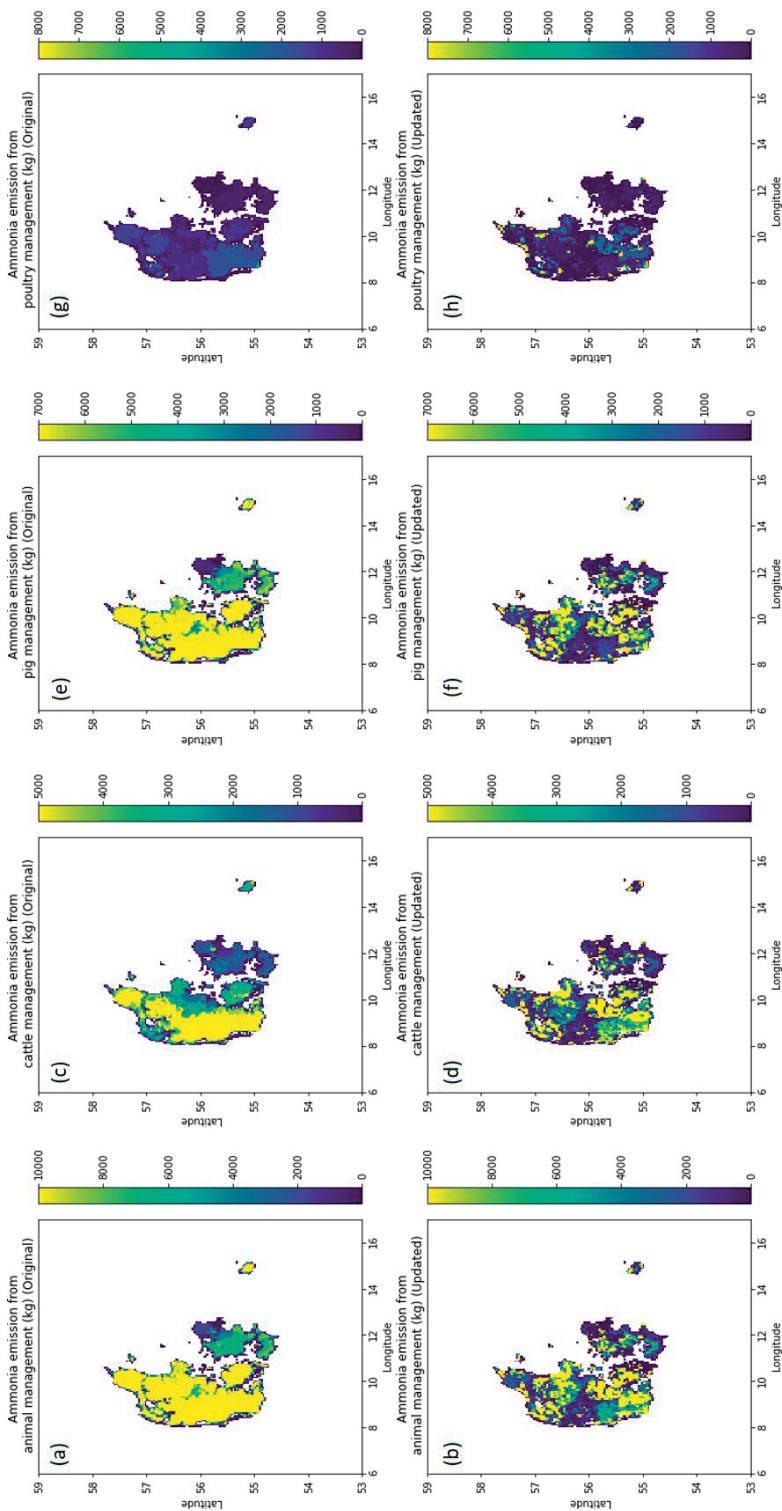
3

Figure 3-6 Maps of total animal management emission (a, b), cattle management emission (c, d), pig management emission (e, f), and poultry management emission (g, h), derived from the standard INTEGRATOR (a, c, e, g) and INTEGRATOR-DK (b, d, f, h). The unit is in kg NH₃.

Portugal

The comparison of Portuguese emissions per sector between the models and reported values is listed in Table 3-6. One can see that the consistency between the original INTEGRATOR (lower by 33%) and the national reporting is much smaller than that for the updated emission total (lower by 5%). The differences in animal management emissions between the original and updated model come from cattle and poultry, which are mainly caused by the differences in animal numbers in cattle and poultry. The density maps of livestock (Figure 3-2) show that the original and updated distributions of cattle and poultry have similar high-density areas, but the updated map indicates a higher magnitude and larger animal number total overall. The cattle management emission total in the updated model is two times larger than that in the original model but closer to the reported emission total. On the contrary, the updated poultry management emission total is almost twice the reported value, while the original total is only 12.3% lower than the reported value. The spatial distribution of animal management emissions from the two models is similar, with the hotspots in the original maps (Figure 3-8(a) (c) (e) (g)) becoming even brighter in the ones in the updated estimates (Figure 3-8(b) (d) (f) (h)). This is more or less corresponding to the livestock distribution in Figure 3-2 because the original animal numbers were scaled using the nationally reported animal number data at the municipality level.

The emission total from manure application witnesses a 24.8% drop from the original model to the updated one, bringing the emission total closer to the reported value. The cattle and poultry populations in the updated model are around 27% and 47% higher than those in the original model. As a result, mineral fertilizer emissions decline, and that from grazing rises in INTEGRATOR-PT. The emission maps of manure application (Figure 3-7(c) (d)) also show more concentrated and new hot spots. For example, Figure 3-7(d) shows a large patch of manure application emission in the south, which does not occur in the original map displayed in Figure 3-7(c). This area does not have the largest livestock density, meaning the cause is in the crop distribution. The census data indicate that the dominant crops in this area are fodder and temporary grassland, whereas the input of the European model version provides a large coverage with olive orchards. Olive is categorized as arable crop with low use of manure. Manure allocated to fodder and temporary grassland is determined by a fraction of total available manure, which is much more than the amount that olive needs. The emission map of mineral fertilizer application from INTEGRATOR-PT (Figure 3-7(f)) is generally lower than the original results (Figure 3-7(e)). The more significant differences are founds in the regions where the animal density is high. The larger cattle population (see Figure 3-2) in INTEGRATOR-PT results in larger grazing emissions (Figure 3-7(h)), with the areas of high emission levels resembling the locations with the highest cattle density.

Table 3-6 Emission totals per sector from the standard INTEGRATOR and INTEGRATOR-PT, compared with officially reported emission totals from EMEP for 2018 (unit: Gg NH$_3$).

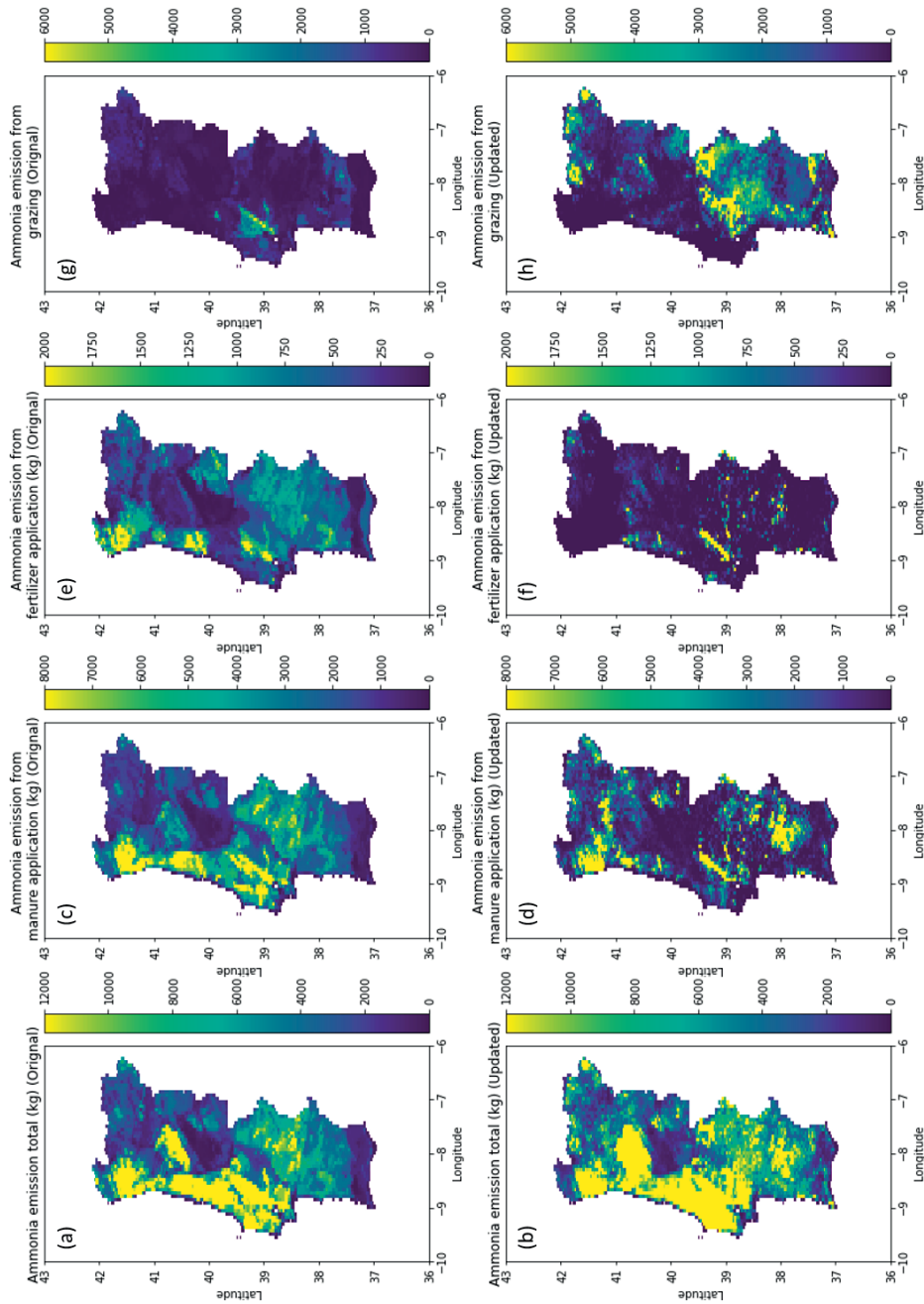|	Portugal		
	Original	**Updated**	**Reported**
Cattle management	2.1	6.0	8.4
Pig management	5.6	6.8	6.0
Poultry management	6.4	14.0	7.3
Manure application	14.5	10.9	11.8
Mineral fertilizer application	2.8	1.0	6.1
Grazing	1.7	7.8	10.0
Total	33.2	47.0	49.6

Figure 3-7 Maps of annual total emission (a, b), emission from manure application (c, d), emission from mineral fertilizer application (e, f), and emission from grazing (g, h), derived from the standard INTEGRATOR (a, c, e, g) and INTEGRATOR-PT (b, d, f, h). The unit is in kg NH$_3$.
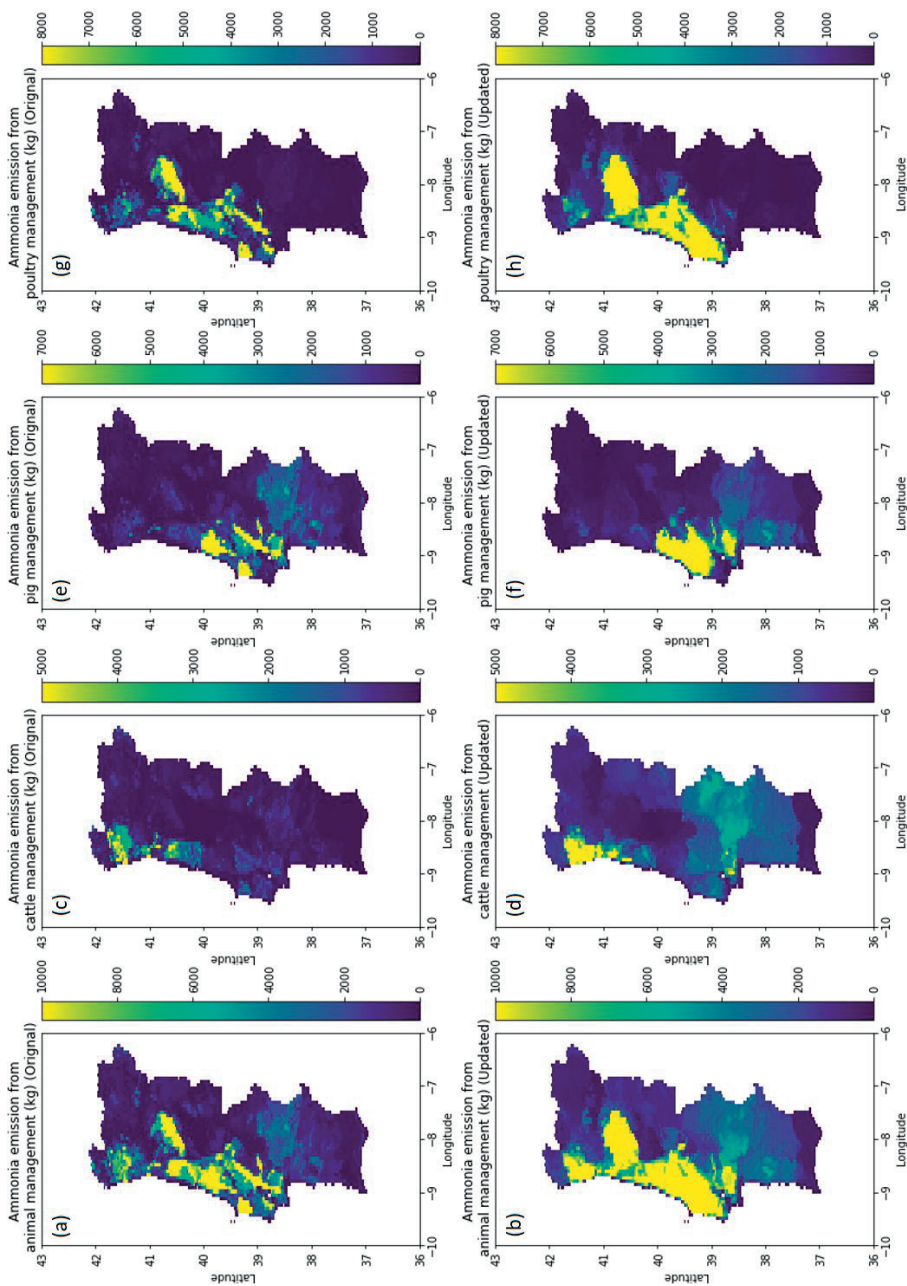
3

Figure 3-8 Maps of total animal management emission (a, b), cattle management emission (c, d), pig management emission (e, f), and poultry management emission (g, h), derived from the standard INTEGRATOR (a, c, e, g) and INTEGRATOR-PT (b, d, f, h). The unit is in kg NH$_3$.

### 3.3.2 Comparison of monthly and season-averaged surface concentrations

The LOTOS-EUROS model performance using the original INTEGRATOR and its updated version were compared to measurements for evaluation. However, due to the lack of measurement data, the assessment was not possible for Portugal. And for Denmark, three out of the five stations provided comparable results for each simulation, which is also insufficient to draw strong conclusions. A much more thorough assessment was conducted for the Netherlands thanks to the large number of ammonia concentration measurements at the MAN stations. Most crops are fertilized in springtime. At the same time, the variability in the emissions from animal housing and manure storage is more subtle, with enhanced emissions during summer due to higher temperatures. Therefore, in agricultural areas, ammonia emissions in springtime (February-April) are dominated by application activities. In contrast, emissions in summer (May-October) are more influenced by animal housing and manure storage. In winter (mid-November to January), there are only emissions from animal housing and manure storage. Therefore, in this study, the MAN monthly measurements were divided into springtime (February-April) and wintertime (Nov-Jan). We investigate the impact of detailed crop and livestock information by looking into the two periods.

Figure 3-9 shows the scatterplot comparison of monthly ammonia surface concentrations between measurements and the modeled outputs. For spring, it is evident that the updated model outperforms the original one, with a narrower spread in the scatter plot that fits more nicely around the y=x line. This finding is also supported statistically. Table 3-7 shows that the updated simulation has a lower bias, higher correlation, better model efficiency, and index of agreement. From the comparisons for wintertime in Figure 3-9 (c) and (d), it is apparent that both are rather noisy with lower correlation. The latter may be due to the larger effect of representativity issues with respect to the location of farms which plays less of a role in spring. Still, all statistical parameters listed in Table 3-7 indicate improvement, although the improvement for the correlation is very modest.. These findings mean that both the crop and livestock inputs have improved the spatial and temporal variability in ammonia emissions.

The comparison above accounts for all monthly observations. We also created the comparison for the averaged concentration values over the spring- and winter periods. Figure 3-10(a) shows that using INTEGRATOR, the model underestimates springtime ammonia surface concentration in the west but overestimates in the east in the Netherlands. Through INTEGRATOR-NL, this phenomenon has been softened, as shown in Figure 3-10(b), although the trend still exists. Figure 3-10(c) indicates that the emission distribution from the original model leads to an overall underestimation of ammonia concentrations during winter. While the updated model performs better in the center of the country, a tendency to overestimate observed levels is found for the (south)east. The

use of actual farm location clearly lifts the modeled concentrations for the stations with the largest concentrations in winter, see Figure 3-11. The scatter plot clearly illustrates a better correlation between the measurements and the updated outputs, verified in Table 3-8. The table confirms that the updated model outperforms all the criteria in both spring and winter, highlighting the improvements in spatial distribution brought by the high-resolution livestock and crop data.

From the comparisons presented above, we can conclude that the detailed crop and livestock distributions and data on the actual animal house locations improved the spatial and temporal distribution of ammonia emissions, highlighting the importance of the availability of the data in ammonia emission modeling.
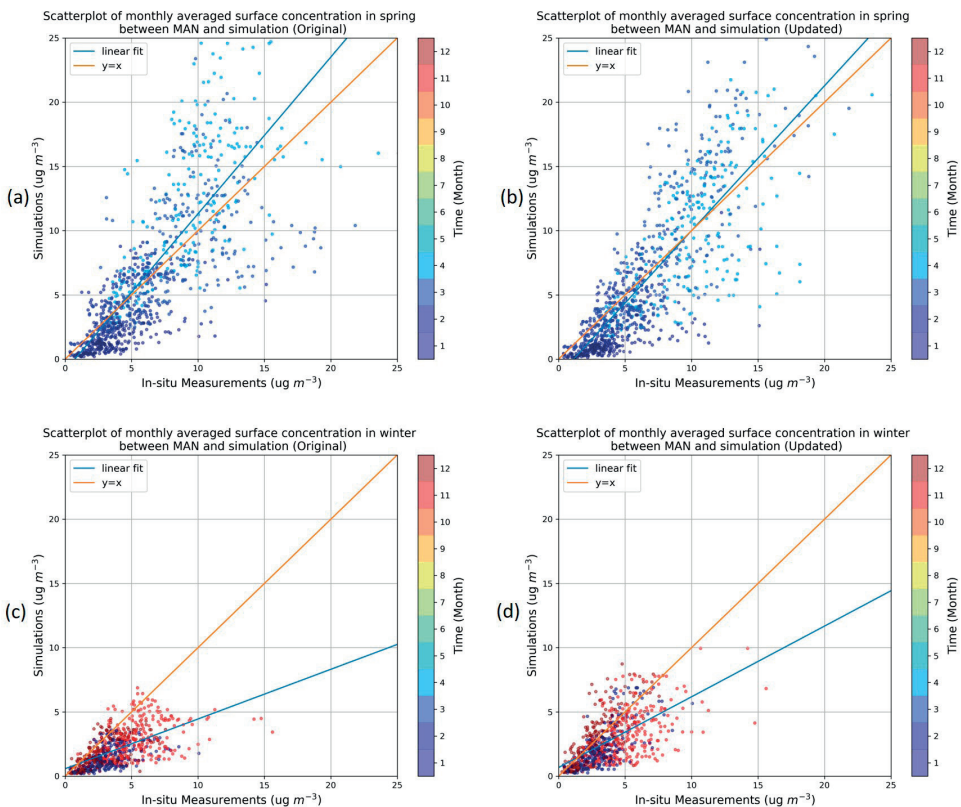
Figure 3-9 The scatterplots of monthly surface concentrations between MAN in situ measurements and simulations. In (a) and (b), all monthly measurements in spring (February -April) are compared with the original and updated modeled results. In (c) and (d), all monthly measurements in summer (May-October) are used for validation of the original and updated model.

Table 3-7 Quality assessment of the comparison of monthly surface concentrations between MAN in situ measurements and model outputs for spring and summer

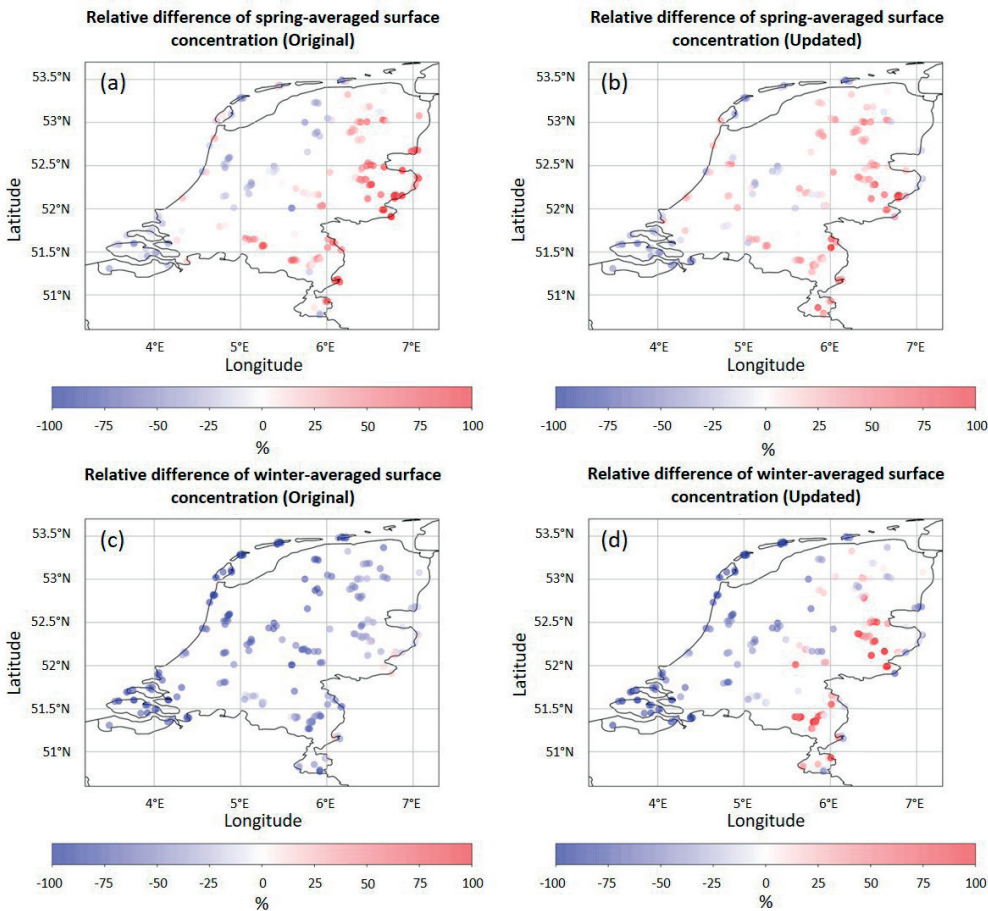| Time block	Scenario	Relative bias (%)	Correlation	NRMSE (%)	NMAE (%)	EF	IA
Spring	*Original*	9	0.73	11	41	0.51	0.79
	Updated	6	0.82	11	39	0.66	0.88
Winter	*Original*	46	0.6	37	91	-2.27	0.59
	Updated	27	0.62	21	55	-0.17	0.73

Figure 3-10 The relative difference of season-averaged surface concentrations between simulations and MAN measurements. (a) and (c) are the maps of the relative difference between the original model and measurements in spring, respectively. (b) and (d) are the maps of the relative difference between the original model and measurements in winter, respectively.
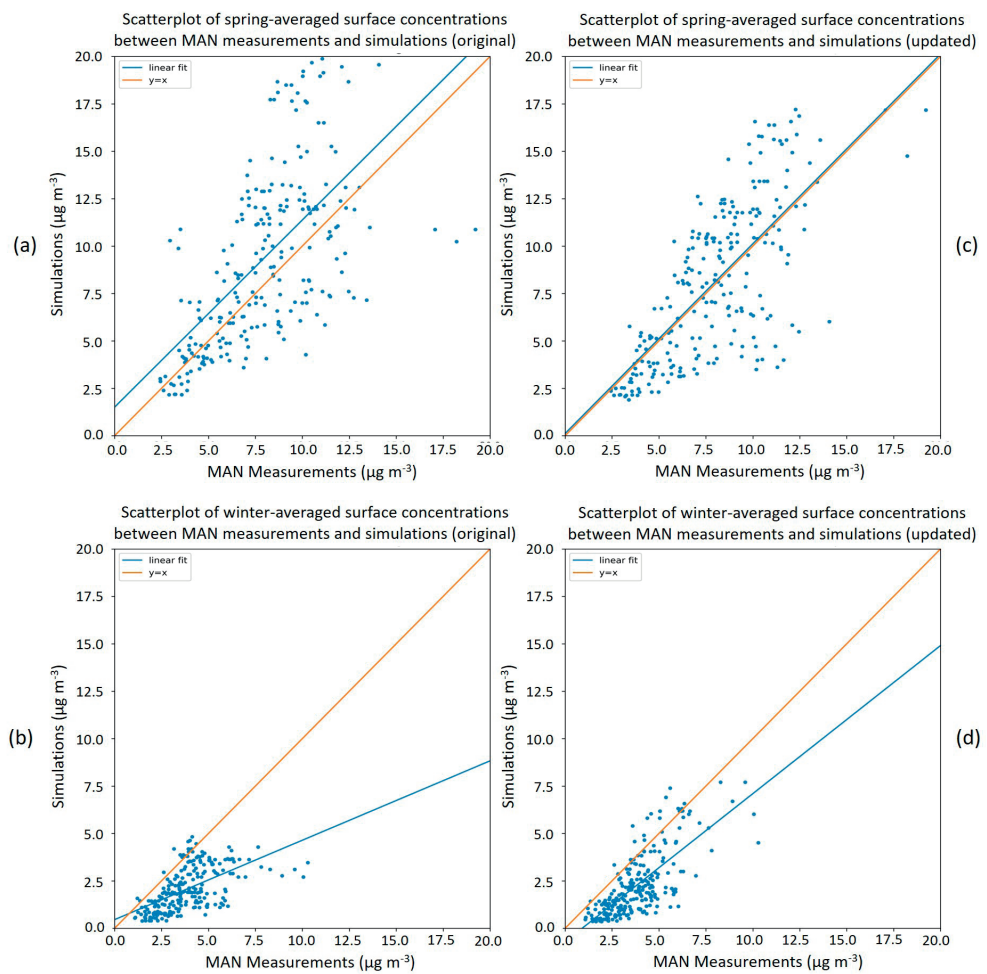
Figure 3-11 The scatterplots of season-averaged surface concentrations between MAN in situ measurements and simulations. In (a) and (b), averaged surface concentration at each station in spring (February-April) are compared with the original and updated modeled results. In (c) and (d), averaged surface concentration at each station in summer (May-October) are used for validation of the original and updated model.

Table 3-8 Quality assessment of the comparison of season-averaged surface concentrations between MAN in situ measurements and model outputs for spring and summer

Time block	Scenario	Relative bias (%)	Correlation	NRMSE (%)	NMAE (%)	EF	IA
Spring	Original	18	0.61	17	32	0.28	0.70
Spring	Updated	2	0.72	18	18	0.52	0.83
Winter	Original	46	0.58	50	88	-2.7	0.54
Winter	Updated	39	0.73	26	72	-0.3	0.71

3.4 Discussion and conclusion

3.4.1 Ammonia emission from animal housing and manure storage

INTEGRATOR does not account for the spatial variation of housing types of each animal category within a country. The emission fractions for animal houses and manure storage in INTEGRATOR are average values per animal category and manure category (solid manure or liquid manure) per country (De Vries et al., 2020a; Kros et al., 2012) only accounting for the percentage of animal houses and manure storage facilities that occur in high, medium, or low emission systems.

The housing emission for the Netherlands (Figure 3-4) has the most detailed spatial resolution, followed by INTEGRATOR-DK (Figure 3-6) and INTEGRATOR-PT (Figure 3-8). This is because INTEGRATOR-NL calculates housing emissions at the farm level, and INTEGRATOR-DK refined the animal number detail. At the same time, we simply conducted a scaling based on national municipality-level data to INTEGRATOR-PT. This method did not increase the spatial details of animal number distribution. In addition, INTEGRATOR-DK and INTEGRATOR-PT still allocate housing emission estimates within an NCU evenly all over the polygon, regardless of the actual locations of animal houses and manure storage facilities. Therefore, as a first step, a land use database can be utilized to exclude nature and urban during the reallocation of emissions. In this way, we can reduce the uncertainties brought by the misallocation of housing emissions. Of course, knowing animal house locations would avoid such a procedure. However, in most countries, data on animal house locations are often unavailable (or not openly available). An alternative detection of livestock houses using satellite imagery may be a viable direction in improving ammonia emission modeling.

Animal houses, distinguished by their distinct traits, such as the hue of the roofs, construction materials, and land use in the surrounding areas, can be identified through satellite images or aerial photography. These methods are both economical and effective for large-scale studies due to the continuous and repeated coverage provided. Sentinel-2,

3

a satellite system that delivers high-resolution multispectral imagery, has gained prominence as an invaluable asset for such tasks. The process of automatically pinpointing the locations of animal dwellings could be executed through a machine-learning algorithm. In addition, using land use maps can aid in zeroing in on the farming regions that typically host these animal accommodations. These maps can also be generated through the use of supervised categorization techniques, wherein representative samples are marked for diverse types of land use such as agriculture, forests, water bodies, and so on.

3.4.2 Ammonia emission from manure and fertilizer application

The more significant improvements in the spatial and temporal distribution of ammonia emissions in springtime indicate that detailed crop distributions are essential for estimating the manure N and fertilizer N distribution. However, a high-resolution crop map is not available for each country or updated on a yearly basis. Nowadays, multitemporal multispectral data collected from optical satellites are being employed to gauge the geographical distribution of an array of crops, courtesy of their efficiency and labor-saving advantages (Yan et al., 2021). Previous research has employed remote sensing information to conduct assessments of time series of vegetation indices, intending to procure data on agricultural land utilization and crop growth (Dubovyk et al., 2015; Marais Sicre et al., 2016; Vaglio Laurin et al., 2018; Waldhoff et al., 2017). The advent of the Sentinel-2 instruments heralds possibilities for more refined differentiation amongst diverse crop categories, attributed to their sensor and orbit features, high-resolution capabilities, and relatively rapid revisit intervals (Belgiu and Csillik, 2018; Kobayashi et al., 2020; Sonobe et al., 2018; Yi et al., 2020). Benevides et al. (2022) derived a parcel-level crop map for the entire area of continental Portugal for 2020 using multitemporal Sentinel-2 data and the Portuguese Land Parcel Identification System (LPIS), achieving an overall accuracy of 85% for the map at the national level. Blickensdörfer et al. (2022) used the assimilation of dense time series data from Sentinel-2 and Landsat 8 in combination with monthly Sentinel-1 composites and environmental data to derive national crop maps for Germany. Combining optical, Sentinel-1, and environmental data increased overall accuracies by 6% to 10%. A remote sensing-based approach to creating a crop map would be beneficial to develop a standardized processing chain of an ammonia emission model that can be applied to any country.

3.4.3 Emission fractions

Ammonia emissions from manure are notably susceptible to climatic conditions (Jiang et al., 2021). Characterizing the proportion of nitrogen in excreta that evaporates as ammonia as a constant value might result in substantial inaccuracies. Sutton et al. (2013) demonstrated that emission rates escalated by a factor of nine within the 5 to 25 degrees Celsius temperature range, with auxiliary influences arising from humidity and

rainfall (Riddick et al., 2017). Skjøth and Geels (2013) accentuated the profound impact that interannual meteorological fluctuations and broader climate variations have on ammonia emissions, attributing it to the high sensitivity of ammonia volatilization to ambient temperature. Furthermore, the quantity of nitrogen released as ammonia after manure is also subject to soil attributes such as pH levels, moisture content, and mineral composition (Raymond et al., 2016).

Research considering the previously discussed effects on ammonia emissions from agricultural activities is limited. A majority of the earlier studies have relied on empirical approaches. For example, Sommer and Hutchings (2001) analyzed diverse empirical models that employed equations derived from experiments to forecast ammonia volatilization after slurry application. Nonetheless, these models typically examined merely one or two variables without delving into the interplay among these factors. Misselbrook et al. (2000) computed ammonia emission fraction under varying agricultural practices in the UK, but incorporating climatic influences in this emission fraction was relatively minimal. An alternative approach to estimating ammonia emission fraction is using process-based models. These models integrate a theoretical comprehension of the pertinent processes (Móring et al., 2016; Nemitz et al., 2001; Sutton et al., 1995). Hafner et al. (2019) developed a semi-empirical dynamic model for predicting ammonia volatilization and emission fractions in field-administered slurry. They estimated values for parameters that measure the impact of predictor variables such as slurry dry matter content, application technique, application volume, incorporation depth (shallow or deep), ambient temperature, wind velocity, and precipitation rate on partitioning and transfer rates. Therefore, instead of using country-specific emission fractions, spatially explicit emission fractions for use in our emission model may be obtained using models which account for meteorology, manure properties, application techniques, etc.

3.4.4 Conclusion and outlook

High-resolution crop maps, municipality-level livestock statistics, and emission fractions based on local experiments were utilized to locally adapt the EU-scale emission model INTEGRATOR to the Netherlands (INTEGRATOR-NL), Denmark (INTEGRATOR-DK) and Portugal (INTEGRATOR-PT), to assess its impact on the spatial variability in agricultural ammonia emissions. INTEGRATOR-NL and INTEGRATOR-DK were previously developed. We updated INTEGRATOR-DK and INTEGRATOR-PT with the official and publicly available crop map and animal number statistics for 2018. The resulting emission estimates from the original INTEGRATOR and the adapted models were compared to each other and also to the officially reported emission totals. Due to the limited availability of measurement data, the updates were only validated for the Netherlands for spring and summer. This was done by comparing the simulated surface concentration using the emission products with MAN in situ measurements. The updated Dutch model improved ammonia distribution

both spatially and temporally, being most evident in spatial distribution (season-averaged surface concentration). As with the Netherlands, the modeled results for Denmark and Portugal introduced regions with large emissions that were not derived in the original model. However, the results for Portugal and Denmark could not be validated due to the lack of measurements, calling for more measurement stations in areas likely to be affected by nitrogen deposition. Nevertheless, our study shows that detailing crop and livestock distributions is an essential step to modeling spatial distribution of ammonia emissions with high resolution. The developed method to process and harmonize different crop and livestock inputs is also useful in obtaining a more detailed spatial distribution of ammonia emissions for other countries.

A comparison of agricultural ammonia emissions for the Netherlands, Denmark, and Portugal using a Europe-wide and locally adapted approaches | **123**

3

Improving spatial and temporal variation of ammonia emissions for the Netherlands using livestock housing information and a Sentinel-2-derived crop map

Ammonia emissions to the atmosphere have a range of negative impacts on environmental quality, human health, and biodiversity. Despite the considerable efforts in quantifying spatially explicit ammonia emissions, there are significant uncertainties in ammonia emission estimates at regional scales. We aimed to improve the modeling of atmospheric ammonia emission variability in space and time across the Netherlands by updating an agricultural ammonia emission model with a newly derived high-resolution crop map and a livestock housing location database of the Netherlands. To generate a crop map of 12 agricultural land cover classes, we applied random forest classification to the multi-temporal multispectral observations of surface reflectance and vegetation indices derived from Sentinel-2. The crop statistics were used to calculate ammonia emission distribution based on nitrogen demand (manure and mineral fertilizer needed) of different crop types using the INTEGRATOR model. Next, the crop map was utilized to spatially allocate the ammonia emissions to a high-resolution grid across the Netherlands. In addition, ammonia emissions from livestock housing systems were introduced as point sources using location data from the Geographic Information Agricultural Business system. The temporal emission variability was updated using a recently developed TIMELINES module. After the spatial and temporal distribution of ammonia emission was obtained with the crop map and housing information, it was imported into the chemistry transport model LOTOS-EUROS to model ammonia surface concentration for validation with in situ measurements.

The performed crop classification has an average accuracy score of 0.73. The derived crop map was compared with Dutch national statistics, and the results showed that the absolute median of the relative difference between Sentinel-2 derived crop areas and national statistical information is around 5%. The newly modeled ammonia monthly surface concentrations compared better with in situ measurements in terms of the magnitude and temporal variability than those derived from the original emission distribution, indicating that the temporal distribution of ammonia emissions was improved. The comparison of modeled and measured annual averaged surface concentrations illustrated that the spatial distribution of ammonia emission was also improved. All model performance indicators significantly improved, and the performance of the updated model was more stable and robust. The improvement was more evident at the stations where livestock housing is the main emission source. This study illustrates that apart from a satellite-derived crop map, information on the locations of animal housing systems also plays an essential role in better estimates of the spatial and temporal distribution of ammonia emissions. It can be worthwhile to extrapolate the method to other regions in Europe and elsewhere.

Abstract

4.1 Introduction

Ammonia (NH_3) emission to the atmosphere has increased substantially on a global scale during the twentieth century in response to the demand for food of a rapidly growing population that leads to enhanced nitrogen fertilization (Erisman et al., 2008). Large increases are mainly witnessed in areas with intense agricultural activities, such as Europe, the US, and China, with declines in the last decade, especially in Europe (Schmitz et al., 2019) and the US (Gilliam et al., 2019) due to legislation. Ammonia is the primary form of reactive nitrogen in the environment (Sutton et al., 2014), and its primary emission source is agriculture which contributes to more than 90% of the total emissions in EU-28 (Elzing and Monteny, 1997; Velthof et al., 2012). Agricultural ammonia is lost to the environment during and after fertilizer and manure application to the land, through animal excretion in housing systems, and during grazing (Erisman et al., 2007; Galloway et al., 2003).

The atmospheric lifetime of ammonia is limited to several hours as it is effectively removed by dry and wet deposition (Schaap et al., 2017a; Fangmeier et al., 1994). Once deposited, the reduced nitrogen components contribute to the acidification and eutrophication of forests and other (vulnerable) terrestrial ecosystems (Bowman et al., 2008; de Vries et al., 2014), which can lead to biodiversity loss (Bobbink et al., 2010; Krupa, 2003; van Dobben and de Vries, 2017; Midolo et al., 2019). In addition, ammonia reacts with sulfuric and nitric acid in the atmosphere, leading to the formation of fine particulate matter (Schaap et al., 2004b), which is an important cause of smog and consequently threatens human health with heart and lung conditions (Brunekreef and Holgate, 2002; Fowler et al., 2009; Pope et al., 2009). Ammonia remains a major concern as either near-zero or increasing trends have been observed in concentration and deposition measurements over large parts of Europe (Colette et al., 2016). Hence, a better understanding of ammonia emission and its fate in the atmosphere is of great significance.

The Netherlands is a densely populated, urbanized, and industrialized country in western Europe. As the second-largest exporter of food and agricultural products globally, the small country has a very intensive agricultural system (Dollmann et al., 2021). Consequently, the Netherlands has the highest ammonia emission density in Europe, with an average of about 3180 kg NH_3-N per square kilometer (Wever et al., 2019). Due to the short lifetime of ammonia in the atmosphere, a large fraction of the emission deposits within the country. It is modeled that Dutch agriculture contributes nearly half of the total nitrogen deposition to its nature areas (Stokstad, 2019). It is estimated that in 118 of 162 Dutch nature reserves, the nitrogen deposition exceeds critical load thresholds by an average of 50% (Stokstad, 2019). As control regulations have been gradually implemented in the last 30 years, the reported ammonia emissions in the Netherlands declined by 51% and 22% respectively between 1993-2005 and between 2005-2014, but the trends in emissions and

concentrations of ammonia diverge over the period 2005–2014 (van Zanten et al., 2017). A recent study into this discrepancy showed that the effects of meteorological variability and changing atmospheric chemical regimes could explain one-third of the difference between the observed and modeled trends in concentrations (Wichink Kruit et al., 2017). The remaining inconsistency was not explained, but an incomplete understanding of the processes involved in ammonia emissions likely plays a crucial role in this context. However, because of expanding dairy operations, Dutch ammonia emissions have not significantly decreased in the last decade (Stokstad, 2019).

There are still significant uncertainties in ammonia emission estimates which are prone to considerable spatial and temporal variability (Battye et al., 2003; Sutton et al., 2003; Erisman et al., 2007; Sutton et al., 2014). Many studies have highlighted that the spatial and temporal variability of ammonia concentrations modeled with chemistry transport models (CTMs) using static time profiles, such as GEOS-Chem (Paulot et al., 2014; Bey et al., 2001), MOZART-4 (Emmons et al., 2010; Liu et al., 2017), CHIMERE (Hamaoui-Laguel et al., 2011, 2014), LOTOS-EUROS (Hendriks et al., 2016), and PMCAMx (Pinder et al., 2006), is poorly represented and needs improvement. Several studies have developed approaches to include meteorology-dependent emission variability in CTMs (Backes et al., 2016; Skjøth et al., 2011; Hendriks et al., 2016). Many studies are based on the work of Skjøth et al. (2004), who proposed a dynamic parameterization of the temporal variation of NH_3 emission based on meteorology, information about agricultural practice, and a simple crop growth model. The parameterization was then improved by including the effect of ventilation rates inside buildings, ambient wind speeds and a more realistic description of temperatures inside animal housing systems (Gyldenkærne et al., 2005). Werner et al. (2015) and Hendriks et al. (2016) showed that replacing the static emission profiles with those account for regional adaptation of meteorology and other variables improves the CTM performance against observations considerably.

At the same time, Ge et al. (2020) developed a novel ammonia emission model for Germany and the Benelux by combing an agricultural emission model (INTEGRATOR (de Vries et al., 2021; Kros et al., 2012)) and an agricultural management model (TIMELINES (Hutchings et al., 2012)). INTEGRATOR provided high-resolution (in the form of polygons called NCUs illustrated in Ge et al. (2020)) spatial distribution of ammonia emission, differentiating types of manure and fertilizer applied on croplands and grassland, grazing, and animal housing systems. TIMELINES (Hutchings et al., 2012) was adapted to provide the timing of manure and fertilizer application on various crops while housing emissions were prescribed following Gyldenkærne et al. (2005). The resulting spatially explicit crop type-, fertilizer type-, and animal housing type-dependent ammonia time profiles were used in the CTM LOTOS-EUROS (Manders et al., 2017). Although the evaluation against observations of ammonia showed a significant improvement, it was recognized that

the spatial representation in the agricultural emission model, the so-called NCUs, which can be rather large areas, is a disadvantage. Within each NCU polygon, the emission is assumed to be evenly distributed, which does not reflect the distribution of crops and animal housing systems within the NCU. Hence, crop distributions and livestock housing information should be taken into account (Ge et al., 2020).

Many studies have used remote sensing data to perform analyses of vegetation indices time series to obtain agricultural land use and crop development information (Dubovyk et al., 2015; Marais Sicre et al., 2016; Vaglio Laurin et al., 2018; Waldhoff et al., 2017). The new Sentinel-2 instruments offer new opportunities to better distinguish between different crop types thanks to their sensor and orbit characteristics, high spatial resolution, and relatively short revisit time (Belgiu and Csillik, 2018; Kobayashi et al., 2020; Yi et al., 2020; Sonobe et al., 2018). Although new crop maps based on sentinel-2 are becoming available (Griffiths et al., 2019), their use for the quantification of agricultural ammonia emissions has not been explored yet.

This study aimed to improve upon the emission model of Ge et al. (2020) by introducing a high-resolution crop map and livestock housing information for the Netherlands. In this paper, we first describe the methodology of crop mapping from Sentinel-2 observations, the subsequent calculation of the spatial and temporal allocation of ammonia emission, which also accounts for livestock housing locations, and the evaluation of the updated emission product with the use of the CTM LOTOS-EUROS and in situ measurements. Next, we provide the results, including the obtained crop map, the updated emission estimates, and the validation of the emission products by comparing modeled surface concentrations with in situ measurements. Finally, we discuss the improvements in the emission model brought by the updated crop map and animal housing information and point out future perspectives for this work.

4

4.2 Methodology

The workflow in this study is separated into three steps (Figure 4-1).

(1) Crop mapping through random forest classification using Sentinel-2 multi-temporal multispectral surface reflectance observations and vegetation indices calculated from surface reflectance.
(2) Adaptation of the spatial and temporal allocation of ammonia emissions by integration of the crop map and livestock housing locations in the INTEGRATOR – TIMELINES emission model, described in Ge et al. (2020).
(3) Simulation of ammonia surface concentrations with the CTM LOTOS-EUROS using the original (without updates on crop map and livestock housing locations) and updated (with updates on crop map and livestock housing locations) ammonia emissions and validation of the simulated surface concentrations with in situ measurements.

Each of the steps is described in detail below.

Crop Classification
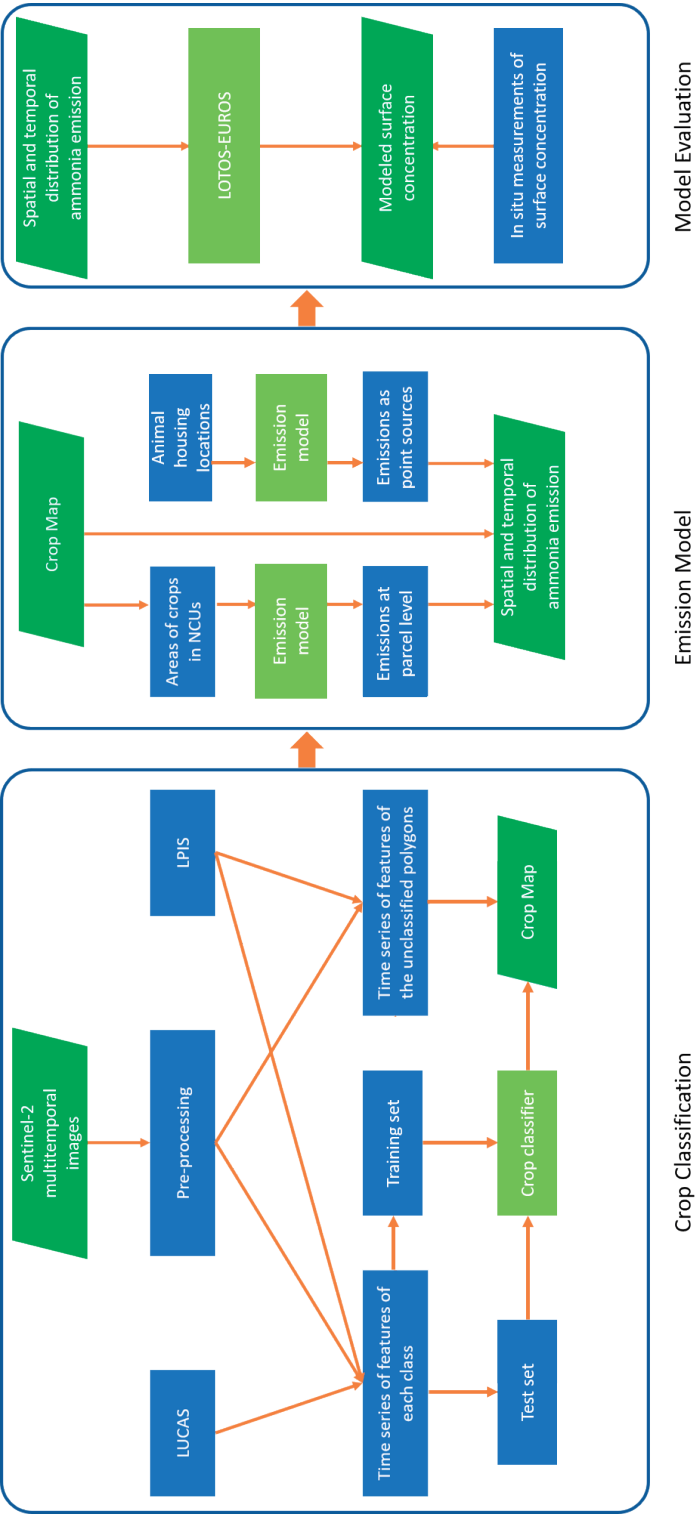
Emission Model

Model Evaluation

Figure 4-1 The schematic workflow in this study is composed of three modules: crop classification that derives a high-resolution crop map of the Netherlands from Sentinel-2 observations, emission model that obtains the spatial and temporal distribution of ammonia emissions, and model evaluation with in situ measurements.

4

4.2.1 Crop mapping with Sentinel-2 observations

Crop mapping is the process of identifying crop types and obtaining the spatial distribution of crops, which can be done with either conventional methods or automated machine learning-based methods. In a machine learning-based framework, crop types are determined using a crop classifier, which is an advanced tree-based, ensemble-based tool built by ground truth data to identify specific spectral and spatiotemporal crop signatures. Nowadays, multitemporal multispectral observations from optical satellites are used to estimate the spatial distribution of various crops due to their benefits of saving time and labor force (Yan et al., 2021). In this study, we conducted crop mapping by applying random forest classification to Sentinel-2 observations. An introduction to Sentinel-2 can be found in Section S4.1 in the supplementary material, and random forest classification will be talked about in the text below. The study area for crop mapping covers not only the Netherlands but also North Rhine-Westphalia of Germany to increase the number of ground truth data. The area was divided into 263 patches of the sizes of 20000 meters by 20000 meters (see Figure 4-2) for data downloading, pre-processing, processing and classification to save processing power and time.

The crop map of the Netherlands is obtained in the following steps:

(i) Collect ground truth land parcels from land surveys and georeferenced land parcels.

(ii) Derive the time series of Sentinel-2 surface reflectance and vegetation indices of the ground truth land parcels.

(iii) Divide the ground truth land parcels into a training set and a test set. Obtain a crop classifier by applying random forest classification and determine the model performance by applying a 5-fold cross-validation.

(iv) Use the classifier to predict crop types for all land parcels, and assess the quality of the obtained crop map by comparing it with other statistical sources.

Details of the various steps are given in the sub-sections below.
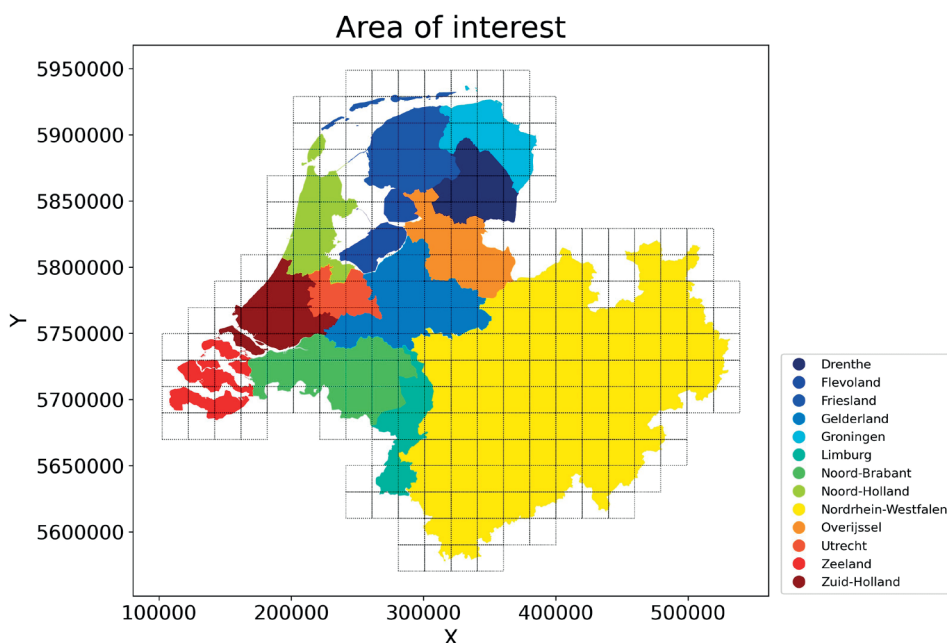
Figure 4-2 The area of interest for crop mapping covers the Netherlands and North-Rhine Westphalia and is divided into 263 patches for data downloading and processing. The coordinates are in WGS84/ UTM 32N coordinate system (EPSG:32632).

4.2.1.1 Ground truth land parcels preparation

Eurostat has carried out the Land Use and Coverage Area frame Survey (LUCAS) every three years since 2006 to identify changes in the European Union in the socioeconomic use of land (for instance, agriculture) (Orgiazzi et al., 2018). LUCAS contains harmonized in situ land cover and land use data collection based on observations made by surveyors throughout Europe (Ballin et al., 2018). The survey is conducted on a 2 km by 2 km grid, which means that land cover information is available at points that are 2 km away from each other. Since Sentinel-2 is available for full-year coverage from 2016 onwards, LUCAS 2018 data on arable crops and grasslands were selected in this study.

To reduce the uncertainties in Sentinel-2 observations and save processing time, we spatially averaged Sentinel-2 observations within each agricultural land parcel instead of looking at pixels. Land Parcel Identification System (LPIS) offers georeferenced polygons of agricultural plots derived from aerial photographs and high-precision satellite images (Zimmermann et al., 2016; Montaghi et al., 2013). The polygons demonstrate the exact shape and size of the land parcels whose contours often intersect with roads or other facilities. Therefore, we utilized QGIS to buffer each ground truth land parcel inwards by 10 meters within its boundary so that tiny and narrow polygons were eliminated and the

remaining polygons were ensured to lay within the farmlands or grassland. For each land parcel that contains a LUCAS point, we assigned the crop information to the land parcel to derive ground truth land parcels. We chose grassland and the 11 most common arable crops presented in the ground truth land parcels as the target classes. The arable crops are barley, flower, fodder, maize, nursery, oat, other cereal, potato, rye, sugar beet, and wheat.

4.2.1.2 Derivation of Sentinel-2 surface reflectance and vegetation indices time series

Satellite data from Sentinel-2 were downloaded through the open-source Python package *sentinelhub* (https://eo-learn.readthedocs.io/en/latest/) to access and process Sentinel-2 spatiotemporal satellite images. The Sentinel-2 observations used for crop mapping were Level 2A Bottom-Of-Atmosphere (BOA) reflectance. For specific days on which no Level 2A BOA reflectance data were available, we conducted pre-processing on Level 1C Top-Of-Atmosphere (TOA) orthoimages to create Level 2A BOA-corrected reflectance images, using the Sen2Cor processor (Main-Knorn et al., 2017). The pre-processing includes atmospheric, terrain, and cirrus correction (Louis et al., 2016; Li et al., 2018). Afterward, scene classification was conducted, resulting in a classification map of three classes of clouds and six other classes of shadows, cloud shadows, vegetation, not vegetated, water, and snow (Louis et al., 2010). Only pixels with less than 25% cloud probability were kept to ensure that all pixels used were under cloud-free conditions to reduce the impact of clouds. Besides, pixels in Sen2Cor's scene classification map labeled *NO DATA*, *Saturated or defective pixel*, *Cloud shadows*, *Cloud medium probability*, *Cloud high probability,* and *Thin cirrus* were regarded as invalid as well. When more than 60% of the pixels in an image were invalid, this image was removed.

In this study, 10-day averages of surface reflectance of 6 bands and 11 vegetation indices from February to November were utilized to derive their temporal patterns for machine learning. Most indices used were normalized differential indices based on differences in reflectance behavior between land cover types. For example, well-nourished, living plants absorb red light and reflect near-infrared light, while dead vegetation absorbs relatively less red light than healthy vegetation (Agapiou et al., 2014). Details on the chosen vegetation indices and their advantages are given in Section S4.2 in the supplementary material. For each parcel, we calculated the time series of the spatially averaged surface reflectance and vegetation indices. Examples of the NDVI and EVI time series of the ground truth land parcels of grassland and maize are given in Section S4.3 in the supplementary material.

It has to be noted that filtering was done to the ground truth parcels based on the 10-day averaged time series of surface reflectance to obtain more uniform ground truth data and to have a similar number of ground truth data for each crop type. When more than eight values were missing or invalid in a time series (30 values in total), the time series was left out. An outlier detection was performed on the observations to determine if an

observation was invalid. For ground truth parcels of each crop type, the mean (R_m) and standard deviation (R_{std}) of surface reflectance at each timestamp were calculated. The observations that lay outside [$R_m - cR_{std}$, $R_m + cR_{std}$] were regarded invalid. The c is a constant that made sure there were no more than 30 valid time series for each crop.

4.2.1.3 Random forest classification

In this study, machine learning with random forest (RF) was used to obtain a crop classifier. The ground truth land parcels were divided into a training set (80%) and a test set (20%) using stratified sampling, which means that the samples were selected in the same proportion as they appeared in the original ground truth data. In this way, we eliminated the sampling bias in a test set and made sure that it represented the entire population. A 5-fold cross-validation was conducted to determine the robustness of the classifier. The ground truth data were divided into five batches, and RF machine learning was performed five times, with each time four batches (80%) being the training set and the remaining batch (20%) being the test set.

A random forest is a collection of a large number of individual decision trees on randomly selected samples (Breiman, 2001). By looking at features, a decision tree makes decisions by splitting nodes into sub-nodes to create relatively pure nodes. A feature, also known as a predictor variable, is an individual measurable property or characteristic used as input for effective algorithms in pattern recognition and classification (Bishop, 2016). This node-splitting process is performed multiple times during the training process until only homogenous nodes are left. Each decision tree returns a classification prediction, and the class with the most votes is the prediction of the forest (Lan et al., 2020). Compared to other algorithms, the random forest algorithm is considered more accurate and robust because of the enormous number of decision trees involved in the process (Guo et al., 2007). Taking the most voted class cancels out potential biases, which helps avoid the overfitting problem. Furthermore, when one set of observations does not have all feature values, RF can deal with the missing value, which is replaced with the median or the proximity-weighted average of all observations of that feature (Cutler et al., 2012). Last but not least, RF can diagnose the relative feature importance, which assists in selecting the most contributing features for classification (Rogers and Gunn, 2006). Variables with low importance might be omitted from the model, making it simpler and faster to fit and predict. RF has achieved efficient classification results in various remote sensing studies, including crop mapping (Hao et al., 2015; Novelli et al., 2016; Pelletier et al., 2016).

Regarding the random forest classification in this study, the 10-day averages of surface reflectance of 6 bands and 11 vegetation indices from February to November resulted in 510 features. The number of trees (ntree) should be chosen as large as possible, especially if the data comprises many predictors. The choice of ntree is usually a compromise

between accuracy and computational speed (Janitza and Hornung, 2018). Goldstein et al. (2010) concluded that for their genome-wide data set, 1000 trees might be sufficient. Díaz-Uriarte and Alvarez de Andrés (2006) found that the results for random forests with 1000 trees and those for RF with 40000 trees were almost the same. Genuer et al. (2008) found out that in the high-dimensional settings, RF with 500 trees yielded very similar out-of-bag (OOB) errors to that with 1000 trees. Following these findings and through experimentation, the number of trees was set to 1000 in this study. Following the random forest classification results reported by Belgiu and Drăguţ (2016) and Gislason et al. (2006), the number of variables used for tree nodes splitting (mtry) was established as the square root of the number of features and was set to 25.

After obtaining the crop classifier with the training set, we applied it to the test set and compared the predictions with the ground truth. The accuracy score of the classifier prediction on the test set, being the fraction of predictions our model succeeded in making, was 0.73. Figure 4-3 shows the importance scores of the features and indicates that vegetation indices generally were given more weight than the Sentinel-2 bands, but there was no dominant feature, with importance values ranging from 0.04 to 0.07. The accuracy scores of the 5-fold cross-validation were 0.67, 0.69, 0.69, 0.73, and 0.74 (0.71 on average), respectively. The resulting crop distributions are very similar. It means that the model was robust and not overfitted. As a result, we did not reduce the number of predictor features for crop mapping.

4.2.1.4 Derivation and validation of the crop map
After we calculated the same features (10-day averages of surface reflectance of 6 bands and 11 vegetation indices from February to November) of all crop parcels in the country in 2017, we applied the classifier to them to obtain a complete crop map of the Netherlands in 2017. Although the crop classifier was validated with the test data, it was important to verify the crop map on a national scale. Therefore, the resulting crop distribution was validated by comparing the predicted crop areas of grassland and the top four arable crops by area (maize, potato, wheat, and sugar beet) in each Dutch province with the official statistics in 2017 from Statistics Netherlands (CBS) (https://opendata.cbs.nl/#/CBS/en/dataset/7100eng/table). In addition, we also compared crop area per province to an online crop map dataset, OneSoil, to see how our map performed compared to a commercial service (https://map.onesoil.ai/).
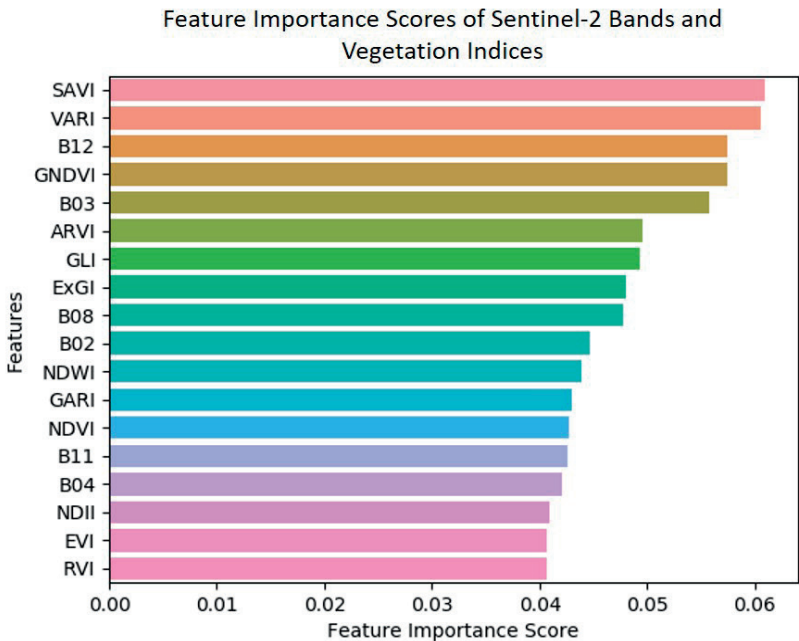
Figure 4-3 Importance values of various feature values (6 satellite bands (B02, B03, B04, B08, B11, B12) and 11 vegetation indices shown in Table S4.1 in the supplementary material Section S4.2) used for machine learning.

4.2.2 Emission modeling with the updated crop map and housing information

As mentioned, the purpose of the study is to update the ammonia emission model described in Ge et al. (2020) with a detailed crop map and locations of animal housing systems. The emission model is composed of two modules, namely, a spatial allocator (INTEGRATOR) and a temporal allocator (TIMELINES) (Ge et al., 2020). The former generates the gridded annual emission map, while the latter disaggregates each gridded annual emission in time. INTEGRATOR is a static nitrogen cycling model which was used to calculate ammonia emissions from animal housing systems and manure and mineral fertilizer application (De Vries et al., 2020a; Kros et al., 2012). For a detailed description of INTEGRATOR, we refer to De Vries et al. (2011) and Ge et al. (2020). For information on the temporal allocator TIMELINES, we refer to Ge et al. (2020). Below, we only describe the critical aspects of the approach to calculate the ammonia emissions from animal housing systems and manure and mineral fertilizer application. To account for the influence of emissions from outside the Netherlands, for example, by long-distance transport, we chose the area of interest that covers the Netherlands and surrounding regions that may affect ammonia concentrations in the country. Therefore, being larger than the study area of crop mapping, the study area of ammonia emission modeling is 2°E−9°E in longitude

and 50°N–54°N in latitude with a step of 0.015625° in longitude and 0.0078125° in latitude, resulting in a spatial resolution of approximately 1.7 km x 1.7 km.

In INTEGRATOR, the total N excreted was calculated by multiplying the number of animals at the NCU level with N excretion rates per animal per country for eight animal categories (dairy cows, other cows, pigs, laying hens, other poultry, sheep and goats, horses and fur animals). A division was made between the excretion of animals in housing systems and grazing animals in pastures based on national data for the number of grazing days. The N excreted in housing systems was derived by multiplying total N excretion with the housing fraction, while the N excreted on land during grazing was calculated by subtracting N excreted in housing systems from total N manure excretion. The total manure production was calculated from the N excreted in housing systems after correcting for losses (gaseous emissions and leaching) in housing systems.

4.2.2.1 Spatial distribution of annual emission from manure and fertilizer application using the crop map

Manure was distributed over grassland and arable crops using various allocation rules. Manure produced by grazing animals all entered grassland. Manure produced for sheep and goats was completely applied to grassland. For other manure, a fraction was applied to arable land, and the remaining fraction went to grassland/fodder crops, according to Menzi et al. (2002). Manure types were lumped into (i) liquid manure of dairy/other cattle, (ii) solid manure of dairy/other cattle, (iii) liquid manure of pigs, (iv) solid manure of pigs, and (v) poultry manure. Regarding fertilizer, a distinction was made between urea and other fertilizer. Manure distribution on arable land was divided over four arable crop groups, adapted after Velthof et al. (2009). The mineral fertilizer N demand of each crop was calculated by a balanced N fertilization approach based on the N demand of each crop (Ge et al., 2020). The ammonia emissions from grazing and application on arable crops and grassland were calculated by multiplying the N inputs by grazing cattle and by manure and fertilizer application with the corresponding N emission fractions.

The derived crop map influences the spatial distribution of ammonia emissions in two ways. First, the crop map leads to changes in manure distribution due to the above allocation rules and fertilizer distribution because of different nitrogen demands. Secondly, instead of evenly distributing emissions within the whole NCU as in Ge et al. (2020), we allocated the crop-dependent application emissions to where the corresponding crops are located within an NCU.

4.2.2.2 *Spatial distribution of annual emission from animal housing systems using livestock housing information*

The ammonia emissions from animal housing systems include emissions in animal houses and manure storage facilities. Ge et al. (2020) pointed out that allocating housing emissions evenly within each NCU was a source of uncertainties in the emission model. Therefore, animal housing locations are useful for treating housing emissions as point sources. Information on the locations of animal housing systems is based on the so-called GIAB (Geographic Information Agricultural Business) system, as used in the INITIATOR model, which is an adapted version of INTEGRATOR built specifically for the Netherlands (de Vries et al., 2015). GIAB includes information on the exact location of all housing systems of each farm in the Netherlands. (GIAB: (Gies et al., 2015); GIABplus: (van Os et al., 2016)). Since we did not have direct access to GIAB, we used INITIATOR output for 2017, from which we extracted the coordinates of animal housing systems in the Netherlands. Then ammonia emissions from animal housing systems within each NCU were evenly assigned to the animal housing systems in that NCU as point sources. The same animal categories in manure types were used in housing systems.

4.2.3 Surface concentration modeling for the evaluation with in situ measurements

To validate the improvement in the emission products brought by the crop map and livestock housing locations, we used the in situ measurements of surface concentrations in the Netherlands. The spatial and temporal distribution of ammonia emissions was imported into LOTOS-EUROS to calculate surface concentrations. LOTOS-EUROS is a 3-dimensional regional CTM (Manders et al., 2017, 2009; Schaap et al., 2008b) that uses a description of the bidirectional surface-atmosphere exchange of ammonia (Wichink Kruit et al., 2017). The model is regularly used to address reactive nitrogen budgets (Banzhaf et al., 2015; Hendriks et al., 2016; van der Graaf et al., 2020, 2018), and we refer to these publications for a detailed model description.

This paper conducted two LOTOS-EUROS simulation runs to quantify the changes in modeled ammonia concentrations brought by the update. The first base simulation (referred to as INT) used the INTEGRATOR ammonia emission, which was distributed as described in Ge et al. (2020). The second (referred to as INT-SEN) utilized the emission information as described in the paper, using the updated crop distributions and livestock housing locations. For both simulations, non-agricultural emissions were derived from the TNO-MACC emission inventory (Kuenen et al., 2014b).

Modeled ammonia surface concentrations were compared to in-situ measurements from the Measuring Ammonia in Nature (MAN) network. In this network, monthly mean ammonia concentrations at 255 sites in 60 Natura2000 areas were monitored (https://man.

rivm.nl/) (Lolkema et al., 2015). Natura2000 areas have been designated to preserve the ecological value of natural areas, and they are protected under European legislation. The ammonia measurements from MAN use low-cost passive samplers. For the measurement method, calibration method, and uncertainties, we referred to Lolkema et al. (2015). When assessing the comparison of monthly and annual averaged concentrations, the stations were divided into three groups, which were determined by the primary source of local ammonia emission. If application emission or housing emission occupied more than 60% of the total emission within the grid where a station was located, this station was categorized as an application-dominated or housing-dominated station, respectively. The remaining stations were called "other stations". In this way, we could inspect the improvement brought by the updated crop map and animal housing systems information separately. In addition, measurements at all stations were also compared with the modeled results to assess the overall performance. The model performance indicators included relative bias, correlation, the normalized root mean square error (NRMSE), normalized mean absolute error (NMAE), model efficiency (EF), and index of agreement (IA) between the measurements and modeled results (see Ge et al. (2020) for the equations). In addition, the fraction of predictions that were within a factor of two of the observations (FAC2) were also calculated as it is a simple and robust measure, which is not overly influenced by the extreme values (high and low) in a time series. (Chang and Hanna, 2004; Hanna and Chang, 2012).

4.3 Results

4.3.1 The derived crop map

The national crop map derived from Sentinel-2 is presented in Figure 4-4. The dominant agricultural land is grassland, with a total area near 1.0 million ha in the Netherlands, which is dominantly distributed in the provinces of Friesland (north), Overijssel (east), and Utrecht (center) (see Figure 4-4(a)). Maize production is mainly found in the eastern part of the country (Drenthe, Eastern Overijssel, Eastern Gelderland, Nord-Brabant, and Limburg). As for potato, oat, wheat, and sugar beet, the distribution is less spread out but concentrated in some highly agriculturally active regions like Flevoland, the coastal areas of Friesland and Groningen, and along the German border in the north-east. Zeeland and Limburg in the south also have potato production but to a lesser extent. Regarding flowers, being a less important crop in terms of area, its fields are correctly identified in the provinces of Flevoland, North Holland, and some smaller areas like Noordwijkerhout and De Zilk. Figure 4-4(b) shows the zoomed crop map of Groningen. One can see that grassland tends to be located in the lands inwards to the west, and arable crops (mainly wheat and potato) are mainly situated in the north by the ocean or to the east.
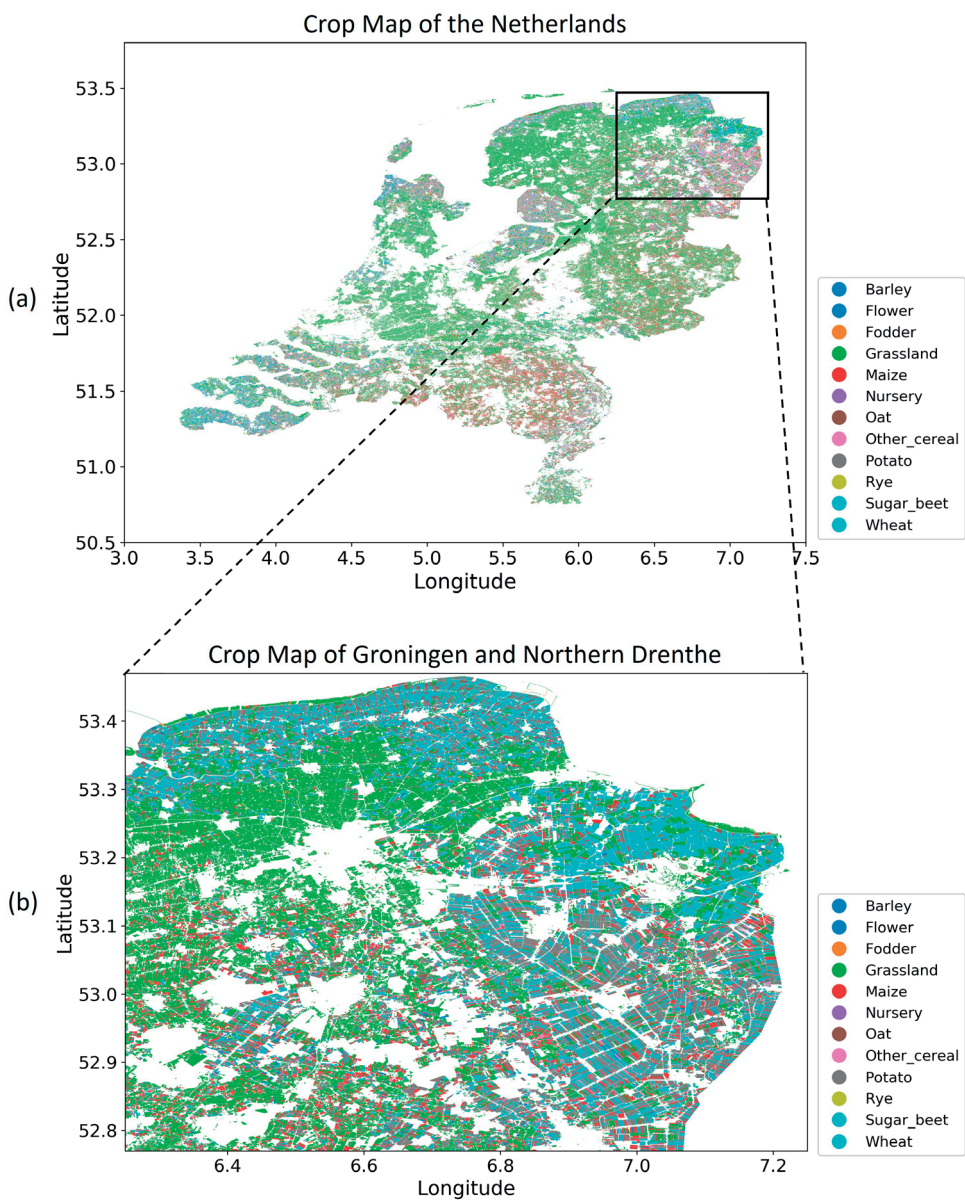
Figure 4-4 Crop Map of the Netherlands (top) and the zoomed map of Groningen (bottom).

Based on the CBS dataset, important arable crops by area in the Netherlands are maize (218 k ha), potato (163 k ha), wheat (116 k ha), sugar beet (85 k ha), vegetables (61 k ha), and barley (30 k ha) (see Table 4-1). Table 4-1 summarizes the total areas of grassland and the six arable crops by area in the Netherlands, comparing estimates from our study with the Dutch statistics from CBS and with the statistics from the OneSoil. The crop areas derived from Sentinel-2 in our study demonstrate better alignment with CBS than those obtained from OneSoil for almost all crops except wheat and vegetables. The absolute median of the relative difference between Sentinel-2 derived crop areas and CBS is around 5 %, while that between OneSoil and CBS is larger than 15 %. The lowest deviations between the derived crop areas and CBS are found for grassland and barley, with the relative difference being −0.8% and 3.0%, respectively. However, the area of wheat obtained in this study is overestimated by 33 %, while OneSoil has a lower relative error of 4.2 %. Moreover, the obtained crop map rarely contains vegetables, while OneSoil also does poorly predict the vegetable area with a 60.7% deviation. We also compared the total area per province of grassland and the top four arable crops with the CBS statistics, and the details are given in Section S4.4 in the supplementary material.

Table 4-1 Total production area for five major arable crops and grassland in the Netherlands (k ha) from Dutch statistics CBS, this study, and the OneSoil database, as well as the relative difference of the two estimates with respect to CBS data in 2017.
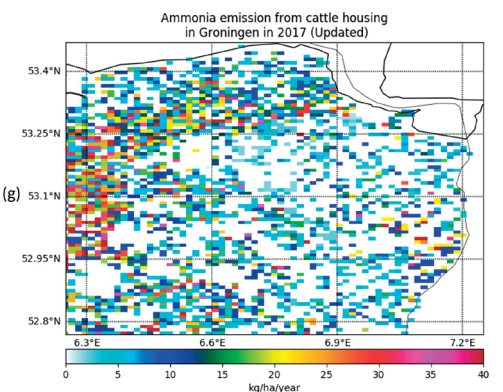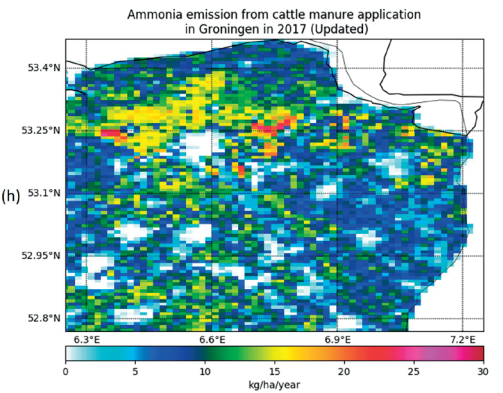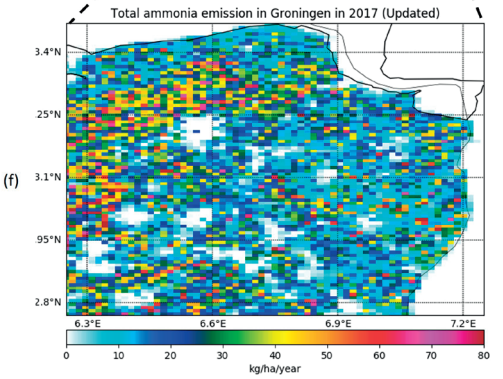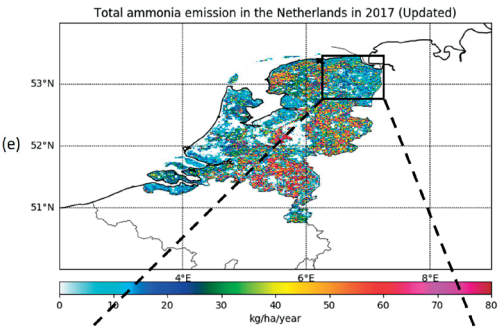
	Grassland	Maize	Potato	Wheat	Sugar beet	Vegetable	Barley
CBS	992	218	163	116	85	61	30
This study	984 (−0.8%)	207 (−5.1%)	171 (+4.9%)	155 (+33.0%)	103 (+20.7%)	0.01 (−100%)	31 (+3.0%)
OneSoil	1139 (+14.8%)	258 (+18.5)	129 (−20.9%)	121 (+4.12%)	138 (+61.5%)	97 (+60.7%)	35 (+16.9%)

4.3.2 Ammonia emission distribution

Figure 4-5 shows the original (left column, without the use of the crop map and livestock housing locations) and updated (right column, with updates on the crop map and livestock housing locations) annual ammonia emission maps in 2017. Figure 4-5(a) and 5(e) show the national emission maps, whereas Figure 4-5(b) and 5(f) are zoomed annual emission maps of Groningen. The updated maps are characterized by a high degree of granularity (spatial details) and a more prominent contrast in ammonia levels between agricultural and natural regions because the updated model only allocated emissions at sources instead of all over the NCUs, which eliminates ammonia emissions in non-agricultural areas. However, the main features of the ammonia emission distribution across the country are comparable to the original data. Cattle housing emissions in Figure 4-5(h) are point sources, so they are less spread out and at larger magnitudes than in Figure 4-5(d). Significant differences in spatial distribution also occur from cattle manure application (Figure 4-5(c) and 5(g)). For example, the application emission level in Figure

4-5(c) is much higher in the north, close to the coast, and other new hot spots appear in central Groningen because the derived crop map affects the spatial allocation of ammonia emissions and introduces new maxima in the distribution. The crop map tells that northern Groningen is mainly occupied by potatoes and wheat. However, the original land use input data of INTEGRATOR indicate that there is broader coverage for vegetables than potatoes in this area. INTEGRATOR regards potato as an arable crop with intermediate manure use, whereas it does not allocate manure to vegetables, which results in more manure allocated here in the updated model. Furthermore, since different crops have different timings of fertilization (Ge et al., 2020), the temporal distribution of the gridded emissions is also affected, causing emission peak shifts over the year. To summarize, the accuracy of the crop distribution in the emission model is significant in estimating manure/fertilizer distribution and the subsequent spatial and temporal distribution of ammonia emission.

4

(a) Total ammonia emission in the Netherlands in 2017 (Original)

(e) Total ammonia emission in the Netherlands in 2017 (Updated)

(b) Total ammonia emission in Groningen in 2017 (Original)

(f) Total ammonia emission in Groningen in 2017 (Updated)

(c) Ammonia emission from cattle manure application in Groningen in 2017 (Original)

(h) Ammonia emission from cattle manure application in Groningen in 2017 (Updated)

(d) Ammonia emission from cattle housing in Groningen in 2017 (Original)

(g) Ammonia emission from cattle housing in Groningen in 2017 (Updated)

<<
**Figure 4-5 Maps of the spatial variation (presented at 1.7km x 1.7km resolution) in annual total
ammonia emission over the Netherlands (a, e), and zoomed map of total emission (b, f), cattle manure
application emission (c, g) and cattle housing emission (d, h) in Groningen.**

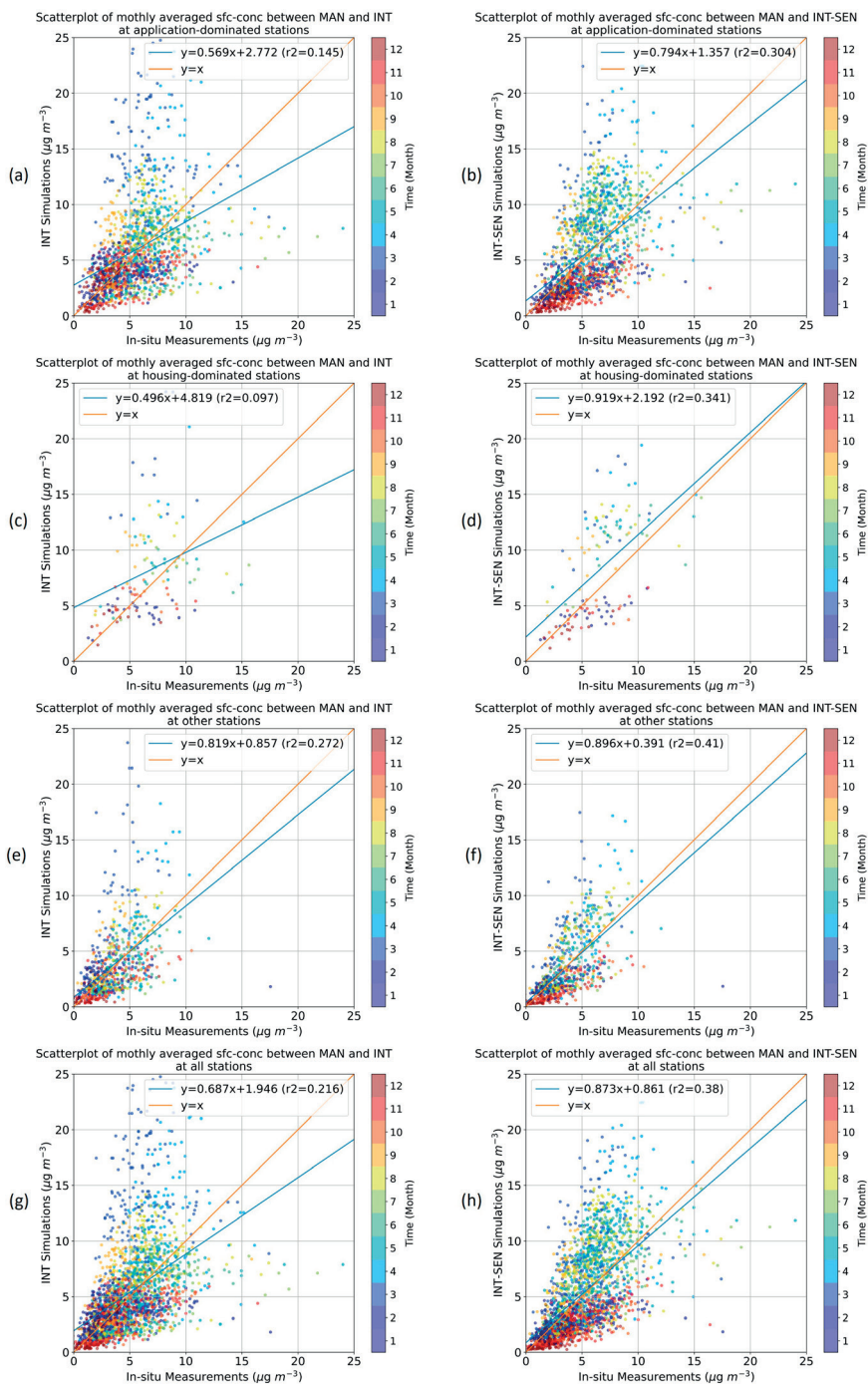## 4.3.3 Comparison of the modeled and measured ammonia surface concentrations

4.3.3.1 *Monthly averaged ammonia surface concentrations*

Figure 4-6 shows two examples comparing ammonia surface concentrations measured
in the MAN network and simulated with the original and updated emission products. In
both Figure 4-6(a) and 6(b), the updated modeled result shows better correspondence
with the measured concentrations, both in absolute magnitude and temporal variability.
Both INT and INT-SEN simulations show the spring and autumn peaks of surface ammonia
concentration at the application-dominated Station Lauwersmeer-De Middelplaat (Figure
4-6(a)). However, the spring peak predicted by the INT scenario is largely overestimated,
while INT-SEN simulated the time series more accurately. Regarding the housing-
dominated Station Sarsven en De Banen- Sarsven (Figure 4-6(b)), the modeled temporal
variabilities in both simulations are relatively similar, except that the average concentration
in the updated INT-SEN simulation is higher than that from the INT simulation and better
aligned with the measurement. The INT simulation shows an earlier spring peak than the
measurements. This is because the original model distributes housing emissions to the
whole NCU, which smoothens spatial characteristics and reduces ammonia levels in the
grid cell. In contrast, the updated model keeps housing emissions where animal housing
systems are located, leading to higher ammonia levels in the grid cell.

4
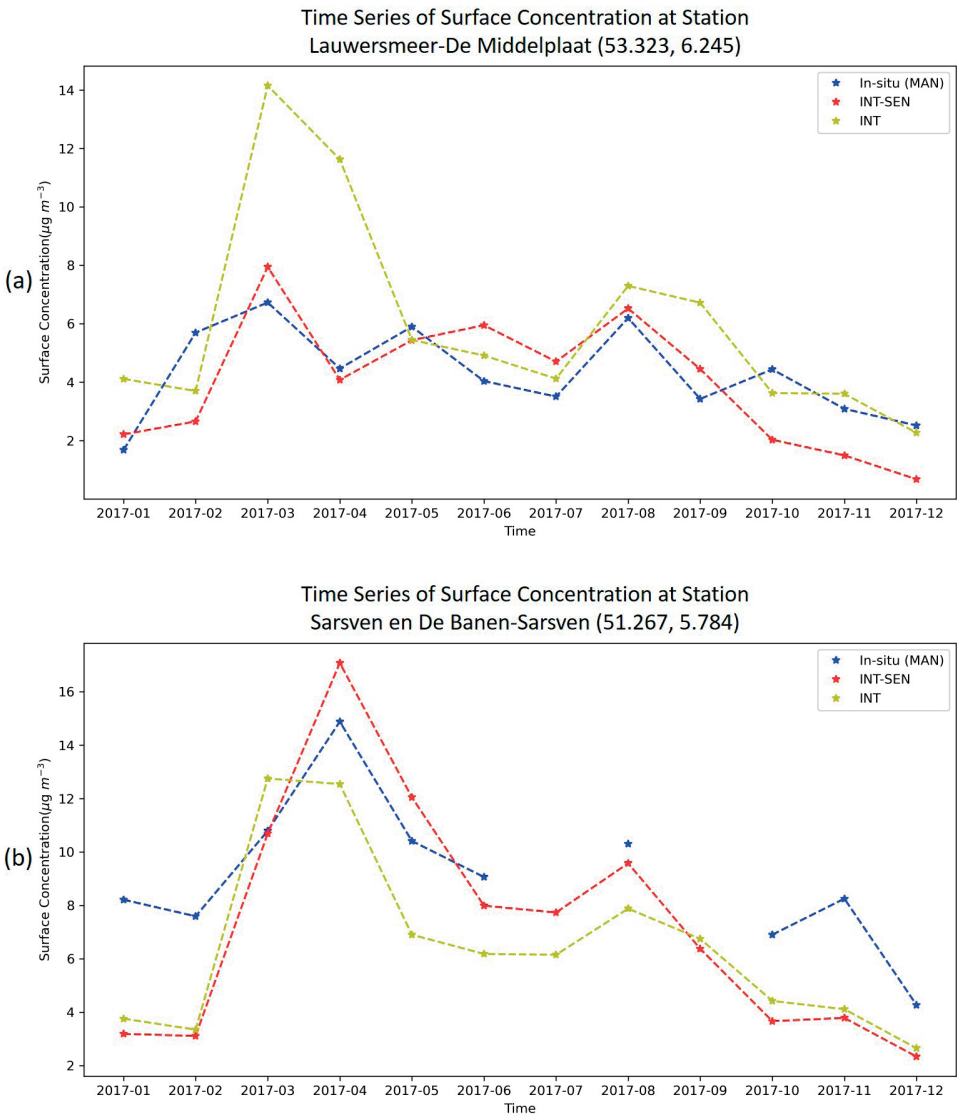
Figure 4-6 Comparison of surface ammonia concentration time series measured in the MAN network and modeled with the original emissions (the INT simulation) and the updated emissions (the INT-SEN simulation) at an application-dominated station (top) and a housing-dominated station (bottom). There were no valid data for July and September.

Figure 4-7 shows the scatter plots comparing modeled and measured monthly averaged surface concentrations at application-dominated stations (Figure 4-7(a) and 7(b)), housing-dominated stations (Figure 4-7(c) and 7(d)), other stations (Figure 4-7(e) and 7(f)) and all stations (Figure 4-7(g) and 7(h)). Table 4-2 presents the model performance indicators for the comparison of simulated and measured monthly averaged surface concentrations in the INT and INT-SEN simulations for the four groups of stations. At application-dominated stations, both simulations seem to over-allocate a considerable amount of emission in springtime (February, March, and April) to account for the fertilization of spring crops. The overestimation in spring in the INT-SEN simulation is less severe, and the spread of the scatter points is narrower (Figure 4-7(b)), resulting in better model performance indicators (see Table 4-2). Similar results are observed in the comparison at other stations. In Figure 4-7(c) and 7(d), there is both under- and overestimation for both comparisons in springtime, with the updated model reducing the deviations compared to the original model. However, for summer, the majority of the scatter points are still located above the y=x line, which means that the tendency to overestimate the ammonia levels in summer remains. At housing-dominated stations, the improvement is more evident, even though the overestimation in summer remains. In Table 4-2, almost all indicators have improved except that the bias for housing-dominated stations remained almost the same (slight increase). Error measures, including relative standard deviation, NRMSE, and NMAE, have dropped substantially, especially for housing-dominated stations. The reductions in relative standard deviation and NMAE are more pronounced than those in the NRMSE. This is because the individual differences are weighted equally in the standard deviation and NMAE calculation, while the NRMSE gives a relatively high weight to large errors (overestimation in spring). In addition, both model efficiency and index of agreement suggest that the INT-SEN simulation can reproduce and predict ammonia surface concentrations in better agreement with in situ measurement. Finally, the FAC2 factors of INT-SEN modeled results are larger than those of INT simulations for any station type, which means that the INT-SEN model is more robust and less influenced by extreme values.

4

Figure 4-7 Scatter plots of monthly averaged modeled and measured ammonia surface concentrations comparing the original (the left panel) and updated (the right panel) modeled results with measurements at application-dominated stations (a, b), housing-dominated stations (c, d), other stations (e, f) and all stations (g, h).

Table 4-2 Quality assessment of the comparison between measured monthly averaged surface concentrations and simulated concentrations with the original (INT) and updated (INT-SEN) INTEGRATOR model

Station type	Simulation	Rel. bias (%)	Rel. std (%)	Correlation	NRMSE	NMAE	EF	IA	FAC2
Application-dominated	INT	6.68	72	0.38	14	45	0.05	0.57	0.75
	INT-SEN	0.53	56	0.55	13	40	0.28	0.71	0.76
Housing-dominated	INT	22.02	69	0.31	20	41	0.04	0.53	0.78
	INT-SEN	22.13	50	0.58	20	33	0.22	0.70	0.84
Other	INT	6.00	80	0.52	12	49	0.25	0.67	0.68
	INT-SEN	3.77	60	0.64	12	44	0.40	0.77	0.74
All	INT	7.58	74	0.46	13	46	0.16	0.64	0.73
	INT-SEN	1.06	58	0.62	12	40	0.29	0.75	0.76

4

4.3.3.2 Annual averaged ammonia surface concentrations

Annual averaged ammonia surface concentrations were also calculated, giving insight into the quality of the spatial distribution of estimated ammonia emissions. Figure 4-8 shows the scatter plots of comparisons between measurements and the two simulations INT and INT-SEN at application-dominated stations, housing-dominated stations, other stations, and all stations. Table 4-3 summarizes model performance indicators for the comparison. At application-dominated stations (Figure 4-8(a) and 8(b)), all indicators have been improved (see Table 4-3), with scatter points being much more concentrically distributed around the y=x line and narrower width of spreading, which corresponds to a higher correlation and lower errors. For housing-dominated stations (Figure 4-8(c) and 8(d)), all indicators except relative bias have been improved (see also Table 4-3). The most remarkable improvement is the increased correlation between observations and predictions at housing-dominated stations (from almost 0 to 0.45) since housing emissions are point sources in the updated model. When looking at all stations (Figure 4-8(g) and 8(h)), we can conclude that the spatial distribution of ammonia emission has been improved.
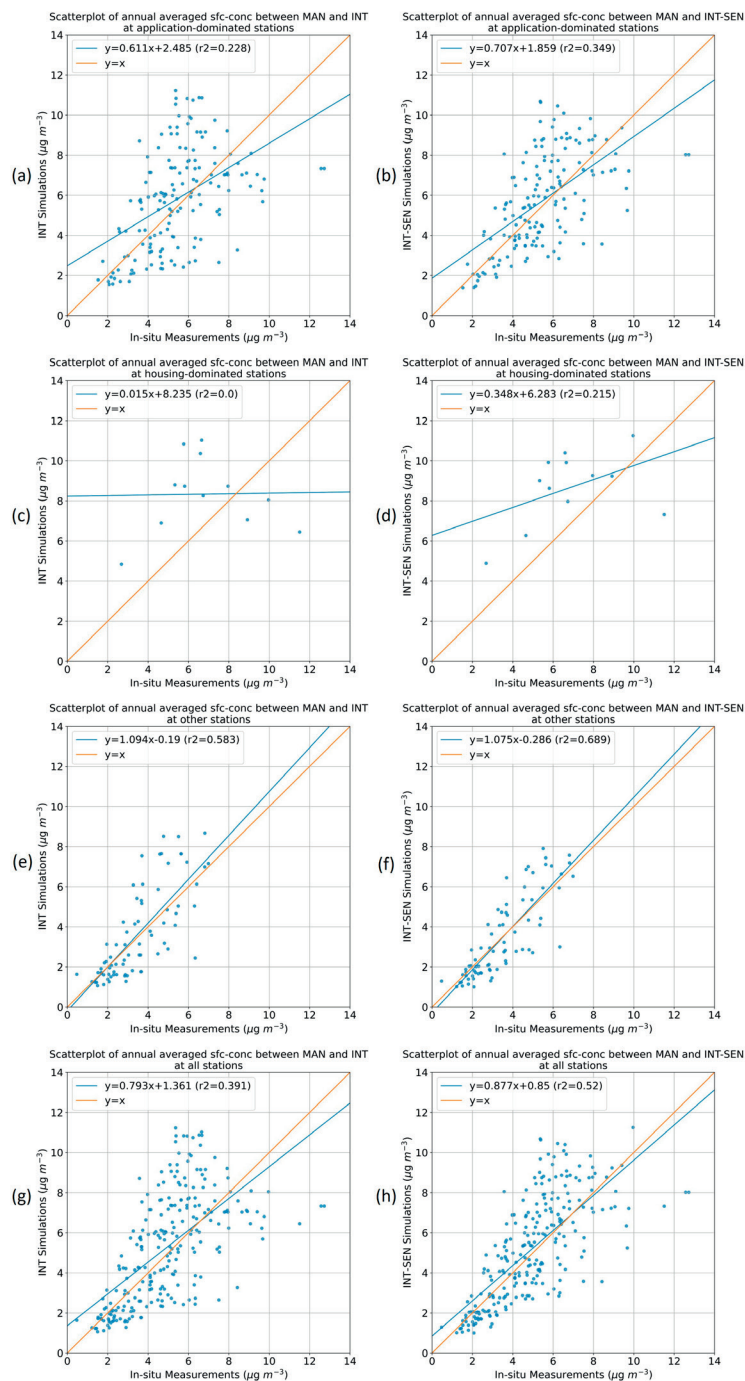
Figure 4-8 Scatterplot plot of annual averaged ammonia surface concentrations comparing the original INT (the left panel) and updated INT-SEN (the right panel) simulated results with measurements at application-dominated stations (a, b), housing-dominated stations (c, d), other stations (e, f) and all stations (g, h).

Table 4-3 Quality assessment of the comparison between measured annual averaged surface concentrations and simulated concentrations with the original (INT) and updated (INT-SEN) INTEGRATOR model

Station type	Simulation	Rel. bias (%)	Rel. std (%)	Correlation	NRMSE	NMAE	EF	IA	FAC2
Application-dominated	INT	6.61	43	0.48	24	32	0.11	0.67	0.93
	INT-SEN	1.02	35	0.59	21	27	0.28	0.76	0.97
Housing-dominated	INT	21.22	42	0.02	52	35	-2.32	0.45	1
	INT-SEN	22.07	32	0.45	43	27	-1.41	0.63	1
Other	INT	3.90	42	0.76	19	31	0.57	0.84	0.92
	INT-SEN	5.76	32	0.83	16	27	0.68	0.89	0.93
All	INT	7.03	44	0.62	21	32	0.35	0.77	0.93
	INT-SEN	0.99	36	0.72	17	27	0.51	0.84	0.96

4.4 Discussion

This paper aimed to improve the spatial and temporal distribution of ammonia emission estimates by updating the agricultural emission model INTEGRATOR with a high-resolution crop map obtained with Sentinel-2 observations and livestock housing information. Their impact on the spatial distribution of manure distribution and N excreted in housing resulted in higher details of ammonia emissions in space and time. Evaluation of the measured and modeled ammonia surface concentration data illustrated that the model improved the spatial and temporal emission estimates, although certain divergences between modeled and observed concentrations remain. Below, we discuss the main directions for improvement based on this work.

4.4.1 Crop mapping

The acquisition of ground truth data plays a major part in developing and validating land cover maps (Foody et al., 2016; Kavzoglu, 2009). This study employed the LUCAS database as the ground truth for machine learning, being one of the most extensive training samples for large-scale crop mapping in Europe. However, there exist some challenges. First of all, geolocation errors related to GPS measurements in the field and image misregistration errors contribute to wrongly classified ground truth data, resulting in a miscalculation of the temporal variability of vegetation indices of the training samples and test samples (Mack et al., 2017). Secondly, LUCAS georeferenced observation points are aligned on a 2 km by 2 km grid, which means that the number of data points for certain crop classes might be too limited. For a selected area, regardless of the size, there may be limited availability of training data for less-grown crops but an abundant number of samples for the most common crop types. For instance, the number of training samples is only five for vegetables compared to more than dozens for other crops and grassland. It is a known challenge to map small-sized classes and estimate the associated accuracy (Stehman, 2000), as larger classes significantly impact overall accuracy. Furthermore, dominant land cover classes in the training data are classified at the expense of smaller classes because the overrepresentation of larger classes in a land cover map mainly affects the validation results of the smaller class. We observed such effects, for example, between wheat, the larger class, and vegetables, the smaller class. Even though vegetables should cover various plants with different temporal patterns in vegetation indices, the training sample of vegetables in this study showed spectral similarities with wheat in the training data. This is why vegetables rarely appeared in our crop map and wheat cover was overestimated.

The spectral properties of a target class and the size of crop parcels also play an essential role in crop mapping. From the extensive validation with the CBS dataset and comparison to the OneSoil database, it can be seen that good validation results were achieved for maize and grassland (see Table 4-1 and Figure S4.2 in the supplementary material Section S4.4),

which have relatively distinct temporal patterns of reflectance and vegetation indices (see Figure S4.1 in the supplementary material Section S4.3). On the contrary, cereal types, including rye, wheat, and oat, have similar phenological and morphological patterns, hampering their spectral differentiation and resulting in lower classification accuracy for the classes. Moreover, smaller parcel sizes may also have affected classification accuracy as the risk of mixing spectral properties with adjacent land covers increases. This hinders the compilation of representative training data and subsequent land cover predictions.

The misclassification in crop types impacts ammonia emission estimates in INTEGRATOR because different arable crop groups have different manure demands. The impact is limited for the cereal types (rye, wheat, and oat) since they are all in the same group of intermediate manure use. However, for instance, when vegetables are classified as wheat, an overestimation in ammonia application emission will occur because no manure is applied to vegetables. In contrast, wheat belongs to the crop group with intermediate manure use.

To further improve classification accuracy, collecting additional training data through manual or automated approaches may help to distinguish spectrally or temporally distinct classes (Radoux et al., 2014). Besides additional ground truth data, integrating other multi-sensor time series such as Landsat-7, Landsat-8, and MODIS, which provides observations of similar nature as Sentinel-2, allows improving the temporal frequency of time series, shortening the revisit time to 2–5 days (Wulder et al., 2015; Drusch et al., 2012). Finally, there have been studies exploring the synergies of optical and high-resolution synthetic aperture radar (SAR) time series (e.g., from Sentinel-1 C-Band) for the mapping and analysis of phenology in agricultural land cover (Mercier et al., 2019; Baumann et al., 2018; Reiche et al., 2018). Unlike optical images, whose quality and availability may be affected by the presence of clouds and haze, SAR sensors can gather data regardless of weather conditions and sun illumination, resulting in a more frequent revisit time (Clerici et al., 2017; Mestre-Quereda et al., 2020). These techniques may be used to discriminate crop types better in the future.

4.4.2 Emission model assessment

After the comparison with MAN in situ measurements, one can see that the updated emission model has improved both the spatial (Table 4-3) and temporal (Table 4-2) distribution of ammonia emission, while the improvement is more evident at housing-dominated stations.

The model simulations at the application-dominated stations (Figure 4-7(a) and 7(b)) showed an overestimation of ammonia surface concentration in springtime (February, March, and April). However, it is less severe when using the improved emission product.

There are three possible explanations. First and foremost, it could be incorrect crop information, which leads to inaccurate manure and fertilizer distribution that affects the spatial distribution, and estimated fertilization day that impacts the temporal distribution of ammonia emissions. In the original emission model, due to outdated land use data in INTEGRATOR and an allocation algorithm distributing emissions from fertilization evenly within each NCU, the derived emission maps are smeared out, even including relatively strong emissions from non-agricultural areas. In the updated model, crops sown and fertilized between spring and autumn can be wrongly classified as spring crops. As a result, emissions that are supposed to occur in late spring are allocated to early spring. Secondly, the emission fractions used to derive ammonia emission from applied nitrogen could be inaccurate. Even though emission fractions influence annual total emissions, more emissions are allocated at peaks than at other times in a year during temporal allocation, leading to larger uncertainties at peaks. The emission fractions in INTEGRATOR are country-dependent constants that only differentiate among manure and fertilizer types. They neglect the influence of meteorological conditions, soil properties, application methods, etc. For example, air temperature has a positive impact on ammonia volatilization (Sommer et al., 1991). When the realistic temperature during fertilization in the Netherlands is lower than the assumed average temperature used to estimate emission fractions in INTEGRATOR, annual application emission totals and spring emissions will be overestimated. The last possible source of overestimation in spring is the misrepresentation of ground station measurement in the simulations. The MAN stations can be seen as points, so the distance between a station and the emission source plays an essential role in the measured values. If a station within a grid cell is located close to a farm, then the effect of overallocation to spring will be strengthened due to higher sensitivity. Even though the spatial resolution of the two model runs is 1.7 km x 1.7 km, it cannot fully represent what a ground station measures.

At housing-dominated stations, the comparison of surface concentrations has low correlations (see Table 4-2), and the spread in the scatter plots is quite wide (Figure 4-7(c) and 7(d)). The updated modeled results have improved, but there still exist considerable errors. Firstly, even though housing emissions are treated as point sources and assigned to where animal housing systems are located, housing emissions are still evenly divided among animal housing systems in one NCU, regardless of the differences in animal numbers and N excretion in the houses due to the lack of data availability. This brings out the errors in the absolute ammonia emission level at individual locations. Secondly, there is still an overestimation in March/April because housing-dominated stations are still affected by the uncertainties of application emissions. Last, the difference in modeled and measured ammonia surface concentrations also comes from the uncertainties of the MAN measurements, including the random uncertainties of a single MAN measurement, the calibration procedure, and the calibration standard (Lolkema et al., 2015). The relative

uncertainty decreases with the magnitude of the ammonia concentration, from 41% to 20% when measured monthly average ammonia concentrations increase from 1 to 20 $\mu g \cdot m^{-3}$ (Lolkema et al., 2015).

Other systematic errors also affect the uncertainty and inaccuracy in the spatial and temporal allocation of ammonia emissions, such as the negligence of alternative emission sources and the spatial variability of emission fractions. For example, animal waste like manure not only goes to storage facilities but also is handled in biogas powerplants, which was not accounted for in the study and will have affected the spatial distribution of ammonia emission depending on biogas powerplant locations. Additionally, the spatial variation of housing type for each animal category in each country was not taken into account. The emission fractions for animal houses and manure storage in INTEGRATOR are a function of animal category and manure category (solid manure or liquid manure) per country (De Vries et al., 2020a; Kros et al., 2012). The differences in countries are related to the animal houses and manure storage facilities that occur (high, medium, or low emission systems). One average housing or storage type per country and animal category is used without distinguishing the differences within a country. Describing the fraction of excreted nitrogen that volatilizes as ammonia as a constant may cause large uncertainties in local scale estimations. Ammonia emissions from animal excretion are highly climate-sensitive (Jiang et al., 2021). Sutton et al. (2013) showed an increase in emission rates of a factor of nine between 5 and 25 degrees Celsius, with additional effects from humidity and precipitation (Riddick et al., 2017). Skjøth and Geels (2013) emphasized the substantial impact of annual variations in meteorology and variations in overall climate on ammonia emissions because the volatilization of ammonia is very sensitive to air temperature. They argued that emissions could easily vary by 20 % for different geographical locations within a country due to overall variations in climate. The amount of nitrogen emitted as ammonia from manure application is also affected by soil properties, such as soil pH, soil moisture, and mineral soil substrate (Raymond et al., 2016). The soil pH can significantly affect ammonia volatilization positively, meaning higher soil-pH values lead to higher rates of ammonia volatilization (Raymond, 2016). There are spatial variations in the geographical distribution of soil pH, and the typical values range between 5.8 to 7.0 depending on the crop types, which is usually lower than the pH of manure (Riddick et al., 2016).

There is limited research on determining the magnitude of ammonia emissions from farming while considering the effects mentioned above. Most of the previous studies used empirical methods. For instance, Sommer and Hutchings (2001) reviewed various empirical models that used experiment-derived equations to predict ammonia volatilization from slurry application. However, only one or two factors were studied, and the interactions between these factors were not investigated. Misselbrook et al. (2000) derived ammonia emission fractions under various farming practices in the UK, but the impacts from climate

are only accounted for to a small extent in these emission factors. Another method for estimating ammonia emission fractions is to use process-based models, which take into account a theoretical understanding of relevant processes (Sutton et al., 1995; Nemitz et al., 2001; Móring et al., 2016). For field-applied slurry, Hafner et al. (2019) built a semi-empirical dynamic model to predict ammonia volatilization as well as emission fractions. Values for parameters that quantify the effects of the following predictor variables on partitioning and transfer rates were estimated: slurry dry matter, application method, application rate, incorporation (shallow or deep), air temperature, wind speed, and rainfall rate. Moreover, along with ammonia emission, soil pH changes simultaneously because the hydrolysis of ammonia production can change the soil pH. Móring et al. (2016) proposed a dynamic scheme for simulating soil pH in a field scale model and had a reasonable approximation against measurement. We think that detailing the emission fraction dynamically could be a worthwhile step to improve the emission model further.

4.5 Conclusions

A Sentinel-2-derived high-resolution crop map and the locations of animal housing systems in the Netherlands were used to update an ammonia emission model, resulting in more refined spatial details and temporal variability of ammonia emissions across the country. Using the crop map and housing information in LOTOS-EUROS, the modeled monthly and annual ammonia surface concentrations compared better with in situ measurements than those derived with the original emission product, indicating that the spatial and temporal distribution of ammonia emission estimates was improved. The model captured the magnitude and temporal variability of in situ measurements at both application-dominated and housing-dominated stations. Almost all model performance indicators have improved, with more significant improvements at housing-dominated stations. However, the model still had uncertainties, illustrated by the overestimated ammonia emission in spring. The findings indicate that including the locations of livestock housing systems and the satellite-derived crop map has improved ammonia emission estimates in space and time, and the methodology can be relatively easily applied to a larger region such as EU-27. The next step to refine the emission model would be replacing the constant emission fractions of animal housing and manure/fertilizer application with spatially explicit ones that account for the spatial variations in explanatory variables related to meteorology, manure properties, application method, and soil properties.

4

CHAPTER 5

Impact of interannual weather variation on ammonia emissions and concentrations in Germany

Ammonia is one of the most impactful pollutants emitted from agricultural activities, harming human health and contributing to biodiversity loss. In ammonia emission inventories, the spatial distribution of annual emissions is mostly approximated by constant empirical emission fractions, which do not account for spatial variability, nor for temporal variability within a year or between years caused by weather variations. Besides, factors like manure properties, soil properties, and manure application techniques also lead to differences in the amount of ammonia emitted into the atmosphere. By not or only partly accounting for these factors, significant uncertainties are introduced into ammonia emission estimates at regional and national scales. In this study, we applied the empirical ALFAM2 model to derive spatially explicit slurry application emission fractions from cropland for use in the large-scale INTEGRATOR model, using the information on slurry properties (dry matter content and pH), manure application rate, application technique, incorporation time, air temperature, wind speed, and rainfall rate. In addition, the impact of weather on the ammonia emissions from animal housing and manure storage systems was included through a temperature-dependent scaling. We applied the method to investigate the year-to-year spatio-temporal variabilities of ammonia emissions and modeled concentrations across Germany from 2015 to 2018. Through the comparison with in situ measurements and satellite-derived observations, we studied how surface concentrations and total columns relate to local meteorology. We found that the spatio-temporal variability in emission fractions improves the ability to reproduce the interannual variability observed in ammonia concentration and total column measurements. This study shows that the developed approach to derive spatially explicit emission fractions can significantly improve ammonia emission modeling and is of great importance for studying the temporal variability between years.

Abstract

5.1 Introduction

Ammonia (NH_3) is an important air pollutant, causing negative effects on human health and biodiversity at elevated concentrations (de Vries, 2021; Li et al., 2014). It reacts with sulphuric and nitric acid in the atmosphere, forming fine particulate matter ($PM_{2.5}$), which leads to increased mortality related to lung disease (Giannadaki et al., 2018; Stokstad, 2014; Wang et al., 2017). Once deposited, it can lead to acidification and eutrophication in soils and surface waters, ultimately resulting in biodiversity loss in terrestrial and aquatic ecosystems (Erisman, 2021; Sutton et al., 2013). In many regions of the world, reactive nitrogen (Nr) deposition, whose essential composition is ammonia, exceeds the critical loads of natural ecosystems (Hettelingh et al., 2017; Forsius et al., 2021). In Germany, the critical loads for eutrophication were estimated to have exceeded 70% of the ecosystem area in 2015 (Schaap et al., 2018). Since European countries have not managed to reduce ammonia emissions strongly, the negative impacts of ammonia emissions are not expected to decline substantially in the near future (European Environment Agency, 2019c).

Agriculture is the dominant source of ammonia emission into the atmosphere, accounting for more than 90% of the emission total in the E.U. (Sintermann et al., 2012). Ammonia emissions from livestock manure and mineral fertilizer constitute a significant but variable proportion of reactive nitrogen loss (Amann et al., 2013; Hafner et al., 2019). Ammonia emissions from livestock manure, which includes manure (urine and feces) in animal houses, manure in storage systems, and manure applied to fields, contribute to nearly 80% of the total agricultural emissions at the European scale (EU27) (de Vries et al., 2011; Leip et al., 2015). Based on EMEP results in 2020, when EMEP revised the country-reported annual emission per sector of 2018, manure management (livestock housing and manure storage) for cattle, pigs, and poultry adds up to about 23%, 15%, and 5% of the annual emission total in Germany, respectively. In addition, the application of manure and mineral fertilizer to fields contributes to around 33% and 12% of the annual total (Reported emission data, 2022).

Accurate estimates of ammonia emission are of great significance for Nr budgets at the field- or farm scale (Sonneveld et al., 2008; Sintermann et al., 2012), landscape scale (Cellier et al., 2011; de Vries et al., 2015), and national or continental scale (de Vries et al., 2011; Kros et al., 2018). The nitrogen flow approach is a common method to model annual ammonia emission within countries where emissions are calculated using emission fractions, which are the ratios between the emitted ammonia to the atmosphere and the total ammoniacal N (TAN) allocated in various agricultural sectors. This methodology has been adopted by Hutchings et al. (2001) for Denmark, Webb and Misselbrook (2004) for the U.K., Gac et al. (2007) for France, (Velthof et al., 2012) for the Netherlands, and by Dämmgen and Hutchings (2008) for Germany.

5

Many experiments on ammonia emission from livestock manure applied to fields have been conducted to develop or evaluate emission fractions (Webb and Misselbrook, 2004; Sintermann et al., 2012). The emission fractions used in the inventories are usually derived by experts averaging over time for each country, not considering either the spatial variability of meteorology or the differences in manure properties, application technique, and incorporation time. The need for including such temporal and spatial differences due to meteorology for accurately assessing ammonia emissions and deposition has been described in several publications (Van Damme et al., 2015; Jiang et al., 2021; Truong et al., 2018; Sommer et al., 2019; Ge et al., 2020). Neglecting such spatial and temporal differences affects the timing of manure and fertilizer application and the related emission fraction. The weather impact is more prominent on the more temporally variable emissions from manure and mineral fertilizer application than the less temporally variable emissions from animal housing and manure storage (Skjøth et al., 2011; Ge et al., 2020).

In assessing the temporal (intra-annual) and spatial variability using the INTEGRATOR model with the agricultural management model TIMELINES, Ge et al. (2020) identified overestimated ammonia emissions in Southern Germany and an underestimation in the country's north. The authors stipulated that this was likely due to using constant ammonia emission fractions for manure application, animal housing, and manure storage all over Germany. Furthermore, several studies have concluded that the currently available emission products do not correctly reflect the impact of inter- and intra-annual variability of ammonia emissions in terms of timing and amount (Backes et al., 2016; Hendriks et al., 2016; Hellsten et al., 2008; Skjøth et al., 2011), highlighting the need to improve the emission fractions for agricultural ammonia emission modeling.

The challenge of estimating field application emissions is formidable because of many influencing variables such as application techniques, manure properties, and the dependence on meteorological conditions. Several models have been developed to predict ammonia emissions from manure applied to fields (Misselbrook et al., 2005; Smith et al., 2009; Gericke et al., 2012; Nicholson et al., 2013; Congreves et al., 2016). Most of these models are empirical or process-based models that contain specific empirical components (Cuddington et al., 2013; Hafner et al., 2019), with each model type having its advantages and disadvantages. Process-based models can more accurately predict complicated responses under specific conditions (Hafner et al., 2019), while empirical models are generally easier to apply since they have fewer parameters and inputs. Process-based models such as the Volt'Air (Génermont and Cellier, 1997) and Manure DNDC (Li et al., 2012) model by principle follow a more mechanistic approach. Volt'Air simulates the gaseous transfers between the soil and the lower atmosphere by dealing with nitrogen's physical and chemical equilibria, the soil surface's energy budget, and the transfers of heat, water, and solutes within the soil profile (Génermont and Cellier, 1997). The Manure DNDC

model is based on thermodynamics and biogeochemical reaction kinetics, controlled by a group of environmental factors (such as temperature, soil moisture, and soil pH) (Li et al., 2012). In contrast, empirical models use relationships based on observed behavior in the field situation. For example, Huijsmans et al. (2018) utilized a logistic regression function to mimic the emission relative to discrete intervals after manure application. The ALFAM (Søgaard et al., 2002) and MANNER (Nicholson et al., 2013) models are two other examples of fully empirical models. They use a Michaelis-Menten function to predict the cumulative emissions simply because the shape of the function is similar to the observed pattern of emission over time. The semi-empirical dynamic model ALFAM2 (Hafner et al., 2019) finds a balance between the simplicity of empirical models and the more accurate representation of processes achieved with a process-based approach and accounts for many control variables. ALFAM2 is the successor of the widely used ALFAM model and is built on a two times larger database of ammonia emissions from field-application experiments than its predecessor. ALFAM2 accounts for the impacts of manure properties (dry matter, slurry pH), meteorology (air temperature, wind speed, and rainfall rate), and application techniques and incorporation time.

This paper aims to improve the spatial and temporal (interannual) variation of ammonia emissions within Germany by replacing country-dependent emission fractions with spatially-explicit gridded matrices using the ALFAM2 model approach. First, we describe the methodology of (1) the INTEGRATOR emission model, which generates spatially resolved N inputs in animal houses (excretion from urine and feces), manure storage systems, N applied to fields by manure and fertilizer application and by grazing; (2) the ALFAM2 model that predicts emission fractions of slurry manure application while accounting for variations in meteorology, manure properties, application techniques, incorporation time and application rates; (3) the chemistry transport model (CTM) LOTOS-EUROS which translates ammonia emission into atmospheric concentrations; and (4) satellite observations of ammonia total columns and in situ measurements of surface concentrations for validation. Subsequently, we evaluate the model performance by comparing modeled results and measurements over Germany from 2015 to 2018 to quantify the improved model's capability to reproduce the interannual variability of annual ammonia emission totals and the spatial and temporal variability of ammonia emissions. Finally, the results, potential shortcomings, and possible future methodological improvements are discussed.

5

5.2 Methodology

A schematic overview of the modeling approach is presented in Figure 5-1. The emission model consists of three modules, including a spatial allocator of manure, compost, and fertilizer N inputs, an emission fraction predictor of those inputs, and a temporal allocator of ammonia emissions. The spatial allocator produces the spatial distribution of N excretion in animal housing and manure system and on the field through manure and mineral fertilizer application and grazing using the INTEGRATOR model. The emission fraction predictor derives emission fractions of slurry application with the ALFAM2 model and emission fractions of animal housing and manure storage using a temperature-based scaling (TBS) algorithm. The INTEGRATOR outputs on grazing emissions and emissions from solid manure and mineral fertilizer application were kept as they were. It has to be noted that emissions from compost and digestate application are not included in INTEGRATOR. However, the official German inventory started to include this sector in 2010. Therefore, we took the reported annual emission total of this sector from European Monitoring and Evaluation Programme (EMEP) and used a top-down algorithm to spatially allocate the emission over Germany. The details can be found in the supplementary material Section S5.1. The temporal allocator creates emission time profiles that distribute gridded annual emissions in time, which also predicts fertilization dates that the emission fraction predictor requires.

The study area was set to be Germany due to data availability. Therefore, the spatial domain was 5°E – 16°E with a resolution of 0.1 degrees in longitude and 46°N – 56°N with a resolution of 0.05 degrees in latitude (approximately 6 x 6 km^2), corresponding to a domain size of 110 pixels by 200 pixels in longitude and latitude, respectively. For each year from 2015 to 2018, the 3D distribution of ammonia emissions (gridded annual emissions and emission time profiles) was then imported into the CTM LOTOS-EUROS to derive surface concentrations and total columns of ammonia. The simulated values were evaluated with remote sensing observations and in situ measurements.
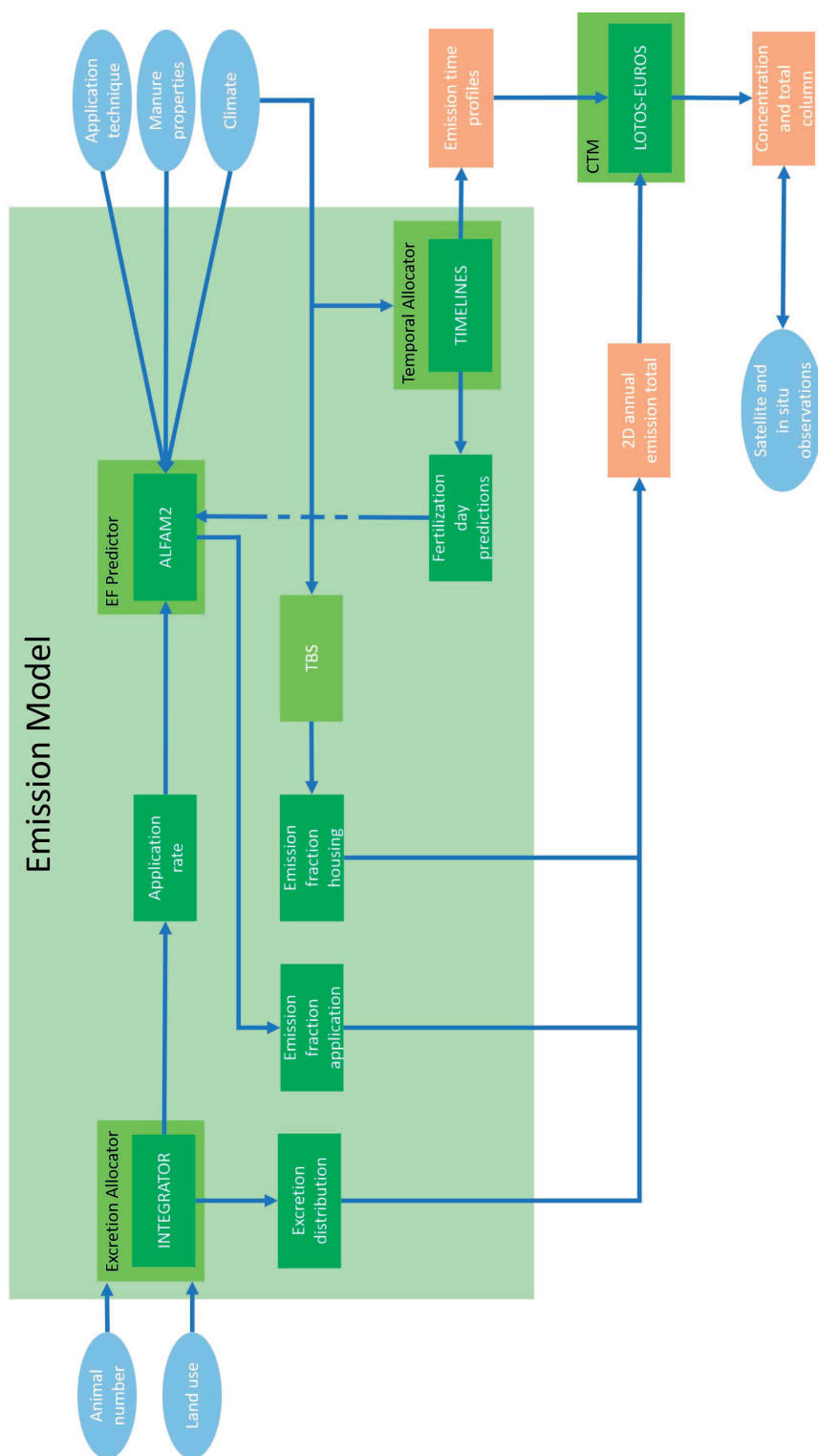
Figure 5-1 Schematic overview of calculating the spatial and temporal distribution of ammonia emissions and validating by the comparison with measurements in this study.

5

5.2.1 Spatial allocator of manure, compost, and fertilizer inputs

5.2.1.1 The INTEGRATOR model

The INTEGRATOR model is a static N cycling model that can assess N emissions from housing, manure storage systems, and the soil (due to manure and mineral fertilizer application) in response to European-scale changes in land use, land management, and climate (De Vries et al., 2011). INTEGRATOR estimates emissions in NitroEurope Classification Units (NCUs), which are multi-part polygons composed of 1 km × 1 km grid cells in the ETRS89/LAEA Europe coordinate system (for a detailed description of NCU, we refer to Ge et al. (2020).

The emission model starts with calculating total N excretion by multiplying the number of animals at the NCU level with the N excretion rate per animal per country for various animal categories (Kros et al., 2012). The total manure production is derived by subtracting gaseous emissions and leaching in housing and manure storage systems from the N excretion. The N excreted within housing systems is the multiplication of N manure excretion and the housing contribution fraction, while the N excreted from grazing on land is obtained by subtracting N excreted in housing systems from total N manure excretion. Manure is then allocated over grassland and arable crop groups using various allocation rules. Manure produced by grazing animals and in housing systems by sheep and goats all enter grassland. A fraction is applied to arable land for other manure, and the remaining fraction is applied to grassland/fodder crops. For the distribution of manure application on arable land, we distinguish three arable crop groups with (i) a relatively high use of manure (sugar beet, barley, rape, and soft wheat), (ii) an intermediate use of manure (potatoes, durum wheat, rye, oats, grain maize, other cereals including triticale, and sunflower), and (iii) low use of manure (fruits, oil crops, grapes, and other crops) using weighing, based on Velthof et al. (2009). Finally, no manure is allocated to dry pulses and rice, fiber crops, other root crops, and vegetables. The amount of mineral fertilizer needed is then estimated with an N-balanced approach, which we refer to Ge et al. (2020) for more details.

After the N excretion distribution of housing, grazing, and manure and fertilizer application is obtained, the gaseous emission of each category is derived by the multiplication with the emission fraction per housing system, for grazing, and manure and fertilizer application, respectively (De Vries et al., 2020a; Kros et al., 2012). The spatial allocator in this study is the subcomponent of INTEGRATOR that produces the N excretion distribution before multiplying emission fractions. The NCU-level N excretion from the spatial allocator was resampled to the grid cells in this paper. Furthermore, N from manure and mineral fertilizer application on the fields was reallocated to the corresponding crops and grassland based on the crop map.

5.2.1.2 Input data

The input data of INTEGRATOR are classified into three categories: biophysical data (soil, land use, and climatic data), agricultural activity data (animal numbers and N excretion rates), and emission information (fractions of N emission, leaching, and runoff). The version of INTEGRATOR in this study was developed for the year 2010 and used by Ge et al. (2020) to improve the spatial details of ammonia emission. Since this study focused on 2015 – 2018, the input data on animal numbers and land use were revised.

Animal numbers

The livestock data in INTEGRATOR (version 2010) were obtained from the FAO database at the country level, using Common Agricultural Policy Regionalised Impact analysis (CAPRI) data for distribution at the NUTS2 level. The data on livestock numbers of various animal categories at the NUTS2 level were downscaled to a $1\,km \times 1\,km$ resolution using expert-based judgment with spatial data sources on land use, slope, altitude, and soil characteristics influencing the livestock carrying capacity (Neumann et al., 2009). However, the animal number data officially reported to EMEP from the German inventory differ substantially from those in FAO used by INTEGRATOR, especially after 2010 (Haenel et al., 2020). There are several reasons for the diverging animal numbers of the two datasets. For cattle (including buffalo), FAOSTAT contains the data of the May census in the years 2011 – 2013, while German inventory uses the data of the November census as required by E.U. regulations. The FAOSTAT animal numbers for cattle only agree with the official German data after 2013. The FAOSTAT numbers of pigs, sheep, and goats are generally not comparable with the number in the German inventory. Because in the German inventory, the number of suckling piglets (i.e., piglets weighing less than 8 kg) is subtracted, the number of sheep number was revised in 2010, and the number of goats was linearly interpolated to fill in missing values (Haenel et al., 2020). Therefore, we adjusted the animal numbers in INTEGRATOR for 2010 to align them with those in the German inventory for the years 2015-2018, according to:

$$N(ani, INT, NUTS)_{2015-2018}$$
$$= N(ani, INT, NUTS)_{2010} \times \frac{N(ani, INT, state)_{2015-2018}}{N(ani, INT, state)_{2010}} \quad (5.1)$$

where $N(ani, INT, state)_{2015-2018}$ is the reported animal numbers per animal type per federal state in Germany averaged over the years 2015-2018 and $N(ani, INT, state)_{2010}$ is the calculated animal numbers per animal type per state in Germany averaged for 2010 in INTEGRATOR, based on the NUTS-level data.

Land use

The standard land use input in INTEGRATOR is the total area of each arable crop or grassland for each NCU based on the year 2010, requiring an update for 2015 – 2018. Thus, we used an updated map of crop and land cover classes for Germany in 2016 based on the crop map developed by Griffiths et al. (2019), who integrated multitemporal multispectral Sentinel-2 and Landsat reflectance data and subsequently generated equidistant, dense, and intra-annual composite time series to provide this national scale map. We used the crop raster map to derive crop areas per NCU for the five years to control the number of variables, assuming that crop rotation in a grid remains semi-constant over the years.

5.2.2 Temporal allocator of ammonia emissions

The usual approach to characterizing the temporal variability in NH_3 emissions is to use time profiles that distribute the annual emission total in a grid cell over a year. Ge et al. (2020) explicitly described the temporal allocation of NH_3 emissions from manure and fertilizer application, grazing, animal housing, and manure storage based on the concepts of Skjøth et al. (2004), Gyldenkærne et al. (2005). The temporal allocator in this study used TIMELINES (Hutchings et al., 2012) to predict the fertilization days for the years between 2015 and 2018 by introducing a thermal time approach. Thermal time is the sum of the positive differences between the daily mean air temperature and a base temperature (0 degrees Celcius). Starting from 1 January, as soon as thermal time on Julian day t reaches the reference thermal time for sowing (or harvesting), it is considered that sowing (or harvesting) occurs on Julian day t. Field operations like manure and mineral fertilizer applications are related to it. The fertilization day predictions were used to construct the time profiles of ammonia emissions from manure and fertilizer application. Regarding the details of the temporal allocator of ammonia emission, we refer to Ge et al. (2020). The fertilization days were also taken into account when we generated meteorological condictions for emission fraction calculations in ALFAM2, which will be elaborated later.

5.2.3 Emission fraction of manure slurry application

Originally, the obtained N distribution in housing systems and on the field is then combined with the corresponding NH_3-N emission fractions in INTEGRATOR, which depend on the animal category, manure type (liquid/solid), and the degree of implementation of emission-reducing techniques per country. In this study, the INTEGRATOR outputs for N slurry application rates were combined with information on meteorology and manure properties for use in the second module (the emission fraction predictor) to calculate the emission fraction of slurry application using the ALFAM2 model.

5.2.3.1 The ALFAM2 model

The ALFAM2 model simulates the behavior of applied total ammoniacal nitrogen (TAN, kg ha^{-1}) over time, based on Chantigny et al. (2004). After the slurry is applied to land, TAN is immediately partitioned between two pools: a "fast" pool representing slurry in direct contact with the atmosphere, and a "slow" pool representing fractions less available for emission due to slurry infiltration (Sommer et al., 2004; Chantigny et al., 2004), adsorption of ammonium (NH_4^+) on cation exchange sites (Pelster et al., 2019), crust formation (Thompson et al., 1990), injection (Webb et al., 2010), or incorporation (Huijsmans, 2003). ALFAM2 parameters value on partitioning and transfer rates, quantifying the effects of slurry application, were estimated from an extensive data set of emissions from cattle and pig slurry (490 field plots in 6 countries from the ALFAM2 database). An analysis of a large subset of the ALFAM2 database showed that most total measured ammonia emission from slurry application generally occurs within 72 hours (Hafner et al., 2018). Consequently, the ALFAM2 model is restricted to a maximum duration of 72 hours (3 days) after slurry application to allow parameter estimation. Therefore, we calculated emission fractions as the relative accumulated emission (ratio between N emitted as ammonia and TAN applied) at the 72nd hour.

Figure 5-2 shows an example of accumulative fractional emission calculated with ALFAM2 for different surface temperature conditions to inspect the impact of temperature. The x-axis represents the number of hours after slurry application (72 hours maximum), and the y-axis is the accumulative fractional emission. Three surface temperature (20, 15, and 10 degrees Celsius) conditions were studied, while other variables remained the same. In this experiment, the TAN was set to be 40 g/kg, and the dry matter of manure is 8% the application method is broadcast with an incorporation time of 2 hours after application. One can see that the largest share of the ammonia emission takes place within the first 6 hours after application, and then it gradually increases at a much lower rate. Furthermore, higher temperature results in higher N loss to the atmosphere in the form of ammonia. The emission fractions for these three temperature scenarios are around 0.40, 0.32, and 0.25, respectively, illustrating the importance of meteorological conditions during application activities.

5
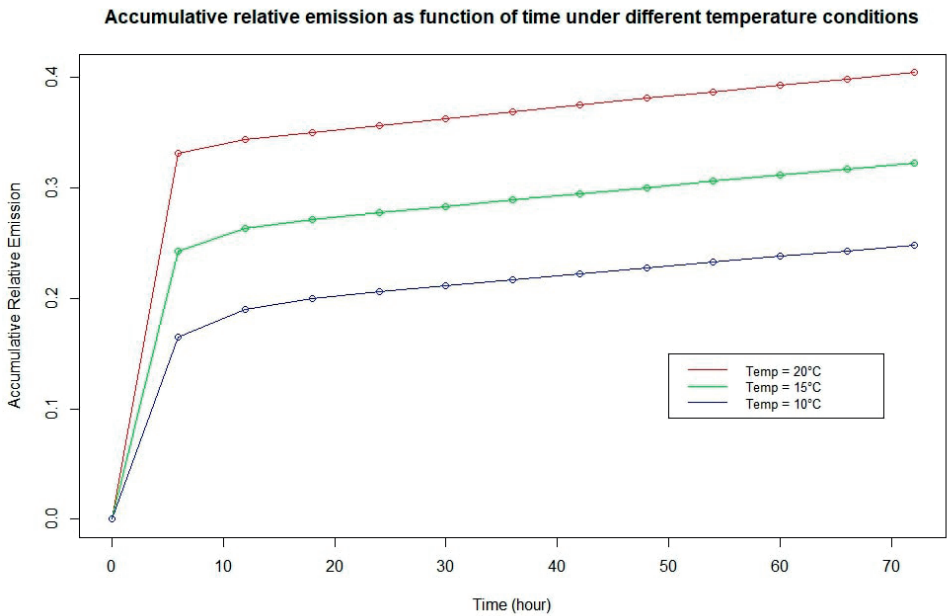
Figure 5-2 Accumulative relative emission as a function of time under average temperature conditions (20, 15, and 10 degrees Celsius).

5.2.3.2 Input data

ALFAM2 input data include slurry dry matter and pH, application rate, application method and incorporation time, air temperature, wind speed, and rainfall rate. Consequently, these variables were included to derive a spatially explicit and dynamic emission fraction product.

Manure properties and application rate

Manure properties accounted for in ALFAM2 include slurry dry matter content and pH. The dry matter values of cattle, pig, and poultry liquid manure were reported averages of different types of manure composition used in INTEGRATOR from the RAMIRAN network (Menzi et al., 2002). The dry matter values of cattle and pig slurry were set to 67 g/kg and 52 g/kg, respectively. The pH of cattle and pig slurry were both set at 7.9 based on Joubin (2018) and Martínez-Suller et al. (2010). The spatial distribution of the slurry application rate was obtained from the excretion allocator described previously.

Application method and incorporation time

Data on the slurry application method in Germany, which differentiates broadcasting, trailing hose, trailing shoe, slot method, cultivator, and injection, were derived from a

survey in 2015, namely Wirtschaftsdünger tierischer Herkunft in landwirtschaftlichen Betrieben/Agrarstrukturerhebung, by the Federal Statistical Office of Germany (Statistisches Bundesamt). This survey gives the area of cropland and grassland on which each application technique was applied at the federal state (Bundesland) level. For arable land, the areas also include a distinction in incorporation time, i.e., no incorporation, incorporation right after application (incorporation time 0), incorporation within one hour (incorporation time <1h), and after one hour (incorporation time > 1h) following application. Since it is unknown which application method is applied on individual fields within a given federal state, we calculated all possible emission fractions for all methods and incorporation options mentioned in the survey with ALFAM2. We then used weighing factors, namely the area per application method per incorporation time divided by the total area, to derive weighted means of emission fractions. An overview of the area percentage of the application techniques on arable land at the state level is given in Table 5-1.

Meteorology

The ALFAM2 model requires air temperature, wind speed, and rainfall rate as meteorological input for emission fraction prediction. We obtained these variables from the ERA5-Land datasets in the Copernicus Climate Data Store (https://cds.climate.copernicus.eu/cdsapp#!/dataset/reanalysis-era5-land). The spatial resolution of the products is 0.1 by 0.1 degrees; thus, it was resampled to the grid in this study. ERA5-Land is a reanalysis dataset providing land variables over several decades at an enhanced resolution compared to ERA5. As previously described, we predicted the fertilization days for each crop from the temporal allocator and calculated the mean air temperature, wind speed, and rainfall rate for the five days before and after the predicted fertilization days. These were the inputs for ALFAM2 so that the data derived could better represent the weather condition during fertilization.

The weighted mean of emission fractions at a location was calculated as:

$$EF(x,y) = \sum \frac{Area_{AT,T_{incorp}}(x,y)}{Area_{sum}(x,y)} EF_{AT,T_{incorp}}(x,y) \tag{5.2}$$

where (x, y) is the coordinates of a location. $Area_{AT,T_{incorp}}(x,y)$ is the area of arable crops or grassland on which application technique AT with a given incorporation time T_{incorp} is used in the German state where (x,y) is located, $Area_{sum}(x,y)$ is the area sum of arable crops or grassland surveyed in the same German state, $EF_{AT,T_{incorp}}(x,y)$ is the predicted emission fraction of application technique AT with incorporation time T_{incorp} from the ALFAM2 model, calculated as:

$$EF_{AT,T_{incorp}}(x,y)$$
$$= f_{ALFAM2}\left(AT, T_{incrop}, T(x,y), W(x,y), P(x,y), DM, pH, R_{app}(x,y)\right) \quad (5.3)$$

where *AT, T_{incorp} , T(x,y), W(x,y), P(x,y), DM, pH, R_{app} (x,y)* are the application method, incorporation time, temperature, wind speed, precipitation rate, manure dry matter, manure pH, and application rate at a given location, respectively.

Table 5-1 Fraction of different application methods and incorporation time applied on arable land per German federal state.

Application technique	Broadcast				Trailing hose				Trailing shoe				Slot injection			
Incorporation time	/	0	<1h	>1h	/	0	<1h	>1h	/	0	<1h	>1h	/	0	<1h	>1h
Baden-Württemberg	0.401	0.033	0.116	0.122	0.165	0.008	0.027	0.029	0.034	0.001	0.005	0.005	0.020	0.004	0.015	0.016
Bayern	0.333	0.095	0.142	0.092	0.028	0.007	0.010	0.007	0.103	0.021	0.032	0.021	0.040	0.020	0.030	0.019
Berlin	1.000	0.000	0.000	0.000	0.000	0.000	0.000	0.000	0.000	0.000	0.000	0.000	0.000	0.000	0.000	0.000
Brandenburg	0.035	0.054	0.058	0.043	0.211	0.104	0.112	0.083	0.024	0.007	0.007	0.005	0.038	0.076	0.082	0.061
Bremen	0.366	0.063	0.091	0.099	0.232	0.010	0.014	0.015	0.072	0.003	0.004	0.005	0.025	0.000	0.000	0.000
Hamburg	0.030	0.055	0.080	0.213	0.257	0.032	0.046	0.124	0.032	0.004	0.006	0.015	0.020	0.014	0.020	0.053
Hessen	0.345	0.036	0.175	0.188	0.113	0.006	0.030	0.032	0.017	0.002	0.008	0.008	0.011	0.003	0.013	0.014
Mecklenburg-Vorpommern	0.093	0.053	0.085	0.065	0.276	0.063	0.101	0.078	0.008	0.002	0.003	0.003	0.020	0.039	0.062	0.048
Niedersachsen	0.165	0.053	0.117	0.060	0.232	0.040	0.088	0.045	0.057	0.008	0.018	0.009	0.020	0.020	0.044	0.023
Nordrhein-Westfalen	0.176	0.030	0.097	0.038	0.380	0.027	0.089	0.035	0.039	0.004	0.012	0.005	0.020	0.009	0.029	0.011
Rheinland-Pfalz	0.367	0.036	0.203	0.154	0.094	0.006	0.033	0.025	0.019	0.001	0.005	0.003	0.017	0.004	0.019	0.015
Saarland	0.327	0.014	0.333	0.185	0.053	0.001	0.027	0.015	0.000	0.000	0.005	0.003	0.031	0.000	0.004	0.002
Sachsen	0.028	0.080	0.021	0.017	0.077	0.089	0.023	0.019	0.025	0.008	0.002	0.002	0.098	0.347	0.090	0.075
Sachsen-Anhalt	0.042	0.058	0.029	0.038	0.213	0.110	0.055	0.072	0.030	0.011	0.006	0.007	0.038	0.135	0.068	0.088
Schleswig-Holstein	0.270	0.043	0.154	0.097	0.248	0.014	0.049	0.031	0.014	0.001	0.003	0.002	0.012	0.009	0.032	0.020

5

5.2.4 Emission fraction of animal housing and manure storage

We used a temperature-based scaling algorithm to derive the spatial and interannual variability of animal housing and manure storage emission fractions. Skjøth et al. (2011) and Gyldenkærne et al. (2005) describe the emission pattern from animal housing and manure storage as below:

$$\begin{cases} Fkt_i = E_i(x,y) \times \big(T_i(x,y)\big)^{0.89}, & T_i(x,y) \geq T_{boundary} \\ T_i(x,y) = \begin{cases} 18 + 0.77 \times (T(x,y) - 12.5), & Houses\ with\ forced\ ventilation \\ T(x,y) + 3, & Open\ animal\ houses \\ T(x,y), & Manure\ storage \end{cases} \end{cases} \quad (5.4)$$

where i refers to the index (1-3) of houses with forced ventilation, open animal houses, and manure storage, respectively. x, y are the coordinates of the emission grid. $E_i(x, y)$ represents the emission for the corresponding agricultural sector within the grid cell. $T_i(x, y)$ is the temperature function. $T(x, y)$ is the 2-meter temperature at the given location. Open houses and manure storage have almost the same emission pattern, except that the indoor temperature in open houses is 3 degrees higher than the outside temperature used for manure storage (Gyldenkærne et al., 2005). $T_{boundary}$ represents lower boundary condition for temperature in animal housing and manure storage, below which emission is set to a constant level, and they are 18, 4, and 1 degree for houses with forced ventilation, open animal houses, and manure storage, respectively.

The concept of temperature-based scaling is to calculate the time profile of the three categories (insulated housing, open housing, and manure storage), using the mean temperature between 2015 and 2018 to represent the averaged pattern of ammonia emission spatially and between years as the base. Subsequently, we used the temperature time series of each year and calculated the deviations from the base at every grid cell, aiming to introduce the variability of the emission fraction based on the deviations. First, we calculated the spatial distribution of the base emission fraction $EF_{i,base}(x, y)$:

$$EF_{i,base}(x,y) = \frac{Fkt'_{i,mean}(x,y)}{mean\big(Fkt'_{i,mean}\big)} \times EF_{i,int} \quad (5.5)$$

where $Fkt'_{i,mean}(x, y)$ is the mean of the function values calculated by the 4-year mean temperature above $T_{boundary}$ at a given location, $mean(Fkt'_{i,mean})$ is the mean of $Fkt'_{i,mean}(x, y)$, $EF_{i,int}$ is the emission fraction introduced in INTEGRATOR. This was under the assumption that the static country-dependent emission fractions represent the emission level with mean temperature conditions over the four years. Subsequently, the gridded emission fraction of housing and storage in each year was calculated as:

$$EF(x, y) = EF_{i,base}(x, y) \times \sum_{t=1}^{n} \frac{Fkt_i(x, y, t)}{Fkt_{i,mean}(x, y, t)} \qquad (5.6)$$

where $Fkt_i(x, y, t)$ is the function value at the hourly time step t in a year at a given location using the original temperature data, $Fkt_{i,mean}(x, y, t)$ is the function value at time step t at a given location using the 4-year mean temperature.

5.2.5 Validation of model estimates to measurements

To validate the emission estimates, we imported the gridded annual emissions and time profiles into LOTOS-EUROS to derive surface concentration and total column which were compared with in situ measurement and satellite observation, respectively.

5.2.5.1 The LOTOS-EUROS model

The LOTOS-EUROS model is an Eulerian chemistry transport model that simulates air pollution in the lower troposphere (Schaap et al., 2008b, 2012; Manders et al., 2017). In this paper, the spatial resolution of LOTOS-EUROS was set to be the same as the emission product, namely 0.1° in longitude and 0.05° in latitude. In the vertical, we applied the well-mixed dynamic boundary layer concept. There are four dynamic layers and a surface layer. The lowest dynamic layer is the mixing layer, followed by three reservoir layers. The model's physical processes include advection, diffusion, dry and wet deposition, chemistry reaction, and sedimentation. LOTOS-EUROS uses a set of temporal factors (monthly, daily, and hourly) to break down annual total emissions into hourly emissions. LOTOS-EUROS has been used for a wide range of applications supporting scientific research. It is used for daily operational air quality forecasts over Europe (Marécal et al., 2015) and the Netherlands (Hendriks et al., 2013), as well as for daily forecasts of dust concentrations over North Africa (Dominguez-Rodriguez et al., 2020), and the forecast of dust storms in China (Jin et al., 2021).

The LOTOS-EUROS CTM was used to simulate surface concentrations and total columns from the emission products. After replacing the gridded annual ammonia emission input with the newly developed emission distribution and replacing the fixed simplified temporal factors with updated spatially explicit time profiles, the improvements can be evaluated by comparing modeling results with in situ measurements and satellite observations.

Three LOTOS-EUROS simulations with a 4-year duration were performed in this study: 1) the base scenario (referred to as *BASE* in this paper) using the gridded annual emissions from the INTEGRATOR output that was scaled by reported country totals (as in Ge et al. (2020)) and the default simplified hourly emission time profile setting in LOTOS-EUROS;

2) a second reference case (referred to as *TIME*) which uses the same gridded annual emissions in *BASE* and the dynamic and a spatially explicit time profile developed with the method from Ge et al. (2020); 3) the test case (referred to as *SPACETIME*) using the gridded N distribution from INTEGRATOR combined with meteorology-dependent emission fractions for slurry application, animal housing and manure storage with ALFAM2 and the same activity time profile as in *TIME*. An overview of the three scenarios is listed in Table 5-2. By comparing the *BASE* and *TIME* scenarios, the impact of dynamic time profiles can be determined since meteorological conditions affect the timing of fertilization practices and thereby the intra-annual time distribution of ammonia emission (Ge et al. (2020)). By comparing the *TIME* and *SPACETIME* scenarios, the improvement introduced by the updated emission fractions in this study can be quantified.

Table 5-2 An overview of emission input the three model runs in this study.

Scenario	Gridded annual emission	Time profile
BASE	INTEGRATOR output with constant emission fractions and scaled with national totals per sector (Ge et al., 2020)	Country-dependent, fixed time profile in LOTOS-EUROS
TIME	INTEGRATOR output with constant emission fractions and scaled with national totals per sector (Ge et al., 2020)	Spatially explicit activity time profile, varying per year depending on meteorological conditions (Ge et al., 2020)
SPACETIME	INTEGRATOR output with meteorology-dependent spatially explicit emission fractions	As above, the timing remains the same but the amplitude is adjusted due to different gridded emissions induced by the meteorology-dependent emission fractions the timing

5.2.5.2 Satellite observations of ammonia total columns

To evaluate the modeled distributions we used satellite observations. The Cross-track Infrared Sounder (CrIS) instrument is a Fourier Transform Spectrometer (FTS) launched by the U.S. NOAA/NASA on both the Suomi National Polar-orbiting Partnership (S-NPP) satellite on 28 October 2011 and the NOAA-20 satellite on 29 November 2017 (Shephard and Cady-Pereira, 2015; Shephard et al., 2020). CrIS is an across-track scanning hyperspectral infrared instrument in a sun-synchronous orbit (824 km) with a 2200 km swath width (±50°) with the total angular field of view consisting of a 3×3 array of circular pixels of 14 km diameter each (nadir spatial resolution). CrIS provides soundings of the atmosphere over three wavelength bands in the infrared with a spectral resolution of 0.625 cm^{-1}. The wavelength range 9.14–15.38 µm (650–1095 cm^{-1}) is used to retrieve ammonia, as the main ammonia infrared absorbing band lies in this spectral region, with the strongest absorption features between 960 and 970 cm-1 (Shephard and Cady-Pereira, 2015).

The CrIS has some advantages in contrast to other instruments. First, it has dense global coverage. In addition, it has improved sensitivity in the boundary layer due to the low

spectral noise of ~0.04 K at 280K (4 times lower than IASI (Clarisse et al., 2009; Van Damme et al., 2017)) in the ammonia spectral region (Zavyalov et al., 2013). Therefore, it has the potential to detect smaller ammonia concentrations than are currently possible with IASI. Furthermore, the early afternoon overpass (a mean local daytime overpass time of 13:30 in the ascending node) coincides with higher thermal contrast (difference between the surface and air temperature), which is a more favorable measurement condition for infrared instruments (Shephard et al., 2020). Lastly, the CrIS fast physical retrieval (Shephard and Cady-Pereira, 2015) provides vertical sensitivity and robust and straightforward retrieval error estimate based on the retrieval input parameter. The CrIS averaging kernel usually has a maximum between 680 hPa and 850 hPa depending on the local conditions and a significant decrease near the surface since the instrument has reduced sensitivity near the surface. We only used the simulated output closest to the measurements in space and time to harmonize modeled and measured total columns during comparison. Furthermore, we applied the linearized averaging kernel (Cao et al., 2022) of each CrIS observation to the corresponding model result when calculating total columns from the LOTOS-EUROS three-dimensional concentrations.

The CrIS v1.6.1 data product was downloaded from https://hpfx.collab.science. gc.ca/~mas001/satellite_ext/cris/snpp/nh3/. Daytime observations between January 2015 and December 2018 were used for this study. Furthermore, only observations with a quality flag of 3 were selected. The measurements with signal-to-noise ratio >2, degrees of freedom >0.8, and thermal contrast >−2 K were selected to filter out anomalous values due to thin clouds, very cold surfaces, and observations with low information content (Shephard et al., 2020).

It has to be noted that there is a background level ammonia total column from CrIS observations. Shephard and Cady-Pereira (2015) determined the minimum ammonia detection limit of CrIS, which is caused by the relatively weak atmospheric spectral signal of ammonia compared with the background infrared signal. The minimum detection limit was assumed to be where SNR is between 1 and 2. When ammonia concentration is low, the infrared signal will also be small. The CrIS instrument has relatively lower minimum detection levels, and here a more conservative limit of 0.9 ppb is assumed to cover most of the conditions found in the observations (Shephard and Cady-Pereira, 2015). Assuming that 1 ppb is equal to a total column $2 \pm 1 \times 10^{15}\, molec / cm^2$, so the lower limits of CrIS was set to be $1.8 \pm 0.9 \times 10^{15}\, molec / cm^2$ (Dammers et al., 2019). However, the threshold used in this paper to exclude the background constant total column is much higher (1×10^{16} $molec / cm^2$), below which a measurement was omitted, because we wanted to focus on the agriculturally active regions.

5.2.5.3 *In situ measurements of ammonia surface concentrations*

In addition to satellite observations of total columns, there are surface concentration measurements that were conducted by the Umweltbundesamt (UBA) research foundation. UBA sets up monitoring stations, providing information on air pollutants to governments and the public. It measures species, including ammonia and greenhouse gases, essential for improving air quality and climate change knowledge. The UBA also collects data from the network of the German federal states. In this study, the in situ data is available for 2015 – 2018 with weekly temporal resolution.

5.2.5.4 *Calculation of the mean surface concentrations and total columns during peak periods*

Emissions from slurry application and animal housing in single grid cells are expected to differentiate after applying the new emission fractions. However, the change is disaggregated into hourly time series using the time profiles, making it less noticeable in an absolute sense and more challenging to detect the improvement brought by our developments. Since the paper aims to reproduce the emission trend brought on by meteorology, we can validate it by analyzing if the new model can reproduce the trends illustrated by the sensitivity of surface concentration and total columns to temperature. This is because the temperature is the most decisive factor for the emission potential since other factors such as application methods and manure properties were kept the same at the state level every year.

The in situ measurements have extensive temporal coverage but low spatial representativeness, while the satellite observations have large spatial coverage but limited temporal continuity due to measurement quality. Therefore, it is more reasonable to look at the ammonia level in a larger region instead of a single location to illustrate the improvements of the new methodology. The UBA measurements and CrIS observations usually show three ammonia level peaks in a year. These are a prominent peak in the time block I between Julian Day 77 and 137 (caused by the first spring fertilization) and a lower peak in the time block II between Julian Day 147 and 197 (due to the second spring fertilization), and a flatter and more subtle peak (representing summer application and housing/storage emissions) in the time block III between Julian Day 207 and 277. Therefore, we calculated the mean surface concentrations and total columns of the three time blocks for each state in the four years and studied the trends against the mean temperature of the corresponding time blocks and states. To identify the models' capability to simulate concentrations in response to temperature, we conducted a comparison between simulated and measured slopes of the response of surface concentration to temperature in the three periods. It has to be noted that during the comparison of surface concentration trend, there was a distinguishment between coastal stations (which only exist in Mecklenburg-Vorpommern and Niedersachsen) and in-land stations. The ammonia

levels measured by coastal stations demonstrated significantly fluctuating patterns due to their unique locations with strong wind and humidity and ammonia's high reactive properties. As a result, they were excluded during the validation.

5.3 Results

5.3.1 Annual emission totals and time series per sector

The emission totals for Germany calculated with the updated emission fractions as categorized in the EMEP database for years from 2015 to 2018 are compared with the ones with the static emission fractions in Table 5-3. The magnitudes of the estimated annual emission totals using weather-dependent emission fractions were only slightly different from those estimated using the original (constant) emission fractions in the INTEGRATOR model for animal housing and manure storage. Some newly estimated emission totals are quite different from the original ones, the deviation is especially apparent for manure application emissions, which increased by 22% (2016) and 29% (2018). The interannual variability of manure application emissions was also induced, even though it was rather limited with the largest relative difference of 6.4% between 2016 and 2018. On the contrary, the emissions from other livestock management sources (animal housing and manure storage) did not change significantly, which was within our expectations. The temperature-based scaling impacted the spatial variation of emissions more than the absolute totals because it was based on the static emission fractions used in INTEGRATOR, representing the averaged ammonia level per sector over the whole country. The largest interannual variation is cattle housing and storage emissions, which is 8.7% between 2016 and 2018.

By comparing the modeled emissions in Table 5-3 with the officially reported data in Table 5-4, one can see that the updated emissions are more aligned with the official data for fertilizer and manure application but less for cattle housing. For other sectors, the results are rather similar. The absolute relative difference in manure application emissions between this study and official data decreased from around 17% to within 10% (1.58% in 2016). In addition, manure housing and storage emissions differ quite dramatically for both the original and updated emissions, especially for cattle (around -26%) and pigs (around +30%). The deviations between reported and modeled emissions from cattle and pig housing and manure storage are caused mainly by excretion rates and emission fractions used in INTEGRATOR. After adding reported emissions from compost and digestate application into INTEGRATOR results, the relative difference between the reported country totals and the updated estimated totals has been reduced except for 2018.

Table 5-3 Comparison of reported emission total per sector and corresponding estimated emission total using the original emission fraction in INTEGRATOR.

EMEP category	Emission using variable emission fraction (kiloton)				Constant EF
	2015	2016	2017	2018	2015-2018
Cattle housing and storage	105	103	104	112	106
Pig housing and storage	121	122	121	127	123
Poultry housing and storage	30	30	30	31	31
Manure application	209	203	213	216	167
Mineral fertilizer application	100	100	100	101	100
Grazing	25	25	25	26	24
Compost application	56	56	55	56	56
Total	648	640	649	669	607

There are also deviations in interannual trends between the reported and newly updated emission estimates. The effect of including temperature change caused a slight increase in the updated modeled emissions in all sectors from 2016 to 2018, with the last increase from manure application (from 203 kton to 216 kton). On the contrary, the reported numbers were either constant or indicated a slight decline (for cattle housing and mineral fertilizer application) during these years, even though the extent is rather low (from 201 kton to 197 kton). The total uncertainty of reported emissions from German agriculture is 10.7%, which is primarily determined by the uncertainties in the manure management of dairy cows and fattening pigs, the application of mineral fertilizers, and the spreading of animal manures (Rösemann et al., 2021). The difference between the updated emission estimates and the reported data lies within the uncertainties.

Table 5-4 Annual ammonia emission total per sector officially reported by Germany between 2015 and 2018.

EMEP category	Reported emission (kiloton)			
	2015	2016	2017	2018
Cattle housing and storage	152	150	148	146
Pig housing and storage	94	93	94	91
Poultry housing and storage	30	30	30	31
Manure application	201	200	199	197
Mineral fertilizer application	105	100	94	74
Grazing	9	9	9	9
Compost application	56	56	55	56
Total	647	639	630	602

An example of the weekly time series of ammonia emission from animal houses, manure storage, and fertilization on various crops from 2015 to 2018 is given in Figure 5-3. Figure 5-3 (top) and Figure 5-3 (bottom) represent the scenarios *TIME* and *SPACETIME* which use the INTEGRATOR annual distribution and the emission estimates with the original and updated emission fractions, respectively. The most noticeable feature in both time series is the seasonal cycle, with ammonia concentrations being at peaks in the warm growing season and at much lower levels during the colder period from late autumn to early spring. There are multiple peaks in concentration amounts during the growing season that can be associated with emissions from fertilization on various crops in spring, emissions from animal housing following increasing temperatures, and emissions from fertilization on winter crops. For both time series, cattle housing emissions experienced a rise from January to summer, followed by a decline till winter. In contrast, pig and poultry housing emissions are more constant over the years. This is because cattle houses are mostly open, while pig and poultry houses are partly or completely closed with forced ventilation. As a result, cattle housing is more sensitive to temperature changes, while the other housings keep a more constant level regardless of the temperature variability.

As expected, the application emission level fluctuates more when using weather-dependent emission fractions (Figure 5-3 (bottom)) than with constant emission fractions (Figure 5-3 (top)) with the most obvious change for fodder maize, since the difference between the original and updated emission fractions of manure application were largest on fodder maize. Figure 5-3 (top) shows that the emission peak is the highest in 2017 (slightly under 1.4 Gg/week) and the lowest in 2016, even though the difference is very small. However, in Figure 5-3 (bottom), the peak in 2018 is about at the same level as in 2017, being the highest among the years. This is because the temperature in 2018 is on average higher than that in 2017, which resulted in higher emission fractions from slurry manure application.
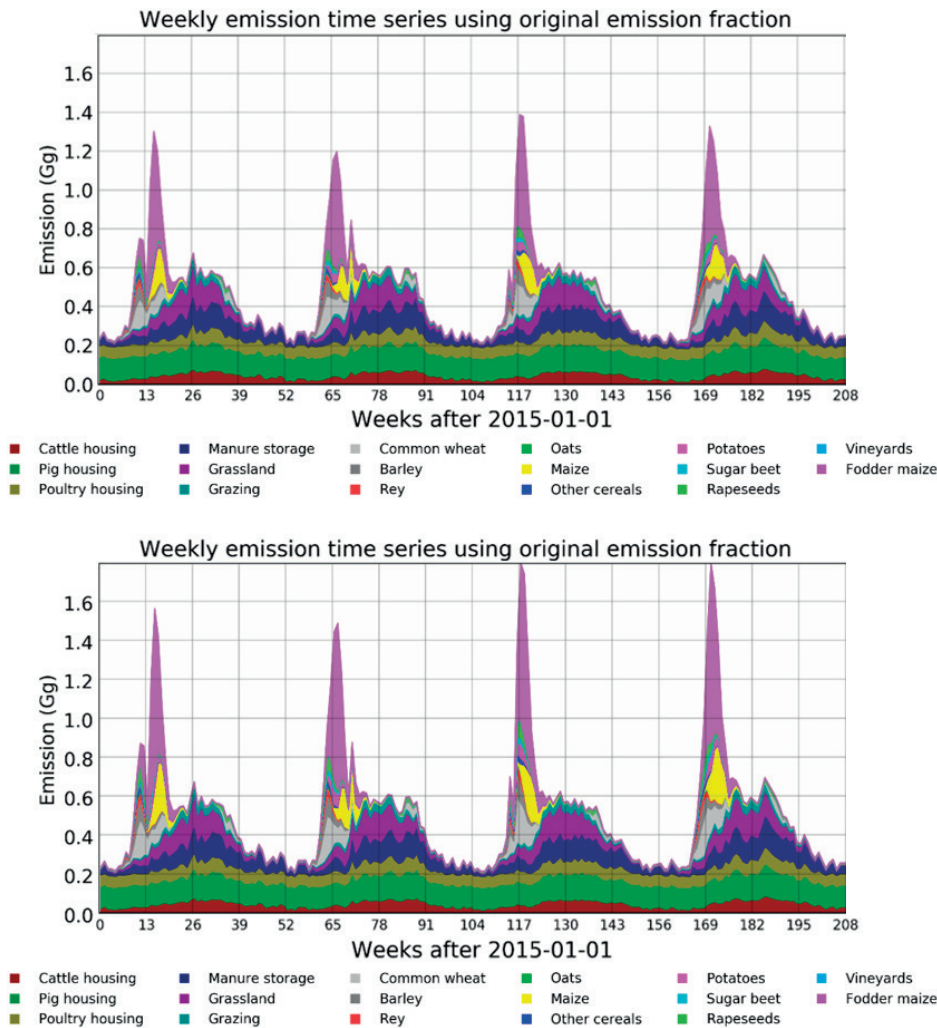
5

Figure 5-3 An example of ammonia emission time series per sector at a selected location in Germany, using INTEGRATOR output scaled with national totals per sector and constant emission fractions (*TIME*, top) and with updated weather dependents emission fractions (*SPACETIME*, bottom).

5.3.2 Simulated and measured surface concentrations in response to temperature

For the three above-mentioned time blocks of 2015 – 2018, we calculated the mean concentrations and the mean temperature for each state. Then, linear regression was performed per time block for each scenario and slopes of the linear regression between the response of surface concentration to temperature were derived. Figure 5-4 compares the slopes (temp-sfcconc coefficient) in all German states during the three time blocks (from up to bottom is the time block I, II, III) derived from the measurements and the three simulation runs (from left to right is the *BASE*, *TIME*, *SPACETIME* scenarios). We then applied linear regression on the slopes, which indicates how well the three simulation runs can represent the changes in surface concentrations brought by temperature in the three periods. It is apparent that from *BASE* to *TIME*, there is an improvement in slope reproduction, illustrated by the linear regression line tilting towards y=x. There is further improvement from *TIME* to *SPACETIME*, but to a lesser extent. As a result, we assessed the quality of the simulated slopes by calculating the statistics illustrated in Table 5-5. One can see that for all three time blocks, the comparison between the measured slopes and the *BASE* results is the worst for almost all indicators except correlation. *SPACETIME* shows a better linear regression coefficient when compared with measurements than *TIME* but it performed worse when it comes to other indicators for the time block I, although not to a large extent. It can be observed from Table 5-5 that the improvement in time blocks I and II, namely in spring, is more obvious than in time block III. To be more specific, all three scenarios do not demonstrate good estimates in summer. This is because the emission in spring is dominated by manure and fertilizer application while emission in summer is more related to animal housing and therefore less sensitive to temperature. To summarize, the improvement from *BASE* to *TIME* is larger than that from *TIME* to *SPACETIME* for all three time blocks. It implies that the meteorology-dependent activity time profile is of greater importance when it comes to the reproduction of interannual variability of surface concentrations.
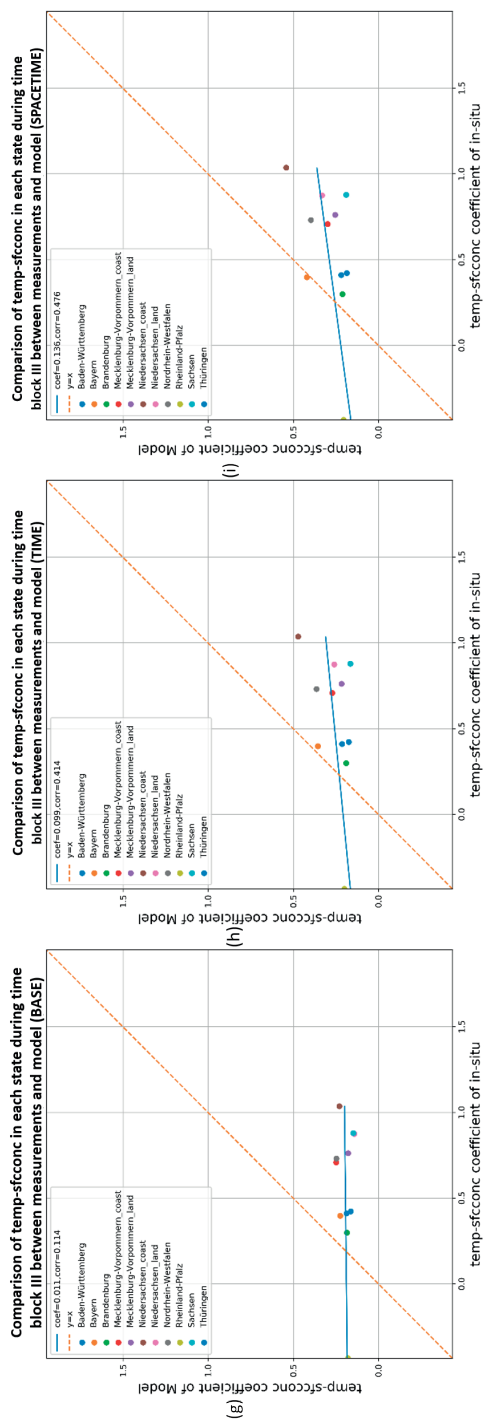
5
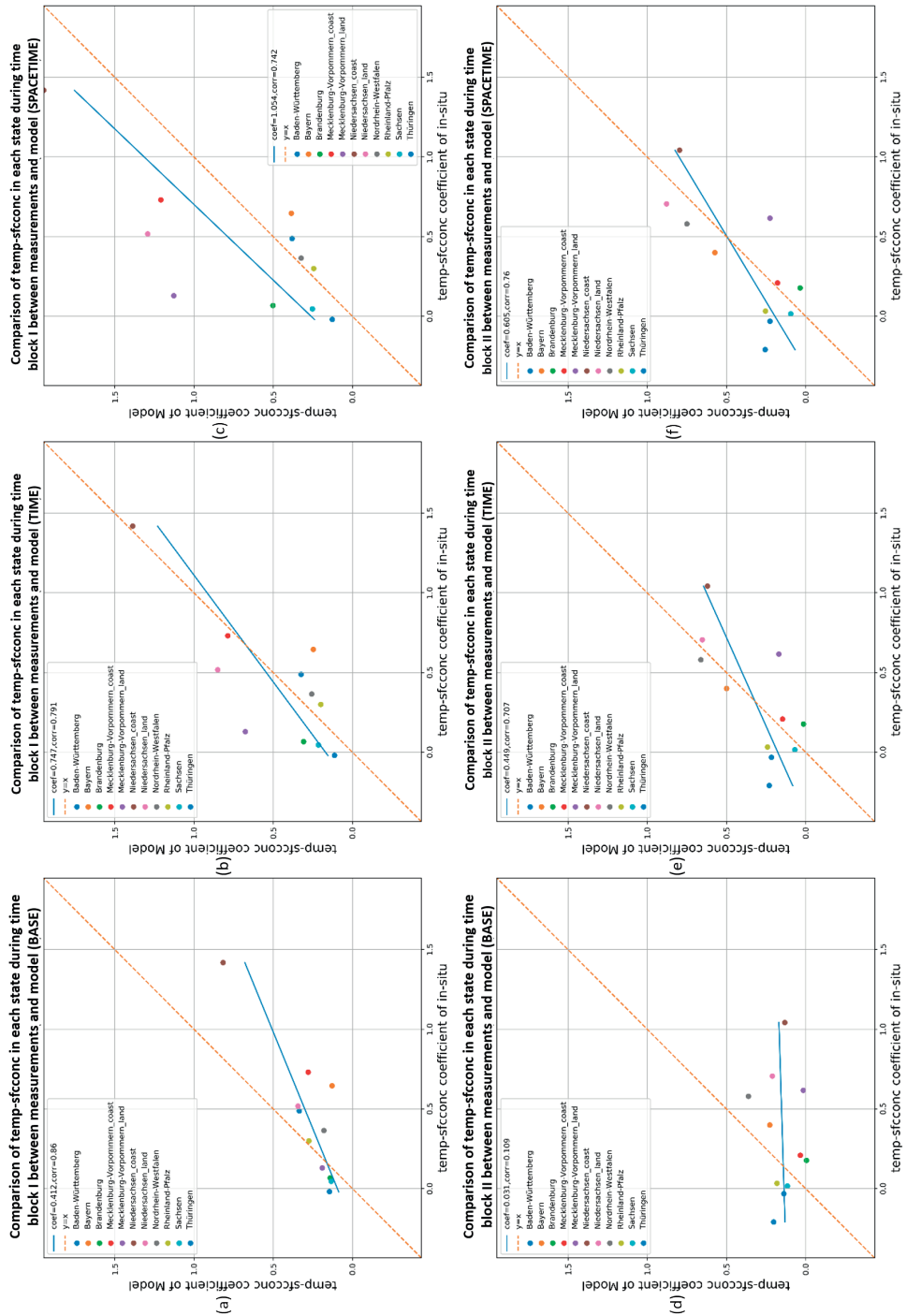
Figure 5-4 Comparison of simulated and measured slopes of surface concentrations to temperature in time block I (top; from Day 77 to 137 linked to first spring fertilization), time block II (middle; from Day 147 to 197 linked to second spring fertilization), and time block III (bottom; from Day 207 to 277 representing summer application and housing/storage emissions) for the *BASE* (left), *TIME* (middle) and *SPACETIME* (right) scenarios. The x-axis is the slope (temp-sfcconc coefficient) from the in situ measurements, the y-axis is the slope from the simulations

Table 5-5 Quality assessment of the comparison based on simulated and measured slopes of surface concentrations in response to temperature. The scenarios with the best statistics are marked green, the second best is marked yellow.

Time block	Scenario	Fitting Coef.	Correlation	NRMSE (%)	NMAE (%)	EF	IA
1	BASE	0.43	0.86	44	82	-1.48	0.75
	TIME	0.73	0.76	22	41	0.48	0.87
	SPACETIME	1.02	0.71	29	51	0.22	0.76
2	BASE	0.07	0.22	110	224	-13.67	0.28
	TIME	0.52	0.74	36	56	0.07	0.82
	SPACETIME	0.70	0.79	25	47	0.50	0.88
3	BASE	0.01	0.09	511	249	-221.42	0.12
	TIME	0.09	0.40	156	156	-25.73	0.31
	SPACETIME	0.13	0.47	127	128	-15.59	0.38

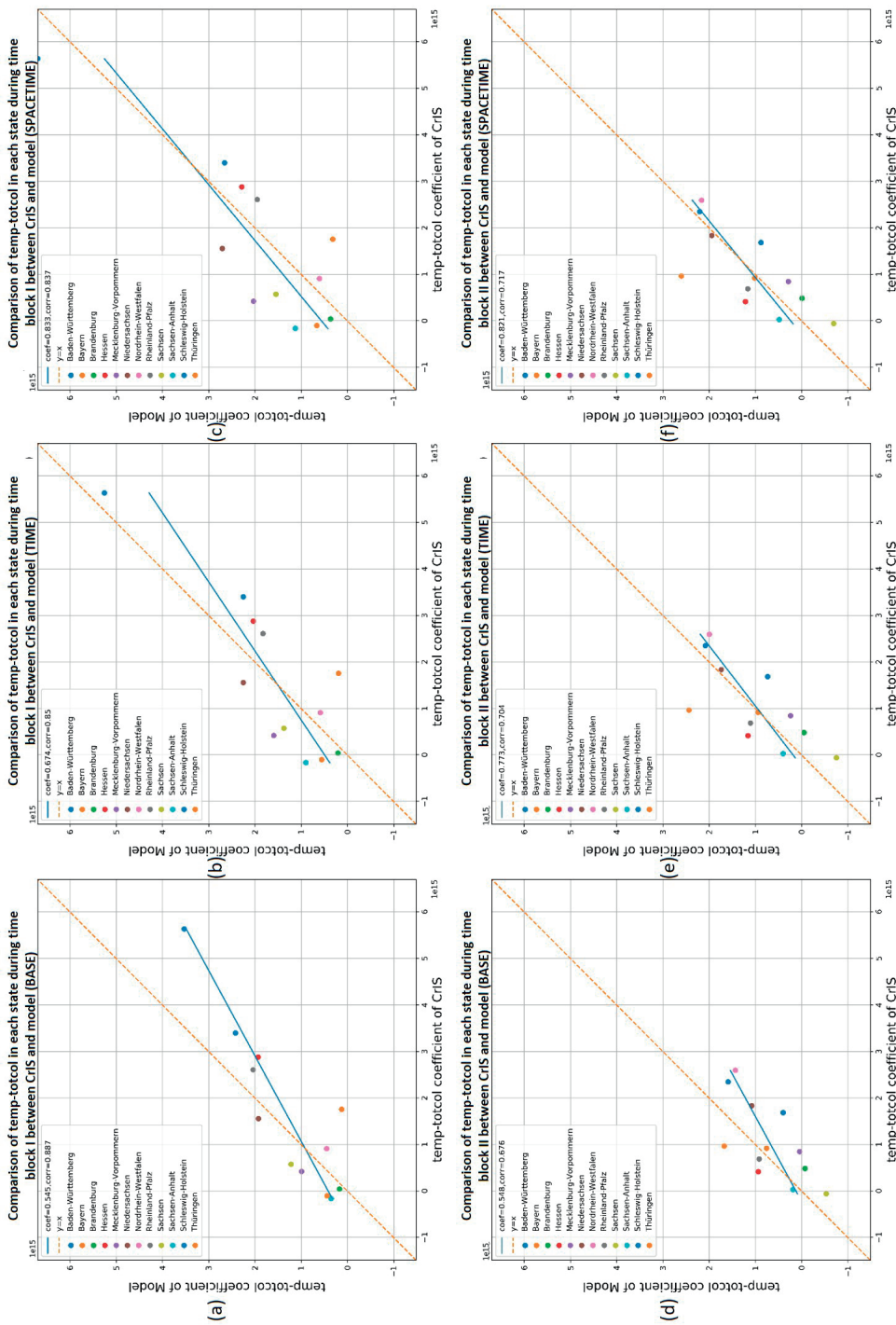## 5.3.3 Simulated and measured total columns in response to temperature

Similar to the comparison of surface concentrations, we also studied the response of averaged total column to temperature during the three time blocks from 2015 to 2018. As an example, the average total column weekly time series of a 1 by 1 degree window in the North Rhine-Westphalia region is shown in Figure 5-5. The red vertical lines are the start of spring peaks based on the observations and the gray shows indicate the wintertime. One can see that the CrIS observations differentiate severely from all three scenarios, especially during wintertime, because the satellite instrument measures the thermal signal and becomes less sensitive under colder conditions (with the signal-to-noise ratio decreasing). The autumn of 2015 witnessed an extremely high peak which is not present in all estimates. However, comparing estimates (*TIME* in Figure 5-5(c) or *SPACETIME* in Figure 5-5(d)) with the satellite measurements (in Figure 5-5(a)) indicates that these predicted the peaks more accurately, while Figure 5-5(b) exposes the limitation of the static time profile in LOTOS-EUROS.

Figure 5-6 shows the comparisons of the slopes (temp-totcol coefficient) of the simulated (from left to right is *BASE*, *TIME*, *SPACETIME*) and measured total column in response to temperature in all German states for the three time blocks (from up to bottom is the time block I, II, III). For the time block I and III, *TIME* and *SPACETIME* both show better predictions of the slope compared to *BASE*. Even though the difference between *TIME* and *SPACETIME* is less noticeable, it is still visible that there is a slight improvement from *TIME* to *SPACETIME*, especially for the time block I. The quality of comparison of trends between total column and temperature is illustrated in Table 5-6. The *SPACETIME* result has outperformed the other two cases in every statistic. Still, the improvement in time block II and III (warmer season) from *TIME* to *SPACETIME* is not as considerable as the comparison of surface concentrations. We can safely conclude that for the springtime, there is an improvement

in reproducing total column slopes from *BASE* to *TIME*, while SPACETIME improves further, but to a smaller extent.
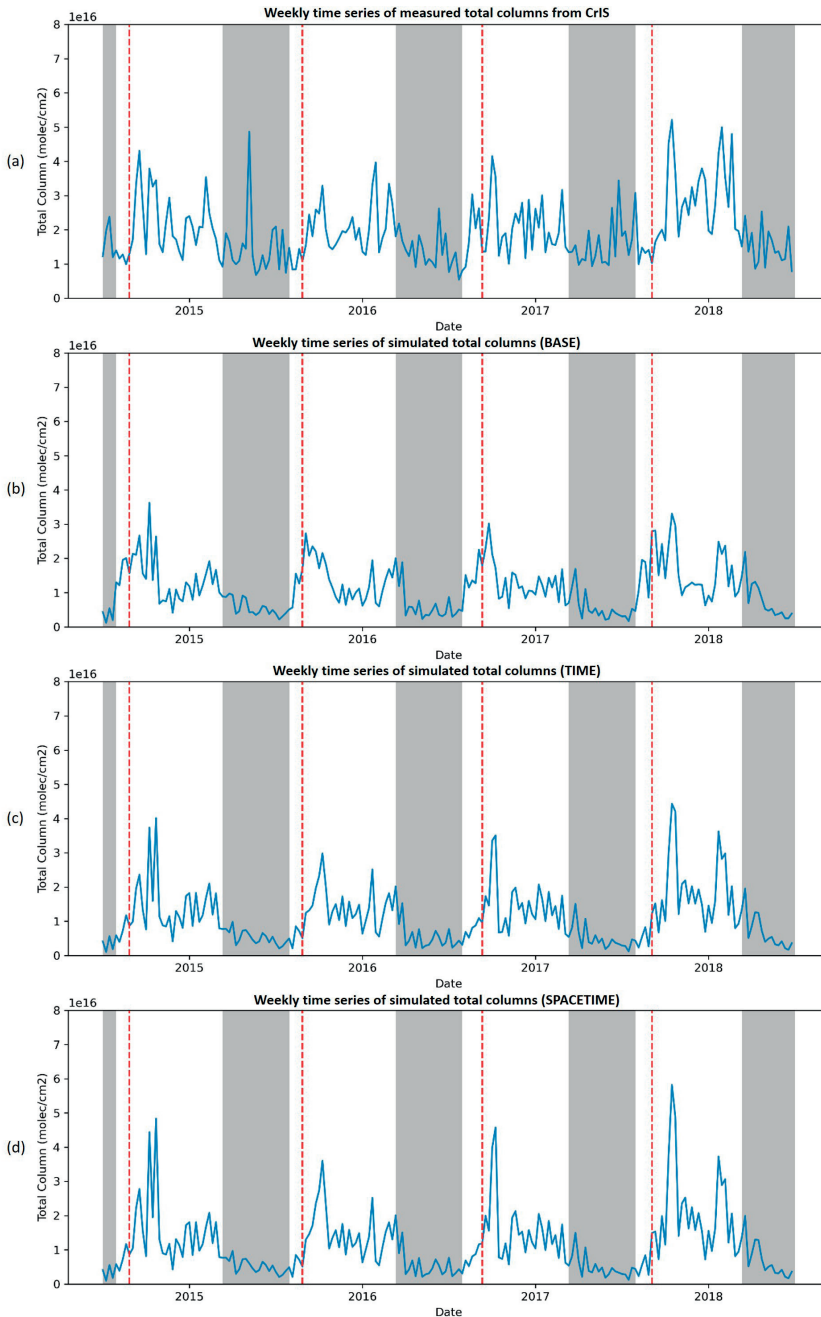
Figure 5-5 Weekly time series of total columns between 2015 and 2018 from CrIS observations (a) and simulations of the runs with the scenarios BASE (b), SPACE (c), and SPACETIME (d). The red vertical lines are the start of spring peaks based on the observations and the gray shows indicate the wintertime.

(a) Comparison of temp-totcol in each state during time block I between CrIS and model (BASE)

(b) Comparison of temp-totcol in each state during time block I between CrIS and model (TIME)

(c) Comparison of temp-totcol in each state during time block I between CrIS and model (SPACETIME)

(d) Comparison of temp-totcol in each state during time block II between CrIS and model (BASE)

(e) Comparison of temp-totcol in each state during time block II between CrIS and model (TIME)

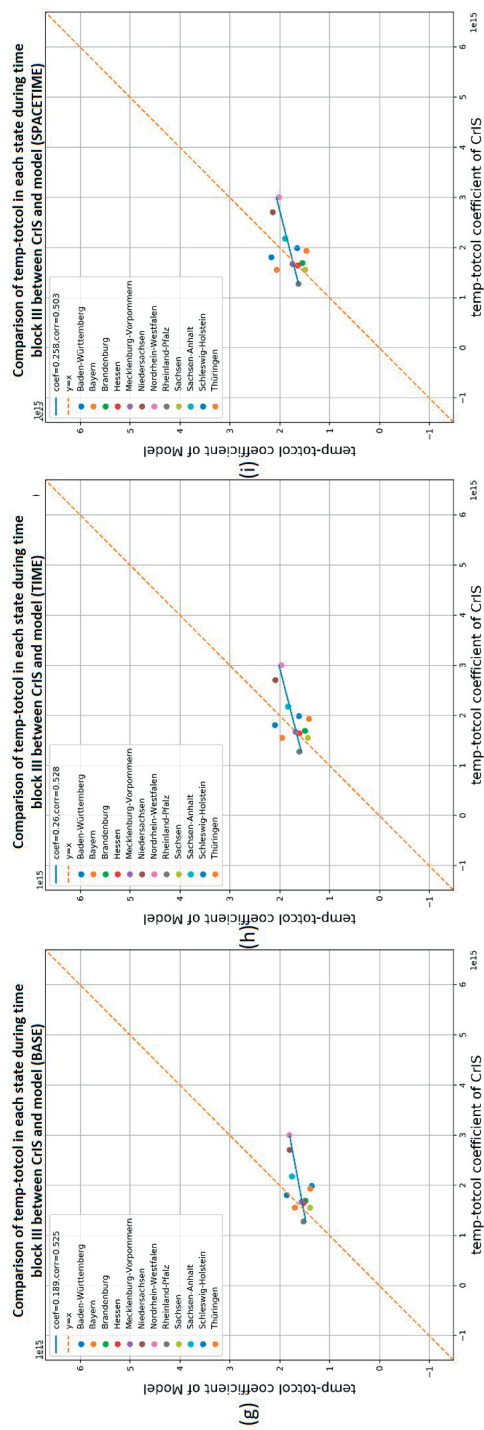(f) Comparison of temp-totcol in each state during time block II between CrIS and model (SPACETIME)

Figure 5-6 Comparison of simulated and measured slopes of total columns to temperature in time block I (top; between Day 77 and 137 linked to first spring fertilization), time block II (middle; between Day 147 and 197 linked to second spring fertilization), and time block III (bottom; between Day 207 and 277 representing summer application and housing/storage emissions) for the *BASE* (left), *TIME* (middle) and *SPACETIME* (right) scenarios. The x-axis is the slope (temp-totcol coefficient) from the satellite measurements, the y-axis is the slope from the simulations.

5

Table 5-6 Quality assessment of the comparison of measured and modeled trends of total columns in the three time blocks. The scenarios with the best statistics are marked green, the second best is marked yellow.

Time block	Scenario	Fitting Coef.	Correlation	NRMSE (%)	NMAE (%)	EF	IA
1	BASE	0.54	0.89	28	61	0.13	0.87
	TIME	0.67	0.85	17	50	0.55	0.90
	SPACETIME	0.83	0.84	15	48	0.64	0.91
2	BASE	0.55	0.68	33	90	-0.14	0.76
	TIME	0.77	0.70	21	56	0.45	0.83
	SPACETIME	0.82	0.72	21	50	0.49	0.84
3	BASE	0.19	0.52	104	25	-8.24	0.46
	TIME	0.26	0.53	65	21	-2.59	0.59
	SPACETIME	0.26	0.50	62	19	-2.12	0.60

5.4 Discussion and Conclusion

This study is based on the previous work of Ge et al. (2020) and included the neglected parameter (meteorology, slurry application techniques and incorporation time, manure properties) in emission fractions estimates. The spatially explicit emission database is aimed to improve the spatial distribution and interannual variability of ammonia emission. We can see a clear improvement in the results but there still exist some uncertainties, which are interpreted and described as follows.

5.4.1 Comparison of annual emission totals and time series

In general, the update of the emission fractions used in INTEGRATOR for housing and manure storage and slurry manure application resulted in a closer agreement between calculated and official reported emissions (except for the year 2018). Still, for some categories differences were substantial. Cattle and pig management (animal housing and manure storage) contributed to around -45 (-30%) and 30 Gg (33%) difference in annual emission, respectively. Since we scaled the animal number distribution input of INTEGRATOR to match the average state sums of the multi-year official data (which does not vary as strongly as the emissions), the difference should not come from animal numbers of cattle and pigs. Therefore, a likely reason is the different methods to estimate excretion from animal numbers. For example, in INTEGRATOR, it was obtained by multiplying animal numbers with excretion rate which stands for the ratio between the total N excreted and the number of animals (kg N per animal) for each animal type. The coefficients of the INTEGRATOR model come from scaling the GAINS model (Asman et al., 2011), which was submitted by national experts (Klimont and Brink, 2004). The official German excretions, however, were derived using an N-balanced approach (Haenel et al., 2014). In the case of

dairy cattle, excretion was calculated by extracting the amount of N retained in weight
gained, exported with milk, and in conception products from the amount of N taken in
with feed (Haenel et al., 2020). This can explain the underestimation in cattle management
emissions reported in this study; a similar explanation can be applied to pig and poultry
management.

To further improve the excretion rates, N excretion rates at the regional level can be
introduced in INTEGRATOR. For example, Velthof (2014) included the impact of the Nitrates
Directive on gaseous N emission in calculating N excretion rates from dairy cattle (in kg per
dairy cow per NUTS-2 region). They found out that the N excretion rate is generally higher
in the north (115 – 135 kg N per cow) than in the south of Germany (larger than 95 – 115
kg N per cow), with the highest rates in Detmold and Amsberg. In addition, Velthof (2014)
showed that N input to grassland (kg N per ha per year) has an impact on N excretion rate
(kg N per cow per year). Under the assumption of a total feed requirement of 7000 kg dry
matter per cow, the N excretion rate increases almost linearly when N input on grassland
increases and the slope rises along with the percentage of grazed grass in the 7000 kg dry
matter feed.

In INTEGRATOR, the excretion of animals in housing systems and of grazing animals in
pastures is separated, based on data for the number of grazing days at the country level.
For the German inventory, N excretions were split into shares for the house, the milking
area, and grazing. The division contributed to both the deviation in cattle management
emission and grazing emission. Instead of being a country-dependent constant, the
division should be more variable as the grazing systems applied and the duration of
daytime grazing together determine the amounts of excretion in animal housing during
grazing seasons for dairy cows (van Bruggen et al., 2012). For instance, van Bruggen et al.
(2010) assumed that for the Netherlands, excretion amounts in animal housing for day
and night grazing and daytime grazing is proportional to the number of barn hours. van
Bruggen et al. (2012) categorized grazing systems into unlimited grazing, limited grazing,
or full-time housing and presented the percentage of N excretion within housing systems
for each grazing system applied. A better survey on the distribution of various grazing
systems is needed to derive more accurate estimates of emissions from housing and
storage systems at the regional level.

Regarding the trend of manure application emissions, the official data showed a gradual
decline over the years, while the updated model output implied a rise between 2016 and
2018. This is because the German inventory used to obtain emission estimates accounts
for changes in animal numbers but not for meteorology between years, while our
simulations included the impact of meteorology but not animal numbers as we used a
4-year average of the reported values. In addition, uncertainties in the predicted emission

fractions affect the simulated emissions. First of all, in many cases, predictions will be based on only limited predictor variables, undoubtedly resulting in inaccurate predictions among locations or even at a single location on different dates (e.g., with differences in soil properties including soil pH and soil water content). Missing variables limit the utility of the ALFAM2 model because, in this case, the ALFAM2 results would be less variable than reality as information on additional driving variables is not available. For example, slurry and soil pH are essential to simulate the impact of the system pH change on ammonia volatilization. In addition, the measurements used to develop ALFAM2 from the individual institutes are not harmonized and balanced, which indicates that the independence of the abundant observations can lead to possible systematic differences. The neglect of variable confoundment (interactions between variables such as soil moisture and manure dry matter) is likely to contribute to bias or inaccurate effect estimates. Therefore, increasing the variety of measurements and improving harmonization through future emission measurement experiments can help to estimate emission fractions better. In particular, emission measurements from regions not well represented in the database would be of great value. It is also essential to include more variables when recording ammonia emissions. Hafner et al. (2018) made a list of minimum recommendations for variables to be measured and reported to ensure valuable results. Systematic biases affect absolute emissions, but not necessarily relative differences. Thus, predictions of relative effects on emission are more accurate than predictions of absolute emission. Since we focused on interannual variation instead of the absolute emission, ALFAM2 was without a doubt of great significance for this study.

The difference in emission total over the years resulted in the same trends of the time series in terms of the magnitudes of peaks (see Figure 1), as they used the same activity time profile. This is why the spring of 2018 witnessed the highest peak over the five years in Figure 1(b) while it was in 2017 in Figure 1(a). If we look at the sector component of the emission time series, the difference mostly came from spring fertilization on fodder maize because fodder maize dominates the crop type in this area and N excretion allocated here is the highest. For other sectors such as animal housing and manure storage, changes from temperature-based scaling were not significant, especially for insulated buildings with forced ventilation like pig and poultry housing (Gyldenkærne et al., 2005). However, cattle housing and manure storage are more sensitive to temperature variation within a year than between years because the temperature-based scaling ensured that the average ammonia emission level corresponds to the original INTEGRATOR output. To achieve a more accurate emission fraction for housing and manure storage, it is of great help to have access to detailed hourly ammonia measurements over a long period on an extensive network. Sommer et al. (2019) pointed out that during the measurements, it is important to record the following factors defining the housing categories and affecting emission: (1) the ratio of slatted floor to concrete floor area for pigs, (2) floor opening

area, (3) distribution of excreta within the building, which is affected by the positioning of feeders and drinkers, and behavior of pigs as related to age and temperature, (4) capacity of in-house storage, (5) age of animals, (6) climate, and (7) feeding practice.

5.4.2 Comparison of simulated and measured slopes of surface concentrations with respect to temperature

Regarding surface concentration's response to temperature (temp-sfcconc calculated as the slope of linear regression), we included the *BASE* scenario to investigate to which extent the updated emission fractions or spatially explicit time profiles improved the estimates compared to in situ measurements. When we compared the slopes temp-sfcconc, the simulations based on the *TIME* scenario compared much better with observations than those from the BASE scenario, while the *SPACETIME* scenario usually outperformed *TIME*, but to a lesser extent. It implies that using a spatially explicit time allocation (Ge et al., 2020) improves the model's ability to detect ammonia interannual variability (brought by meteorology), while the utilization of weather-dependent emission fractions improves the simulations further. The improvement was bigger in spring than in summer, which may be caused by three reasons. First, the summer ammonia level in the model was usually dominated by animal housing and manure storage, among which only cattle housing is more sensitive to temperature since cattle houses were considered open houses. As a result, the slope temp-sfcconc brought from the slurry application emission fraction is less noticeable. Another reason is that the absolute temperature is higher in summer. Sutton et al. (2013) concluded from the results of various field campaigns that the percentage of N volatilized as ammonia increased exponentially as a function of average temperature. Bleizgys et al. (2013) also found similar correlations from experiment results from a naturally ventilated open cowshed lab, namely, ammonia increased emission gains at higher temperatures. This behavior was also captured by the modeled results from ALFAM2. It means that the calculated emission fractions are more sensitive to uncertainties. Another factor that could affect the quality of the trend comparisons is the separation of the three time blocks. Time block I (from Day 77 to 137) is linked to first spring fertilization), time block II (between Day 147 and 197) is related to second spring fertilization), and time block III (from Day 207 to 277) represents summer application and housing/storage emissions). The separation was derived using visual inspection to distinguish multiple fertilizations. However, as Ge et al. (2020) pointed out, the sowing (fertilization) day of a certain crop varies according to temperature, rainfall, and legislative constraints, with the temperature being the dominant factor. Therefore, when it comes to a relatively larger country like Germany, the separation of time blocks might be more flexible.

5

5.4.3 Comparison of simulated and measured slopes of total columns with respect to temperature

Regarding simulated slopes of total columns with respect to temperature (temp-totcol), the simulations based on the *TIME* scenario compared much better with observations than those from the BASE scenario for time blocks I and II, but the improvement was much less visible for time block III, as well as from *TIME* to *SPACETIME* was weaker. Therefore, we can come to a similar conclusion that spatially explicit time profiles (Ge et al., 2020) improve the model's ability to detect ammonia interannual variability, while the newly developed emission fractions improve the simulations more, especially for springtime. The improvements in total column slopes are not very apparent in summer, which could be caused by the following reasons. One possible reason is the uncertainties in total column measurement from the CrIS instrument. Even though the higher temperature in summer makes CrIS more sensitive, the uncertainties in summer are also higher.

Another factor is that we defined a threshold before calculating averaged total columns per state to only include the ammonia hot spot during the agriculturally active period. Because 1) there is a minimum detection value of ammonia in CrIS observations and 2) we wanted to exclude background ammonia levels over the non-agricultural area (forest and urban). It should be mentioned that the threshold to exclude background ammonia also has an impact on the overall performance. We also did a sensitivity study on how the threshold can impact the quality of the comparison. When the threshold increased from 0 to approximately $1 \times 10^{16} \, molec / cm^2$, the improvement in calculated total column slope in the *SPACETIME* scenario went from unclear (random trends) to gradually visible. After $1 \times 10^{16} \, molec / cm^2$, the improvement of *SPACETIME* declined, especially for time block III. It means that the model performance worsens when selectively focusing on high levels of ammonia in summer, which could be caused by the spatial allocation of emissions from animal housing and manure storage. Emissions from animal houses and manure storage facilities should be seen as point sources, but due to the absence of information on the locations of animal houses, we evenly distributed them all over the NCUs, which smoothens the emission hot spots of animal housing. During the first stage of the threshold increase from 0 to approximately $1 \times 10^{16} \, molec / cm^2$, the background constant ammonia was gradually excluded. The second stage of the threshold increase after $1 \times 10^{16} \, molec / cm^2$, however, exposed the shortcoming of the spatial allocation of housing emissions. Since housing emissions were more spread out instead of point sources, they were excluded as well. This also explains the reduced improvement over summer because housing emissions became more dominant as application emissions in summer dropped compared to spring. Consequently, access to the coordinates of animal houses to attribute emissions to the right locations would be helpful. Ge et al. (2022) confirmed for the Netherlands that the improvement brought about by the detailed information on housing locations is significant. Without housing locations, the emissions

from animal houses and manure storage facilities were distributed all over the NCU, which resulted in smoothened spatial characteristics.

We also compared the weekly total column time series of a selected 1 by 1 degree window from CrIS observations with the modeled results from the three scenarios (Figure 5-5). When it comes to spring peaks, the *BASE* scenario always overestimated the total columns at the beginning of the year because the fixed time profile used does not account for the actual practice of fertilization which is affected by temperature and resembles the spring peak earlier than reality. On the contrary, for both the *TIME* and *SPACETIME* cases which used the same time profile, the spring peaks synchronized with CrIS measurements, which also validates the time profile algorithm of Ge et al. (2020). In addition, the comparison in winter seemed quite poor. This is because satellite observations measure in the infrared portion of the radiation source. When the thermal signal is decreased under colder conditions (such as in winter), the overall signal-to-noise ratio (SNR) and sensitivity will reduce (Dammers et al., 2019). Furthermore, the number of observations that pass the quality criteria is much lower than in spring and summer. Therefore, we focused on the period between 1 March and 30 September. Shephard et al. (2020) proposed to average CrIS observations over longer periods (e.g. monthly, seasonal, and annual) instead of weekly.

The comparison of the ammonia total column implies that better satellite data is of great importance, which requires higher spatial resolution, higher sensitivity and shorter revisit time. The revisit time can be improved by assimilating various data sources such as IASI, but data harmonization would be needed. For now, satellite measurements are valuable for the validation of ammonia budgets over a larger region or a long period. It is however not yet sufficient for point sources or grid cells of limited size less than the measurements' spatial resolution.

5.4.4 Conclusions and outlook

In this study, we presented an ammonia emission inventory using weather (air temperature, wind speed, and rainfall rate) dependent emission fractions for slurry application to crops (obtained with ALFAM2), and temperature-dependent emission fractions for animal housing and manure storage, aiming to improve the model's ability to reproduce interannual variation observed in satellite observations and in situ measurements. The emission fractions for slurry application also accounted for differences in dry matter content and pH of the slurry and slurry application method. The newly modeled annual emission totals (and manure application emissions) were closer to the officially reported values (except for 2018), but deviations in some categories (cattle and pig housing/storage) remained relatively large. For emissions from animal housing and manure storage, the temperature-based scaling method affects the spatial distribution and temporal distribution within a

year and between years, rather than the absolute magnitude. Compared to a national generic time allocation of emission within the year, a spatially explicit time profile already largely improved the ability to reproduce interannual ammonia surface concentrations and total columns. The updated weather-dependent emission fractions further improved the comparison of simulated and measured surface concentrations and total columns. This study showed that modeling the variability of ammonia emissions is a crucial step to improve the performance (the comparison of predicted and observed variability in ammonia concentration levels) of chemistry transport models.

To further develop the modeling of ammonia emissions from agriculture, priorities should focus on improving both the spatial and temporal distribution of emission estimates, as well as the retrievals of ground-based surface concentrations and satellite-derived total columns for validation. Several aspects can improve ammonia emission modeling. First of all, the spatial details of basic input data for the model can be refined, including livestock and crop distributions, animal housing locations, fertilizer use, application techniques and incorporation times, and timing of fertilization. Secondly, the ammonia emission functions (emission fractions and temporalization) should be further developed by better accounting for impacts of site conditions, including crop type, climate, and soil properties, which are regionally available. Last but not least, data affecting the N manure input, and thus the ammonia emission, can also be ameliorated, including N excretion rates and the division of N excretion over grazing and housing. In situ measurements offer great possibilities for the validation of temporal variations while satellite-derived observations can be used to validate the spatial variation in large-scale estimates of ammonia emissions. However, most ground stations in Western Europe offer concentrations at the monthly resolution, which is not detailed enough to validate the timing of emission from manure and fertilizer application. The progressing development of satellite remote sensing nowadays provides great opportunities for better constraining ammonia emissions in space and time. Since approximately 2018, CrIS and IASI satellite observations, combined with relevant emission inventory, have been widely to calculate NH_3 emission fluxes and identify ammonia emission hotspots at the global scale (Dammers et al., 2019; Clarisse et al., 2019; Luo et al., 2022; Evangeliou et al., 2021; Van Damme et al., 2018). At the regional scale, it is also feasible to make use of satellite data, combined with high-resolution emission inventories, to reduce the uncertainties in ammonia emission and deposition in space and time. For instance, we can take advantage of the averaging kernels and error covariance matrix provided in the CrIS retrieved product to provide top-down constraints on the ammonia emissions (Cao et al., 2020; Shephard et al., 2020). Examples of use at the regional scale are still quite limited with notable examples of their application in the UK (Marais et al., 2021), the US (Chen et al., 2021), and China (Liu et al., 2022). To improve ammonia total columns observed by CrIS, we can refine the retrievals over elevated concentration values on high

elevations wintertime conditions and enhance the a-priori profiles and constraints used in the retrieval (Shephard et al., 2020).

5

CHAPTER 6

Synthesis

In this final chapter, I summarize the main results of my Ph.D. project by answering the research questions formulated in the introduction (Section 6.1). I then discuss the uncertainties brought by the model inputs, model methodologies and in the measurements of ammonia, with their impacts on the resulting temporal and spatial distribution of ammonia emissions and the validation, including suggestions for follow-up research (Section 6.2).

6.1 Research questions and outcome

The alteration of the global nitrogen cycle by human activities has resulted in increased reactive nitrogen (N_r) losses to the environment, surpassing numerous thresholds for human and ecosystem health. As N deposition is shifting towards ammonium-dominant, excess ammonia emissions negatively impact human health, cause acidification and eutrophication of ecosystems, and eventually, biodiversity loss. However, ammonia emissions are challenging to estimate, resulting in significant uncertainties in regional budgets and distributions of NH_3 (and its deposition) in both space and time. Addressing this issue, this Ph.D. thesis aimed to improve agricultural ammonia emission estimates by combining and refining existing models and assimilating remote sensing and various datasets on agricultural activities, meteorology, national surveys, etc. Various ground-based and satellite measurements of ammonia levels at different spatial and temporal resolutions were used to validate the modeled results and evaluate the uncertainties in the distribution of ammonia estimates.

The main research question of this thesis was: What are the improvements in the ammonia emission distribution in space and time if we account for variations in meteorology, agricultural practices, crop distributions, and livestock and animal house distributions? This main question was divided into four sub-questions, being evaluated in four chapters:
- What are the impacts of different agricultural practices and their timing based on meteorology (Chapter 2)?
- What are the impacts of detailed crop and livestock distributions and emission fractions based on country-specific information (Chapter 3)?
- What are the impacts of detailed livestock housing information and remote sensed crop distributions (Chapter 4)?
- What are the impacts of manure characteristics, meteorology, and application techniques (Chapter 5)?

In Figure 6-1 A schematic overview of the thesis with answers to the research questions., the results of these questions are summarized, while detailed results on the improvements of the ammonia emission distribution in space and time are described below.
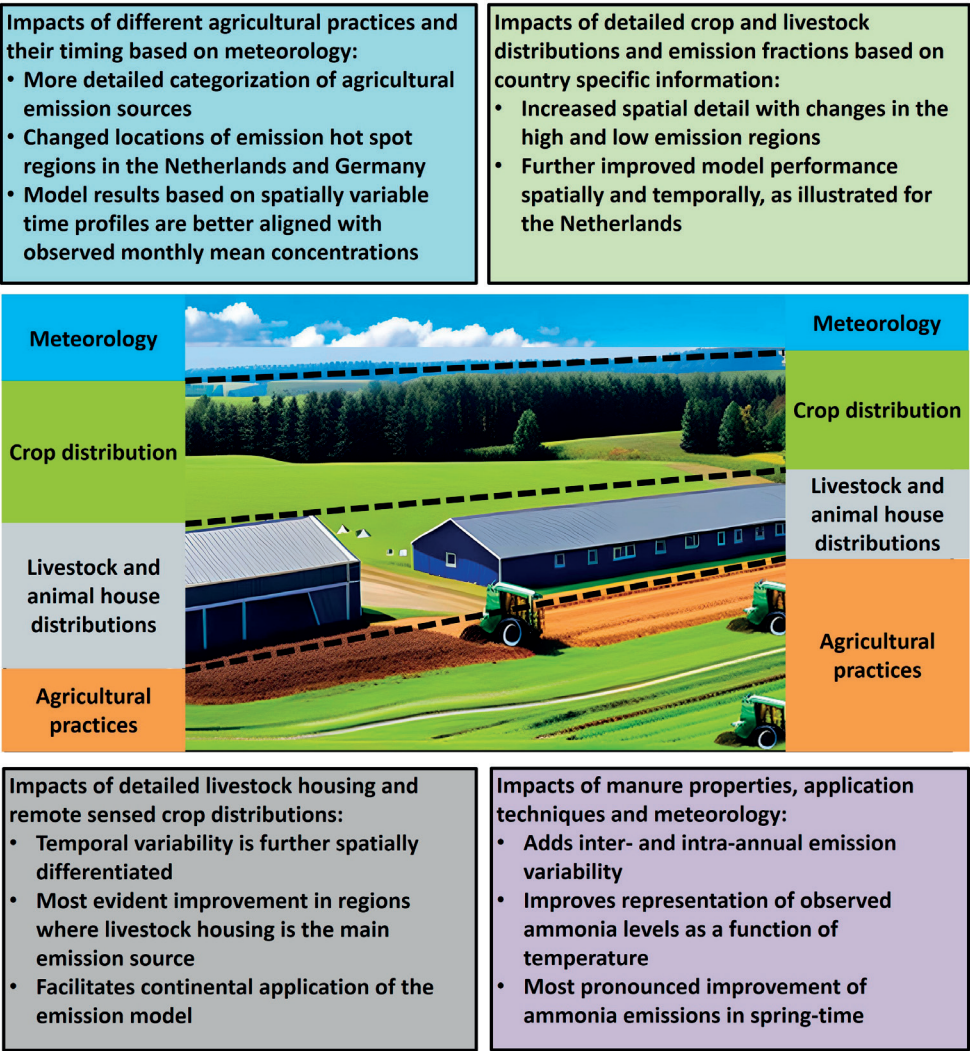
Impacts of different agricultural practices and their timing based on meteorology:
- More detailed categorization of agricultural emission sources
- Changed locations of emission hot spot regions in the Netherlands and Germany
- Model results based on spatially variable time profiles are better aligned with observed monthly mean concentrations

Impacts of detailed crop and livestock distributions and emission fractions based on country specific information:
- Increased spatial detail with changes in the high and low emission regions
- Further improved model performance spatially and temporally, as illustrated for the Netherlands

Meteorology

Crop distribution

Livestock and animal house distributions

Agricultural practices

Meteorology

Crop distribution

Livestock and animal house distributions

Agricultural practices

Impacts of detailed livestock housing and remote sensed crop distributions:
- Temporal variability is further spatially differentiated
- Most evident improvement in regions where livestock housing is the main emission source
- Facilitates continental application of the emission model

Impacts of manure properties, application techniques and meteorology:
- Adds inter- and intra-annual emission variability
- Improves representation of observed ammonia levels as a function of temperature
- Most pronounced improvement of ammonia emissions in spring-time

Figure 6-1 A schematic overview of the thesis with answers to the research questions.

Impacts of different agricultural practices and their timing based on meteorology

A novel NH_3 emission model comprising a spatial and temporal allocator was developed. The spatial allocator (INTEGRATOR) offers enhanced spatial detail and can differentiate between various agricultural sources such as animal housing, manure storage, grazing, manure application, and fertilizer application. The temporal allocator (TIMELINES) is spatially explicit and dynamic, considering land use, local weather, and legislative restrictions. The updated emissions in the CTM LOTOS-EUROS allow tracking of the source contributions to modeled NH_3 surface concentrations and total columns, enabling better

interpretation and future enhancements. Compared to results based on the original MACC emissions, new hotspots emerged in southeastern Germany, while the east of the Netherlands saw smoother spatial characteristics due to the allocation algorithm. Compared with in situ measurements, the time series of surface concentrations from the updated model showed better alignment with in situ measurements than those from the original model, which indicates a better representation of the temporal dynamics by the dynamic and spatially explicit time profiles. Compared to in situ measurement, the updated results no longer overestimated surface concentrations from January to March as much as the original model. The updated model increased correlation and reduced errors compared to the original one. The performance of the updated model also showed improved consistency and robustness. However, there were still large differences between the IASI observations and the modeled total columns from the original and updated model. Apart from the uncertainties of IASI observations, possible sources of uncertainty are crop and livestock distribution, constant excretion rates and emission fractions, and the negligence of manure transport.

In short, this study confirmed that modeling the spatio-temporal emission variability based on estimating the timing of agricultural management activities is a promising way forward. As more accurate and comprehensive input datasets emerge and as the methodology progresses, this strategy holds the potential to be expanded to encompass the whole of Europe.

Impacts of detailed crop and livestock distributions and emission fractions based on country-specific information

The European-scale emission model INTEGRATOR was adapted to the Netherlands, Denmark, and Portugal using locally available information on crop and livestock distributions and ammonia emission fractions in the different countries. In the original model, crop and livestock distributions were upscaled to NCU polygons from European datasets, and the emission fractions were country-dependent. We used locally adapted versions of INTEGRATOR for the Netherlands and Denmark, coupled with updated crop and livestock distribution, to derive annual emission maps. For Portugal, a standardized approach to applying INTEGRATOR with more detailed local inputs was developed with the following aspects: 1) the NCU polygons were refined by being combined with the municipality boundaries; 2) livestock distribution and a crop map were obtained from official publications and resampled to the NCUs; 3) emission fractions were updated based on country-specific information. The resulting emission products showed changes in ammonia distribution due to different livestock distributions. Annual emission has more spatial details because of the high-resolution crop distribution. The emissions were validated with in situ measurements. The updated emissions showed increased spatial details with changes in the high and low emission regions. The total column products

from CrIS proved too coarse to validate the spatial distributions, especially for the high-resolution emissions in relatively small countries. The comparison of monthly and annual averaged surface concentrations with in situ measurements showed larger improvements in springtime than in summertime for the Netherlands, indicated by higher correlations with in situ measurements and lower errors in spring. Unfortunately, such a comparison could not be made for Portugal and Denmark due to lacking surface concentration measurements.

Despite the limitations in validation, this study showed that the use of local data on crop and livestock distributions has the potential to improve the ammonia emission distribution in space and time. First, it shows that using detailed crop distribution improved the spatial distribution in ammonia emission estimates but also temporally, especially the spring time emissions. Furthermore, the farm-level livestock number and location data improved the spatial distribution of ammonia emissions in winter, during which animal housing dominated ammonia emissions.

Impacts of detailed livestock housing information and remote sensed crop distributions

High-resolution crop maps and livestock distributions are generally unavailable for the different EU countries, although they are essential in ammonia emission modeling. A Sentinel-2-derived high-resolution crop map and the locations of animal housing systems in the Netherlands were thus used when applying the INTEGRATOR model, resulting in more refined and improved spatial details and temporal variability of ammonia emissions across the country. The performed crop classification has an average accuracy score of 0.73. The derived crop map was compared with Dutch national statistics, and the results showed that the absolute median of the relative difference between Sentinel-2 derived crop areas and national statistical information is around 5%. After using the ammonia emissions in LOTOS-EUROS, the newly modeled ammonia monthly surface concentrations compared better with in situ measurements in terms of the magnitude and temporal variability than those derived from the original emission distribution, indicating that the temporal distribution of ammonia emissions was improved. The comparison of modeled and measured annual averaged surface concentrations illustrated that the spatial distribution of ammonia emission was also improved. All model performance indicators significantly improved, and the performance of the updated model was more stable and robust. The improvement was more evident at the stations where livestock housing is the main emission source.

This study illustrates that apart from a satellite-derived crop map, information on the locations of animal housing systems also plays an essential role in better estimates of the spatial and temporal distribution of ammonia emissions. The model still has uncertainties,

illustrated by the overestimated ammonia emission in spring. This could be caused by the misclassification of crops or the wrongly predicted fertilization days. Besides, constant emission fractions for manure/fertilizer application that do not account for spatial variation in meteorological conditions can also contribute to uncertainties. Nevertheless, the findings indicate that including the locations of livestock housing systems and the satellite-derived crop map has improved ammonia emission estimates in space and time, supporting the use of the methodology in a larger region such as EU-27.

Impacts of meteorology, manure application techniques, manure properties, and soil properties

We presented an ammonia emission inventory using weather (air temperature, wind speed, and rainfall rate) dependent emission fractions for slurry application to crops (obtained with ALFAM2) and temperature-dependent emission fractions for animal housing and manure storage, aiming to improve the model's ability to reproduce interannual variation observed in satellite observations and in situ measurements. The emission fractions for slurry application also accounted for differences in dry matter content and pH of the slurry and slurry application method. The interannual sensitivity of surface concentration and total column to temperature was calculated for early spring, late spring and summer between 2014 and 2018. Compared to a national generic time allocation of emission within the year, the spatially explicit time profile largely improved the ability to reproduce the interannual sensitivity of surface concentrations and total columns to temperature. The updated weather-dependent emission fractions brought the improvement further. The improvement was more pronounced in early spring fertilization, followed by late spring fertilization. However, the summer period did not show a noticeable change because animal housing and manure storage dominated ammonia emission at this time.

This study shows that the developed approach to derive spatially explicit emission fractions can significantly improve ammonia emission modeling and is of great importance for studying the temporal variability between years.

Overall, the research carried out in this thesis clearly improved the spatial and temporal variability in agricultural ammonia emissions in Western Europe by (i) improving the spatial distribution of livestock and animal houses and of arable crops and grassland, (ii) by accounting for the variation in manure application techniques and their timing, and (iii) and by accounting for the impact of manure composition and meteorological conditions on the variation in ammonia emissions fractions.

6

6.2 Discussion and outlook

This thesis was devoted to improving agricultural ammonia emissions' spatial and temporal distribution through more detailed inputs derived from remote sensing, developed models, and statistics, accounting for variations in meteorology, agricultural practices, crop distributions, and livestock and animal house distributions. The updated model was validated for the short-term (1 year in Chapters 2, 3, and 4) and long-term (4 years in Chapter 5) periods.

There are several ways to enhance emission estimates' spatial and temporal precision in ammonia emission modeling. Firstly, the spatial resolution of basic input data for the model can be improved. This includes refining data on livestock and crop distribution, the location of animal housing facilities, fertilizer use, application methods, incorporation times, and fertilization timing. Secondly, the development of ammonia emission functions (emission fractions and temporalization) should consider more thoroughly the impact of site-specific conditions, such as crop type, climate, and soil characteristics, which are readily available on a regional basis. Finally, data that influence the nitrogen input from manure, and consequently the ammonia emission, can be improved. This includes refining nitrogen excretion rates and the distribution of nitrogen excretion between grazing and housing. Apart from reducing the uncertainties in all these input data, improving the accuracy of ground-level surface concentrations and satellite-acquired total columns for validation is also vital to evaluate uncertainties in the modeled results.

Below, the impacts of uncertain input data on the uncertainties in the resulting temporal and spatial distribution of ammonia emissions are first discussed, followed by uncertainties in the measurement and use of satellite observations, including suggestions for follow-up research.

Uncertainties in emission timing

Uncertainties in the temporal distribution of ammonia emissions are affected by the approach to predict fertilization days, also by accounting for the trafficability of the soil and the possibility of multiple fertilizations during the growing season, as discussed in detail below.

Thermal sum approach for fertilization day prediction

One of the uncertainties in the temporal allocation of application emissions is the peak day of application emission, which is predicted using a thermal sum approach in TIMELINES. From the comparison of surface concentrations with in situ measurements, we learned that the model tends to overestimate emissions at the beginning of the growing season. One plausible explanation for the discrepancy could be that the reference

temperature sums in TIMELINES, used to predict fertilization days, are inaccurate and require adjustment. The TIMELINES model relies heavily on empirical data on sowing and harvesting dates currently used within the CGMS to calculate thermal time thresholds. The reference temperature sums are spatially explicit but remain the same between years. They also cover a subset of current crop varieties. Nowadays, it is widely accepted that the global and regional climate is changing and that biological systems quickly respond visibly to changes in the climate (Peñuelas and Filella, 2001; Walther et al., 2002). Therefore, the reference temperature sums may need to be updated to improve the model's ability to accurately simulate the timing of field operations for all types of arable crops at various locations across Europe. As a result, a more comprehensive analysis is needed to fine-tune the relationships between different field operations (Hutchings et al., 2012).

One way to improve the accuracy of reference thermal sums for sowing days and related fertilization days for each crop is to use phenological data. Phenology is the study of periodically recurring patterns of growth and development of plants and animal behavior during the year (Lieth, 1974). Phenological data are, therefore, a valuable source of information for agricultural advisory activities and climate research (Richardson et al., 2013). In Germany, a phenological observation network is operated by Germany's national meteorological service (Deutscher Wetterdienst, DWD). Currently, about 1200 observers contribute to this network, most of whom voluntarily. Each year's reference thermal sums of sowing for each crop can be calculated using the sowing day observations in the DWD phenology data and meteorology. Subsequently, the relationship between reference thermal sums and other parameters, such as altitude, latitude, and average temperature, can be explored for multiple years. For example, machine learning can be utilized to quantify the relationship. In this way, we can derive more accurate reference thermal sums for each crop at any location in the same region in any year (unpublished work).

Derivation of sowing days from remote sensing
We now used the thermal sum approach to predict crops' sowing days and then linked it to the fertilization days. However, satellite remote sensing technology advancements also offer opportunities for a more direct assessment of the fertilization days because fertilization significantly alters the physiological status of crops and, consequently, their spectral and radar signatures. The European Space Agency's Sentinel-1 and Sentinel-2 satellites stand out among the various satellite systems available due to their high temporal resolution and diverse sensing capabilities. Sentinel-1 is a radar imaging system capable of providing data regardless of weather conditions, which is critical for continuous monitoring of agricultural practices. Meanwhile, Sentinel-2 offers high-resolution multispectral imagery, which is essential for assessing vegetation health. Multitemporal observations, the repeated observations of a specific area over time, allow for the monitoring of temporal changes and trends in crop growth stages, plant health,

and farming practices in agriculture. By analyzing multitemporal Sentinel-1 and Sentinel-2 data, it is possible to infer when fertilization on crops occurs.

The high-resolution multispectral data from Sentinel-2 can be used to calculate vegetation indices such as the Normalized Difference Vegetation Index (NDVI). A sudden increase in NDVI following a period of stable or decreasing values can indicate that the crops have been fertilized and are experiencing enhanced growth. Sentinel-1's Synthetic Aperture Radar (SAR) data can be used to monitor soil moisture (Paloscia et al., 2013). Changes in soil moisture can indicate irrigation activities, often accompanying fertilization in many agricultural systems. An increase in soil moisture not linked to rainfall can also suggest a fertilization event. By analyzing the temporal trends of these indicators, it is possible to identify significant changes likely associated with fertilization events. To validate these findings, the estimated fertilization dates, with actual fertilization dates recorded by farmers or agricultural managers, can be obtained from phenological observations.

De Martonne-Index and soil type
The timing of fertilization is affected by trafficability. Modeling trafficability on farmlands can be complex as it involves numerous variables, including weather conditions, soil type, and agricultural practices, which can all influence the ability of vehicles to traverse the landscape.

In our model, the De Martonne-Index was used to predict excessive rainfall as an indicator for unfavorable trafficability and thus fertilization and related emissions being put off. The threshold of De Martonne-Index was decided with a visual inspection for Flanders and expanded to the whole area of interest. The value is considered a pragmatic, empirical, and essential value. When the threshold is set too small, the time profile will be delayed too far because precipitation is too often considered excessive for fertilization operations. A more elaborate trafficability algorithm is required to account for regional differences.

Apart from rainfall, there are other factors related to trafficability and the timing of fertilization, such as soil type and soil moisture content. Different soil types have different properties that can influence trafficability, such as texture, structure, and compaction. For instance, clayey soils can become extremely sticky and potentially more impassable than sandy soils when wet. Soil surveys or soil maps can provide information on the distribution of different soil types within the area of interest.

Moisture content affects soil compaction, shear strength, and, thus, trafficability (Cokca et al., 2004). The infiltration rate, or the rate at which water enters the soil, is critical to model the changes in soil moisture content, which depends on the soil's physical properties, the precipitation's intensity and duration, and the initial soil moisture content. Various

infiltration models exist, such as the Green and Ampt model and Philip's model (Chahinian et al., 2005). After calculating the amount of water infiltrating the soil, one can model the change in soil moisture content using a soil water balance equation, which considers inputs (precipitation), outputs (evapotranspiration), and changes in storage (soil moisture).

Multiple fertilizations on potatoes and grassland

In our study, we assumed that fertilization occurs only at the start of the growing season, while multiple fertilizations can also be practiced for crops. Multiple fertilizations, or split applications, arise from the need to better match the supply of nutrients with the plant's demand at different stages of its growth cycle. This concept can be applied to all crops but holds specifically for potatoes with a significant nutrient demand, particularly nitrogen, phosphorus, and potassium, to ensure optimal growth and productivity due to their high yield potential. Multiple fertilizations throughout the growth period can have several advantages. First, potatoes absorb nutrients more efficiently when applied closer to the time of greatest need, such as during tuber initiation and bulking stages. Multiple fertilizations can enhance tuber yield and quality by optimizing nutrient availability. Second, using all the fertilizer at the time of planting can lead to nutrient losses before the plant can utilize them effectively, and applying fertilizer in stages reduces the risk of nutrient leaching or runoff. This is especially common when large amounts of nutrients are applied at once under heavy rain. It thus minimizes the risk of environmental issues like water contamination.

The timing of these fertilizations generally follows key stages in the potato plant's growth cycle. A portion of the fertilizer is applied at planting to ensure the potato plants have the nutrients necessary for initial growth. The second time occurs when the potato plant begins to form tubers. It's a critical phase that requires additional nutrients, particularly phosphorus, and potassium, to support tuber development. Potatoes are fertilized for the third time when the tubers grow rapidly and have the highest nutrient demand, especially nitrogen, and potassium. Some growers apply additional fertilizer in the late season to ensure the plants have enough nutrients to complete their growth cycle. However, this is less common and depends on the specific nutrient needs of the crop and soil fertility levels.

One common method to derive key stages in the potato plant's growth cycle and to enable the best timing of multiple fertilizations of crops, is to use a crop growth model. A widely-used crop model for potatoes is the SUBSTOR-Potato model integrated within the DSSAT (Decision Support System for Agrotechnology Transfer) suite (Jones et al., 2003), which simulates the daily dynamics of water, nitrogen, biomass, phenology, and tuber yield accumulation of potato. The model recognizes five developmental stages: pre-planting, sprout elongation, emergence, tuber initiation, and maturity. The model uses

6

five genotype-specific parameters that control plant growth and development processes, including leaf area expansion, tuber initiation, potential tuber growth rate, and tuber growth cessation. Various relative temperature functions are used to modify leaf, root, and tuber growth, photosynthesis, and tuber initiation. Potato growth and development are simulated based on the accumulation and partitioning of biomass in relation to intercepted radiation, photoperiodicity, and temperature. For details, the reader is referred to Griffin et al. (1993) and Singh et al. (1998).

Similarly to potatoes, temporary grasslands have specific nutrient needs that vary throughout the growing season. Insight into the proper fertilization time for grassland is critical because they are a dominant "crop", a vital component of many farming systems, serving as a source of forage for livestock and a way to improve soil health and fertility. Applying fertilizer multiple times throughout the year can help meet these needs more effectively. Regarding timing, fertilizations are often planned in Early Spring, After Each Cutting or Grazing, and Late Summer or Fall. A fertilizer application in early spring can provide nutrients to support the initial flush of growth after winter dormancy. Grasslands typically need additional nutrients to recover after being cut for hay or grazed by livestock. As such, another round of fertilizer is often applied at this time to promote regrowth. Some farmers apply additional fertilizer in late summer or fall to prepare the grassland for winter and ensure a solid start for the next growing season. This is particularly common if the grassland is being overwintered. Although fixed periods of cutting may be set to prescribe the variability easily, remote sensing may be used to prescribe it better.

In Chapter 4, the ammonia emission model with the updated crop map indicates that total ammonia emission from manure and fertilizer application on grassland is approximately 87% more than that on all arable crops in the Netherlands in 2017. The National Emission Model for Ammonia (NEMA), which calculates the total NH_3 emission from agriculture in the Netherlands, simulates that 22 Gg $N-NH_3$ is emitted annually from manure application on grassland. In comparison, only 11 Gg $N-NH_3$ comes from manure application on arable land (Velthof et al., 2012). Therefore, given the magnitude of ammonia emissions, we recommend first elaborating on the grassland application emissions as a follow-up.

Uncertainties in the spatial distribution of ammonia emissions

Uncertainties in the spatial distribution of ammonia emissions are affected by the spatial variability in (i) manure and fertilizer N inputs, such as N excretion rates, animal grazing periods, housing locations, crop distributions, fertilizer application rates, and manure transport; and (ii) ammonia emission fractions of manure N inputs by grazing, application and in animal houses, which are discussed in detail below.

Nitrogen (N) excretion rates

Nitrogen (N) excretion rates (kg N per animal) for each animal type are used to obtain the total N excreted per animal type in NCUs in INTEGRATOR after being multiplied with animal numbers. The N excretion rates in INTEGRATOR for EU-27 are country-specific and come from the GAINS model (Asman et al., 2011), based on estimates of national experts (Klimont and Brink, 2004). However, there exists spatial variability within the country since N excretion rates are influenced by several factors, including an animal's diet, age, weight, and productivity. It means that there are uncertainties in the spatial distribution of N excreted and, subsequently, the spatial distribution of manure N and ammonia emissions.

The amount and type of nitrogen in an animal's diet significantly affect its nitrogen excretion rate. Animals fed a diet high in protein (nitrogen) generally excrete more nitrogen. The digestibility of the diet also plays a role – diets that are more digestible result in lower nitrogen excretion as the animal's body utilizes more of the consumed nitrogen. Age can also impact nitrogen excretion rates as it is often correlated with an animal's metabolism and size. Younger animals may utilize more dietary nitrogen for tissue synthesis and thus excrete less, while older animals may excrete more of the nitrogen they consume due to slower metabolic rates. Larger animals generally consume more food and nitrogen, leading to higher nitrogen excretion rates. However, there can be exceptions, where larger animals may excrete less nitrogen because they are more efficient at converting feed into body mass. Productivity, such as milk production in dairy cows or egg production in hens, can also influence nitrogen excretion rates. High-productivity animals often have specially formulated diets designed to maximize their output. These diets can be high in protein to promote growth or milk/egg production, leading to higher nitrogen excretion rates. However, these animals may also be more efficient at utilizing dietary nitrogen, which could counterbalance this effect.

6

One way to increase the spatial variability in N excretion rates in INTEGRATOR is to use insight into their variation at the regional level. For example, Velthof (2014) found out that the N excretion rate from dairy cattle is generally higher in the north (115 – 135 kg N per cow) than in the south of Germany (larger than 95 – 115 kg N per cow). In addition, Velthof (2014) also showed that N input to grassland (kg N per ha per year) has an impact on N excretion rate (kg N per cow per year). Under the assumption of a total feed requirement of 7000 kg dry matter per cow, the N excretion rate increases almost linearly when N input on grassland increases and the slope rises along with the percentage of grazed grass. More surveys and experiments are needed to derive excretion rates with higher spatial details. For example, information on animal weight, feed, etc., can be gathered. Regional N excretion rates can then be derived using an N-balanced approach (Haenel et al., 2014). In the case of dairy cattle, excretion can be calculated by extracting the amount of N retained

in weight gained, exported with milk, and in animal products from the amount of N taken in with feed (Haenel et al., 2020).

Grazing periods

The INTEGRATOR model distinguishes between the excretion of animals in housing systems and those grazing in pastures, utilizing data on the number of grazing days at the national level. The assumed constant partitioning most likely contributed to discrepancies in cattle management and grazing emissions. Rather than a country-specific constant, this partitioning should be more flexible as the type of grazing system used and the duration of daily grazing collectively determine the amount of excretion in animal housing during the grazing seasons for dairy cows (van Bruggen et al., 2012). For example, van Bruggen et al. (2010) postulated that in the Netherlands, the excretion amounts in animal housing for both day-night and daytime grazing are proportionate to the number of barn hours. Van Bruggen et al. (2012) grouped grazing systems into unrestricted grazing, limited grazing, or full-time housing. They provided the percentage of N excretion within housing systems for each type of grazing system applied. A more comprehensive survey of the variety of grazing systems is needed to produce more precise estimates of emissions from housing and storage systems at the regional level.

Animal housing locations

Chapter 4 confirmed for the Netherlands that the improvement brought about by detailed information on housing locations is significant. Without housing locations, the emissions from animal houses and manure storage facilities were distributed all over the NCU, which resulted in smoothened spatial characteristics. However, in most countries, data on animal house locations are unavailable (or not openly available). Therefore, an alternative detection of livestock houses using satellite imagery may be a viable direction in improving ammonia emission modeling.

Animal houses, with their unique characteristics of roof color, material, and surrounding land use, can be detected using satellite imagery, which provides an efficient and cost-effective tool for large-scale surveys with its consistent coverage and repeated measurements. Particularly, the Sentinel-2 satellite system, offering high-resolution multispectral imagery, has emerged as a powerful resource for such applications. The automatic detection of animal houses can be achieved using a machine learning model, which is trained and validated with ground truth data. Once ground truth data of animal houses are collected, feature extraction from Sentinel-2 images can be performed to identify the specific characteristics of animal houses that correspond to roof color and material. Spectral indices such as the Normalized Difference Vegetation Index (NDVI), Normalized Difference Water Index (NDWI), and Built-Up Index (BUI) can help distinguish between various roof materials and colors based on their unique spectral signatures. After

extracting the relevant features, a machine learning model can be trained using algorithms such as Random Forest and Convolutional Neural Networks (CNN). Following the classification, it is essential to validate the results, based on which classification parameters can be fine-tuned as necessary to improve the accuracy of animal house detection. Land use maps can be utilized to narrow down the agricultural areas where animal houses are located. Similar to crop mapping in Chapter 4, supervised classification techniques can be applied to the Sentinel-2 imagery, where training samples are identified for different land use types, such as agriculture, forest, water, etc., creating a comprehensive land use map.

Crop distribution

Crop distribution mainly affects the spatial variation in the application of manure and mineral N fertilizers. There are several factors that affect the accuracy of the crop classification. Firstly, inaccuracies related to GPS measurements in the field and errors in image registration can lead to the misclassification of ground truth data of crops, which can result in incorrect calculations of the temporal variability of vegetation indices in training and test samples. Secondly, the arrangement of georeferenced observation points in the LUCAS system, which follows a 2 km by 2 km grid, may lead to insufficient data points for certain crop classes. Regardless of its size, training data for less prevalent crops may be scarce in any given area, while data for more common crop types might be abundant. This causes an overrepresentation of larger classes in a land cover map, primarily affecting the validation results of the smaller classes.

The spectral attributes of a specific class and the size of crop parcels are crucial factors in crop mapping. Maize and grassland exhibit relatively unique temporal reflectance and vegetation index patterns. Conversely, cereal types like rye, wheat, and oat share similar phenological and morphological patterns, making their spectral differentiation challenging and reducing classification accuracy for these classes. Moreover, a class like vegetable encompasses various plants with different temporal patterns in vegetation indices. More refined categorization is needed to identify various vegetables. Additionally, the classification accuracy may be negatively impacted by smaller parcel sizes as the likelihood of spectral properties blending with neighboring land covers rises. This complicates the collection of representative training data and subsequent land cover predictions.

To enhance classification accuracy, gathering extra training data through manual or automated methods could assist in distinguishing spectrally or temporally unique classes. In addition, incorporating other multi-sensor time series such as Landsat-7 and Landsat-8, which offer observations akin to those of Sentinel-2, can improve the temporal frequency of time series, reducing the revisit time to between 2–5 days (Wulder et al., 2021). Furthermore, the synergies of optical and high-resolution synthetic aperture radar

(SAR) time series (for example, from Sentinel-1 C-Band) can also improve crop mapping (Blickensdörfer et al., 2022). Unlike optical images, which can be affected by weather conditions and sunlight, SAR sensors can collect data regardless of these factors, providing more frequent revisit times (Villarroya-Carpio et al., 2022). These techniques may offer better discrimination of crop types in future studies.

Mineral fertilizer applied to crops
Our study uses the N-balanced approach to estimate the amount of mineral fertilizer required for crops based on crop yields and N demand per crop. Apart from using more recent and region-specific data on mineral fertilizer application rates and crop yields, there are several ways of improving the accuracy and spatial resolution. First, information on crop rotation patterns can provide more accurate fertilizer estimates since crop rotation and intercropping influence soil N levels and crop N demand. Besides, more detailed information on the contribution of organic matter and other organic sources of N, such as cover crops, manure, and compost in the N balance approach, likely improves the estimate as these sources can supplement or even replace the need for mineral fertilizers. Moreover, incorporating data on crop residue management can help improve the accuracy of fertilizer estimates since the management of crop residues can significantly affect soil N levels. Finally, remote sensing can provide detailed information on within-field variability in crop yields and soil characteristics, allowing for more precise fertilizer application estimates.

Emission fractions of manure application and animal housing
Apart from the spatial variability in manure (and fertilizer) N inputs, the spatial distribution of ammonia emissions is also affected by the spatial variability in ammonia emission fractions of manure application and animal housing. Predictions of those fractions, as a function of site conditions affecting their spatial variation, often rely on a limited set of predictor variables. This can inevitably lead to inaccuracies across different locations or even at a single location on varying dates. The absence of relevant variables, such as soil pH and water content, restricts the effectiveness of the ALFAM2 model. Slurry and soil pH are critical to simulate the system's pH change impact on ammonia volatilization. Furthermore, ignoring confounding variables (interactions between variables like soil moisture and dry matter of manure) might contribute to biased or inaccurate effect estimates by ALFAM2. Consequently, current predictions about relative effects on emission tend to be more accurate than predictions of absolute emission. There is a need for diversifying measurements that include a broader range of variables and enhancing their harmonization via future emission measurement experiments.

The emission fractions for animal houses and manure storage in INTEGRATOR are a function of animal category and manure category (solid manure or liquid manure) per

country (de Vries et al., 2022). The differences in countries are related to the animal houses and manure storage facilities that occur (high, medium, or low emission systems). On average, housing or storage type per country and animal category is used without distinguishing the spatial variation of housing type for each animal category in each country. Modifications resulting from the temperature-based scaling were not notably significant because the temperature-based scaling ensured that the average ammonia emission level matched the initial output from the INTEGRATOR model. To attain a more precise emission fraction for housing and manure storage, having access to comprehensive hourly ammonia measurements over an extended period across a broad network can be incredibly beneficial. Sommer et al. (2019) highlighted that during these measurements, it's essential to account for several factors: (1) the proportion of slatted floor to concrete floor area in pig pens, (2) the area of floor openings, (3) the distribution of excreta within the structure, (4) the capacity for in-house storage, (5) the age of the animals, (6) the local climate, and (7) feeding practices.

Manure transport

The INTEGRATOR model presumes that emissions from a specific animal, including housing, storage, and manure application, occur where the animal resides, thereby overlooking the transport of manure from areas with surplus to those experiencing shortages. Manure transport becomes more significant in regions with intensive animal livestock. Hendriks et al. (2016) discovered that manure transport occupied approximately one-third of the manure applied annually in Flanders. Therefore, ignoring manure transport contributes to uncertainties in emission estimates. Incorporating manure transport data can serve as a valuable tool to enhance the spatial distribution of emissions.

Predicting the amount and location of manure transport in a model involves a comprehensive process combining various data types and several assumptions, as summarized by de Vries et al. (2023) in view of a manure transport model in the Netherlands. First, comprehensive data on the location and number of livestock need to be gathered according to livestock types (cattle, poultry, swine, etc.), as each type produces manure with different nutrient contents. Next, high-resolution livestock population data can be utilized to estimate manure production. With the manure production estimates at hand, one can identify regions of manure surplus (where manure production surpasses the land's capacity to utilize it) and deficit (where there's potential land to absorb more manure than locally produced). Potential manure transport can be modeled based on the identified surplus and deficit areas, which involves calculating the cost of transport (depending on distance, road infrastructure, etc.) and the benefit of nutrient value to crops. Commonly, the model assumes that manure would be transported from surplus to deficit areas, prioritizing closer regions to minimize transport costs. The actual transport might be influenced by various regulatory constraints like restrictions on manure application

6

rates, times, or locations, which must be incorporated into the model (de Vries et al., 2023). If available, actual manure transport from transportation records, surveys, or other data sources can be used to validate the model, which determines the model's accuracy and pinpoint areas for refinement.

Uncertainties in the measurement and use of satellite observations
Uncertainties in CrIS and IASI measurements
Both CrIS and IASI are interferometric sensors that provide high-spectral-resolution, long-wavelength infrared radiance data. The retrieval of ammonia from them is challenging due to the weak spectral signal of ammonia and the interference from other atmospheric constituents.

One of the major challenges in retrieving ammonia from satellite observations is the interference from other gases, particularly water vapor. This is due to overlapping absorption features in the infrared spectrum. Algorithms must accurately account for these interferences to avoid significant biases in ammonia retrieval. In addition, ammonia concentrations in the atmosphere are generally low, resulting in a weak spectral signal. This resulted in the limited availability of valid measurements or observations with low uncertainties. Integrating CrIS data with IASI data has been shown to improve spatial and temporal coverage, providing a more comprehensive picture of global ammonia distributions (Dammers et al., 2019).

The limited availability of in situ measurements is a recurring issue during the validations of the models. The nature of high reactivity makes it challenging to measure ammonia. Besides, the cost of maintaining and operating the instruments can be high. Even though the MAN network is extensive, it measures ammonia concentrations in nature areas at a monthly resolution, which reduces its representativeness in space and time.

There have been studies on the retrieval of ammonia concentrations from satellite data using atmospheric temperature and humidity profiles. Errors in these profiles can introduce significant uncertainties in the ammonia retrievals, which calls for significant improvements. Dammers et al. (2016) proposed that tower measurement campaigns are essential for enhancing the comprehension of the vertical profile. Li et al. (2017) noted an evident seasonal fluctuation in the vertical distribution of ammonia, with the slope of the ammonia concentration gradient varying throughout the year. They observed relatively high ground concentrations of ammonia during winter, attributing this to the shallower boundary layer in colder months, which could potentially trap ammonia emissions and decrease ammonia concentrations at higher altitudes.

Inverse emission modeling using satellite data

The progressing development of satellite remote sensing provides great opportunities for better-constraining ammonia emissions in space and time. CrIS and IASI satellite observations, combined with relevant emission inventory, have been widely used to calculate NH_3 emission fluxes and identify ammonia emission hotspots at the global scale (Dammers et al., 2019; Clarisse et al., 2019; Luo et al., 2022; Evangeliou et al., 2021; Van Damme et al., 2018).

Several studies have shown that IASI observations can be used to infer global and regional patterns of ammonia emissions. For instance, Van Damme et al. (2014) used IASI observations in an inversion model to estimate global ammonia emissions. Similarly, Fortems-Cheiney et al. (2016) used IASI data to assess the impact of agricultural practices on ammonia emissions in Europe. Compared to IASI, CrIS has a higher spectral resolution but a narrower swath width, making it less suitable for global studies but potentially more useful for regional studies. Cao et al. (2020) used CrIS observations and GEOS-Chem to estimate monthly NH_3 emissions over the contiguous US, and found they are 33% higher than the prior emissions which likely underestimated most agricultural emissions. We can also take advantage of the averaging kernels and error covariance matrix provided in the CrIS retrieved product to provide top-down constraints on the ammonia emissions (Cao et al., 2020; Shephard et al., 2020). Examples of use at the regional scale are still quite limited, with notable examples of their application in the UK (Marais et al., 2021), the US (Chen et al., 2021), and China (Liu et al., 2022).

Ongoing and future work in this field includes the development of improved retrieval algorithms, refining the inverse models, and integrating satellite data with ground-based measurements and model simulations for a more comprehensive understanding of the ammonia cycle.

6

References

References

Aber, J., McDowell, W., Nadelhoffer, K., Magill, A., Berntson, G., Kamakea, M., McNulty, S., Currie, W., Rustad, L., and Fernandez, I.: Nitrogen Saturation in Temperate Forest Ecosystems: Hypotheses revisited, Bioscience, 48, 921–934, https://doi.org/10.2307/1313296, 1998.

Agapiou, A., Alexakis, D. D., Sarris, A., and Hadjimitsis, D. G.: Evaluating the Potentials of Sentinel-2 for Archaeological Perspective, Remote Sens., 6, 2176–2194, https://doi.org/10.3390/rs6032176, 2014.

Amann, M., Klimont, Z., and Wagner, F.: Regional and Global Emissions of Air Pollutants: Recent Trends and Future Scenarios, https://doi.org/10.1146/annurev-environ-052912-173303, 38, 31–55, https://doi.org/10.1146/ANNUREV-ENVIRON-052912-173303, 2013.

Anderson, N., Strader, R., and Davidson, C.: Airborne reduced nitrogen: ammonia emissions from agriculture and other sources, Environ. Int., 29, 277–286, https://doi.org/10.1016/S0160-4120(02)00186-1, 2003.

Arogo, J., Westerman, P., Heber, A., Robarge, W., and Classen, J.: Ammonia Emissions from Animal Feeding Operations, Anim. Agric. Environ. Natl. Cent. Manure Anim. Waste Manag. White Pap., 2002.

Asman, W. A. H.: Modelling the atmospheric transport and deposition of ammonia and ammonium: an overview with special reference to Denmark, Atmos. Environ., 35, 1969–1983, https://doi.org/10.1016/S1352-2310(00)00548-3, 2001.

Asman, W. A. H., Klimont, Z., and Winiwarter, W.: A Simplified Model of Nitrogen Flows from Manure Management, IR-11-030, IIASA, Laxenburg, Austria, 2011.

Backes, A., Aulinger, A., Bieser, J., Matthias, V., and Quante, M.: Ammonia emissions in Europe, part I: Development of a dynamical ammonia emission inventory, Atmos. Environ., 131, 55–66, https://doi.org/10.1016/j.atmosenv.2016.01.041, 2016.

Baker, J. P. and Schofield, C. L.: Aluminum toxicity to fish in acidic waters, Water. Air. Soil Pollut., 18, 289–309, https://doi.org/10.1007/BF02419419, 1982.

Ballin, M., Barcaroli, G., Masselli, M., and Scarnó, M.: Redesign sample for Land Use/Cover Area frame Survey (LUCAS) 2018, Eurostat, https://doi.org/10.2785/132365, 2018.

Baltas, E.: Spatial distribution of climatic indices in northern Greece, Meteorol. Appl., https://doi.org/10.1002/met.7, 2007.

Banzhaf, S., Schaap, M., Kranenburg, R., Manders, A. M. M., Segers, A. J., Visschedijk, A. J. H., Van Der Gon, H. A. C. D., Kuenen, J. J. P., Van Meijgaard, E., Van Ulft, L. H., Cofala, J., and Builtjes, P. J. H.: Dynamic model evaluation for secondary inorganic aerosol and its precursors over Europe between 1990 and 2009, Geosci. Model Dev., 8, 1047–1070, https://doi.org/10.5194/gmd-8-1047-2015, 2015.

Bassett, M. and Seinfeld, J. H.: Atmospheric equilibrium model of sulfate and nitrate aerosols, Atmos. Environ., 17, 2237–2252, https://doi.org/10.1016/0004-6981(83)90221-4, 1983.

Battye, W., Aneja, V. P., and Roelle, P. A.: Evaluation and improvement of ammonia emissions inventories, Atmos. Environ., https://doi.org/10.1016/S1352-2310(03)00343-1, 2003.

R

Baumann, M., Levers, C., Macchi, L., Bluhm, H., Waske, B., Gasparri, N. I., and Kuemmerle, T.: Mapping continuous fields of tree and shrub cover across the Gran Chaco using Landsat 8 and Sentinel-1 data, Remote Sens. Environ., 216, 201–211, https://doi.org/10.1016/j.rse.2018.06.044, 2018.

Beer, R., Shephard, M. W., Kulawik, S. S., Clough, S. A., Eldering, A., Bowman, K. W., Sander, S. P., Fisher, B. M., Payne, V. H., Luo, M., Osterman, G. B., and Worden, J. R.: First satellite observations of lower tropospheric ammonia and methanol, Geophys. Res. Lett., 35, https://doi.org/10.1029/2008GL033642, 2008.

Behera, S. N. and Sharma, M.: Transformation of atmospheric ammonia and acid gases into components of $PM_{2.5}$: an environmental chamber study., Environ. Sci. Pollut. Res. Int., 19, 1187–1197, https://doi.org/10.1007/s11356-011-0635-9, 2012.

Belgiu, M. and Csillik, O.: Sentinel-2 cropland mapping using pixel-based and object-based time-weighted dynamic time warping analysis, Remote Sens. Environ., https://doi.org/10.1016/j.rse.2017.10.005, 2018.

Belgiu, M. and Drăguţ, L.: Random forest in remote sensing: A review of applications and future directions, ISPRS J. Photogramm. Remote Sens., 114, 24–31, https://doi.org/10.1016/j.isprsjprs.2016.01.011, 2016.

Benevides, P., Costa, H., Moreira, F. D., and Caetano, M.: Mapping annual crops in Portugal with Sentinel-2 data, in: Proc.SPIE, 122620M, https://doi.org/10.1117/12.2636125, 2022.

Berkhout, A. J. C., Swart, D. P. J., Volten, H., Gast, L. F. L., Haaima, M., Verboom, H., Stefess, G., Hafkenscheid, T., and Hoogerbrugge, R.: Replacing the AMOR with the miniDOAS in the ammonia monitoring network in the Netherlands, Atmos. Meas. Tech., 10, 4099–4120, https://doi.org/10.5194/amt-10-4099-2017, 2017.

Bey, I., Jacob, D. J., Yantosca, R. M., Logan, J. A., Field, B. D., Fiore, A. M., Li, Q., Liu, H. Y., Mickley, L. J., and Schultz, M. G.: Global modeling of tropospheric chemistry with assimilated meteorology: Model description and evaluation, J. Geophys. Res. Atmos., 106, 23073–23095, https://doi.org/10.1029/2001JD000807, 2001.

Bishop, C. M.: Pattern Recognition and Machine Learning, Springer New York, 2016.

Bleeker, A.: Quantification of nitrogen deposition and its uncertainty with respect to critical load exceedances, Vrije Universiteit Amsterdam, 2018.

Bleizgys, R., Bagdonienė, I., and Baležentienė, L.: Reduction of the Livestock Ammonia Emission under the Changing Temperature during the Initial Manure Nitrogen Biomineralization, Sci. World J., 2013, 825437, https://doi.org/10.1155/2013/825437, 2013.

Blickensdörfer, L., Schwieder, M., Pflugmacher, D., Nendel, C., Erasmi, S., and Hostert, P.: Mapping of crop types and crop sequences with combined time series of Sentinel-1, Sentinel-2 and Landsat 8 data for Germany, Remote Sens. Environ., 269, 112831, https://doi.org/10.1016/j.rse.2021.112831, 2022.

Bobbink, Bal, D. V, van Dobben, H. F., Jansen, A. J. M., Nijssen, M., Siepel, H., Schaminée, J. H. J., Smits, N. A. C., and de Vries, W.: The effects of nitrogen deposition on the structure and functioning of ecosystems, 2013.

Bobbink, R., Hornung, M., and Roelofs, J. G. M.: The effects of air-borne nitrogen pollutants on species diversity in natural and semi-natural European vegetation, J. Ecol., 86, 717–738, https://doi.org/10.1046/j.1365-2745.1998.8650717.x, 1998.

Bobbink, R., Hicks, K., Galloway, J., Spranger, T., Alkemade, R., Ashmore, M., Bustamante, M., Cinderby, S., Davidson, E., Dentener, F., Emmett, B., Erisman, J. W., Fenn, M., Gilliam, F., Nordin, A., Pardo, L., and De Vries, W.: Global assessment of nitrogen deposition effects on terrestrial plant diversity: A synthesis, Ecol. Appl., https://doi.org/10.1890/08-1140.1, 2010.

Boldo, E., Medina, S., Le Tertre, A., Hurley, F., Mücke, H.-G., Ballester, F., Aguilera, I., and group, D. E. on behalf of the A.: Apheis: Health Impact Assessment of Long-term Exposure to PM2.5 in 23 European Cities, Eur. J. Epidemiol., 21, 449–458, https://doi.org/10.1007/s10654-006-9014-0, 2006.

Bougouin, A., Leytem, A., Dijkstra, J., Dungan, R. S., and Kebreab, E.: Nutritional and Environmental Effects on Ammonia Emissions from Dairy Cattle Housing: A Meta-Analysis, J. Environ. Qual., 45, 1123–1132, https://doi.org/10.2134/jeq2015.07.0389, 2016.

Bouwman, A. F.: Long-term Scenarios of Livestock-Crop-Land Use Interactions in Developing Countries., Food and Agriculture Organizatio of the United Nations (FAO), Rome., 1997.

Bouwman, A. F., Van Vuuren, D. P., Derwent, R. G., and Posch, M.: A Global Analysis of Acidification and Eutrophication of Terrestrial Ecosystems, Water. Air. Soil Pollut., 141, 349–382, https://doi.org/10.1023/A:1021398008726, 2002.

Bouwmeester, R. J. B., Vlek, P. L. G., and Stumpe, J. M.: Effect of Environmental Factors on Ammonia Volatilization from a Urea-Fertilized Soil, Soil Sci. Soc. Am. J., 49, 376–381, https://doi.org/10.2136/sssaj1985.03615995004900020021x, 1985.

Bowman, W. D., Cleveland, C. C., Halada, Ĺ., Hreško, J., and Baron, J. S.: Negative impact of nitrogen deposition on soil buffering capacity, Nat. Geosci., 1, 767–770, https://doi.org/10.1038/ngeo339, 2008.

Breiman, L.: Random Forests, Mach. Learn., 45, 5–32, https://doi.org/10.1023/A:1010933404324, 2001.

ten Brink, H., Otjes, R., Jongejan, P., and Kos, G.: Monitoring of the ratio of nitrate to sulphate in size-segregated submicron aerosol in the Netherlands, Atmos. Res., 92, 270–276, https://doi.org/10.1016/j.atmosres.2008.12.003, 2009.

van Bruggen, C., de Bode, M. J. C., Evers, A. G., van der Hoek, K. W., Luesink, H. H., and van Schijndel, M. W.: Gestandaardiseerde berekeningsmethode voor dierlijke mest en mineralen : standaardcijfers 1990-2008, Centraal Bureau voor de Statistiek, 2010.

van Bruggen, C., Groenestein, C. M., de Haan, B. J., Hoogeveen, M. W., Huijsmans, J. F. M., Sluis, S. M., and Velthof, G. L.: Ammonia emissions from animal manure and inorganic fertilisers in 2009 : calculated with the Dutch National Emissions Model for Ammonia (NEMA), Wettelijke Onderzoekstaken Natuur & Milieu, 2012.

Brunekreef, B. and Holgate, S. T.: Air pollution and health, https://doi.org/10.1016/S0140-6736(02)11274-8, 2002.

R

Buendia, E., Tanabe, K., Kranjc, A., Jamsranjav, B., Fukuda, M., Ngarize, S., Osako, A., Pyrozhenko, Y., Shermanau, P., and Federici, S.: 2019 Refinement to the 2006 IPCC Guidelines for National Greenhouse Gas Inventories, 2019.

Bussink, D. W.: Ammonia volatilization from grassland receiving nitrogen fertilizer and rotationally grazed by dairy cattle, Fertil. Res., 33, 257–265, https://doi.org/10.1007/BF01050881, 1992.

Bussink, D. W.: Relationships between ammonia volatilization and nitrogen fertilizer application rate, intake and excretion of herbage nitrogen by cattle on grazed swards, Fertil. Res., 38, 111–121, https://doi.org/10.1007/BF00748771, 1994.

Bussink, D. W. and Oenema, O.: Ammonia volatilization from dairy farming systems in temperate areas: a review, Nutr. Cycl. Agroecosystems, 51, 19–33, https://doi.org/10.1023/A:1009747109538, 1998.

Cao, H., Henze, D. K., Shephard, M. W., Dammers, E., Cady-Pereira, K., Alvarado, M., Lonsdale, C., Luo, G., Yu, F., Zhu, L., Danielson, C. G., and Edgerton, E. S.: Inverse modeling of NH3 sources using CrIS remote sensing measurements, Environ. Res. Lett., 15, 104082, https://doi.org/10.1088/1748-9326/abb5cc, 2020.

Cao, H., Henze, D. K., Zhu, L., Shephard, M. W., Cady-Pereira, K., Dammers, E., Sitwell, M., Heath, N., Lonsdale, C., Bash, J. O., Miyazaki, K., Flechard, C., Fauvel, Y., Wichink Kruit, R., Feigenspan, S., Brümmer, C., Schrader, F., Twigg, M. M., Leeson, S., Tang, Y. S., Stephens, A. C. M., Braban, C., Vincent, K., Meier, M., Seitler, E., Geels, C., Ellermann, T., Sanocka, A., and Capps, S. L.: 4D-Var Inversion of European NH3 Emissions Using CrIS NH3 Measurements and GEOS-Chem Adjoint With Bi-Directional and Uni-Directional Flux Schemes, J. Geophys. Res. Atmos., 127, e2021JD035687, https://doi.org/10.1029/2021JD035687, 2022.

Cellier, P., Durand, P., Hutchings, N., Dragosits, U., Theobald, M., Drouet, J.-L., Oenema, O., Bleeker, A., Breuer, L., Dalgaard, T., Duretz, S., Kros, J., Loubet, B., Olesen, J. E., Merot, P., Viaud, V., de Vries, W., and Sutton, M. A.: Nitrogen flows and fate in rural landscapes, in: The European Nitrogen Assessment: Sources, Effects and Policy Perspectives, edited by: Sutton, M. A., Howard, C. M., Erisman, J. W., Billen, G., Bleeker, A., Grennfelt, P., van Grinsven, H., and Grizzetti, B., Cambridge University Press, Cambridge, 229–248, 2011.

Chahinian, N., Moussa, R., Andrieux, P., and Voltz, M.: Comparison of infiltration models to simulate flood events at the field scale, J. Hydrol., 306, 191–214, https://doi.org/10.1016/j.jhydrol.2004.09.009, 2005.

Chamberlain, A. C. and Spence, R.: Transport of gases to and from grass and grass-like surfaces, Proc. R. Soc. London. Ser. A. Math. Phys. Sci., 290, 236–265, https://doi.org/10.1098/rspa.1966.0047, 1997.

Chang, J. C. and Hanna, S. R.: Air quality model performance evaluation, Meteorol. Atmos. Phys., 87, 167–196, https://doi.org/10.1007/S00703-003-0070-7/METRICS, 2004.

Chantigny, M. H., Rochette, P., Angers, D. A., Massé, D., and Côté, D.: Ammonia Volatilization and Selected Soil Characteristics Following Application of Anaerobically Digested Pig Slurry, Soil Sci. Soc. Am. J., 68, 306–312, https://doi.org/10.2136/SSSAJ2004.3060, 2004.

Charlson, R. J., Langner, J., Rodhe, H., Leovy, C. B., and Warren, S. G.: Perturbation of the northern hemisphere radiative balance by backscattering from anthropogenic sulfate aerosols, Tellus B, https://doi.org/10.1034/j.1600-0889.1991.t01-1-00013.x, 1991.

Chen, Y., Shen, H., Kaiser, J., Hu, Y., Capps, S. L., Zhao, S., Hakami, A., Shih, J.-S., Pavur, G. K., Turner, M. D., Henze, D. K., Resler, J., Nenes, A., Napelenok, S. L., Bash, J. O., Fahey, K. M., Carmichael, G. R., Chai, T., Clarisse, L., Coheur, P.-F., Van Damme, M., and Russell, A. G.: High-resolution hybrid inversion of IASI ammonia columns to constrain US ammonia emissions using the CMAQ adjoint model, Atmos. Chem. Phys., 21, 2067–2082, https://doi.org/10.5194/acp-21-2067-2021, 2021.

Clarisse, L., Clerbaux, C., Dentener, F., Hurtmans, D., and Coheur, P. F.: Global ammonia distribution derived from infrared satellite observations, Nat. Geosci., 2, 479–483, https://doi.org/10.1038/ngeo551, 2009.

Clarisse, L., Shephard, M. W., Dentener, F., Hurtmans, D., Cady-Pereira, K., Karagulian, F., Van Damme, M., Clerbaux, C., and Coheur, P. F.: Satellite monitoring of ammonia: A case study of the San Joaquin Valley, J. Geophys. Res. Atmos., 115, https://doi.org/10.1029/2009JD013291, 2010.

Clarisse, L., Van Damme, M., Clerbaux, C., and Coheur, P.-F.: Tracking down global NH3 point sources with wind-adjusted superresolution, Atmos. Meas. Tech., 12, 5457–5473, https://doi.org/10.5194/amt-12-5457-2019, 2019.

Claverie, M., Ju, J., Masek, J. G., Dungan, J. L., Vermote, E. F., Roger, J.-C., Skakun, S. V, and Justice, C.: The Harmonized Landsat and Sentinel-2 surface reflectance data set, Remote Sens. Environ., 219, 145–161, https://doi.org/10.1016/j.rse.2018.09.002, 2018.

Clerbaux, C., Boynard, A., Clarisse, L., George, M., Hadji-Lazaro, J., Herbin, H., Hurtmans, D., Pommier, M., Razavi, A., Turquety, S., Wespes, C., and Coheur, P. F.: Monitoring of atmospheric composition using the thermal infrared IASI/MetOp sounder, Atmos. Chem. Phys., https://doi.org/10.5194/acp-9-6041-2009, 2009.

Clerici, N., Calderón, C. A. V., and Posada, J. M.: Fusion of Sentinel-1A and Sentinel-2A data for land cover mapping: a case study in the lower Magdalena region, Colombia, J. Maps, 13, 718–726, https://doi.org/10.1080/17445647.2017.1372316, 2017.

Cokca, E., Erol, O., and Armangil, F.: Effects of compaction moisture content on the shear strength of an unsaturated clay, Geotech. Geol. Eng., 22, 285–297, https://doi.org/10.1023/B:GEGE.0000018349.40866.3e, 2004.

Colette, A., Aas, W., Banin, L., Braban, C. F., Ferm, M., Ortiz, A. G., Ilyin, I., Mar, K., Pandolfi, M., Putaud, J.-P., Shatalov, V., Solberg, S., Spindler, G., Tarasova, O., Vana, M., Adani, M., Almodovar, P., Berton, E., Bessagnet, B., Bohlin-Nizzetto, P., Boruvkova, J., Breivik, K., Briganti, G., Cappelletti, A., Cuvelier, K., Derwent, R., D'Isidoro, M., Fagerli, H., Funk, C., Vivanco, M. G., Haeuber, R., Hueglin, C., Jenkins, S., Kerr, J., de Leeuw, F., Lynch, J., Manders, A., Mircea, M., Pay, M. T., Pritula, D., Querol, X., Raffort, V., Reiss, I., Roustan, Y., Sauvage, S., Scavo, K., Simpson, D., Smith, R. I., Tang, Y. S., Theobald, M., Torseth, K., Tsyro, S., van Pul, A., Vidic, S., Wallasch, M., and Wind, P.: Air pollution trends in the EMEP region between 1990 and 2012, Norwegian Institute for Air Research, Kjeller, Norway, 2016.

R

Congreves, K. A., Grant, B. B., Dutta, B., Smith, W. N., Chantigny, M. H., Rochette, P., and Desjardins, R. L.: Predicting ammonia volatilization after field application of swine slurry: DNDC model development, Agric. Ecosyst. Environ., 219, 179–189, https://doi.org/10.1016/j.agee.2015.10.028, 2016.

Crews, T. E. and Peoples, M. B.: Can the Synchrony of Nitrogen Supply and Crop Demand be Improved in Legume and Fertilizer-based Agroecosystems? A Review, Nutr. Cycl. Agroecosystems, 72, 101–120, https://doi.org/10.1007/s10705-004-6480-1, 2005.

Crippa, M., Guizzardi, D., Muntean, M., Schaaf, E., Dentener, F., van Aardenne, J. A., Monni, S., Doering, U., Olivier, J. G. J., Pagliari, V., and Janssens-Maenhout, G.: Gridded emissions of air pollutants for the period 1970--2012 within EDGAR v4.3.2, Earth Syst. Sci. Data, 10, 1987–2013, https://doi.org/10.5194/essd-10-1987-2018, 2018.

Croitoru, A. E., Holobaca, I. H., Lazar, C., Moldovan, F., and Imbroane, A.: Air temperature trend and the impact on winter wheat phenology in Romania, Clim. Change, https://doi.org/10.1007/s10584-011-0133-6, 2012.

Cuddington, K., Fortin, M.-J., Gerber, L. R., Hastings, A., Liebhold, A., O'Connor, M., and Ray, C.: Process-based models are required to manage ecological systems in a changing world, Ecosphere, 4, art20, https://doi.org/10.1890/ES12-00178.1, 2013.

Cutler, A., Cutler, D. R., and Stevens, J. R.: Random Forests, Ensemble Mach. Learn., 157–175, https://doi.org/10.1007/978-1-4419-9326-7_5, 2012.

Effects of air pollution on natural ecosystems: https://www.daera-ni.gov.uk/topics/protect-environment/effects-air-pollution-natural-ecosystems, last access: 24 June 2023.

Van Damme, M., Wichink Kruit, R. J., Schaap, M., Clarisse, L., Clerbaux, C., Coheur, P.-F., Dammers, E., Dolman, A. J., and Erisman, J. W.: Evaluating 4 years of atmospheric ammonia (NH3) over Europe using IASI satellite observations and LOTOS-EUROS model results, J. Geophys. Res. Atmos., 119, 9549–9566, https://doi.org/10.1002/2014JD021911, 2014a.

Van Damme, M., Clarisse, L., Heald, C. L., Hurtmans, D., Ngadi, Y., Clerbaux, C., Dolman, A. J., Erisman, J. W., and Coheur, P. F.: Global distributions, time series and error characterization of atmospheric ammonia (NH3) from IASI satellite observations, Atmos. Chem. Phys., 14, 2905–2922, https://doi.org/10.5194/acp-14-2905-2014, 2014b.

Van Damme, M., Clarisse, L., Dammers, E., Liu, X., Nowak, J. B., Clerbaux, C., Flechard, C. R., Galy-Lacaux, C., Xu, W., Neuman, J. A., Tang, Y. S., Sutton, M. A., Erisman, J. W., and Coheur, P. F.: Towards validation of ammonia (NH3) measurements from the IASI satellite, Atmos. Meas. Tech., 8, 1575–1591, https://doi.org/10.5194/amt-8-1575-2015, 2015.

Van Damme, M., Whitburn, S., Clarisse, L., Clerbaux, C., Hurtmans, D., and Coheur, P.-F.: Version 2 of the IASI NH3 neural network retrieval algorithm: near-real-time and reanalysed datasets, Atmos. Meas. Tech., 10, 4905–4914, https://doi.org/10.5194/amt-10-4905-2017, 2017.

Van Damme, M., Clarisse, L., Whitburn, S., Hadji-Lazaro, J., Hurtmans, D., Clerbaux, C., and Coheur, P.-F.: Industrial and agricultural ammonia point sources exposed, Nature, 564, 99–103, https://doi.org/10.1038/s41586-018-0747-1, 2018.

Van Damme, M., Clarisse, L., Franco, B., Sutton, M. A., Erisman, J. W., Wichink Kruit, R., van Zanten, M., Whitburn, S., Hadji-Lazaro, J., Hurtmans, D., Clerbaux, C., and Coheur, P.-F.: Global, regional and national trends of atmospheric ammonia derived from a decadal (2008–2018) satellite record, Environ. Res. Lett., 16, 55017, https://doi.org/10.1088/1748-9326/abd5e0, 2021.

Dammers, E.: Measuring atmospheric ammonia with remote sensing, Vrije Universiteit Amsterdam, 2017.

Dammers, E., Vigouroux, C., Palm, M., Mahieu, E., Warneke, T., Smale, D., Langerock, B., Franco, B., Van Damme, M., Schaap, M., Notholt, J., and Erisman, J. W.: Retrieval of ammonia from ground-based FTIR solar spectra, Atmos. Chem. Phys., 15, 12789–12803, https://doi.org/10.5194/acp-15-12789-2015, 2015.

Dammers, E., Palm, M., Van Damme, M., Vigouroux, C., Smale, D., Conway, S., Toon, G. C., Jones, N., Nussbaumer, E., Warneke, T., Petri, C., Clarisse, L., Clerbaux, C., Hermans, C., Lutsch, E., Strong, K., Hannigan, J. W., Nakajima, H., Morino, I., Herrera, B., Stremme, W., Grutter, M., Schaap, M., Wichink Kruit, R. J., Notholt, J., Coheur, P. F., and Erisman, J. W.: An evaluation of IASI-NH3 with ground-based Fourier transform infrared spectroscopy measurements, Atmos. Chem. Phys., 16, 10351–10368, https://doi.org/10.5194/acp-16-10351-2016, 2016.

Dammers, E., Schaap, M., Haaima, M., Palm, M., Wichink Kruit, R. J., Volten, H., Hensen, A., Swart, D., and Erisman, J. W.: Measuring atmospheric ammonia with remote sensing campaign: Part 1 – Characterisation of vertical ammonia concentration profile in the centre of The Netherlands, Atmos. Environ., 169, 97–112, https://doi.org/10.1016/j.atmosenv.2017.08.067, 2017.

Dammers, E., McLinden, C. A., Griffin, D., Shephard, M. W., Van Der Graaf, S., Lutsch, E., Schaap, M., Gainairu-Matz, Y., Fioletov, V., Van Damme, M., Whitburn, S., Clarisse, L., Cady-Pereira, K., Clerbaux, C., Coheur, P. F., Erisman, J. W., Francois Coheur, P., and Erisman, J. W.: NH3 emissions from large point sources derived from CrIS and IASI satellite observations, Atmos. Chem. Phys., 19, 12261–12293, https://doi.org/10.5194/acp-19-12261-2019, 2019.

Dämmgen, U. and Hutchings, N. J.: Emissions of gaseous nitrogen species from manure management: A new approach, Environ. Pollut., 154, 488–497, https://doi.org/10.1016/J.ENVPOL.2007.03.017, 2008.

Dennis, R. L., Mathur, R., Pleim, J. E., and Walker, J. T.: Fate of ammonia emissions at the local to regional scale as simulated by the Community Multiscale Air Quality model, Atmos. Pollut. Res., https://doi.org/10.5094/apr.2010.027, 2010.

Dentener, F. J. and Crutzen, P. J.: A three-dimensional model of the global ammonia cycle, J. Atmos. Chem., 19, 331–369, https://doi.org/10.1007/BF00694492, 1994.

Díaz-Uriarte, R. and Alvarez de Andrés, S.: Gene selection and classification of microarray data using random forest, BMC Bioinformatics, 7, 3, https://doi.org/10.1186/1471-2105-7-3, 2006.

van Dobben, H. F. and de Vries, W.: The contribution of nitrogen deposition to the eutrophication signal in understorey plant communities of European forests, Ecol. Evol., 7, 214–227, https://doi.org/10.1002/ECE3.2485, 2017.

R

Dollmann, S., Vermeulen, L., and Husman, A. M. de R.: Untangling the Governance of Public Health Aspects of Manure in The Netherlands, Int. J. Environ. Res. Public Health, 18, https://doi.org/10.3390/IJERPH182312472, 2021.

Dominguez-Rodriguez, A., Baez-Ferrer, N., Rodríguez, S., Avanzas, P., Abreu-Gonzalez, P., Terradellas, E., Cuevas, E., Basart, S., and Werner, E.: Saharan Dust Events in the Dust Belt -Canary Islands- and the Observed Association with in-Hospital Mortality of Patients with Heart Failure, J. Clin. Med. 2020, Vol. 9, Page 376, 9, 376, https://doi.org/10.3390/JCM9020376, 2020.

Dore, A. J., Kryza, M., Hall, J. R., Hallsworth, S., Keller, V. J. D., Vieno, M., and Sutton, M. A.: The influence of model grid resolution on estimation of national scale nitrogen deposition and exceedance of critical loads, Biogeosciences, 9, 1597–1609, https://doi.org/10.5194/bg-9-1597-2012, 2012.

Dragosits, U., Theobald, M. R., Place, C. J., Lord, E., Webb, J., Hill, J., ApSimon, H. M., and Sutton, M. A.: Ammonia emission, deposition and impact assessment at the field scale: a case study of sub-grid spatial variability, Environ. Pollut., 117, 147–158, https://doi.org/10.1016/S0269-7491(01)00147-6, 2002.

Drusch, M., Del Bello, U., Carlier, S., Colin, O., Fernandez, V., Gascon, F., Hoersch, B., Isola, C., Laberinti, P., Martimort, P., Meygret, A., Spoto, F., Sy, O., Marchese, F., and Bargellini, P.: Sentinel-2: ESA's Optical High-Resolution Mission for GMES Operational Services, Remote Sens. Environ., 120, 25–36, https://doi.org/10.1016/j.rse.2011.11.026, 2012.

Dubovyk, O., Menz, G., Lee, A., Schellberg, J., Thonfeld, F., and Khamzina, A.: SPOT-Based Sub-Field Level Monitoring of Vegetation Cover Dynamics: A Case of Irrigated Croplands, Remote Sens., 7, 6763–6783, https://doi.org/10.3390/rs70606763, 2015.

Duyzer, J., Nijenhuis, B., and Weststrate, H.: Monitoring and Modelling of Ammonia Concentrations and Deposition in Agricultural Areas of The Netherlands, Water, Air Soil Pollut. Focus, 1, 131–144, https://doi.org/10.1023/A:1013186517683, 2001.

Global Air Pollutant Emissions: https://edgar.jrc.ec.europa.eu/index.php/dataset_ap61, last access: 23 June 2023.

EEA: European Union emission inventory report 1990 –2015 under the UNECE Convention on Long-range Transboundary Air Pollution, EEA Technical report, https://doi.org/10.2800/478321, 2017.

Eichhorn, M., Scheftelowitz, M., Reichmuth, M., Lorenz, C., Louca, K., Schiffler, A., Keuneke, R., Bauschmann, M., Ponitka, J., Manske, D., and Thrän, D.: Spatial Distribution of Wind Turbines, Photovoltaic Field Systems, Bioenergy, and River Hydro Power Plants in Germany, Data, 4, https://doi.org/10.3390/data4010029, 2019.

Elzing, A. and Monteny, G. J.: Modeling and experimental determination of ammonia emissions rates from a scale model dairy-cow house, Trans. Am. Soc. Agric. Eng., 1997.

Emmons, L. K., Walters, S., Hess, P. G., Lamarque, J.-F., Pfister, G. G., Fillmore, D., Granier, C., Guenther, A., Kinnison, D., Laepple, T., Orlando, J., Tie, X., Tyndall, G., Wiedinmyer, C., Baughcum, S. L., and Kloster, S.: Description and evaluation of the Model for Ozone and Related chemical Tracers, version 4 (MOZART-4), Geosci. Model Dev., 3, 43–67, https://doi.org/10.5194/gmd-3-43-2010, 2010.

Erisman, J. W.: How ammonia feeds and pollutes the world, Science (80-.)., 374, 685–686, https://doi.org/10.1126/SCIENCE.ABM3492, 2021.

Erisman, J. W. and Draaijers, G. P. J.: Atmospheric deposition in relation to acidification and eutrophication, Elsiever, Netherlands, 1995.

Erisman, J. W., Bleeker, A., and Jaarsveld, H. Van: Atmospheric deposition of ammonia to semi-natural vegetation in the Netherlands—methods for mapping and evaluation, Atmos. Environ., 32, 481–489, https://doi.org/10.1016/S1352-2310(97)00276-8, 1998.

Erisman, J. W., Hensen, A., Mosquera, J., Sutton, M., and Fowler, D.: Deposition monitoring networks: what monitoring is required to give reasonable estimates of ammonia/ammonium?, Environ. Pollut., 135, 419–431, https://doi.org/10.1016/j.envpol.2004.11.015, 2005.

Erisman, J. W., Bleeker, A., Galloway, J., and Sutton, M. S.: Reduced nitrogen in ecology and the environment, https://doi.org/10.1016/j.envpol.2007.06.033, 2007.

Erisman, J. W., Sutton, M. A., Galloway, J., Klimont, Z., and Winiwarter, W.: How a century of ammonia synthesis changed the world, Nat. Geosci., https://doi.org/10.1038/ngeo325, 2008.

Erisman, J. W., Galloway, J., Seitzinger, S., Bleeker, A., and Butterbach-Bahl, K.: Reactive nitrogen in the environment and its effect on climate change, Curr. Opin. Environ. Sustain., 3, 281–290, https://doi.org/10.1016/j.cosust.2011.08.012, 2011.

European Environment Agency: Air quality in Europe : 2019 report, Publications Office, https://doi.org/doi/10.2800/822355, 2019a.

European Environment Agency: EMEP/EEA air pollutant emission inventory guidebook 2019, 2019b.

European Environment Agency: NEC Directive reporting status 2019, 2019c.

Evangeliou, N., Balkanski, Y., Eckhardt, S., Cozic, A., Van Damme, M., Coheur, P.-F., Clarisse, L., Shephard, M. W., Cady-Pereira, K. E., and Hauglustaine, D.: 10-year satellite-constrained fluxes of ammonia improve performance of chemistry transport models, Atmos. Chem. Phys., 21, 4431–4451, https://doi.org/10.5194/acp-21-4431-2021, 2021.

Famulari, D., Fowler, D., Nemitz, E., Hargreaves, K. J., Storeton-West, R. L., Rutherford, G., Tang, Y. S., Sutton, M. A., and Weston, K. J.: Development of a low-cost system for measuring conditional time-averaged gradients of SO2 and NH3., Environ. Monit. Assess., 161, 11–27, https://doi.org/10.1007/s10661-008-0723-6, 2010.

Fangmeier, A., Hadwiger-Fangmeier, A., Van der Eerden, L., and Jäger, H. J.: Effects of atmospheric ammonia on vegetation-A review, Environ. Pollut., https://doi.org/10.1016/0269-7491(94)90008-6, 1994.

Ferm, M.: Method for determination of atmospheric ammonia, Atmos. Environ., 13, 1385–1393, https://doi.org/10.1016/0004-6981(79)90107-0, 1979.

Fink, M., Feller, C., Scharpf, H.-C., Weier, U., Maync, A., Ziegler, J., Paschold, P.-J., and Strohmeyer, K.: Nitrogen, phosphorus, potassium and magnesium contents of field vegetables - Recent data for fertiliser recommendations and nutrient balances, J. Plant Nutr. Soil Sci., 162, 71–73, https://doi.org/10.1002/(SICI)1522-2624(199901)162:1<71::AID-JPLN71>3.0.CO;2-0, 1999.

R

Flechard, C. R., Spirig, C., Neftel, A., and Ammann, C.: The annual ammonia budget of fertilised cut grassland – Part 2: Seasonal variations and compensation point modeling, Biogeosciences, 7, 537–556, https://doi.org/10.5194/bg-7-537-2010, 2010.

Flechard, C. R., Nemitz, E., Smith, R. I., Fowler, D., Vermeulen, A. T., Bleeker, A., Erisman, J. W., Simpson, D., Zhang, L., Tang, Y. S., and Sutton, M. A.: Dry deposition of reactive nitrogen to European ecosystems: a comparison of inferential models across the NitroEurope network, Atmos. Chem. Phys., 11, 2703–2728, https://doi.org/10.5194/acp-11-2703-2011, 2011.

Flechard, C. R., Massad, R.-S., Loubet, B., Personne, E., Simpson, D., Bash, J. O., Cooter, E. J., Nemitz, E., and Sutton, M. A.: Advances in understanding, models and parameterizations of biosphere-atmosphere ammonia exchange, Biogeosciences, 10, 5183–5225, https://doi.org/10.5194/bg-10-5183-2013, 2013.

Foody, G. M., Pal, M., Rocchini, D., Garzon-Lopez, C. X., and Bastin, L.: The Sensitivity of Mapping Methods to Reference Data Quality: Training Supervised Image Classifications with Imperfect Reference Data, ISPRS Int. J. Geo-Information, 5, https://doi.org/10.3390/ijgi5110199, 2016.

Forsius, M., Posch, M., Holmberg, M., Vuorenmaa, J., Kleemola, S., Augustaitis, A., Beudert, B., Bochenek, W., Clarke, N., de Wit, H. A., Dirnböck, T., Frey, J., Grandin, U., Hakola, H., Kobler, J., Krám, P., Lindroos, A. J., Löfgren, S., Pecka, T., Rönnback, P., Skotak, K., Szpikowski, J., Ukonmaanaho, L., Valinia, S., and Váňa, M.: Assessing critical load exceedances and ecosystem impacts of anthropogenic nitrogen and sulphur deposition at unmanaged forested catchments in Europe, Sci. Total Environ., 753, 141791, https://doi.org/10.1016/J.SCITOTENV.2020.141791, 2021.

Fortems-Cheiney, A., Dufour, G., Hamaoui-Laguel, L., Foret, G., Siour, G., Van Damme, M., Meleux, F., Coheur, P.-F., Clerbaux, C., Clarisse, L., Favez, O., Wallasch, M., and Beekmann, M.: Unaccounted variability in NH3 agricultural sources detected by IASI contributing to European spring haze episode, Geophys. Res. Lett., 43, 5475–5482, https://doi.org/10.1002/2016GL069361, 2016.

Fowler, D.: Wet and Dry Deposition of Sulphur and Nitrogen Compounds from the Atmosphere BT - Effects of Acid Precipitation on Terrestrial Ecosystems, edited by: Hutchinson, T. C. and Havas, M., Springer US, Boston, MA, 9–27, https://doi.org/10.1007/978-1-4613-3033-2_3, 1980.

Fowler, D., Pilegaard, K., Sutton, M. A., Ambus, P., Raivonen, M., Duyzer, J., Simpson, D., Fagerli, H., Fuzzi, S., Schjoerring, J. K., Granier, C., Neftel, A., Isaksen, I. S. A., Laj, P., Maione, M., Monks, P. S., Burkhardt, J., Daemmgen, U., Neirynck, J., Personne, E., Wichink-Kruit, R., Butterbach-Bahl, K., Flechard, C., Tuovinen, J. P., Coyle, M., Gerosa, G., Loubet, B., Altimir, N., Gruenhage, L., Ammann, C., Cieslik, S., Paoletti, E., Mikkelsen, T. N., Ro-Poulsen, H., Cellier, P., Cape, J. N., Horváth, L., Loreto, F., Niinemets, Ü., Palmer, P. I., Rinne, J., Misztal, P., Nemitz, E., Nilsson, D., Pryor, S., Gallagher, M. W., Vesala, T., Skiba, U., Brüggemann, N., Zechmeister-Boltenstern, S., Williams, J., O'Dowd, C., Facchini, M. C., de Leeuw, G., Flossman, A., Chaumerliac, N., and Erisman, J. W.: Atmospheric composition change: Ecosystems-Atmosphere interactions, https://doi.org/10.1016/j.atmosenv.2009.07.068, 2009.

Fowler, D., Coyle, M., Skiba, U., Sutton, M. A., Cape, J. N., Reis, S., Sheppard, L. J., Jenkins, A., Grizzetti, B., Galloway, J. N., Vitousek, P., Leach, A., Bouwman, A. F., Butterbach-Bahl, K., Dentener, F., Stevenson,

D., Amann, M., and Voss, M.: The global nitrogen cycle in the twenty-first century., Philos. Trans. R. Soc. London. Ser. B, Biol. Sci., 368, 20130164, https://doi.org/10.1098/rstb.2013.0164, 2013.

Gac, A., Béline, F., Bioteau, T., and Maguet, K.: A French inventory of gaseous emissions (CH4, N2O, NH3) from livestock manure management using a mass-flow approach, Livest. Sci., https://doi.org/10.1016/j.livsci.2007.09.006, 2007.

Galle, B., Klemedtsson, L., Bergqvist, B., Ferm, M., Kåre Törnqvist, Griffith, D. W. T., Jensen, N.-O., and Hansen, F.: Measurements of ammonia emissions from spreading of manure using gradient FTIR techniques, Atmos. Environ., 34, 4907–4915, https://doi.org/10.1016/S1352-2310(00)00220-X, 2000.

Galloway, J. N.: 10.12 - The Global Nitrogen Cycle, edited by: Holland, H. D. and Turekian, K. K. B. T.-T. on G. (Second E., Pergamon, Oxford, 475–498, https://doi.org/10.1016/B978-0-08-095975-7.00812-3, 2003.

Galloway, J. N. and Cowling, E. B.: Reactive nitrogen and the world: 200 years of change., Ambio, 31, 64–71, https://doi.org/10.1579/0044-7447-31.2.64, 2002.

Galloway, J. N., Aber, J. D., Erisman, J. W., Seitzinger, S. P., Howarth, R. W., Cowling, E. B., and Cosby, B. J.: The Nitrogen Cascade, Bioscience, 53, 341–356, https://doi.org/10.1641/0006-3568(2003)053[0341:TNC]2.0.CO;2, 2003.

Galloway, J. N., Dentener, F. J., Capone, D. G., Boyer, E. W., Howarth, R. W., Seitzinger, S. P., Asner, G. P., Cleveland, C. C., Green, P. A., Holland, E. A., Karl, D. M., Michaels, A. F., Porter, J. H., Townsend, A. R., and Vöosmarty, C. J.: Nitrogen Cycles: Past, Present, and Future, Biogeochemistry, 70, 153–226, https://doi.org/10.1007/s10533-004-0370-0, 2004.

Galloway, J. N., Bleeker, A., and Erisman, J. W.: The Human Creation and Use of Reactive Nitrogen: A Global and Regional Perspective, Annu. Rev. Environ. Resour., 46, 255–288, https://doi.org/10.1146/annurev-environ-012420-045120, 2021.

Ge, X., Schaap, M., Kranenburg, R., Segers, A., Reinds, G. J., Kros, H., and de Vries, W.: Modeling atmospheric ammonia using agricultural emissions with improved spatial variability and temporal dynamics, Atmos. Chem. Phys., 20, 16055–16087, https://doi.org/10.5194/acp-20-16055-2020, 2020.

Ge, X., Schaap, M., Dammers, E., Shephard, M., and de Vries, W.: Impact of interannual weather variation on ammonia emissions and concentrations in Germany, Agric. For. Meteorol., 334, 109432, https://doi.org/10.1016/j.agrformet.2023.109432, 2023a.

Ge, X., Schaap, M., and de Vries, W.: Improving spatial and temporal variation of ammonia emissions for the Netherlands using livestock housing information and a Sentinel-2-derived crop map, Atmos. Environ. X, 17, 100207, https://doi.org/10.1016/j.aeaoa.2023.100207, 2023b.

Geels, C., Andersen, H. V, Skjøth, C. A., Christensen, J. H., Ellermann, T., Løfstrøm, P., Gyldenkærne, S., Brandt, J., Hansen, K. M., Frohn, L. M., and Hertel, O.: Improved modelling of atmospheric ammonia over Denmark using the coupled modelling system DAMOS, Biogeosciences, 9, 2625–2647, https://doi.org/10.5194/bg-9-2625-2012, 2012.

R

Génermont, S. and Cellier, P.: A mechanistic model for estimating ammonia volatilization from slurry applied to bare soil, Agric. For. Meteorol., 88, 145–167, https://doi.org/10.1016/S0168-1923(97)00044-0, 1997.

Genuer, R., Poggi, J.-M., and Tuleau, C.: Random Forests: some methodological insights, 2008.

Gericke, D., Bornemann, L., Kage, H., and Pacholski, A.: Modelling Ammonia Losses After Field Application of Biogas Slurry in Energy Crop Rotations, Water, Air, Soil Pollut., 223, 29–47, https://doi.org/10.1007/s11270-011-0835-4, 2012.

Giannadaki, D., Giannakis, E., Pozzer, A., and Lelieveld, J.: Estimating health and economic benefits of reductions in air pollution from agriculture, Sci. Total Environ., 622–623, 1304–1316, https://doi.org/10.1016/j.scitotenv.2017.12.064, 2018.

Gies, T. J. A., van, O., Smidt, R. A., Naeff, H., and Vos, E.: Geografisch Informatiesysteem Agrarische Bedrijven (GIAB) : gebruikershandleiding 2010, 2015.

Gilliam, F. S., Burns, D. A., Driscoll, C. T., Frey, S. D., Lovett, G. M., and Watmough, S. A.: Decreased atmospheric nitrogen deposition in eastern North America: Predicted responses of forest ecosystems, Environ. Pollut., 244, 560–574, https://doi.org/10.1016/J.ENVPOL.2018.09.135, 2019.

Giordano, S., Bailly, S., Landrieu, L., and Chehata, N.: Temporal Structured Classification of Sentinel 1 and 2 Time Series for Crop Type Mapping, 2018.

Gislason, P. O., Benediktsson, J. A., and Sveinsson, J. R.: Random Forests for land cover classification, Pattern Recognit. Lett., 27, 294–300, https://doi.org/10.1016/j.patrec.2005.08.011, 2006.

Gitelson, A. A., Kaufman, Y. J., and Merzlyak, M. N.: Use of a green channel in remote sensing of global vegetation from EOS-MODIS, Remote Sens. Environ., 58, 289–298, https://doi.org/10.1016/S0034-4257(96)00072-7, 1996.

Gitelson, A. A., Merzlyak, M. N., and Chivkunova, O. B.: Optical Properties and Nondestructive Estimation of Anthocyanin Content in Plant Leaves, Photochem. Photobiol., 74, 38–45, https://doi.org/10.1562/0031-8655(2001)0740038OPANEO2.0.CO2, 2001.

Gobron, N., Pinty, B., Verstraete, M. M., and Widlowski, J.-L.: Advanced vegetation indices optimized for up-coming sensors: Design, performance, and applications, IEEE Trans. Geosci. Remote Sens., 38, 2489–2505, https://doi.org/10.1109/36.885197, 2000.

Gocht, A. and Britz, W.: EU-wide farm type supply models in CAPRI--How to consistently disaggregate sector models into farm type models, J. Policy Model., 33, 146–167, 2011.

Goldstein, B. A., Hubbard, A. E., Cutler, A., and Barcellos, L. F.: An application of Random Forests to a genome-wide association dataset: Methodological considerations & new findings, BMC Genet., 11, 49, https://doi.org/10.1186/1471-2156-11-49, 2010.

Goot, E. van der: Spatial interpolation of daily meteorological data for the Crop Growth Monitoring System (CGMS), in: Proceedings of seminar on data spatial distribution in meteorology and climatology, 28 September - 3 October 1997, Volterra, Italy, 141–153, 1998.

van der Graaf, S. C., Dammers, E., Schaap, M., Willem Erisman, J., Erisman, J. W., Willem Erisman, J., and Erisman, J. W.: Technical note: How are NH3 dry deposition estimates affected by combining

the LOTOS-EUROS model with IASI-NH3 satellite observations?, Atmos. Chem. Phys., 18, 13173–13196, https://doi.org/10.5194/acp-18-13173-2018, 2018.

van der Graaf, S. C., Kranenburg, R., Segers, A. J., Schaap, M., and Erisman, J. W.: Satellite-derived leaf area index and roughness length information for surface–atmosphere exchange modelling: a case study for reactive nitrogen deposition in north-western Europe using LOTOS-EUROS v2.0 , Geosci. Model Dev., 13, 2451–2474, https://doi.org/10.5194/gmd-13-2451-2020, 2020.

van der Graaf, S., Dammers, E., Segers, A., Kranenburg, R., Schaap, M., Shephard, M. W., and Erisman, J. W.: Data assimilation of CrIS NH3 satellite observations for improving spatiotemporal NH3 distributions in LOTOS-EUROS, Atmos. Chem. Phys., 22, 951–972, https://doi.org/10.5194/acp-22-951-2022, 2022.

Griffin, T. S., Johnson, B. S., Ritchie, J. T., Project, I., Science, U. of H. (Honolulu). D. of A. and S., and Science, M. S. U. D. of C. and S.: A Simulation Model for Potato Growth and Development: SUBSTOR-potato Version 2.0, Michigan State University, Department of Crop and Soil Sciences, 1993.

Griffiths, P., Nendel, C., and Hostert, P.: Intra-annual reflectance composites from Sentinel-2 and Landsat for national-scale crop and land cover mapping, Remote Sens. Environ., 220, 135–151, https://doi.org/10.1016/j.rse.2018.10.031, 2019.

Guo, Y., Hastie, T., and Tibshirani, R.: Regularized linear discriminant analysis and its application in microarrays, Biostatistics, 8, 86–100, https://doi.org/10.1093/biostatistics/kxj035, 2007.

Gyldenkærne, S., Skjøth, C. A., Hertel, O., and Ellermann, T.: A dynamical ammonia emission parameterization for use in air pollution models, J. Geophys. Res. Atmos., 110, 1–14, https://doi.org/10.1029/2004JD005459, 2005.

Haenel, H.-D., Rösemann, C., Dämmgen, U., Poddey, E., Freibauer, A., Wulf, S., Eurich-Menden, B., Döhler, H., Schreiner, C., Bauer, B., and Osterburg, B.: Calculations of gaseous and particulate emissions from German agriculture 1990 - 2012: Report on methods and data (RMD) Submission 2014; Berechnung von gas- und partikelförmigen Emissionen aus der deutschen Landwirtschaft 1990 - 2012: Report zu Methoden u, Johann Heinrich von Thünen-Institut, Braunschweig, https://doi.org/10.3220/REP_17_2014, 2014.

Haenel, H.-D., Rösemann, C., Dämmgen, U., Döring, U., Wulf, S., Eurich-Menden, B., Freibauer, A., Döhler, H., Schreiner, C., Osterburg, B., and Fuß, R.: Calculations of gaseous and particulate emissions from German agriculture 1990 - 2018: Input data and emission results, https://doi.org/10.3220/DATA20200312140923, 2020.

Hafner, S. D., Pacholski, A., Bittman, S., Burchill, W., Bussink, W., Chantigny, M., Carozzi, M., Génermont, S., Häni, C., Hansen, M. N., Huijsmans, J., Hunt, D., Kupper, T., Lanigan, G., Loubet, B., Misselbrook, T., Meisinger, J. J., Neftel, A., Nyord, T., Pedersen, S. V., Sintermann, J., Thompson, R. B., Vermeulen, B., Vestergaard, A. V., Voylokov, P., Williams, J. R., and Sommer, S. G.: The ALFAM2 database on ammonia emission from field-applied manure: Description and illustrative analysis, Agric. For. Meteorol., 258, 66–79, https://doi.org/10.1016/J.AGRFORMET.2017.11.027, 2018.

Hafner, S. D., Pacholski, A., Bittman, S., Carozzi, M., Chantigny, M., Génermont, S., Häni, C., Hansen, M. N., Huijsmans, J., Kupper, T., Misselbrook, T., Neftel, A., Nyord, T., and Sommer, S. G.: A flexible

R

semi-empirical model for estimating ammonia volatilization from field-applied slurry, Atmos. Environ., 199, 474–484, https://doi.org/10.1016/j.atmosenv.2018.11.034, 2019.

Hamaoui-Laguel, L., Meleux, F., Beekmann, M., Bessagnet, B., Génermont, S. S., and Cellier, P.: Modelling agricultural ammonia emissions : impact on particulate matter formation, in: Conference "'Nitrogen & global change : key findings - future challenges,"' 2011.

Hamaoui-Laguel, L., Meleux, F., Beekmann, M., Bessagnet, B., Génermont, S., Cellier, P., and Létinois, L.: Improving ammonia emissions in air quality modelling for France, Atmos. Environ., 92, 584–595, https://doi.org/10.1016/j.atmosenv.2012.08.002, 2014.

Hanna, S. and Chang, J.: Acceptance criteria for urban dispersion model evaluation, Meteorol. Atmos. Phys., 116, 133–146, https://doi.org/10.1007/S00703-011-0177-1/TABLES/6, 2012.

Hansen-Kuhn, K., Holden, P., Hudson, U., Jensen, A., and Mathias, E.: Fleischatlas 2014 - Daten und Fakten über Tiere als Nahrungsmittel, Fleischatlas, 2014.

Hao, P., Zhan, Y., Wang, L., Niu, Z., and Shakir, M.: Feature Selection of Time Series MODIS Data for Early Crop Classification Using Random Forest: A Case Study in Kansas, USA, Remote Sens., 7, 5347–5369, https://doi.org/10.3390/rs70505347, 2015.

Hardisky, M. A., Klemas, V., and Smart, M.: The influence of soil salinity, growth form, and leaf moisture on the spectral radiance of, Spartina alterniflora, 49, 77–83, 1983.

Hellsten, S., Dragosits, U., Place, C. J., Vieno, M., Dore, A. J., Misselbrook, T. H., Tang, Y. S., and Sutton, M. A.: Modelling the spatial distribution of ammonia emissions in the UK, Environ. Pollut., 154, 370–379, https://doi.org/10.1016/J.ENVPOL.2008.02.017, 2008.

Hempel, S., Saha, C. K., Fiedler, M., Berg, W., Hansen, C., Amon, B., and Amon, T.: Non-linear temperature dependency of ammonia and methane emissions from a naturally ventilated dairy barn, Biosyst. Eng., 145, 10–21, https://doi.org/10.1016/j.biosystemseng.2016.02.006, 2016.

Hendriks, C., Kranenburg, R., Kuenen, J., van Gijlswijk, R., Wichink Kruit, R., Segers, A., Denier van der Gon, H., and Schaap, M.: The origin of ambient particulate matter concentrations in the Netherlands, Atmos. Environ., 69, 289–303, https://doi.org/10.1016/J.ATMOSENV.2012.12.017, 2013.

Hendriks, C., Kranenburg, R., Kuenen, J. J. P., Van den Bril, B., Verguts, V., and Schaap, M.: Ammonia emission time profiles based on manure transport data improve ammonia modelling across north western Europe, Atmos. Environ., 131, 83–96, https://doi.org/10.1016/j.atmosenv.2016.01.043, 2016.

Hertel, O., Ellermann, T., Palmgren, F., Berkowicz, R., Løfstrøm, P., Frohn, L. M., Geels, C., Skjøth, C. A., Brandt, J., Christensen, J., Kemp, K., and Ketzel, M.: Integrated air-quality monitoring - Combined use of measurements and models in monitoring programmes, Environ. Chem., 4, 65–74, https://doi.org/10.1071/EN06077, 2007.

Hettelingh, J., Posch, M., and Slootweg, J.: European critical loads: database, biodiversity and ecosystems at risk : CCE Final Report 2017, , https://doi.org/10.21945/RIVM-2017-0155, 2017.

Hicks, B. B.: A climatology of wet deposition scavenging ratios for the United States, Atmos. Environ., 39, 1585–1596, https://doi.org/10.1016/j.atmosenv.2004.10.039, 2005.

Hristov, A. N., Hanigan, M., Cole, A., Todd, R., McAllister, T. A., Ndegwa, P. M., and Rotz, A.: Review: Ammonia emissions from dairy farms and beef feedlots, Can. J. Anim. Sci., 91, 1–35, https://doi.org/10.4141/CJAS10034, 2011.

Huete, A., Didan, K., Miura, T., Rodriguez, E. P., Gao, X., and Ferreira, L. G.: Overview of the radiometric and biophysical performance of the MODIS vegetation indices, Remote Sens. Environ., 83, 195–213, https://doi.org/10.1016/S0034-4257(02)00096-2, 2002.

Huete, A. R.: A soil-adjusted vegetation index (SAVI), Remote Sens. Environ., 25, 295–309, https://doi.org/10.1016/0034-4257(88)90106-X, 1988.

Huijnen, V., Williams, J., van Weele, M., van Noije, T., Krol, M., Dentener, F., Segers, A., Houweling, S., Peters, W., de Laat, J., Boersma, F., Bergamaschi, P., van Velthoven, P., Le Sager, P., Eskes, H., Alkemade, F., Scheele, R., Nédélec, P., and Pätz, H.-W.: The global chemistry transport model TM5: description and evaluation of the tropospheric chemistry version 3.0, Geosci. Model Dev., 3, 445–473, https://doi.org/10.5194/gmd-3-445-2010, 2010.

Huijsmans, J., Holterman, H., Vermeulen, G., Stolk, A., and Pul, W. V: Simulating emission of ammonia after liquid manure applicaton on arable land : Preliminary performance assessment of the Volt'air model for manure application conditions in the Netherlands, 2014.

Huijsmans, J. F. M.: Manure application and ammonia volatilization, 160 pp., 2003.

Huijsmans, J. F. M. and Hol, J. M. G.: Ammoniakemissie bij het in een tweede werkgang onderwerken van dunne varkensmest op bouwland, IMAG, 1995.

Huijsmans, J. F. M., Hol, J. M. G., and Hendriks, M. M. W. B.: Effect of application technique, manure characteristics, weather and field conditions on ammonia volatilization from manure applied to grassland, Netherlands J. Agric. Sci., 49, 323–342, https://doi.org/10.1016/S1573-5214(01)80021-X, 2001.

Huijsmans, J. F. M., Vermeulen, G. D., Hol, J. M. G., and Goedhart, P. W.: A model for estimating seasonal trends of ammonia emission from cattle manure applied to grassland in the Netherlands, Atmos. Environ., 173, 231–238, https://doi.org/10.1016/J.ATMOSENV.2017.10.050, 2018.

Hussein, T., Smolik, J., Kerminen, V.-M., and Kulmala, M.: Modeling Dry Deposition of Aerosol Particles onto Rough Surfaces, Aerosol Sci. Technol., 46, 44–59, https://doi.org/10.1080/02786826.2011.605814, 2012.

Hutchings, N. J., Sommer, S. G., Andersen, J. M., and Asman, W. A. H.: A detailed ammonia emission inventory for Denmark, Atmos. Environ., 35, 1959–1968, https://doi.org/10.1016/S1352-2310(00)00542-2, 2001.

Hutchings, N. J., Reinds, G. J., Leip, A., Wattenbach, M., Bienkowski, J. F., Dalgaard, T., Dragosits, U., Drouet, J. L., Durand, P., Maury, O., and De Vries, W.: A model for simulating the timelines of field operations at a European scale for use in complex dynamic models, Biogeosciences, 9, 4487–4496, https://doi.org/10.5194/bg-9-4487-2012, 2012.

Hyde, B. P., Carton, O. T., O'Toole, P., and Misselbrook, T. H.: A new inventory of ammonia emissions from Irish agriculture, Atmos. Environ., https://doi.org/10.1016/S1352-2310(02)00692-1, 2003.

R

Immitzer, M., Vuolo, F., and Atzberger, C.: First Experience with Sentinel-2 Data for Crop and Tree Species Classifications in Central Europe, Remote Sens., 8, https://doi.org/10.3390/rs8030166, 2016.

Inglada, J., Arias, M., Tardy, B., Hagolle, O., Valero, S., Morin, D., Dedieu, G., Sepulcre, G., Bontemps, S., Defourny, P., and Koetz, B.: Assessment of an Operational System for Crop Type Map Production Using High Temporal and Spatial Resolution Satellite Optical Imagery, Remote Sens., 7, 12356–12379, https://doi.org/10.3390/rs70912356, 2015.

Janitza, S. and Hornung, R.: On the overestimation of random forest's out-of-bag error, PLoS One, 13, e0201904, 2018.

Jiang, J., Stevenson, D. S., Uwizeye, A., Tempio, G., and Sutton, M. A.: A climate-dependent global model of ammonia emissions from chicken farming, Biogeosciences, 18, 135–158, https://doi.org/10.5194/bg-18-135-2021, 2021.

Jin, J., Segers, A., Lin, H. X., Henzing, B., Wang, X., Heemink, A., and Liao, H.: Position correction in dust storm forecasting using LOTOS-EUROS v2.1: Grid-distorted data assimilation v1.0, Geosci. Model Dev., 14, 5607–5622, https://doi.org/10.5194/GMD-14-5607-2021, 2021.

Jones, J. W., Hoogenboom, G., Porter, C. H., Boote, K. J., Batchelor, W. D., Hunt, L. A., Wilkens, P. W., Singh, U., Gijsman, A. J., and Ritchie, J. T.: The DSSAT cropping system model, Eur. J. Agron., 18, 235–265, https://doi.org/10.1016/S1161-0301(02)00107-7, 2003.

Jordan, C. F.: Derivation of Leaf-Area Index from Quality of Light on the Forest Floor, Ecology, 50, 663–666, https://doi.org/10.2307/1936256, 1969.

Joubin, M. L.: Animal slurry acidification: effects of slurry characteristics, use of different acids, slurry pH buffering : Student work, 2018.

Kaufman, Y. J. and Tanre, D.: Atmospherically resistant vegetation index (ARVI) for EOS-MODIS, IEEE Trans. Geosci. Remote Sens., 30, 261–270, https://doi.org/10.1109/36.134076, 1992.

Kavzoglu, T.: Increasing the accuracy of neural network classification using refined training data, Environ. Model. Softw., 24, 850–858, https://doi.org/10.1016/j.envsoft.2008.11.012, 2009.

Khaniabadi, Y. O., Goudarzi, G., Daryanoosh, S. M., Borgini, A., Tittarelli, A., and De Marco, A.: Exposure to PM10, NO2, and O3 and impacts on human health, Environ. Sci. Pollut. Res., 24, 2781–2789, https://doi.org/10.1007/s11356-016-8038-6, 2017.

Kim, K.-H., Kabir, E., and Kabir, S.: A review on the human health impact of airborne particulate matter, Environ. Int., 74, 136–143, https://doi.org/https://doi.org/10.1016/j.envint.2014.10.005, 2015.

Klimont, Z. and Brink, C.: Modeling of Emissions of Air Pollutants and Greenhouse Gases from Agricultural Sources in Europe, IR-04-048, IIASA, Laxenburg, Austria, 2004.

Kobayashi, N., Tani, H., Wang, X., and Sonobe, R.: Crop classification using spectral indices derived from Sentinel-2A imagery, J. Inf. Telecommun., https://doi.org/10.1080/24751839.2019.1694765, 2020.

Kranenburg, R., Quade, M., Dammers, E., Hendriks, C., Van den Bril, B., Verguts, V., and Schaap, M.: Improving the timing of manure application emissions for modelling ammonia, 2016.

Kros, H., van Os, J., Voogd, J. C., Groenendijk, P., van Bruggen, C., te Molder, R., and Ros, G.: Ruimtelijke allocatie van mesttoediening en ammoniakemissie: beschrijving mestverdelingsmodule

INITIATOR versie 5, Wageningen Environmental Research, Netherlands, https://doi.org/10.18174/474513, 2019.

Kros, J., Heuvelink, G. B. M., Reinds, G. J., Lesschen, J. P., Ioannidi, V., and De Vries, W.: Uncertainties in model predictions of nitrogen fluxes from agro-ecosystems in Europe, Biogeosciences, 9, 4573–4588, https://doi.org/10.5194/bg-9-4573-2012, 2012.

Kros, J., Hutchings, N. J., Kristensen, I. T. I. S., Kristensen, I. T. I. S., Børgesen, C. D., Voogd, J. C., Dalgaard, T., and de Vries, W.: A comparison of disaggregated nitrogen budgets for Danish agriculture using Europe-wide and national approaches, Sci. Total Environ., 643, 890–901, https://doi.org/10.1016/j.scitotenv.2018.06.267, 2018.

Krupa, S. V.: Effects of atmospheric ammonia (NH3) on terrestrial vegetation: A review, https://doi.org/10.1016/S0269-7491(02)00434-7, 2003.

Kryza, M., Dore, A. J., Błaś, M., and Sobik, M.: Modelling deposition and air concentration of reduced nitrogen in Poland and sensitivity to variability in annual meteorology, J. Environ. Manage., 92, 1225–1236, https://doi.org/10.1016/j.jenvman.2010.12.008, 2011.

Kuenen, J., Denier van der Gon, H., Visschedijk, A., van der Brugh, H., and Gijlswijk, R.: MACC European emission inventory for the years 2003–2007, TNO-report, 49, 2011.

Kuenen, J. J. P., Visschedijk, A. J. H., Jozwicka, M., and Denier van der Gon, H. A. C.: TNO-MACC_II emission inventory; a multi-year (2003–2009) consistent high-resolution European emission inventory for air quality modelling, Atmos. Chem. Phys., 14, 10963–10976, https://doi.org/10.5194/acp-14-10963-2014, 2014a.

Kuenen, J. J. P., Visschedijk, A. J. H., Jozwicka, M., and Denier Van Der Gon, H. A. C.: TNO-MACC-II emission inventory; A multi-year (2003-2009) consistent high-resolution European emission inventory for air quality modelling, Atmos. Chem. Phys., 14, 10963–10976, https://doi.org/10.5194/acp-14-10963-2014, 2014b.

Kuhn, T.: The revision of the German Fertiliser Ordinance in 2017, Food Resour. Econ. Discuss. Pap. 2017, https://doi.org/10.22004/ag.econ.262054, 2017.

Ladha, J. K., Peoples, M. B., Reddy, P. M., Biswas, J. C., Bennett, A., Jat, M. L., and Krupnik, T. J.: Biological nitrogen fixation and prospects for ecological intensification in cereal-based cropping systems, F. Crop. Res., 283, 108541, https://doi.org/10.1016/j.fcr.2022.108541, 2022.

Lan, T., Hu, H., Jiang, C., Yang, G., and Zhao, Z.: A comparative study of decision tree, random forest, and convolutional neural network for spread-F identification, Adv. Sp. Res., 65, 2052–2061, https://doi.org/10.1016/j.asr.2020.01.036, 2020.

Larrinaga, A. R. and Brotons, L.: Greenness Indices from a Low-Cost UAV Imagery as Tools for Monitoring Post-Fire Forest Recovery, Drones, 3, https://doi.org/10.3390/drones3010006, 2019.

Leen, J. B., Yu, X. Y., Gupta, M., Baer, D. S., Hubbe, J. M., Kluzek, C. D., Tomlinson, J. M., and Hubbell, M. R.: Fast in situ airborne measurement of ammonia using a mid-infrared off-axis ICOS spectrometer, Environ. Sci. Technol., https://doi.org/10.1021/es401134u, 2013.

de Leeuw, F. A. A. M.: A set of emission indicators for long-range transboundary air pollution, Environ. Sci. Policy, 5, 135–145, https://doi.org/10.1016/S1462-9011(01)00042-9, 2002.

R

Leip, A., Billen, G., Garnier, J., Grizzetti, B., Lassaletta, L., Reis, S., Simpson, D., Sutton, M. A., De Vries, W., Weiss, F., and Westhoek, H.: Impacts of European livestock production: nitrogen, sulphur, phosphorus and greenhouse gas emissions, land-use, water eutrophication and biodiversity, Environ. Res. Lett., 10, 115004, https://doi.org/10.1088/1748-9326/10/11/115004, 2015.

Lelieveld, J., Evans, J. S., Fnais, M., Giannadaki, D., and Pozzer, A.: The contribution of outdoor air pollution sources to premature mortality on a global scale, Nature, 525, 367–371, https://doi.org/10.1038/nature15371, 2015.

Li, C., Salas, W., Zhang, R., Krauter, C., Rotz, A., and Mitloehner, F.: Manure-DNDC: A biogeochemical process model for quantifying greenhouse gas and ammonia emissions from livestock manure systems, Nutr. Cycl. Agroecosystems, 93, 163–200, https://doi.org/10.1007/S10705-012-9507-Z/TABLES/10, 2012.

Li, J., Yang, X., Maffei, C., Tooth, S., and Yao, G.: Applying Independent Component Analysis on Sentinel-2 Imagery to Characterize Geomorphological Responses to an Extreme Flood Event near the Non-Vegetated Río Colorado Terminus, Salar de Uyuni, Bolivia, Remote Sens., 10, https://doi.org/10.3390/rs10050725, 2018.

Li, Y., Schwandner, F. M., Sewell, H. J., Zivkovich, A., Tigges, M., Raja, S., Holcomb, S., Molenar, J. V, Sherman, L., Archuleta, C., Lee, T., and Collett, J. L.: Observations of ammonia, nitric acid, and fine particles in a rural gas production region, Atmos. Environ., 83, 80–89, https://doi.org/10.1016/j.atmosenv.2013.10.007, 2014.

Li, Y., Thompson, T. M., Van Damme, M., Chen, X., Benedict, K. B., Shao, Y., Day, D., Boris, A., Sullivan, A. P., Ham, J., Whitburn, S., Clarisse, L., Coheur, P. F., and Collett, J. L.: Temporal and spatial variability of ammonia in urban and agricultural regions of northern Colorado, United States, Atmos. Chem. Phys., https://doi.org/10.5194/acp-17-6197-2017, 2017.

Lieth, H.: Purposes of a Phenology Book BT - Phenology and Seasonality Modeling, edited by: Lieth, H., Springer Berlin Heidelberg, Berlin, Heidelberg, 3–19, https://doi.org/10.1007/978-3-642-51863-8_1, 1974.

Liu, L., Zhang, X., Xu, W., Liu, X., Li, Y., Lu, X., Zhang, Y., and Zhang, W.: Temporal characteristics of atmospheric ammonia and nitrogen dioxide over China based on emission data, satellite observations and atmospheric transport modeling since 1980, Atmos. Chem. Phys., 17, 9365–9378, https://doi.org/10.5194/acp-17-9365-2017, 2017.

Liu, P., Ding, J., Liu, L., Xu, W., and Liu, X.: Estimation of surface ammonia concentrations and emissions in China from the polar-orbiting Infrared Atmospheric Sounding Interferometer and the FY-4A Geostationary Interferometric Infrared Sounder, Atmos. Chem. Phys., 22, 9099–9110, https://doi.org/10.5194/acp-22-9099-2022, 2022.

Lolkema, D. E., Noordijk, H., Stolk, A. P., Hoogerbrugge, R., Van Zanten, M. C., and Van Pul, W. A. J.: The Measuring Ammonia in Nature (MAN) network in the Netherlands, Biogeosciences, https://doi.org/10.5194/bg-12-5133-2015, 2015.

Lonsdale, C. R., Hegarty, J. D., Cady-Pereira, K. E., Alvarado, M. J., Henze, D. K., Turner, M. D., Capps, S. L., Nowak, J. B., Neuman, J. A., Middlebrook, A. M., Bahreini, R., Murphy, J. G., Markovic, M. Z., VandenBoer, T. C., Russell, L. M., and Scarino, A. J.: Modeling the diurnal variability of agricultural

ammonia in Bakersfield, California, during the CalNex campaign, Atmos. Chem. Phys., 17, 2721–2739, https://doi.org/10.5194/acp-17-2721-2017, 2017.

Loubet, B., Asman, W. A. H., Theobald, M. R., Hertel, O., Tang, Y. S., Robin, P., Hassouna, M., Dämmgen, U., Genermont, S., Cellier, P., and Sutton, M. A.: Ammonia Deposition Near Hot Spots: Processes, Models and Monitoring Methods BT - Atmospheric Ammonia: Detecting emission changes and environmental impacts, edited by: Sutton, M. A., Reis, S., and Baker, S. M. H., Springer Netherlands, Dordrecht, 205–267, https://doi.org/10.1007/978-1-4020-9121-6_15, 2009.

Louis, J., Charantonis, A., Berthelot, B., and Lacoste-Francis, H.: Cloud Detection for Sentinel-2, Living planet symposium, in: EUROPEAN SPACE AGENCY -PUBLICATIONS- ESA SP, Living planet symposium, 499, 2010.

Louis, J., Debaecker, V., Pflug, B., Main-Knorn, M., Bieniarz, J., Mueller-Wilm, U., Cadau, E., and Gascon, F.: SENTINEL-2 SEN2COR: L2A Processor for Users, in: Proceedings Living Planet Symposium 2016, 1–8, 2016.

Lovarelli, D., Conti, C., Finzi, A., Bacenetti, J., and Guarino, M.: Describing the trend of ammonia, particulate matter and nitrogen oxides: The role of livestock activities in northern Italy during Covid-19 quarantine., Environ. Res., 191, 110048, https://doi.org/10.1016/j.envres.2020.110048, 2020.

Luo, Z., Zhang, Y., Chen, W., Van Damme, M., Coheur, P.-F., and Clarisse, L.: Estimating global ammonia NH3 emissions based on IASI observations from 2008 to 2018, Atmos. Chem. Phys., 22, 10375–10388, https://doi.org/10.5194/acp-22-10375-2022, 2022.

Mack, B., Leinenkugel, P., Kuenzer, C., and Dech, S.: A semi-automated approach for the generation of a new land use and land cover product for Germany based on Landsat time-series and Lucas in-situ data, Remote Sens. Lett., 8, 244–253, https://doi.org/10.1080/2150704X.2016.1249299, 2017.

Main-Knorn, M., Pflug, B., Louis, J., Debaecker, V., Müller-Wilm, U., and Gascon, F.: Sen2Cor for Sentinel-2, https://doi.org/10.1117/12.2278218, 2017.

Manders, A. M. M., Schaap, M., and Hoogerbrugge, R.: Testing the capability of the chemistry transport model LOTOS-EUROS to forecast PM10 levels in the Netherlands, Atmos. Environ., 43, 4050–4059, https://doi.org/10.1016/j.atmosenv.2009.05.006, 2009.

Manders, A. M. M., Builtjes, P. J. H., Curier, L., Gon, H. A. C. D. Vander, Hendriks, C., Jonkers, S., Kranenburg, R., Kuenen, J. J. P., Segers, A. J., Timmermans, R. M. A., Visschedijk, A. J. H., Wichink Kruit, R. J., Pul, W. A. J. V., Sauter, F. J., Van Der Swaluw, E., Swart, D. P. J., Douros, J., Eskes, H., Van Meijgaard, E., Van Ulft, B., Van Velthoven, P., Banzhaf, S., Mues, A. C., Stern, R., Fu, G., Lu, S., Heemink, A., Van Velzen, N., and Schaap, M.: Curriculum vitae of the LOTOS-EUROS (v2.0) chemistry transport model, Geosci. Model Dev., https://doi.org/10.5194/gmd-10-4145-2017, 2017.

Mannheim, T., Braschkat, J., and Marschner, H.: Measurement of ammonia emission after liquid manure application: II. Comparison of the wind tunnel and the IHF method under field conditions, Zeitschrift für Pflanzenernährung und Bodenkd., 158, 215–219, https://doi.org/10.1002/jpln.19951580302, 1995.

R

Marais, E. A., Pandey, A. K., Van Damme, M., Clarisse, L., Coheur, P.-F., Shephard, M. W., Cady-Pereira, K. E., Misselbrook, T., Zhu, L., Luo, G., and Yu, F.: UK Ammonia Emissions Estimated With Satellite Observations and GEOS-Chem, J. Geophys. Res. Atmos., 126, e2021JD035237, https://doi.org/10.1029/2021JD035237, 2021.

Marais Sicre, C., Inglada, J., Fieuzal, R., Baup, F., Valero, S., Cros, J., Huc, M., and Demarez, V.: Early Detection of Summer Crops Using High Spatial Resolution Optical Image Time Series, Remote Sens., 8, https://doi.org/10.3390/rs8070591, 2016.

Marécal, V., Peuch, V. H., Andersson, C., Andersson, S., Arteta, J., Beekmann, M., Benedictow, A., Bergström, R., Bessagnet, B., Cansado, A., Chéroux, F., Colette, A., Coman, A., Curier, R. L., Van Der Gon, H. A. C. D., Drouin, A., Elbern, H., Emili, E., Engelen, R. J., Eskes, H. J., Foret, G., Friese, E., Gauss, M., Giannaros, C., Guth, J., Joly, M., Jaumouillé, E., Josse, B., Kadygrov, N., Kaiser, J. W., Krajsek, K., Kuenen, J., Kumar, U., Liora, N., Lopez, E., Malherbe, L., Martinez, I., Melas, D., Meleux, F., Menut, L., Moinat, P., Morales, T., Parmentier, J., Piacentini, A., Plu, M., Poupkou, A., Queguiner, S., Robertson, L., Rouïl, L., Schaap, M., Segers, A., Sofiev, M., Tarasson, L., Thomas, M., Timmermans, R., Valdebenito, Van Velthoven, P., Van Versendaal, R., Vira, J., and Ung, A.: A regional air quality forecasting system over Europe: The MACC-II daily ensemble production, Geosci. Model Dev., 8, 2777–2813, https://doi.org/10.5194/GMD-8-2777-2015, 2015.

Martin, R. S., Ilyinskaya, E., and Oppenheimer, C.: The enigma of reactive nitrogen in volcanic emissions, Geochim. Cosmochim. Acta, 95, 93–105, https://doi.org/10.1016/j.gca.2012.07.027, 2012.

Martínez-Suller, L., Provolo, G., Brennan, D., Howlin, T., Carton, O. T., Lalor, S. T. J., and Richards, K. G.: A note on the estimation of nutrient value of cattle slurry using easily determined physical and chemical parameters, Irish J. Agric. Food Res., 49, 93–97, 2010.

Masero, F., Perrin, M. A., Dey, S., and Mougel, V.: Dinitrogen Fixation: Rationalizing Strategies Utilizing Molecular Complexes, Chem. – A Eur. J., 27, 3892–3928, https://doi.org/10.1002/chem.202003134, 2021.

Massad, R.-S., Nemitz, E., and Sutton, M. A.: Review and parameterisation of bi-directional ammonia exchange between vegetation and the atmosphere, Atmos. Chem. Phys., 10, 10359–10386, https://doi.org/10.5194/acp-10-10359-2010, 2010.

McDuffie, E. E., Smith, S. J., O'Rourke, P., Tibrewal, K., Venkataraman, C., Marais, E. A., Zheng, B., Crippa, M., Brauer, M., and Martin, R. V: A global anthropogenic emission inventory of atmospheric pollutants from sector- and fuel-specific sources (1970--2017): an application of the Community Emissions Data System (CEDS), Earth Syst. Sci. Data, 12, 3413–3442, https://doi.org/10.5194/essd-12-3413-2020, 2020.

Menut, L., Bessagnet, B., Briant, R., Cholakian, A., Couvidat, F., Mailler, S., Pennel, R., Siour, G., Tuccella, P., Turquety, S., and Valari, M.: The CHIMERE v2020r1 online chemistry-transport model, Geosci. Model Dev., 14, 6781–6811, https://doi.org/10.5194/gmd-14-6781-2021, 2021.

Menzi, H., Pain, B., and Sommer, S. G.: Manure management: The European perspective, in: Proc. 4th int. livestock waste management symp. and technology expo, Penang, Malaysia (Ong, H.K. et al. (eds.)). ISBN 983-99519-2-0, 35–44, 2002.

Mercier, A., Betbeder, J., Rumiano, F., Baudry, J., Gond, V., Blanc, L., Bourgoin, C., Cornu, G., Ciudad, C., Marchamalo, M., Poccard-Chapuis, R., and Hubert-Moy, L.: Evaluation of Sentinel-1 and 2 Time Series for Land Cover Classification of Forest–Agriculture Mosaics in Temperate and Tropical Landscapes, Remote Sens., 11, https://doi.org/10.3390/rs11080979, 2019.

Mestre-Quereda, A., Lopez-Sanchez, J. M., Vicente-Guijalba, F., Jacob, A. W., and Engdahl, M. E.: Time-Series of Sentinel-1 Interferometric Coherence and Backscatter for Crop-Type Mapping, IEEE J. Sel. Top. Appl. Earth Obs. Remote Sens., 13, 4070–4084, https://doi.org/10.1109/JSTARS.2020.3008096, 2020.

Midolo, G., Alkemade, R., Schipper, A. M., Benítez-López, A., Perring, M. P., and De Vries, W.: Impacts of nitrogen addition on plant species richness and abundance: A global meta-analysis, Glob. Ecol. Biogeogr., 28, 398–413, https://doi.org/10.1111/GEB.12856, 2019.

Misselbrook, T. H., Van Der Weerden, T. J., Pain, B. F., Jarvis, S. C., Chambers, B. J., Smith, K. A., Phillips, V. R., and Demmers, T. G. M.: Ammonia emission factors for UK agriculture, Atmos. Environ., 34, 871–880, https://doi.org/10.1016/S1352-2310(99)00350-7, 2000.

Misselbrook, T. H., Nicholson, F. A., and Chambers, B. J.: Predicting ammonia losses following the application of livestock manure to land, Bioresour. Technol., 96, 159–168, https://doi.org/10.1016/j.biortech.2004.05.004, 2005.

Montaghi, A., Larsen, R., and Greve, M. H.: Accuracy assessment measures for image segmentation goodness of the Land Parcel Identification System (LPIS) in Denmark, Remote Sens. Lett., 4, 946–955, https://doi.org/10.1080/2150704X.2013.817709, 2013.

Monteny, G.-J. and Hartung, E.: Ammonia emissions in agriculture, edited by: Monteny, G.-J. and Hartung, E., Wageningen Academic Publishers, The Netherlands, https://doi.org/10.3920/978-90-8686-611-3, 2007.

Monteny, G. J.: Modelling of ammonia emissions from dairy cow houses, 112, Instituut voor Mechanisatie, Arbeid en Gebouwen, , 2000.

Morán, M., Ferreira, J., Martins, H., Monteiro, A., Borrego, C., and González, J. A.: Ammonia agriculture emissions: From EMEP to a high resolution inventory, Atmos. Pollut. Res., 7, 786–798, https://doi.org/10.1016/j.apr.2016.04.001, 2016.

Móring, A., Vieno, M., Doherty, R. M., Laubach, J., Taghizadeh-Toosi, A., and Sutton, M. A.: A process-based model for ammonia emission from urine patches, GAG (Generation of Ammonia from Grazing): description and sensitivity analysis, Biogeosciences, 13, 1837–1861, https://doi.org/10.5194/bg-13-1837-2016, 2016.

Mura, M., Bottalico, F., Giannetti, F., Bertani, R., Giannini, R., Mancini, M., Orlandini, S., Travaglini, D., and Chirici, G.: Exploiting the capabilities of the Sentinel-2 multi spectral instrument for predicting growing stock volume in forest ecosystems, Int. J. Appl. Earth Obs. Geoinf., 66, 126–134, https://doi.org/10.1016/j.jag.2017.11.013, 2018.

Navarro, G., Caballero, I., Silva, G., Parra, P.-C., Vázquez, Á., and Caldeira, R.: Evaluation of forest fire on Madeira Island using Sentinel-2A MSI imagery, Int. J. Appl. Earth Obs. Geoinf., 58, 97–106, https://doi.org/10.1016/j.jag.2017.02.003, 2017.

R

Nemitz, E., Milford, C., and Sutton, M. A.: A two-layer canopy compensation point model for describing bi-directional biosphere-atmosphere exchange of ammonia, Q. J. R. Meteorol. Soc., 127, 815–833, https://doi.org/10.1002/qj.49712757306, 2001.

Neumann, K., Elbersen, B. S., Verburg, P. H., Staritsky, I., Pérez-Soba, M., de Vries, W., and Rienks, W. A.: Modelling the spatial distribution of livestock in Europe, Landsc. Ecol., https://doi.org/10.1007/s10980-009-9357-5, 2009.

Ng, W.-T., Rima, P., Einzmann, K., Immitzer, M., Atzberger, C., and Eckert, S.: Assessing the Potential of Sentinel-2 and Pléiades Data for the Detection of Prosopis and Vachellia spp. in Kenya, https://doi.org/10.3390/rs9010074, 2017.

Nicholson, F. A., Chambers, B. J., and Walker, A. W.: Ammonia Emissions from Broiler Litter and Laying Hen Manure Management Systems, Biosyst. Eng., 89, 175–185, https://doi.org/10.1016/j.biosystemseng.2004.06.006, 2004.

Nicholson, F. A., Bhogal, A., Chadwick, D., Gill, E., Gooday, R. D., Lord, E., Misselbrook, T., Rollett, A. J., Sagoo, E., Smith, K. A., Thorman, R. E., Williams, J. R., and Chambers, B. J.: An enhanced software tool to support better use of manure nutrients: MANNER-NPK, Soil Use Manag., 29, 473–484, https://doi.org/10.1111/sum.12078, 2013.

Nilsson, J.: Critical Loads for Sulphur and Nitrogen BT - Air Pollution and Ecosystems, 85–91, 1988.

Nimmermark, S. and Gustafsson, G.: Influence of temperature, humidity and ventilation rate on the release of odour and ammonia in a floor housing system for laying hens, Influ. Temp., 2005.

Nimmermark, S., Lund, V., Gustafsson, G., and Eduard, W.: Ammonia, dust and bacteria in welfare-oriented systems for laying hens., Ann. Agric. Environ. Med., 16, 103–113, 2009.

Noordijk, H., Braam, M., Rutledge-Jonker, S., Hoogerbrugge, R., Stolk, A. P., and van Pul, W. A. J.: Performance of the MAN ammonia monitoring network in the Netherlands, Atmos. Environ., 228, 117400, https://doi.org/10.1016/j.atmosenv.2020.117400, 2020.

Novelli, A., Aguilar, M. A., Nemmaoui, A., Aguilar, F. J., and Tarantino, E.: Performance evaluation of object based greenhouse detection from Sentinel-2 MSI and Landsat 8 OLI data: A case study from Almería (Spain), Int. J. Appl. Earth Obs. Geoinf., 52, 403–411, https://doi.org/10.1016/j.jag.2016.07.011, 2016.

Nowak, J. B., Neuman, J. A., Bahreini, R., Brock, C. A., Middlebrook, A. M., Wollny, A. G., Holloway, J. S., Peischl, J., Ryerson, T. B., and Fehsenfeld, F. C.: Airborne observations of ammonia and ammonium nitrate formation over Houston, Texas, J. Geophys. Res. Atmos., https://doi.org/10.1029/2010JD014195, 2010.

Orgiazzi, A., Ballabio, C., Panagos, P., Jones, A., and Fernández-Ugalde, O.: LUCAS Soil, the largest expandable soil dataset for Europe: a review, Eur. J. Soil Sci., 69, 140–153, https://doi.org/10.1111/EJSS.12499, 2018.

van Os, J., Jeurissen, L. J. J., and Naeff, H. S. D.: Geografisch informatiesysteem voor de emissieregistratie van landbouwbedrijven;: GIABplus-bestand 2013 – Status A, Wettelijke Onderzoekstaken Natuur & Milieu, https://doi.org/10.18174/386756, 2016.

Palchowdhuri, Y., Valcarce-Diñeiro, R., King, P., and Sanabria-Soto, M.: Classification of multi-temporal spectral indices for crop type mapping: a case study in Coalville, UK, J. Agric. Sci., 156, 24–36, https://doi.org/10.1017/S0021859617000879, 2018.

Paloscia, S., Pettinato, S., Santi, E., Notarnicola, C., Pasolli, L., and Reppucci, A.: Soil moisture mapping using Sentinel-1 images: Algorithm and preliminary validation, Remote Sens. Environ., 134, 234–248, https://doi.org/10.1016/j.rse.2013.02.027, 2013.

Pasqualotto, N., Delegido, J., Van Wittenberghe, S., Rinaldi, M., and Moreno, J.: Multi-Crop Green LAI Estimation with a New Simple Sentinel-2 LAI Index (SeLI), Sensors, 19, https://doi.org/10.3390/s19040904, 2019.

Paull, J.: A Century of Synthetic Fertilizer:1909-2009, 2009.

Paulot, F., Jacob, D. J., Pinder, R. W., Bash, J. O., Travis, K., and Henze, D. K.: Ammonia emissions in the United States, European Union, and China derived by high-resolution inversion of ammonium wet deposition data: Interpretation with a new agricultural emissions inventory (MASAGE_NH3), J. Geophys. Res. Atmos., 119, 4343–4364, https://doi.org/10.1002/2013JD021130, 2014.

Paulot, F., Malyshev, S., Nguyen, T., Crounse, J. D., Shevliakova, E., and Horowitz, L. W.: Representing sub-grid scale variations in nitrogen deposition associated with land use in a global Earth system model: implications for present and future nitrogen deposition fluxes over North America, Atmos. Chem. Phys., 18, 17963–17978, https://doi.org/10.5194/acp-18-17963-2018, 2018.

Paustian, K., Ravindranath, N. H., and van Amstel, A. R.: 2006 IPCC Guidelines for National Greenhouse Gas Inventories, [s.n.], 2006.

Pelletier, C., Valero, S., Inglada, J., Champion, N., and Dedieu, G.: Assessing the robustness of Random Forests to map land cover with high resolution satellite image time series over large areas, Remote Sens. Environ., 187, 156–168, https://doi.org/10.1016/j.rse.2016.10.010, 2016.

Pelster, D. E., Watt, D., Strachan, I. B., Rochette, P., Bertrand, N., and Chantigny, M. H.: Effects of Initial Soil Moisture, Clod Size, and Clay Content on Ammonia Volatilization after Subsurface Band Application of Urea, J. Environ. Qual., 48, 549–558, https://doi.org/10.2134/JEQ2018.09.0344, 2019.

Peñuelas, J. and Filella, I.: Phenology. Responses to a warming world., Science, 294, 793–795, https://doi.org/10.1126/science.1066860, 2001.

Pinder, R. W., Pekney, N. J., Davidson, C. I., and Adams, P. J.: A process-based model of ammonia emissions from dairy cows: Improved temporal and spatial resolution, Atmos. Environ., 38, 1357–1365, https://doi.org/10.1016/j.atmosenv.2003.11.024, 2004.

Pinder, R. W., Adams, P. J., Pandis, S. N., and Gilliland, A. B.: Temporally resolved ammonia emission inventories: Current estimates, evaluation tools, and measurement needs, J. Geophys. Res. Atmos., 111, 1–14, https://doi.org/10.1029/2005JD006603, 2006.

Pitcairn, C. E. R., Leith, I. D., van Dijk, N., Sheppard, L. J., Sutton, M. A., and Fowler, D.: The Application of Transects to Assess the Effects of Ammonia on Woodland Groundflora BT - Atmospheric Ammonia: Detecting emission changes and environmental impacts, edited by: Sutton, M. A.,

R

Reis, S., and Baker, S. M. H., Springer Netherlands, Dordrecht, 59–69, https://doi.org/10.1007/978-1-4020-9121-6_5, 2009.

Plöchl, M.: Neural network approach for modelling ammonia emission after manure application on the field, Atmos. Environ., https://doi.org/10.1016/S1352-2310(01)00281-3, 2001.

Pope, C. A., Ezzati, M., and Dockery, D. W.: Fine-Particulate Air Pollution and Life Expectancy in the United States, N. Engl. J. Med., https://doi.org/10.1056/nejmsa0805646, 2009.

Poteko, J., Zähner, M., and Schrade, S.: Effects of housing system, floor type and temperature on ammonia and methane emissions from dairy farming: A meta-analysis, Biosyst. Eng., 182, 16–28, https://doi.org/10.1016/j.biosystemseng.2019.03.012, 2019.

Pul, A. van, Jaarsveld, H. Van, Meulen, T. van der, and Velders, G.: Ammonia concentrations in the Netherlands: spatially detailed measurements and model calculations, Atmos. Environ., 38, 4045–4055, https://doi.org/10.1016/j.atmosenv.2004.03.051, 2004.

Van Pul, A., Hertel, O., Geels, C., Dore, A. J., Vieno, M., van Jaarsveld, H. A., Bergström, R., Schaap, M., and Fagerli, H.: Modelling of the Atmospheric Transport and Deposition of Ammonia at a National and Regional Scale BT - Atmospheric Ammonia: Detecting emission changes and environmental impacts, edited by: Sutton, M. A., Reis, S., and Baker, S. M. H., Springer Netherlands, Dordrecht, 301–358, https://doi.org/10.1007/978-1-4020-9121-6_19, 2009.

Qian, P. and Schoenau, J. J.: Availability of nitrogen in solid manure amendments with different C:N ratios, Can. J. Soil Sci., 82, 219–225, https://doi.org/10.4141/S01-018, 2002.

Radoux, J., Lamarche, C., Van Bogaert, E., Bontemps, S., Brockmann, C., and Defourny, P.: Automated Training Sample Extraction for Global Land Cover Mapping, Remote Sens., 6, 3965–3987, https://doi.org/10.3390/rs6053965, 2014.

Raymond, J.: Use of Stable Isotopes to Trace the Fate of Applied Nitrogen in Forest Plantations to Evaluate Fertilizer Efficiency and Ecosystem Impacts, 2016.

Raymond, J. E., Fox, T. R., Strahm, B. D., and Zerpa, J.: Ammonia volatilization following nitrogen fertilization with enhanced efficiency fertilizers and urea in loblolly pine (Pinus taeda L.) plantations of the southern United States, For. Ecol. Manage., 376, 247–255, https://doi.org/10.1016/j.foreco.2016.06.015, 2016.

Reiche, J., Verhoeven, R., Verbesselt, J., Hamunyela, E., Wielaard, N., and Herold, M.: Characterizing Tropical Forest Cover Loss Using Dense Sentinel-1 Data and Active Fire Alerts, Remote Sens., 10, https://doi.org/10.3390/rs10050777, 2018.

Reis, S., Pinder, R. W., Zhang, M., Lijie, G., and Sutton, M. A.: Reactive nitrogen in atmospheric emission inventories, Atmos. Chem. Phys., 9, 7657–7677, https://doi.org/10.5194/acp-9-7657-2009, 2009.

Renard, J. J., Calidonna, S. E., and Henley, M. V: Fate of ammonia in the atmosphere—a review for applicability to hazardous releases, J. Hazard. Mater., 108, 29–60, https://doi.org/10.1016/j.jhazmat.2004.01.015, 2004.

Reuss, J. O. and Johnson, D. W.: Acid Deposition and the Acidification of Soils and Waters, in: Ecological Studies, 1986.

Richardson, A. D., Keenan, T. F., Migliavacca, M., Ryu, Y., Sonnentag, O., and Toomey, M.: Climate change, phenology, and phenological control of vegetation feedbacks to the climate system, Agric. For. Meteorol., 169, 156–173, https://doi.org/10.1016/j.agrformet.2012.09.012, 2013.

Richardson, D., Felgate, H., Watmough, N., Thomson, A., and Baggs, E.: Mitigating release of the potent greenhouse gas N2O from the nitrogen cycle – could enzymic regulation hold the key?, Trends Biotechnol., 27, 388–397, https://doi.org/10.1016/j.tibtech.2009.03.009, 2009.

Riddick, S., Ward, D., Hess, P., Mahowald, N., Massad, R., and Holland, E.: Estimate of changes in agricultural terrestrial nitrogen pathways and ammonia emissions from 1850 to present in the Community Earth System Model, Biogeosciences, 13, 3397–3426, https://doi.org/10.5194/bg-13-3397-2016, 2016.

Riddick, S. N., Blackall, T. D., Dragosits, U., Tang, Y. S., Moring, A., Daunt, F., Wanless, S., Hamer, K. C., and Sutton, M. A.: High temporal resolution modelling of environmentally-dependent seabird ammonia emissions: Description and testing of the GUANO model, Atmos. Environ., 161, 48–60, https://doi.org/10.1016/j.atmosenv.2017.04.020, 2017.

Wanneer mest uitrijden: https://www.rvo.nl/onderwerpen/agrarisch-ondernemen/mest/gebruiken-en-uitrijden/wanneer-mest-uitrijden.

Ritter, A. and Muñoz-Carpena, R.: Performance evaluation of hydrological models: Statistical significance for reducing subjectivity in goodness-of-fit assessments, J. Hydrol., https://doi.org/10.1016/j.jhydrol.2012.12.004, 2013.

Robarge, W. P., Walker, J. T., McCulloch, R. B., and Murray, G.: Atmospheric concentrations of ammonia and ammonium at an agricultural site in the southeast United States, Atmos. Environ., 36, 1661–1674, https://doi.org/10.1016/S1352-2310(02)00171-1, 2002.

Rogers, J. and Gunn, S.: Identifying feature relevance using a random forest, Lect. Notes Comput. Sci. (including Subser. Lect. Notes Artif. Intell. Lect. Notes Bioinformatics), 3940 LNCS, 173–184, https://doi.org/10.1007/11752790_12/COVER, 2006.

Rösemann, C., Haenel, H.-D., Vos, C., Dämmgen, U., Döring, U., Wulf, S., Eurich-Menden, B., Freibauer, A., Döhler, H., Schreiner, C., Osterburg, B., and Fuß, R.: Calculations of gaseous and particulate emissions from German agriculture 1990 - 2019: Report on methods and data (RMD) Submission 2021; Berechnung von gas- und partikelförmigen Emissionen aus der deutschen Landwirtschaft 1990 - 2019: Report zu Methoden u, Johann-Heinrich-von-Thünen-Institut, Braunschweig, Germany, https://doi.org/10.3220/REP1616572444000, 2021.

Rotz, C. A.: Management to reduce nitrogen losses in animal production., J. Anim. Sci., 82 E-Suppl, E119-137, https://doi.org/10.2527/2004.8213_supplE119x, 2004a.

Rotz, C. A.: The Integrated Farm System Model: A Tool for Developing more Economically and Environmentally Sustainable Farming Systems for the Northeast, https://doi.org/10.13031/2013.16116, 2004b.

Rouse J. W., J., Haas, R. H., Schell, J. A., and Deering, D. W.: Monitoring Vegetation Systems in the Great Plains with Erts, in: NASA Special Publication, vol. 351, 309, 1974.

R

Sanchis, E., Calvet, S., Prado, A. del, and Estellés, F.: A meta-analysis of environmental factor effects on ammonia emissions from dairy cattle houses, Biosyst. Eng., 178, 176–183, https://doi.org/10.1016/j.biosystemseng.2018.11.017, 2019.

Sanz-Cobena, A., Lassaletta, L., Estellés, F., Del Prado, A., Guardia, G., Abalos, D., Aguilera, E., Pardo, G., Vallejo, A., Sutton, M. A., Garnier, J., and Billen, G.: Yield-scaled mitigation of ammonia emission from N fertilization: the Spanish case, Environ. Res. Lett., 9, 125005, https://doi.org/10.1088/1748-9326/9/12/125005, 2014.

Sapek, A.: Ammonia Emissions from Non-Agricultural Sources, Polish J. Environ. Stud., 22, 2013.

Saveyn, H. and Eder, P.: End-of-waste criteria for biodegradable waste subjected to biological treatment (compost & digestate) : technical proposals, Publications Office, https://doi.org/doi/10.2788/6295, 2014.

Schaap, M., Müller, K., and ten Brink, H. M.: Constructing the European aerosol nitrate concentration field from quality analysed data, Atmos. Environ., 36, 1323–1335, https://doi.org/10.1016/S1352-2310(01)00556-8, 2002.

Schaap, M., Spindler, G., Schulz, M., Acker, K., Maenhaut, W., Berner, A., Wieprecht, W., Streit, N., Müller, K., Brüggemann, E., Chi, X., Putaud, J.-P., Hitzenberger, R., Puxbaum, H., Baltensperger, U., and ten Brink, H.: Artefacts in the sampling of nitrate studied in the "INTERCOMP" campaigns of EUROTRAC-AEROSOL, Atmos. Environ., 38, 6487–6496, https://doi.org/10.1016/j.atmosenv.2004.08.026, 2004a.

Schaap, M., van Loon, M., ten Brink, H. M., Dentener, F. J., and Builtjes, P. J. H.: Secondary inorganic aerosol simulations for Europe with special attention to nitrate, Atmos. Chem. Phys., https://doi.org/10.5194/acp-4-857-2004, 2004b.

Schaap, M., Timmermans, R. M. A., Roemer, M., Boersen, G. A. C., Builtjes, P. J. H., Sauter, F. J., Velders, G. J. M., and Beck, J. P.: The LOTOS-EUROS model: description, validation and latest developments, Int. J. Environ. Pollut., 32, 270, https://doi.org/10.1504/ijep.2008.017106, 2008a.

Schaap, M., Timmermans, R. M. A., Roemer, M., Boersen, G. A. C., Builtjes, P. J. H., Sauter, F. J., Velders, G. J. M., and Beck, J. P.: The LOTOS EUROS model: description, validation and latest developments, Int. J. Environ. Pollut., 32, 270, https://doi.org/10.1504/ijep.2008.017106, 2008b.

Schaap, M., Segers, A., Curier, L., Eskes, H., and Kumar, U.: LOTOS-EUROS regional forecasting system and performances, 36, 1–36, 2012.

Schaap, M., Banzhaf, S., Scheuschner, T., Geupel, M., Hendriks, C., Kranenburg, R., Nagel, H.-D., Segers, A. J., von Schlutow, A., Wichink Kruit, R., and Builtjes, P. J. H.: Atmospheric nitrogen deposition to terrestrial ecosystems across Germany, Biogeosciences Discuss., 1–24, https://doi.org/10.5194/BG-2017-491, 2017a.

Schaap, M., Wichink Kruit, R., Hendriks, C., Kranenburg, R., Segers, A., Builtjes, P., and Banzhaf, S.: Modelling and assessment of acidifying and eutrophying atmospheric deposition to terrestrial ecosystems (PINETI2), 2017b.

Schaap, M., Hendriks, C., Kranenburg, R., Kuenen, J., Segers, A., Schlutow, A., Nagel, H. D., Ritter, A., and Banzhaf, S.: PINETI-3: Modellierung atmosphärischer Stoffeinträge von 2000 bis 2015 zur

Bewertung der ökosystem-spezifischen Gefährdung von Biodiversität durch Luftschadstoffe in Deutschland, Texte Umweltbundesamt, 79, 149, 2018.

Schjoerring, J. K. and Mattsson, M.: Quantification of ammonia exchange between agricultural cropland and the atmosphere: Measurements over two complete growth cycles of oilseed rape, wheat, barley and pea, Plant Soil, https://doi.org/10.1023/A:1004851001342, 2001.

Schleyer, R., Bieber, E., and Wallasch, M.: Das Luftmessnetz des Umweltbundesamtes, Umweltbundesamt, 2013.

Schmitz, A., Sanders, T. G. M., Bolte, A., Bussotti, F., Dirnböck, T., Johnson, J., Peñuelas, J., Pollastrini, M., Prescher, A. K., Sardans, J., Verstraeten, A., and de Vries, W.: Responses of forest ecosystems in Europe to decreasing nitrogen deposition, Environ. Pollut., 244, 980–994, https://doi.org/10.1016/J.ENVPOL.2018.09.101, 2019.

Schobesberger, S., Franchin, A., Bianchi, F., Rondo, L., Duplissy, J., Kürten, A., Ortega, I. K., Metzger, A., Schnitzhofer, R., Almeida, J., Amorim, A., Dommen, J., Dunne, E. M., Ehn, M., Gagné, S., Ickes, L., Junninen, H., Hansel, A., Kerminen, V.-M., Kirkby, J., Kupc, A., Laaksonen, A., Lehtipalo, K., Mathot, S., Onnela, A., Petäjä, T., Riccobono, F., Santos, F. D., Sipilä, M., Tomé, A., Tsagkogeorgas, G., Viisanen, Y., Wagner, P. E., Wimmer, D., Curtius, J., Donahue, N. M., Baltensperger, U., Kulmala, M., and Worsnop, D. R.: On the composition of ammonia–sulfuric-acid ion clusters during aerosol particle formation, Atmos. Chem. Phys., 15, 55–78, https://doi.org/10.5194/acp-15-55-2015, 2015.

Schofield, C. L.: Acid precipitation: Effects on fish, Ambio, 5, 228–230, 1976.

Seedorf, J., Hartung, J., Schröder, M., Linkert, K. H., Phillips, V. R., Holden, M. R., Sneath, R. W., Short, J. L., White, R. P., Pedersen, S., Takai, H., Johnsen, J. O., Metz, J. H. M., Groot Koerkamp, P. W. G., Uenk, G. H., and Wathes, C. M.: Concentrations and emissions of airborne endotoxins and microorganisms in livestock buildings in Northern Europe, J. Agric. Eng. Res., https://doi.org/10.1006/jaer.1997.0281, 1998a.

Seedorf, J., Hartung, J., Schröder, M., Linkert, K. H., Pedersen, S., Takai, H., Johnsen, J. O., Metz, J. H. M., Groot Koerkamp, P. W. G., Uenk, G. H., Phillips, V. R., Holden, M. R., Sneath, R. W., Short, J. L., White, R. P., and Wathes, C. M.: Temperature and moisture conditions in livestock buildings in Northern Europe, J. Agric. Eng. Res., https://doi.org/10.1006/jaer.1997.0284, 1998b.

Shephard, M. W. and Cady-Pereira, K. E.: Cross-track Infrared Sounder (CrIS) satellite observations of tropospheric ammonia, Atmos. Meas. Tech., 8, 1323–1336, https://doi.org/10.5194/AMT-8-1323-2015, 2015.

Shephard, M. W., Cady-Pereira, K. E., Luo, M., Henze, D. K., Pinder, R. W., Walker, J. T., Rinsland, C. P., Bash, J. O., Zhu, L., Payne, V. H., and Clarisse, L.: TES ammonia retrieval strategy and global observations of the spatial and seasonal variability of ammonia, Atmos. Chem. Phys., 11, 10743–10763, https://doi.org/10.5194/acp-11-10743-2011, 2011.

Shephard, M. W., Dammers, E., E. Cady-Pereira, K., K. Kharol, S., Thompson, J., Gainariu-Matz, Y., Zhang, J., A. McLinden, C., Kovachik, A., Moran, M., Bittman, S., E. Sioris, C., Griffin, D., J. Alvarado, M., Lonsdale, C., Savic-Jovcic, V., and Zheng, Q.: Ammonia measurements from space with the

R

Cross-track Infrared Sounder: Characteristics and applications, Atmos. Chem. Phys., 20, 2277–2302, https://doi.org/10.5194/ACP-20-2277-2020, 2020.

Shimshock, J. P. and De Pena, R. G.: Below-cloud scavenging of tropospheric ammonia, Tellus B Chem. Phys. Meteorol., 41, 296–304, https://doi.org/10.3402/tellusb.v41i3.15082, 1989.

Shoko, C., Mutanga, O., Dube, T., and Slotow, R.: Characterizing the spatio-temporal variations of C3 and C4 dominated grasslands aboveground biomass in the Drakensberg, South Africa, Int. J. Appl. Earth Obs. Geoinf., 68, 51–60, https://doi.org/10.1016/j.jag.2018.02.006, 2018.

Simpson, D., Aas, W., Bartnicki, J., Berge, H., Bleeker, A., Cuvelier, K., Dentener, F., Dore, T., Erisman, J. W., Fagerli, H., Flechard, C., Hertel, O., van Jaarsveld, H., Jenkin, M., Schaap, M., Semeena, V. S., Thunis, P., Vautard, R., and Vieno, M.: Atmospheric transport and deposition of reactive nitrogen in Europe, in: The European Nitrogen Assessment: Sources, Effects and Policy Perspectives, edited by: Sutton, M. A., Howard, C. M., Erisman, J. W., Billen, G., Bleeker, A., Grennfelt, P., van Grinsven, H., and Grizzetti, B., Cambridge University Press, Cambridge, 298–316, 2011.

Simpson, D., Benedictow, A., Berge, H., Bergström, R., Emberson, L. D., Fagerli, H., Flechard, C. R., Hayman, G. D., Gauss, M., Jonson, J. E., Jenkin, M. E., Nyíri, A., Richter, C., Semeena, V. S., Tsyro, S., Tuovinen, J.-P., Valdebenito, Á., and Wind, P.: The EMEP MSC-W chemical transport model – technical description, Atmos. Chem. Phys., 12, 7825–7865, https://doi.org/10.5194/acp-12-7825-2012, 2012.

Singh, U., Matthews, R. B., Griffin, T. S., Ritchie, J. T., Hunt, L. A., and Goenaga, R.: Modeling growth and development of root and tuber crops BT - Understanding Options for Agricultural Production, edited by: Tsuji, G. Y., Hoogenboom, G., and Thornton, P. K., Springer Netherlands, Dordrecht, 129–156, https://doi.org/10.1007/978-94-017-3624-4_7, 1998.

Sintermann, J., Neftel, A., Ammann, C., Häni, C., Hensen, A., Loubet, B., and Flechard, C. R.: Are ammonia emissions from field-applied slurry substantially over-estimated in European emission inventories?, Biogeosciences, 9, 1611–1632, https://doi.org/10.5194/BG-9-1611-2012, 2012.

Sintermann, J., Dietrich, K., Häni, C., Bell, M., Jocher, M., and Neftel, A.: A miniDOAS instrument optimised for ammonia field measurements, Atmos. Meas. Tech., 9, 2721–2734, https://doi.org/10.5194/amt-9-2721-2016, 2016.

Skiba, U., Medinets, S., Cardenas, L. M., Carnell, E. J., Hutchings, N. J., and Amon, B.: Assessing the contribution of soil NOx emissions to European atmospheric pollution, Environ. Res. Lett., 16, 25009, https://doi.org/10.1088/1748-9326/abd2f2, 2021.

Skjøth, C. A. and Geels, C.: The effect of climate and climate change on ammonia emissions in Europe, Atmos. Chem. Phys., 13, 117–128, https://doi.org/10.5194/acp-13-117-2013, 2013.

Skjøth, C. A., Hertel, O., Gyldenkaerne, S., and Ellermann, T.: Implementing a dynamical ammonia emission parameterization in the large-scale air pollution model ACDEP, J. Geophys. Res. Atmos., 109, https://doi.org/10.1029/2003JD003895, 2004.

Skjøth, C. A., Geels, C., Berge, H., Gyldenkaerne, S., Fagerli, H., Ellermann, T., Frohn, L. M., Christensen, J., Hansen, K. M., Hansen, K. M., and Hertel, O.: Spatial and temporal variations in ammonia emissions ĝ€" a freely accessible model code for Europe, Atmos. Chem. Phys., 11, 5221–5236, https://doi.org/10.5194/acp-11-5221-2011, 2011.

Smith, E., Gordon, R., Bourque, C., Campbell, A., Génermont, S., Rochette, P., and Mkhabela, M.: Simulated management effects on ammonia emissions from field applied manure, J. Environ. Manage., 90, 2531–2536, https://doi.org/10.1016/j.jenvman.2009.01.012, 2009.

Smith, K. A., Jackson, D. R., Misselbrook, T. H., Pain, B. F., and Johnson, R. A.: PA—Precision Agriculture: Reduction of Ammonia Emission by Slurry Application Techniques, J. Agric. Eng. Res., 77, 277–287, https://doi.org/10.1006/jaer.2000.0604, 2000.

Snell, H. G. J., Seipelt, F., and Weghe, H. F. A. V. den: Ventilation Rates and Gaseous Emissions from Naturally Ventilated Dairy Houses, Biosyst. Eng., 86, 67–73, https://doi.org/10.1016/S1537-5110(03)00113-2, 2003.

Søgaard, H. T., Sommer, S. G., Hutchings, N. J., Huijsmans, J. F. M., Bussink, D. W., and Nicholson, F.: Ammonia volatilization from field-applied animal slurry-the ALFAM model, Atmos. Environ., https://doi.org/10.1016/S1352-2310(02)00300-X, 2002.

Someya, Y., Imasu, R., Shiomi, K., and Saitoh, N.: Atmospheric ammonia retrieval from the TANSO-FTS/GOSAT thermal infrared sounder, Atmos. Meas. Tech., 13, 309–321, https://doi.org/10.5194/amt-13-309-2020, 2020.

Sommer, S. G. and Hutchings, N. J.: Ammonia emission from field applied manure and its reduction—invited paper, Eur. J. Agron., 15, 1–15, https://doi.org/10.1016/S1161-0301(01)00112-5, 2001.

Sommer, S. G. and Olesen, J. E.: Effects of Dry Matter Content and Temperature on Ammonia Loss from Surface-Applied Cattle Slurry, J. Environ. Qual., 20, 679–683, https://doi.org/10.2134/jeq1991.00472425002000030029x, 1991.

Sommer, S. G., Olesen, J. E., and Christensen, B. T.: Effects of temperature, wind speed and air humidity on ammonia volatilization from surface applied cattle slurry, J. Agric. Sci., 117, 91–100, https://doi.org/10.1017/S0021859600079016, 1991.

Sommer, S. G., Schjoerring, J. K., and Denmead, O. T.: Ammonia Emission from Mineral Fertilizers and Fertilized Crops, Adv. Agron., 82, 557–622, https://doi.org/10.1016/S0065-2113(03)82008-4, 2004.

Sommer, S. G., Webb, J., and Hutchings, N. D.: New Emission Factors for Calculation of Ammonia Volatilization From European Livestock Manure Management Systems, Front. Sustain. Food Syst., 3, 101, https://doi.org/10.3389/FSUFS.2019.00101/BIBTEX, 2019.

Sonneveld, M. P. W., Schröder, J. J., Vos, J. A. de, Monteny, G. J., Mosquera, J., Hol, J. M. G., Lantinga, E. A., Verhoeven, F. P. M., and Bouma, J.: A Whole-Farm Strategy to Reduce Environmental Impacts of Nitrogen, J. Environ. Qual., 37, 186–195, https://doi.org/10.2134/JEQ2006.0434, 2008.

Sonobe, R., Yamaya, Y., Tani, H., Wang, X., Kobayashi, N., and Mochizuki, K.: Crop classification from Sentinel-2-derived vegetation indices using ensemble learning, J. Appl. Remote Sens., 12, 1–16, https://doi.org/10.1117/1.JRS.12.026019, 2018.

Spranger, T., Kunze, F., Gauger, T., Nagel, D., Bleeker, A., and Draaijers, G.: Critical Loads Exceedances in Germany and their Dependence on the Scale of Input Data, Water, Air Soil Pollut. Focus, 1, 335–351, https://doi.org/10.1023/A:1011548425913, 2001.

Starmans, D. A. J. and van der Hoek, K. W. (Eds.): Ammonia, the case of The Netherlands, Wageningen Academic Publishers, Netherlands, 2007.

R

Stehman, S. V: Practical Implications of Design-Based Sampling Inference for Thematic Map Accuracy Assessment, Remote Sens. Environ., 72, 35–45, https://doi.org/10.1016/S0034-4257(99)00090-5, 2000.

Stokstad, E.: Ammonia Pollution From Farming May Exact Hefty Health Costs, Science (80-.)., 343, 238 LP – 238, https://doi.org/10.1126/science.343.6168.238, 2014.

Stokstad, E.: Nitrogen crisis threatens Dutch environment-and economy, Science (80-.)., 366, 1180–1181, https://doi.org/10.1126/science.366.6470.1180, 2019.

Stolk, A., Noordijk, H., and van Zanten, M.: Drogedepositiemetingen van ammoniak in Natura 2000-gebied Bargerveen, 2014.

Sutton, M. A., Fowler, D., Burkhardt, J. K., and Milford, C.: Vegetation atmosphere exchange of ammonia: Canopy cycling and the impacts of elevated nitrogen inputs, Water, Air, Soil Pollut., https://doi.org/10.1007/BF01186137, 1995.

Sutton, M. A., Asman, W. A. H., Ellermann, T., Van Jaarsveld, J. A., Acker, K., Aneja, V., Duyzer, J., Horvath, L., Paramonov, S., Mitosinkova, M., Tang, Y. S., Achermann, B., Gauger, T., Bartniki, J., Neftel, A., and Erisman, J. W.: Establishing the link between ammonia emission control and measurements of reduced nitrogen concentrations and deposition, https://doi.org/10.1023/A:1021834132138, 2003.

Sutton, M. A., Reis, S., Riddick, S. N., Dragosits, U., Nemitz, E., Theobald, M. R., Tang, Y. S., Braban, C. F., Vieno, M., Dore, A. J., Mitchell, R. F., Wanless, S., Daunt, F., Fowler, D., Blackall, T. D., Milford, C., Flechard, C. R., Loubet, B., Massad, R., Cellier, P., Personne, E., Coheur, P. F., Clarisse, L., Van Damme, M., Ngadi, Y., Clerbaux, C., Skjøth, C. A., Geels, C., Hertel, O., Wichink Kruit, R. J., Pinder, R. W., Bash, J. O., Walker, J. T., Simpson, D., Horváth, L., Misselbrook, T. H., Bleeker, A., Dentener, F., and de Vries, W.: Towards a climate-dependent paradigm of ammonia emission and deposition, Philos. Trans. R. Soc. B Biol. Sci., 368, 20130166, https://doi.org/10.1098/rstb.2013.0166, 2013.

Sutton, M. A., Skiba, U. M., van Grinsven, H. J. M., Oenema, O., Watson, C. J., Williams, J., Hellums, D. T., Maas, R., Gyldenkaerne, S., Pathak, H., and Winiwarter, W.: Green economy thinking and the control of nitrous oxide emissions, Environ. Dev., https://doi.org/10.1016/j.envdev.2013.10.002, 2014.

van der Swaluw, E., Asman, W. A. H., and Hoogerbrugge, R.: The Dutch National Precipitation Chemistry Monitoring Network over the period 1992-2004, 2010.

Swart, D., Zhang, J., van der Graaf, S., Rutledge-Jonker, S., Hensen, A., Berkhout, S., Wintjen, P., van der Hoff, R., Haaima, M., Frumau, A., van den Bulk, P., Schulte, R., van Zanten, M., and van Goethem, T.: Field comparison of two novel open-path instruments that measure dry deposition and emission of ammonia using flux-gradient and eddy covariance methods, Atmos. Meas. Tech., 16, 529–546, https://doi.org/10.5194/amt-16-529-2023, 2023.

Theobald, M. R., Dragosits, U., Place, C. J., Smith, J. U., Sozanska, M., Brown, L., Scholefield, D., Del Prado, A., Webb, J., Whitehead, P. G., Angus, A., Hodge, I. D., Fowler, D., and Sutton, M. A.: Modelling nitrogen fluxes at the landscape scale, Water, Air, Soil Pollut. Focus, 4, 135–142, https://doi.org/10.1007/s11267-004-3023-3, 2004.

Thompson, R. B., Pain, B. F., and Rees, Y. J.: Ammonia volatilization from cattle slurry following surface application to grassland: II. Influence of application rate, wind speed and applying slurry in narrow bands, Plant Soil, 125, 119–128, 1990.

Timmermans, R., van Pinxteren, D., Kranenburg, R., Hendriks, C., Fomba, K. W., Herrmann, H., and Schaap, M.: Evaluation of modelled LOTOS-EUROS with observational based PM10 source attribution, Atmos. Environ. X, 14, 100173, https://doi.org/10.1016/j.aeaoa.2022.100173, 2022.

Todd, L. A., Ramanathan, M., Mottus, K., Katz, R., Dodson, A., and Mihlan, G.: Measuring chemical emissions using open-path Fourier transform infrared (OP-FTIR) spectroscopy and computer-assisted tomography, Atmos. Environ., 35, 1937–1947, https://doi.org/10.1016/S1352-2310(00)00546-X, 2001.

Trebs, I., Meixner, F. X., Slanina, J., Otjes, R., Jongejan, P., and Andreae, M. O.: Real-time measurements of ammonia, acidic trace gases and water-soluble inorganic aerosol species at a rural site in the Amazon Basin, Atmos. Chem. Phys., 4, 967–987, https://doi.org/10.5194/acp-4-967-2004, 2004.

Van Tricht, K., Gobin, A., Gilliams, S., and Piccard, I.: Synergistic Use of Radar Sentinel-1 and Optical Sentinel-2 Imagery for Crop Mapping: A Case Study for Belgium, Remote Sens., 10, https://doi.org/10.3390/rs10101642, 2018.

Truong, A. H., Kim, M. T., Nguyen, T. T., Nguyen, N. T., and Nguyen, Q. T.: Methane, Nitrous Oxide and Ammonia Emissions from Livestock Farming in the Red River Delta, Vietnam: An Inventory and Projection for 2000–2030, Sustain. 2018, Vol. 10, Page 3826, 10, 3826, https://doi.org/10.3390/SU10103826, 2018.

Reported emission data: https://www.ceip.at/webdab-emission-database/reported-emissiondata, last access: 15 November 2022.

Unsworth, M. H. and Wilshaw, J. C.: Wet, occult and dry deposition of pollutants on forests, Agric. For. Meteorol., 47, 221–238, https://doi.org/10.1016/0168-1923(89)90097-X, 1989.

Vaglio Laurin, G., Belli, C., Bianconi, R., Laranci, P., and Papale, D.: Early mapping of industrial tomato in Central and Southern Italy with Sentinel 2, aerial and RapidEye additional data, J. Agric. Sci., 156, 396–407, https://doi.org/10.1017/S0021859618000400, 2018.

Velthof, G. L.: Report Task 1 of Methodological studies in the field of Agro-Environmental Indicators. Lot 1 excretion factors Final Draft, 2014.

Velthof, G. L. and Kuikman, P. J.: Beperking van lachgasemissie uit gewasresten; een systeemanalyse, Alterra, Netherlands, 2000.

Velthof, G. L., Oudendag, D., Witzke, H. P., Asman, W. A. H., Klimont, Z., and Oenema, O.: Integrated Assessment of Nitrogen Losses from Agriculture in EU-27 using MITERRA-EUROPE, J. Environ. Qual., 38, 402, https://doi.org/10.2134/jeq2008.0108, 2009.

Velthof, G. L., van Bruggen, C., Groenestein, C. M., de Haan, B. J., Hoogeveen, M. W., and Huijsmans, J. F. M.: A model for inventory of ammonia emissions from agriculture in the Netherlands, Atmos. Environ., 46, 248–255, https://doi.org/10.1016/j.atmosenv.2011.09.075, 2012.

Velthof, G. L., Hou, Y., and Oenema, O.: Nitrogen excretion factors of livestock in the European Union: a review, J. Sci. Food Agric., 95, 3004–3014, https://doi.org/10.1002/jsfa.7248, 2015.

R

Verrelst, J., Rivera, J. P., Veroustraete, F., Muñoz-Marí, J., Clevers, J. G. P. W., Camps-Valls, G., and Moreno, J.: Experimental Sentinel-2 LAI estimation using parametric, non-parametric and physical retrieval methods – A comparison, ISPRS J. Photogramm. Remote Sens., 108, 260–272, https://doi.org/10.1016/j.isprsjprs.2015.04.013, 2015.

Villarroya-Carpio, A., Lopez-Sanchez, J. M., and Engdahl, M. E.: Sentinel-1 interferometric coherence as a vegetation index for agriculture, Remote Sens. Environ., 280, 113208, https://doi.org/10.1016/j.rse.2022.113208, 2022.

Vitousek, P. M., Mooney, H. A., Lubchenco, J., and Melillo, J. M.: Human Domination of Earth's Ecosystems BT - Urban Ecology: An International Perspective on the Interaction Between Humans and Nature, edited by: Marzluff, J. M., Shulenberger, E., Endlicher, W., Alberti, M., Bradley, G., Ryan, C., Simon, U., and ZumBrunnen, C., Springer US, Boston, MA, 3–13, https://doi.org/10.1007/978-0-387-73412-5_1, 2008.

Vitousek, P. M., Menge, D. N. L., Reed, S. C., and Cleveland, C. C.: Biological nitrogen fixation: rates, patterns and ecological controls in terrestrial ecosystems, Philos. Trans. R. Soc. B Biol. Sci., 368, 20130119, https://doi.org/10.1098/rstb.2013.0119, 2013.

Uitrijregeling: https://www.vlm.be/nl/themas/Mestbank/bemesting/aanwenden-van-mest/uitrijregeling/Paginas/default.aspx.

Uitrijregeling volgens type meststof: https://www.vlm.be/nl/themas/Mestbank/bemesting/aanwenden-van-mest/uitrijregeling/uitrijregeling-volgens-type-meststof/Paginas/default.aspx.

Volten, H., Bergwerff, J. B., Haaima, M., Lolkema, D. E., Berkhout, A. J. C., van der Hoff, G. R., Potma, C. J. M., Wichink Kruit, R. J., van Pul, W. A. J., and Swart, D. P. J.: Two instruments based on differential optical absorption spectroscopy (DOAS) to measure accurate ammonia concentrations in the atmosphere, Atmos. Meas. Tech., 5, 413–427, https://doi.org/10.5194/amt-5-413-2012, 2012.

de Vries, W.: Impacts of nitrogen emissions on ecosystems and human health: A mini review, Curr. Opin. Environ. Sci. Heal., 21, 100249, https://doi.org/10.1016/J.COESH.2021.100249, 2021.

de Vries, W., Leip, A., Reinds, G. J., Kros, J., Lesschen, J. P., and Bouwman, A. F.: Comparison of land nitrogen budgets for European agriculture by various modeling approaches, Environ. Pollut., 159, 3254–3268, https://doi.org/10.1016/j.envpol.2011.03.038, 2011.

de Vries, W., Dobbertin, M. H., Solberg, S., van Dobben, H. F., and Schaub, M.: Impacts of acid deposition, ozone exposure and weather conditions on forest ecosystems in Europe: an overview, Plant Soil, 380, 1–45, https://doi.org/10.1007/s11104-014-2056-2, 2014.

de Vries, W., Kros, J., Dolman, M. A., Vellinga, T. V., de Boer, H. C., Gerritsen, A. L., Sonneveld, M. P. W., and Bouma, J.: Environmental impacts of innovative dairy farming systems aiming at improved internal nutrient cycling: A multi-scale assessment, Sci. Total Environ., 536, 432–442, https://doi.org/10.1016/j.scitotenv.2015.07.079, 2015.

de Vries, W., Schulte-Uebbing, L., Kros, H., Voogd, J. C., and Louwagie, G.: Spatially explicit boundaries for agricultural nitrogen inputs in the European Union to meet air and water quality targets, Sci. Total Environ., 786, 147283, https://doi.org/10.1016/J.SCITOTENV.2021.147283, 2021.

de Vries, W., Schulte-Uebbing, L., Kros, H., and Voogd, J. C.: Assessment of spatially explicit actual, required and critical nitrogen inputs in EU-27 agriculture, Wageningen Environmental Research, Netherlands, https://doi.org/10.18174/578175, 2022.

de Vries, W., Kros, J., Voogd, J. C., and Ros, G. H.: Integrated assessment of agricultural practices on large scale losses of ammonia, greenhouse gases, nutrients and heavy metals to air and water, Sci. Total Environ., 857, 159220, https://doi.org/10.1016/j.scitotenv.2022.159220, 2023.

De Vries, W., Schulte-Uebbing, L., and Kros, J.: Assessment of spatially explicit actual, required and critical nitrogen inputs in EU-27 agriculture (in press), Wageningen, 2020a.

De Vries, W., Schulte-Uebbing, L., and Kros, J.: Spatially explicit needed increase in nitrogen use efficiency in European agricultural soils in view of air and water quality, 2020b.

Waldhoff, G., Lussem, U., and Bareth, G.: Multi-Data Approach for remote sensing-based regional crop rotation mapping: A case study for the Rur catchment, Germany, Int. J. Appl. Earth Obs. Geoinf., 61, 55–69, https://doi.org/10.1016/j.jag.2017.04.009, 2017.

Walker, J. T., Beachley, G., Amos, H. M., Baron, J. S., Bash, J., Baumgardner, R., Bell, M. D., Benedict, K. B., Chen, X., Clow, D. W., Cole, A., Coughlin, J. G., Cruz, K., Daly, R. W., Decina, S. M., Elliott, E. M., Fenn, M. E., Ganzeveld, L., Gebhart, K., Isil, S. S., Kerschner, B. M., Larson, R. S., Lavery, T., Lear, G. G., Macy, T., Mast, M. A., Mishoe, K., Morris, K. H., Padgett, P. E., Pouyat, R. V, Puchalski, M., Pye, H. O. T., Rea, A. W., Rhodes, M. F., Rogers, C. M., Saylor, R., Scheffe, R., Schichtel, B. A., Schwede, D. B., Sexstone, G. A., Sive, B. C., Sosa Echeverría, R., Templer, P. H., Thompson, T., Tong, D., Wetherbee, G. A., Whitlow, T. H., Wu, Z., Yu, Z., and Zhang, L.: Toward the improvement of total nitrogen deposition budgets in the United States., Sci. Total Environ., 691, 1328–1352, https://doi.org/10.1016/j.scitotenv.2019.07.058, 2019.

Walther, G.-R., Post, E., Convey, P., Menzel, A., Parmesan, C., Beebee, T. J. C., Fromentin, J.-M., Hoegh-Guldberg, O., and Bairlein, F.: Ecological responses to recent climate change, Nature, 416, 389–395, https://doi.org/10.1038/416389a, 2002.

Wang, D., Wan, B., Qiu, P., Su, Y., Guo, Q., Wang, R., Sun, F., and Wu, X.: Evaluating the Performance of Sentinel-2, Landsat 8 and Pléiades-1 in Mapping Mangrove Extent and Species, Remote Sens., 10, https://doi.org/10.3390/rs10091468, 2018.

Wang, Y., Dong, H., Zhu, Z., Gerber, P. J., Xin, H., Smith, P., Opio, C., Steinfeld, H., and Chadwick, D.: Mitigating Greenhouse Gas and Ammonia Emissions from Swine Manure Management: A System Analysis, Environ. Sci. Technol., 51, 4503–4511, https://doi.org/10.1021/acs.est.6b06430, 2017.

Warner, J. X., Wei, Z., Strow, L. L., Dickerson, R. R., and Nowak, J. B.: The global tropospheric ammonia distribution as seen in the 13-year AIRS measurement record, Atmos. Chem. Phys., 16, 5467–5479, https://doi.org/10.5194/acp-16-5467-2016, 2016.

Webb, J. and Misselbrook, T. H.: A mass-flow model of ammonia emissions from UK livestock production, Atmos. Environ., https://doi.org/10.1016/j.atmosenv.2004.01.023, 2004.

Webb, J., Pain, B., Bittman, S., and Morgan, J.: The impacts of manure application methods on emissions of ammonia, nitrous oxide and on crop response—A review, Agric. Ecosyst. Environ., 137, 39–46, https://doi.org/10.1016/J.AGEE.2010.01.001, 2010.

R

Weijers, E. P., Schaap, M., Nguyen, L., Matthijsen, J., van der Gon, H. A. C., ten Brink, H. M., and Hoogerbrugge, R.: Anthropogenic and natural constituents in particulate matter in the Netherlands, Atmos. Chem. Phys., 11, 2281–2294, https://doi.org/10.5194/acp-11-2281-2011, 2011.

Werner, M., Kryza, M., Geels, C., Ellermann, T., and Skjøth, C. A.: Spatial, temporal and vertical distribution of ammonia concentrations over Europe -- comparing a~static and dynamic approach with WRF-Chem, Atmos. Chem. Phys. Discuss., 15, 22935–22973, https://doi.org/10.5194/acpd-15-22935-2015, 2015a.

Werner, M., Skjøth, C. A., Kryza, M., and Dore, A. J.: Understanding emissions of ammonia from buildings and the application of fertilizers: an example from Poland, Biogeosciences, 12, 3623–3638, https://doi.org/10.5194/bg-12-3623-2015, 2015b.

Wever, D., Coenen, P., Dröge, R., Geilenkirchen, G. P., 't Hoen, M., Honig, E., WWR, K., Leekstra, A. J., Lagerwerf, L. A., te Molder, R. A. B., Peek, C. J., Smeets, W. L. M., van der Sluis, S. M., and Vonk, J.: Informative Inventory Report 2019 : Emissions of transboundary air pollutants in the Netherlands 1990-2017, https://doi.org/10.21945/RIVM-2019-0016, 2019.

Whalen, J. K., Thomas, B. W., and Sharifi, M.: Chapter One - Novel Practices and Smart Technologies to Maximize the Nitrogen Fertilizer Value of Manure for Crop Production in Cold Humid Temperate Regions, vol. 153, edited by: Sparks, D. L. B. T.-A. in A., Academic Press, 1–85, https://doi.org/10.1016/bs.agron.2018.09.002, 2019.

Whitburn, S., Van Damme, M., Clarisse, L., Bauduin, S., Heald, C. L., Hadji-Lazaro, J., Hurtmans, D., Zondlo, M. A., Clerbaux, C., and Coheur, P.-F.: A flexible and robust neural network IASI-NH3 retrieval algorithm, J. Geophys. Res. Atmos., 121, 6581–6599, https://doi.org/10.1002/2016JD024828, 2016.

Whitehead, D. C. and Raistrick, N.: The volatilization of ammonia from cattle urine applied to soils as influenced by soil properties, Plant Soil, https://doi.org/10.1007/BF02185383, 1993.

Wichink Kruit, R. J., van Pul, W. A. J., Sauter, F. J., van den Broek, M., Nemitz, E., Sutton, M. A., Krol, M., and Holtslag, A. A. M.: Modeling the surface-atmosphere exchange of ammonia, Atmos. Environ., 44, 945–957, https://doi.org/10.1016/j.atmosenv.2009.11.049, 2010.

Wichink Kruit, R. J., Schaap, M., Sauter, F. J., Van Zanten, M. C., and Van Pul, W. A. J.: Modeling the distribution of ammonia across Europe including bi-directional surface-atmosphere exchange, Biogeosciences, 9, 5261–5277, https://doi.org/10.5194/bg-9-5261-2012, 2012.

Wichink Kruit, R. J., Aben, J., de Vries, W., Sauter, F., van der Swaluw, E., van Zanten, M. C., and van Pul, W. A. J.: Modelling trends in ammonia in the Netherlands over the period 1990–2014, Atmos. Environ., 154, 20–30, https://doi.org/10.1016/j.atmosenv.2017.01.031, 2017.

Williams, M. W. and Tonnessen, K. A.: CRITICAL LOADS FOR INORGANIC NITROGEN DEPOSITION IN THE COLORADO FRONT RANGE, USA, Ecol. Appl., 10, 1648–1665, https://doi.org/10.1890/1051-0761(2000)010[1648:CLFIND]2.0.CO;2, 2000.

Willmott, C. J.: On The Validation of Models, Phys. Geogr., 2, 184–194, https://doi.org/10.1080/02723646.1981.10642213, 1981.

Wu, C., Wang, G., Li, J., Li, J., Cao, C., Ge, S., Xie, Y., Chen, J., Liu, S., Du, W., Zhao, Z., and Cao, F.: Non-agricultural sources dominate the atmospheric NH3 in Xi'an, a megacity in the semi-arid region of China, Sci. Total Environ., 722, 137756, https://doi.org/10.1016/j.scitotenv.2020.137756, 2020.

Wulder, M. A., Hilker, T., White, J. C., Coops, N. C., Masek, J. G., Pflugmacher, D., and Crevier, Y.: Virtual constellations for global terrestrial monitoring, Remote Sens. Environ., 170, 62–76, https://doi.org/10.1016/j.rse.2015.09.001, 2015.

Wulder, M. A., Hermosilla, T., White, J. C., Hobart, G., and Masek, J. G.: Augmenting Landsat time series with Harmonized Landsat Sentinel-2 data products: Assessment of spectral correspondence, Sci. Remote Sens., 4, 100031, https://doi.org/10.1016/j.srs.2021.100031, 2021.

Wyer, K. E., Kelleghan, D. B., Blanes-Vidal, V., Schauberger, G., and Curran, T. P.: Ammonia emissions from agriculture and their contribution to fine particulate matter: A review of implications for human health, J. Environ. Manage., 323, 116285, https://doi.org/10.1016/j.jenvman.2022.116285, 2022.

Xue, J. and Su, B.: Significant Remote Sensing Vegetation Indices: A Review of Developments and Applications, J. Sensors, 2017, 1353691, https://doi.org/10.1155/2017/1353691, 2017.

Yan, S., Yao, X., Zhu, D., Liu, D., Zhang, L., Yu, G., Gao, B., Yang, J., and Yun, W.: Large-scale crop mapping from multi-source optical satellite imageries using machine learning with discrete grids, Int. J. Appl. Earth Obs. Geoinf., 103, 102485, https://doi.org/10.1016/j.jag.2021.102485, 2021.

Yi, Z., Jia, L., and Chen, Q.: Crop Classification Using Multi-Temporal Sentinel-2 Data in the Shiyang River Basin of China, Remote Sens., 12, https://doi.org/10.3390/rs12244052, 2020.

van Zanten, M. C., Wichink Kruit, R. J., Hoogerbrugge, R., Van der Swaluw, E., and van Pul, W. A. J.: Trends in ammonia measurements in the Netherlands over the period 1993–2014, Atmos. Environ., 148, 352–360, https://doi.org/10.1016/j.atmosenv.2016.11.007, 2017.

Zavyalov, V., Esplin, M., Scott, D., Esplin, B., Bingham, G., Hoffman, E., Lietzke, C., Predina, J., Frain, R., Suwinski, L., Han, Y., Major, C., Graham, B., and Phillips, L.: Noise performance of the CrIS instrument, J. Geophys. Res. Atmos., 118, 13,108-13,120, https://doi.org/10.1002/2013JD020457, 2013.

Zhang, L., Vet, R., O'Brien, J. M., Mihele, C., Liang, Z., and Wiebe, A.: Dry deposition of individual nitrogen species at eight Canadian rural sites, J. Geophys. Res. Atmos., 114, https://doi.org/10.1029/2008JD010640, 2009.

Zimmermann, J., Fealy, R. M., Lydon, K., Mockler, E. M., O'Brien, P., Packham, I., Smith, G., and Green, S.: The Irish Land-Parcels Identification System (LPIS)–Experiences in ongoing and recent environmental research and land cover mapping, Biol. Environ. Proc. R. Irish Acad., 116B, 53–62, https://doi.org/10.3318/bioe.2016.04, 2016.

Zimmermann, P. H., Feichter, J., Rath, H. K., Crutzen, P. J., and Weiss, W.: A global three-dimensional source-receptor model investigation using 85Kr, Atmos. Environ., 23, 25–35, https://doi.org/10.1016/0004-6981(89)90094-2, 1989.

Zöll, U., Brümmer, C., Schrader, F., Ammann, C., Ibrom, A., Flechard, C. R., Nelson, D. D., Zahniser, M., and Kutsch, W. L.: Surface--atmosphere exchange of ammonia over peatland using QCL-based eddy-covariance measurements and inferential modeling, Atmos. Chem. Phys., 16, 11283–11299, https://doi.org/10.5194/acp-16-11283-2016, 2016.

R

Appendix

Supplementary material to Chapter 2:
Modeling atmospheric ammonia using agricultural emissions with improved spatial variability and temporal dynamics

S2.1 Statistical indices used to assess the performance of the models

To evaluate the performance of the updated model and compare it with that of the original model, we calculated the normalized root mean square error (NRMSE), the normalized mean absolute error (NMAE), the model efficiency (EF) and the index of agreement between the modeled results (predictions) and measurements.

The root mean square error of n predicted values of a regression's dependent variable, with $\hat{y}_i$ being the i-th prediction and y_i being the i-th estimate, is computed as the square root of the mean of the squares of the deviations:

$$\text{RMSE} = \sqrt{\frac{\sum_{i=1}^{n}(\hat{y}_i - y_i)^2}{n}}$$

(Eq. S2.1)

The NRMSE indicates RMSE in a relative sense, by dividing RMSE by the difference between the maximum and minimum observed values:

$$\text{NRMSE} = \frac{\text{RMSE}}{y_{max} - y_{min}}$$

(Eq. S2.2)

The normalized mean Absolute Error (MAE) is interpreted as the average absolute difference between y_i and $\hat{y}_i$, with reference to the mean of observations:

$$NMAE = \frac{\sum_{i=1}^{n}|\hat{y}_i - y_i|}{n} / \bar{y}$$

(Eq. S2.3)

The model efficiency coefficient is used to illustrate predictive power. It can range from $-\infty$ to 1. An efficiency of 1 indicates a perfect match of simulations to observations (Ritter and Muñoz-Carpena, 2013). The closer the model efficiency is to 1, the more accurate the model is.

$$EF = 1 - \frac{\sum_{i=1}^{n}(\hat{y}_i - y_i)^2}{\sum_{i=1}^{n}(y_i - \bar{y})^2}$$

(Eq. S2.4)

Last but not least, the index of agreement (d) statistic was also employed, which represents the ratio of the mean square error and the potential error (Willmott, 1981). The agreement value of 1 indicates a perfect match, and 0 indicates no agreement at all. However, it is overly sensitive to extreme values due to the squared differences (Willmott, 1981).

$$d = 1 - \frac{\sum_{i=1}^{n}(\hat{y}_i - y_i)^2}{\sum_{i=1}^{n}(|\hat{y}_i - \bar{y}| + |y_i - \bar{y}|)^2}$$

(Eq. S2.5)

A

S2.2 Methodology to allocate manure application over grassland and arable crop groups

In the INTEGRATOR model, manure is distributed over grassland and different crop groups using various allocation rules. Manure produced by grazing animals and in housing systems by sheep and goats all enters grassland. For other manure, a fraction is applied to arable land and the remaining fraction is applied to grassland/fodder crops, distinguishing (i) liquid manure of dairy cattle, other cattle and pigs, (ii) solid manure of dairy cattle, other cattle and pigs and (iii) poultry manure. For the distribution of manure application on arable land, we distinguish three arable crop groups with (i) a relatively high use of manure (sugar beet, barley, rape, and soft wheat), (ii) an intermediate use of manure (potatoes, durum wheat, rye, oats, grain maize, other cereals including triticale, and sunflower), and (iii) low use of manure (fruits, citrus, olives, oil crops, citrus, grapes and other crops) using weighing, based on Velthof et al. (2009). Finally, no manure is allocated to dry pulses and rice, fiber crops, other root crops and vegetables.

As the last step, mineral fertilizer is distributed over crops on country level using a balanced N fertilization approach:

1. The total N demand in a NUTS 2 region is calculated as the sum of N in harvested products and in crop residues. The N in harvested crops is calculated from the crop yield and the N content in crop yield. The yields of arable crops for each country were derived from FAOSTAT on a country basis, and the N contents of harvested crop products were based on literature. The N in crop residues is calculated by dividing the N removed in harvest with an N index.
2. The fertilizer N demand of each crop was calculated by subtracting the non-fertilizer N input from the total N demand and then divided by the N use efficiency (NUE).
3. The N fertilizer estimates for each NUTS 2 region were aggregated at country level and compared with reported country-level N fertilizer consumption. Scaling factors (the ratio of the known and calculated country-level N fertilizer consumption) were then applied to ensure consistency.

S2.3 Fertilizer and crop categorization in the MACC-INTEGRATOR combined emission inventory
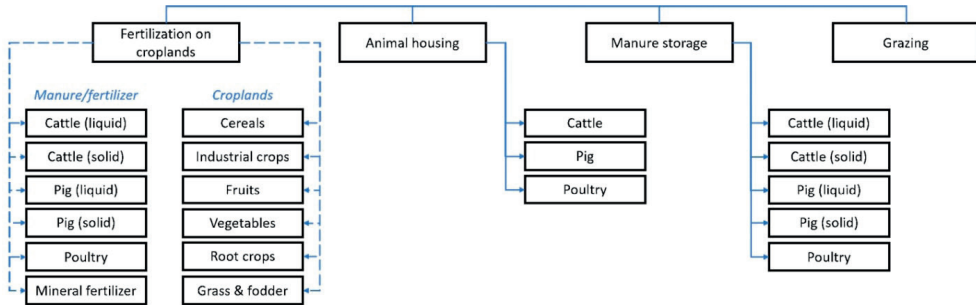
Figure S2.1 Categorization in the MACC-INTEGRATOR combined emission inventory. There are six fertilizer types and six crop types, resulting in 36 categories regarding fertilization. Together with three animal housing types, five manure storage types, and grazing, there are 45 categories in the new NH$_3$ emission model.

S2.4 Calculation of the temporal variation of ammonia emission due to grazing, animal housing and manure storage

For the temporal variation of NH_3 emission from fertilization on grassland, we used the parameterizations of Skjøth et al. (2004) for Danish conditions using a gauss-function as given below:

$$\begin{cases} F_{grass} = E(x,y) \times e^{0.0223T(t)} e^{0.0419W(t)} \times \dfrac{e^{(\frac{(t-\mu)^2}{-2\sigma^2})}}{\sigma\sqrt{2\pi}} \\ \mu = T_{sum1400}(x,y) + 4 \end{cases} \quad \text{(Eq. S2.6)}$$

where t is the actual time of the year, $E(x,y)$ is the total emission from fertilization on grassland within a grid cell, μ is the mean value for the Gaussian distribution, T(t) is the air temperature in Celsius, W(t) is the wind speed (m/s) for the applied time step (t). μ is the Julian day on which the thermal sum reaches 1400, except that the starting day of thermal time calculation is 1st March, instead of 1st January. μ depends on local climatology, so it differs from grid cell to grid cell. σ is the spread of the gauss function and is equated to 60 days, which means that grazing occurs in a relatively long period of time.

Regarding emissions from grazing on grassland, it is generally dependent on the release time of the cattle, the availability of grass, and the length of the growing season (Gyldenkærne et al., 2005). The availability of grass is then primarily a function of precipitation, soil humidity, soil fertility, and fertilization. For a region that has a relatively even distribution of the precipitation during summer, such as the study area in this paper,

Gyldenkærne et al. (2005) suggested that a model following grass growth could be used to represent the characteristics of grazing emissions. Therefore, as the work of Skjøth et al. (2004), here emission from grazing is assumed to follow the same pattern as grown grass in Eq. S2.6.

Emission patterns from animal housing and manure storage are based on Skjøth et al. (2011)and Gyldenkærne et al. (2005) as given below:

$$
\begin{cases}
Fkt_i = \frac{E_i(x,y)}{Epot_i(x,y)} \times (T_i(x,y))^{0.89}, & T_i(x,y) \geq T_{boundary} \\
T_i(x,y) = \begin{cases} 18 + 0.77 \times (T(x,y) - 12.5), & \textit{Insulated houses} \\ T(x,y) + 3, & \textit{Open houses} \\ T(x,y), & \textit{Manure storage} \end{cases}
\end{cases}
\qquad \text{(Eq. S2.7)}
$$

where i refers to the index (1-3) of insulated housing, open housing and manure storage, respectively. x, y are the coordinates of the emission grid. $E_i(x,y)$ represents the emission for the corresponding agricultural sector within the grid cell. $Epot_i(x,y)$ is a constant emission potential scaling factor for a given grid cell and can be neglected for simplicity (Elzing and Monteny, 1997). $T_i(x,y)$ is temperature function which is different for housing, open housing and manure storage. $T(x,y)$ is the 2-meter temperature at the given location and is obtained from the ECMWF data portal. It can be seen from Eq. S2.7 that open houses and manure storage have almost the same emission pattern except that the indoor temperature in open houses is 3 degrees higher than the outside temperature used for manure storage (Gyldenkærne et al., 2005). $T_{boundary}$ represents lower boundary condition for temperature in animal housing and manure storage, below which emission is set to a constant level, and they are 18, 4, and 1 degree, respectively.

Pigs and poultry have a high lower critical temperature (LCT) between 6 to 20 degrees, below which an animal must expend additional energy to maintain normal body temperature and essential body functions. So in colder climates, they are usually kept in insulated buildings with forced ventilation to maintain a fixed temperature throughout the year (Seedorf et al., 1998b). On the contrary, cattle have a very low LCT and are therefore often kept in open barns (Seedorf et al., 1998a). However, there still might be some insulated cattle barns with forced ventilation in colder climates (Gyldenkærne et al., 2005). Consequently, the function for forced ventilation is used to represent the temporal variation of pig and poultry housing emission, while the mean of functions of insulated houses with forced ventilation and open houses is calculated to characterize cattle housing emission. In terms of manure storage, it is assumed that the emissions from manure storage of all animal types have the same pattern.

S2.5 Comparison of sowing day estimates

Comparisons between sowing days calculated in this study and by Hutchings et al. (2012) were made for verification. Figure S2.2 depicts an example of the calculated sowing days of potatoes. Only the dates for years between 1985 and 2000 are selected for comparison because Hutchings et al. (2012) used predicted temperature data for years after 2000. The sowing days are in good alignment with only a few outliers away from line y=x.
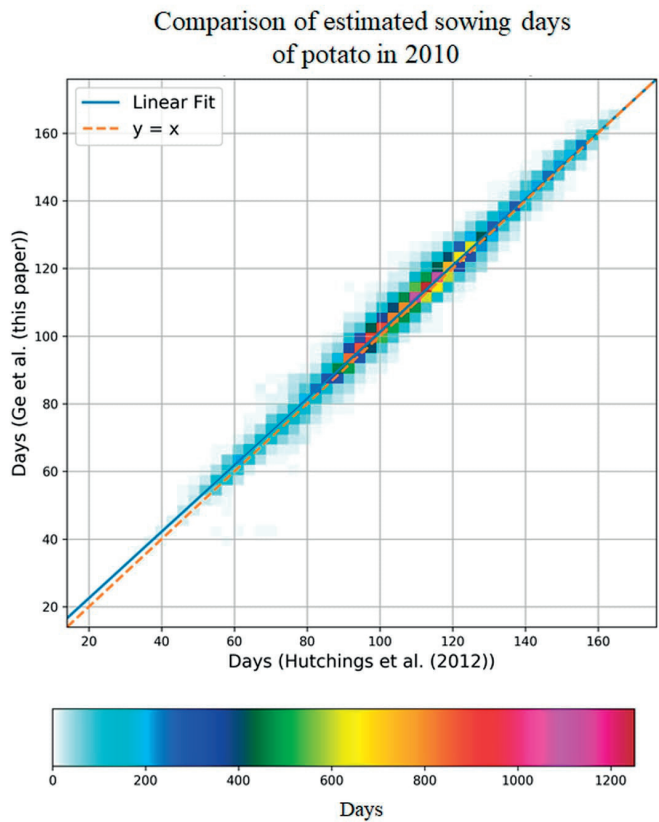

Figure S2.2 The density plot comparing sowing day estimates of potato between 1985 and 1995 by Hutchings et al. (2012) (x-axis) and in this study (y-axis).

S2.6 Spatial variation in sowing day estimates for winter wheat and spring wheat

Figure S2.3 shows that the sowing days of winter wheat and spring wheat generally have the opposite trends. For winter wheat, even though the differences between daily mean temperature and the base temperature are larger in the south, the greater reference thermal sum makes it take a longer time to reach this thermal sum. Whereas for spring wheat, the reference thermal sum in the south is less than that in the north, resulting in earlier sowing day than in the north.
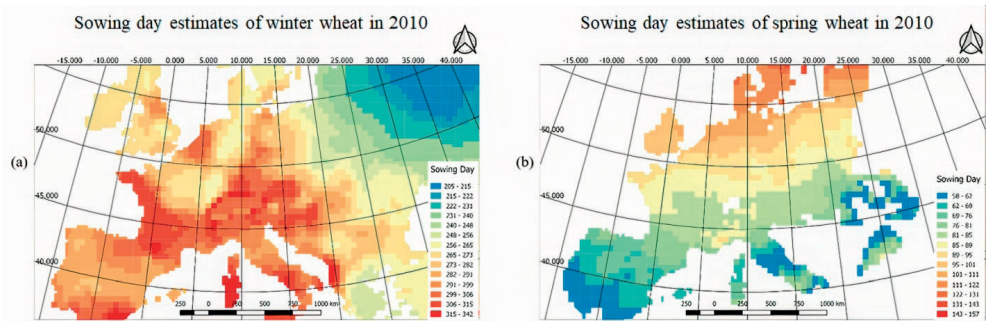

Figure S2.3 Two examples of estimated sowing days over Europe from the TIMELINES model for winter wheat (a) and spring wheat (b) in 2010.

## S2.7 Time series of the weekly De Martonne-Index

Figure S2.4 shows that the weekly De Martonne-Index at location coordinate (48.98, 8.14) approximately ranges between 0 and 6.5 in 2010. High indices are observed around Day 30 before the first spring application period as well as at the end of the year. On these occasions, the index reaches values well above 3.
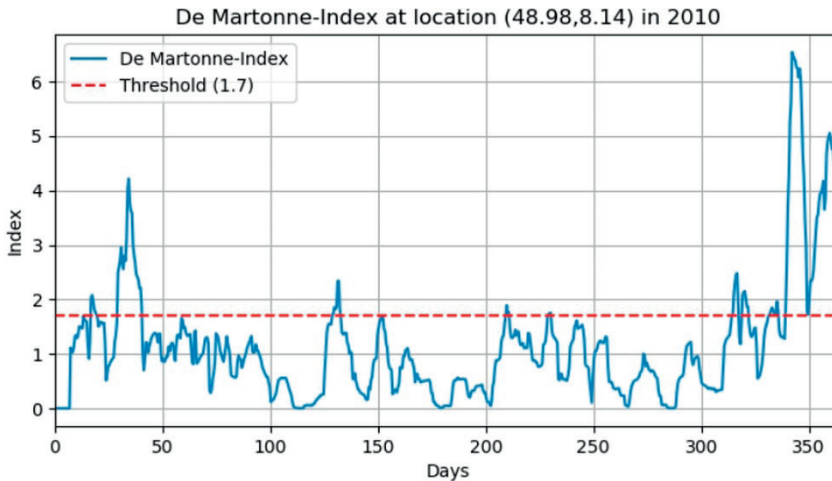
Figure S2.4 An example of the time series of the weekly De Martonne-Index at (48.98, 8.14). A threshold of 1.7 is determined, above which precipitation is considered to be excessive.

A

S2.8 Examples of ammonia emission time profiles

Examples of NH_3 emission time profiles during development at the location (47.41°*N*, 10.98°*E*) in latitude/longitude in 2010 are presented in Fig. H1. The left panel represents time profiles of the application of cattle liquid manure on cereals, while the right panel demonstrates that of pig liquid manure application on grass and fodder. Four rows indicate the four phases during the development of the time profiles. First and foremost, the initial emission time profiles (first row) in both panels were obtained using fertilization day estimation from TIMELINES and the emission function in Eq. (2.1), taking into account local climatology including temperature and wind speed. Subsequently, the emission strengths of Sundays were set to baseline since manure and fertilizer application were prohibited, as is shown in the second row. Furthermore, in the third row, prohibition on fertilization after late fall and before early spring (exact dates vary from country to country) did not affect the time profile on the left panel since the emission function lies within the period where fertilization is allowed. However, for the right panel, part of the third peak exceeded the last allowed date for application. Thus, the part outside the application ban was cut out, and the rest of the peak was scaled accordingly. Finally, the impact of excessive rain on emission was accounted for in the last row. On each day where the De Martonne-Index exceeded the threshold 1.7, the emission curve before this day remained as it is, while the rest was shifted to the next possible day. It is possible that in the final time profile, emission lies slightly outside the permitted period for fertilization. However, it is allowed under the assumption that the government allows a delay in manure and fertilizer application due to weather.
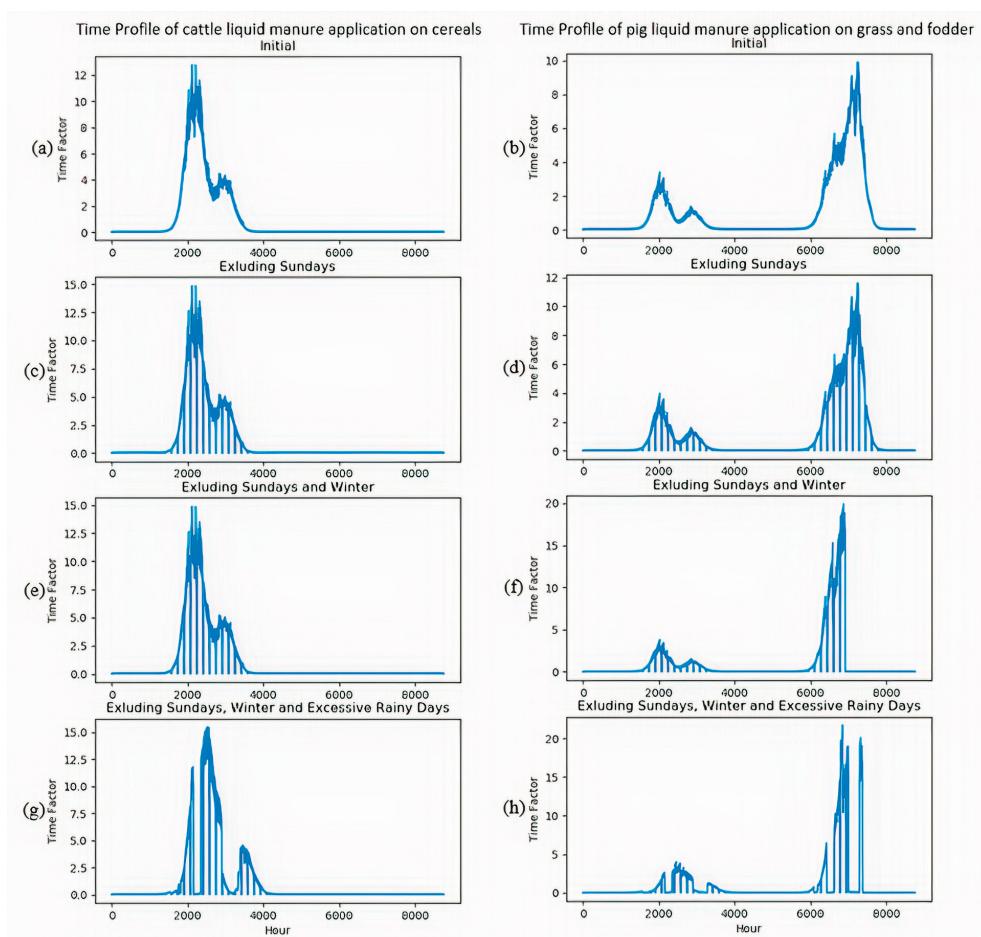
Figure S2.5 Two examples of NH_3 emission time profile during the four phases of development at location (47.41, 10.98) in latitude/longitude: cattle slurry application on cereals (left panel), and pig liquid manure application on grass and fodder (right panel).

A

S2.9 Land use information of the selected in situ measurement sites

Table S2.1 Information on the selected in situ measurement sites.

Station Code	Network	Latitude	Longitude	Existing Land Use
DEUB028	UBA	54.44	12.72	Cereal, industrial crop, grassland, manure storage, animal housing
DEUB005	UBA	52.8	10.76	Cereal, root crop, industrial crop, grassland, manure storage, animal housing
DENI054	UBA	52.36	9.71	Cereal, root crop, industrial crop, grassland, manure storage, animal housing
DEBY151	UBA	47.81	10.72	Grassland, manure storage, animal housing
NL63-4	MAN	51.40	5.66	Grassland, manure storage, animal housing

S2.10 Monthly statistics and spatial distribution of the number of valid IASI measurements
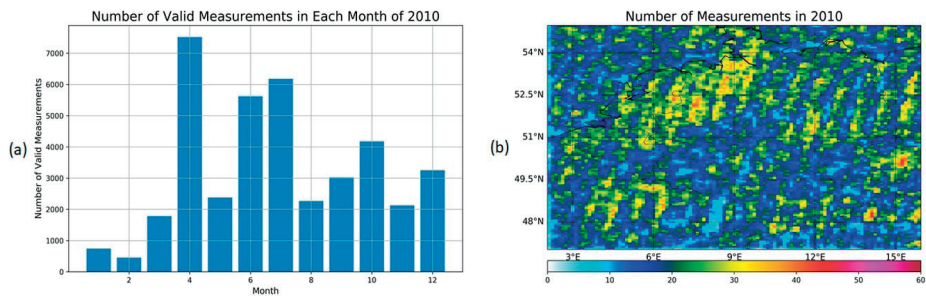

Figure S2.6 The bar plot of the number of IASI measurements as a function of measuring month (a). The spatial distribution of the number of valid IASI measurements (b).

Supplementary material to Chapter 4:
Improving spatial and temporal variation of ammonia emissions for the Netherlands using livestock housing information and a Sentinel-2-derived crop map

S4.1 The Sentinel-2 twin satellites
Until quite recently, the low spatiotemporal information of satellite data made large-scale crop mapping challenging. Since 2015, Sentinel-2 twin satellites (launched in 2015 and 2017) have been providing global data with a swath width of 290 km and a revisit time of five days at the equator (Claverie et al., 2018; Van Tricht et al., 2018). The optical sensor (MSI) on the satellites covers 13 spectral bands (443–2190 nm) from visible to shortwave infrared, as well as three spectral bands in the red-edge region, centered at 705 nm, 740 nm, and 783 nm (Wang et al., 2018; Drusch et al., 2012). The spatial resolution of satellite data is 10 m (visible bands 2–4, and near-infrared band 8), 20 m (six red edge and shortwave infrared bands 5–7, 8a, and 11–12), and 60 m (three atmospheric correction bands 1 and 9–10) (Pasqualotto et al., 2019; Verrelst et al., 2015). Recent studies have proven the feasibility of the application of Sentinel-2 to study vegetation phenology and growth (Immitzer et al., 2016; Palchowdhuri et al., 2018; Ng et al., 2017), above-ground biomass of grasslands (Shoko et al., 2018), forest growing stock volume (Mura et al., 2018) and forest fires (Navarro et al., 2017).

S4.2 The advantages of various vegetation indices
Table S1 shows the vegetation indices used in this study for crop mapping and their advantages. The most common index may be the Normalized Difference Vegetation Index (NDVI) (Rouse J. W. et al., 1974). The Green Normalized Difference Vegetation Index (GNDVI), replacing the red band with the green band in NDVI calculation, is more sensitive to variation in chlorophyll content than NDVI (Gitelson et al., 1996). Similar to GNDVI, The Normalized Difference Infrared Index (NDII) uses the B11 infrared band instead of the green band, making it sensitive to changes in the water content of plant canopies. Empirically derived normalized differential products have been unstable due to soil, atmosphere effects, and saturation effects of high-density vegetation. Therefore, a few indices that counter these effects were also included. The Soil Adjusted Vegetation Index (SAVI) minimizes soil brightness influences (Huete, 1988). The Enhanced Vegetation Index (EVI) outperforms the NDVI in high biomass areas where NDVI values are saturated (Huete et al., 2002). The Green Atmospherically Resistant Index (GARI) counters the effects of atmospheric interference, demonstrating much higher sensitivity to chlorophyll content and lower sensitivity to atmospheric interference (Gitelson et al., 1996). The Visible Atmospherically Resistant Index (VARI) mitigates illumination differences and atmospheric effects by emphasizing vegetation in the visible portion of the spectrum, which is ideal

for RGB or color images. The Atmospheric Reflection Vegetation Index (ARVI) eliminates atmospheric disturbances (Kaufman and Tanre, 1992).

In addition, the Green Leaf Index (GLI) indicates the greenness using RGB bands in aerial and satellite imagery. Ranging from -1 to +1, GLI indicates soil and non-living features when negative, and green leaves and stems when positive. The Excess Green Index (ExGI) contrasts the green portion of the spectrum against red and blue to distinguish vegetation from the soil. Larrinaga and Brotons (2019) show that it does better than other indices in distinguishing vegetation. Ratio Vegetation Index (RVI) (Jordan, 1969) can be used to estimate and monitor above-ground biomass, especially in densely vegetated areas. However, it is sensitive to atmospheric effects when vegetation cover is less than 50% (Xue and Su, 2017).

Table S4.1 Description of the vegetation indices used in machine learning.

Abbreviation	Name	Derivation	Advantage
NDVI (Rouse J. W. et al., 1974)	Normalized Difference Vegetation Index	$\dfrac{B08 - B04}{B08 + B04}$	Distinguishes different stages of plants from other objects
GNDVI (Gitelson et al., 1996)	Green Normalized Difference Vegetation Index	$\dfrac{B08 - B03}{B08 + B03}$	Sensitive to variation in chlorophyll content
NDII (Hardisky et al., 1983)	Normalized Difference 819/1600	$\dfrac{B08 - B11}{B08 + B11}$	Sensitive to changes in the water content of plant canopies
SAVI (Huete, 1988)	Soil Adjusted Vegetation Index	$1.5 * \dfrac{B08 - B04}{B08 + B04 + 0.5}$	Minimizes soil brightness influences
EVI (Huete et al., 2002)	Enhanced Vegetation Index	$2.5 * \dfrac{B08 - B04}{B08 + 6 * B04 - 7.5 * B02 + 1}$	Outperforms NDVI in areas of high biomass
GARI (Gitelson et al., 1996)	Green Atmospherically Resistant Vegetation Index	$\dfrac{B08 - [B03 - (B02 - B04)]}{B08 - [B03 + (B02 - B04)]}$	Sensitive to chlorophyll content and insensitive to atmospheric interference
VARI (Gitelson et al., 2001)	Visible Atmospherically Resistant Index	$\dfrac{B05 - 1.7 * B04 + 0.7 * B02}{B05 + 2.3 * B04 - 1.3 * B02}$	Mitigates illumination differences and atmospheric effects
ARVI (Kaufman and Tanre, 1992)	Atmospherically Resistant Vegetation Index	$\dfrac{B08 - [B04 - (B02 - B04)]}{B08 + [B04 - (B02 - B04)]}$	Eliminates atmospheric disturbances
GLI (Gobron et al., 2000)	Green Leaf Index	$\dfrac{2 * B03 - B05 - B02}{2 * B03 + B05 + B02}$	Distinguishes green leaves and stems from soil and non-living features
ExGI (Larrinaga and Brotons, 2019)	Excess Green Index	$2 * B03 - B04 - B02$	Distinguishes vegetation from soil
RVI (Jordan, 1969; Xue and Su, 2017)	Simple Ratio 800/670 Ratio Vegetation Index	$\dfrac{B08}{B04}$	Sensitive to above-ground biomass, especially in densely vegetated areas

A

S4.3 Examples of NDVI and EVI time series of the ground truth polygons of grassland and maize

Figure S4.1 demonstrates two examples, i.e., the NDVI and EVI time series of the ground truth polygons of grassland and maize in 2018. One can see that even though the parcels of each crop are located in different locations, the same crop type shares similarities in the temporal variability of the features.
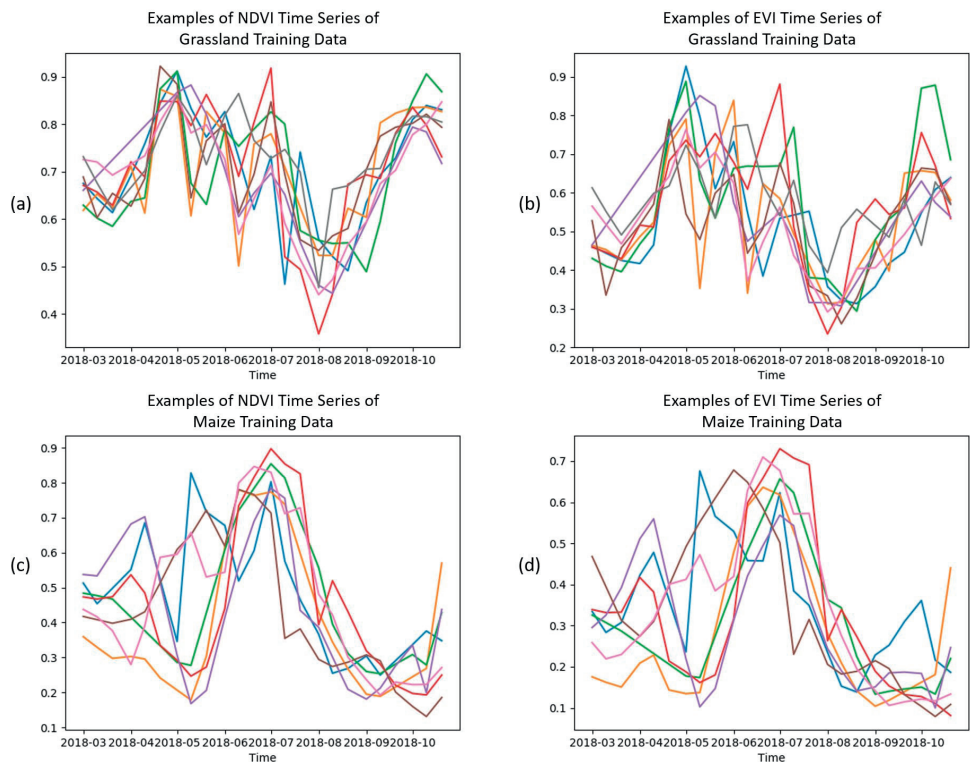
Figure S4.1 Examples of NDVI and EVI time series of grassland and maize training data. Lines of different colors represent individual land parcel.

For grassland, NDVI values (Figure S4.1 (a)) varied between 0.4 (August) and 0.9 (May/October), whereas EVI (Figure S4.1 (b)) values ranged from 0.3 (August) to 0.9 (May). The trends for both indices were similar. The values first increased from March to May, reaching the peak because grass started growing and showing more greenness in this period. Then they dropped between May and August to the lowest point, possibly due to mowing or the drought in 2018. Afterward, they climbed again up to the second peak in October, which adequately characterizes the regrowth period for summer grasses. Regarding maize, NDVI values (Figure S4.1 (c)) varied between 0.2 (May/October) and 0.9 (July), and the EVI (Figure S4.1 (d)) values ranged from 0.1 (May/October) to 0.7 (July). The trends of

the two indices were different from those of grassland. The two indices slightly decreased from March to May, and then they ascended dramatically to the peak in July. The slight decrease in the early year might be related to plowing, after which bare soil is exposed on the surface. The drastic jump represents the growing season of maize. In the end, the values gradually decreased to the bottom due to harvest.

S4.4 Validation of crop map by official provincial crop area data

Figure S4.2 shows the distribution of the crop areas across the Dutch provinces for the top four arable crops by area and grassland. Inspecting the variability between the provinces shows that regional production patterns in our study are in relative closer accordance with CBS than those of OneSoil, with a few exceptions. In terms of crop areas, our map did worse predicting potato in Groningen and Drenthe, and sugar beet in Flevoland. Another exception worth noting is the nationwide overestimation of wheat, especially in Groningen and Zeeland, which two factors can explain. Firstly, the categorization in our study distinguishes fewer crop types than CBS. Therefore, we will inevitably misclassify the additional CBS crop types into another class, such as wheat. Secondly, we found that vegetables are often misclassified as wheat, which leads to overestimating wheat and underestimating vegetables. This misclassification can be related to the low number of training data for vegetables from LUCAS, leading to a less robust and accurate classifier for vegetables. Furthermore, vegetable is a very heterogeneous category, including a large variety of plants whose growing seasons differ from one to another. Hence, misidentification is prone to happen with such a small training set.

A
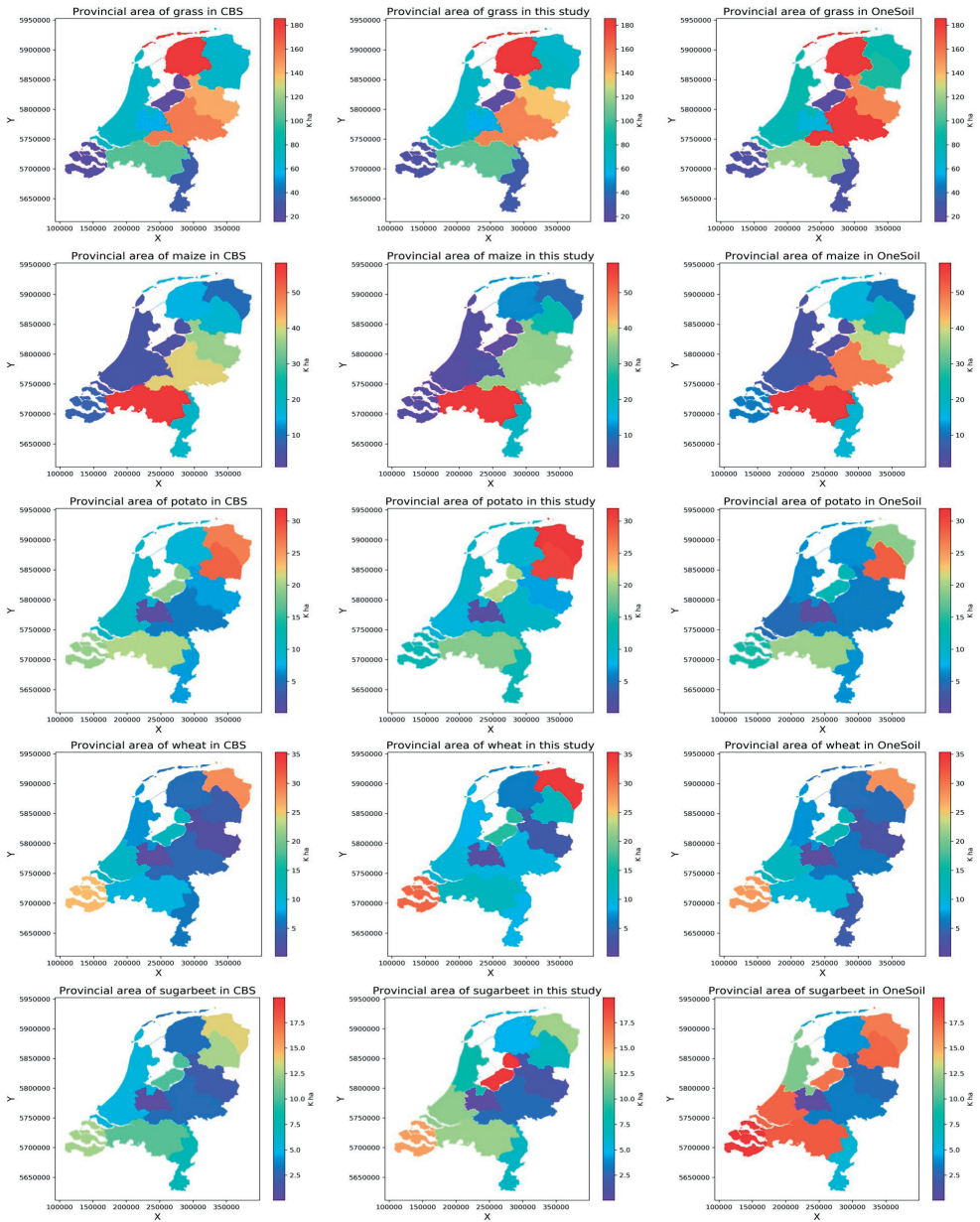
Figure S4.2 Provincial total production area of grassland (row 1) and major arable crops (maize, potato, wheat, sugar beet) from Row 2 to Row 5) from CBS data (left), this study (middle), and OneSoil database (right). The coordinates are in WGS84/UTM 32N (EPSG:32632)

Supplementary material to Chapter 5:
Impact of interannual weather variation on ammonia emissions and concentrations in Germany

S5.1 Spatial allocation of ammonia emissions from compost and digestate application

Since 2010, the addition of compost (including digestate) has strongly increased in Germany due to enhanced biogas production. To properly account for the ammonia emissions from compost in space, we estimated the amounts and the location where it is applied from data on the locations, and capacities of the bioenergy plants in Germany in the so-called DBFZ database (Eichhorn et al., 2019). The DBFZ bioenergy database includes data on the location and capacity (in kWel; Kilowatt Electricity) of plants that produce biogas/biomethane and biomass. The former leaves behind digestate, while the latter produces compost. Digestate is the material remaining after the anaerobic digestion of a biodegradable feedstock, while compost is produced by aerobic digestion-decomposition by aerobes. Digestate is technically not composted although it is similar to it in physical and chemical characteristics. Both digestate and compost can also be used as soil conditioners. In Southern Germany as well as in Hesse and parts of Rhineland-Palatinate mainly small to medium-scale biogas plants with average capacities below 350 kWel are installed. In contrast, the average plant size in North and East Germany (Lower Saxony, Brandenburg, Saxony-Anhalt) is significantly higher (> 500 kWel), in Mecklenburg-Western Pomerania even > 600 kWel.

The capacity of the compost plant, which is an indicator of how much bioenergy it produces and thus how much compost/digestate it leaves behind, was used as a weight to downscale the given total ammonia emission numbers due to compost application emission for the whole of Germany. This amount was then allocated within a 50 km radius of the plant (see below) according to the solid manure allocation over crops and grass. The range of 50 km was based on Saveyn and Eder (2014), which stated that bioenergy plants generally supply their product within 50 km of the plant. We further treated compost and digestate similar to cattle solid manure, so 85% is applied to arable land while the remaining is applied to grassland, according to the data from Menzi et al. (2002), and we also assumed that the ammonia emission fraction of compost is also similar to solid manure.

A

More specifically a top-down algorithm was applied to allocate the officially reported German national emission in space using a weighted method that uses bioenergy plant locations and plant capacities and a crop map according to:

$$\text{NH3em}_{\text{plant,loc}} = \text{Capacity}_{\text{plant,loc}} / \text{Capacity}_{\text{plants}} \text{ x NH3em}_{\text{Germany}},$$

where Capacity$_{plants}$ is the capacity of a plant in Germany at a given location, Capacity$_{plants}$ is the capacity of all plants in Germany and NH3em$_{Germany}$ is officially reported German national ammonia emission from compost. For each plant, the amount thus downscaled is then allocated on land within 50 km of the considered plant according to the solid manure distribution approach, according to:

1. Averaged gridded availability for arable land and grassland

$$Avail_{grid,grass} = \frac{Avail_{plant} * 0.15}{Area_{circle,grass}} \qquad \text{(Eq. S5.1)}$$

$$Avail_{grid,arable} = \frac{Avail_{plant} * 0.85}{Area_{circle,arable}} \qquad \text{(Eq. S5.2)}$$

where $Avail_{plant}$ is the total availability of compost produced from a bioenergy plant, it is assumed to be linearly correlated to the capacity, namely $Avail_{plant} = C * Capacity_{plant}$, where C is a constant. $Area_{circle,grass}$, $Area_{circle,arable}$ are the total area of grassland and arable land located within a 50 km radius of a plant, respectively.

2. Averaged gridded availability applied to each arable crop

$$Avail_{grid,crop} = Avail_{grid,arable} * W = \frac{Avail_{plant} * 0.85}{Area_{circle,arable}} * W \quad \text{(Eq. S5.3)}$$

where W is the weighing factor which varies per crop depending on manure use. 1.0 for group I, 0.50 for group II and 0.25 for group III, and 0.0 for group IV. Group I (high use of manure): maize, sugar beet, rape, and permanent industrial crops; group II (intermediate use of manure): common wheat, durum wheat, barley, rye, oats, other cereals, potatoes, sunflower; group III (low use of manure): citrus fruits/oranges, apples, other fruit, vineyards, other wines, table grapes, olive groves, table olives, other oil crops and; group IV (no use of manure): rice, other root crops, soya, fiber crops, cotton, tobacco, non-permanent industrial crops, dry pulses, tomatoes, other fresh vegetables, floriculture, and nurseries.

3. Gridded emission weight for each arable crop and grassland

$$EmisWeight_{grid,grass} = Avail_{grid,grass} * Area_{grid,grass} * EF_{grass}$$
$$= \frac{Avail_{plant} * 0.15}{Area_{circle,grass}} * Area_{grid,grass} * EF_{grass} \qquad \text{(Eq. S5.4)}$$

$$EmisWeight_{grid,crop} = Avail_{grid,crop} * Area_{grid,crop} * EF_{crop}$$

$$= \frac{Avail_{plant} * 0.85}{Area_{circle,arable}} * W * Area_{grid,crop} * EF_{crop} \qquad \text{(Eq. S5.5)}$$

where $Area_{grid,grass}$, $Area_{grid,crop}$ are the area of grassland and each arable land located within a grid, EF_{grass}, EF_{crop} are the emission fraction of compost application.

As a result, we obtained the gridded emission weights for each crop. The spatial distribution of compost application emission is therefore

$$E_{i,x,y} = E * \frac{W_{i,x,y}}{\sum W_{i,x,y}} \qquad \text{(Eq. S5.6)}$$

where $E_{i,x,y}$ is compost application emission on crop i at location (x,y), $W_{i,x,y}$ is the emission weight of compost application on crop i at location (x,y), E is the averaged total emission from compost application in the year 2015 – 2018 officially reported to EMEP. We regarded compost as cattle solid manure for simplicity, so the emissions were added to emissions from cattle solid manure applied to crops.

A

Acknowledgments
About the author

Acknowledgments

This challenging journey has come to an end. I want to express my deepest gratitude to all those who have contributed to completing this journey. Your support and encouragement along the way have made it possible; this achievement is dedicated to all of you. I want to express my heartfelt thanks to all the participants willing to volunteer their invaluable time and experiences. I am deeply grateful to everyone who contributed to the realization of the thesis.

First and foremost, I am profoundly grateful to my supervision team for their guidance, insights, and tireless dedication to my research. Their mentorship has been the key to shaping the direction of this thesis and in my growth as a researcher. In particular, I extend my most profound appreciation to my promotor, Wim, for offering precious opportunities and constant support during my PhD There are many things you have taught me, especially the HOWs: how to interact with other researchers and manage and organize research. Without your dedication and energy, the studies covered in the thesis would not have been fulfilled. Even though you had a demanding schedule, you always made time to provide feedback and help me with documentation and progress. A similar gratitude belongs to my co-promotor, Martijn. You not only assisted me with the scientific and technical aspects of the studies but also taught me to look at things in the bigger picture and keep my focus on track. Your encouragement inspired me to continue trying and experimenting with efficiency.

I thank my colleagues and fellow researchers at TNO and WUR for helping me with my studies, Richard, Arjo, Enrico, Hans, Jan Cees, etc. You have provided a stimulating academic environment and offered valuable discussions that have broadened my perspective. You shared your pupillometry expertise and provided precious knowledge on modeling and measurements. Whenever I was stuck with technical problems, you came to the rescue and solved them in no time.

I would also like to thank my amazing colleagues, who have become dear friends and made my research time extra joyful. Maddy, we started around the same time at WUR and immediately clicked. I thoroughly enjoy our coffee breaks and university activities together. You introduced your friends to me when I was entirely new to WUR. I missed our dinner and bar nights and Liberation Day celebrations together; it was always a great time with you. Ilan, we never ran out of topics for heated discussions and "arguments". You love data science as I do, so we are always on the same frequency and immediately understand each other. You are a fantastic researcher as well as a DJ. The nights out with you were always full of fun and laughter. Jillian, you are so kind and innocent. We talked about culture, politics, and all sorts of things; I love how our conversations often amused

AA

you. I had my first ever Amsterdam canal trip with you and other guys. It was one of the most Amsterdam-ish things ever, and I enjoyed every second of it. I am so glad that we still sometimes work at the same locations and honored that you are my paranymph.

To my roommate and friend in Wageningen, Yannis and Daniel, I am so lucky to have met you. We have had great nights relaxing and outing. The random YouTube meme viewings were ridiculously funny, and Yannis being utterly confused by me and Daniel was even more amusing. You helped me relieve stress from work and made my time in this small town so much better. To my friends and neighbors in Amsterdam, Kai, Polina, Alyson, etc., thank you for your company, especially during the pandemic. I do not know how I would have spent the difficult time without you.

To my beloved family, I am so fortunate and honored to have your unwavering support, understanding, and encouragement during this journey. Your belief in me has been my greatest motivation. I am aware that my absence during these years made me miss a lot of big moments in our family. Grandpa, I regret to this day that I could not accompany you in the last moments of your life. My big brother, I wish to be there during your ups and downs and celebrate your recent breakthrough. My dearest cousin, I cannot believe I missed your wedding and wish I could have gotten to know my brother-in-law better. I want to thank my family for accompanying my parents when I was absent.

Of course, thanks must go to my mom and dad. You did not understand my research but tried your best to support and encourage me to do what I wanted. Without your constant support, I would never have had a chance to start and finish a PhD or even come to Europe for my study. You gave me the opportunity to see the world, and I am forever grateful. I know you act strict on the surface, but you are the most sensitive when knowing I have a difficult time. In this way, you encourage me to keep improving myself and make me confident but also humble at the same time.

Thank you.

About the author

SCAN ME

AA

**Netherlands Research School for the
Socio-Economic and Natural Sciences of the Environment**

D I P L O M A

for specialised PhD training

The Netherlands research school for the
Socio-Economic and Natural Sciences of the Environment
(SENSE) declares that

Xinrui Ge

born on the 8th of January 1992 in Yichang, China

has successfully fulfilled all requirements of the
educational PhD programme of SENSE.

Wageningen, the 10th of October 2023

Chair of the SENSE board   The SENSE Director

Prof. dr. Martin Wassen   Prof. Philipp Pattberg

The SENSE Research School has been accredited by the Royal Netherlands Academy of Arts and Sciences (KNAW)

K O N I N K L I J K E   N E D E R L A N D S E
A K A D E M I E   V A N   W E T E N S C H A P P E N

The SENSE Research School declares that **Xinrui Ge** has successfully fulfilled all requirements
of the educational PhD programme of SENSE with a
work load of 33.0 EC, including the following activities:

SENSE PhD Courses

o   Environmental research in context (2017)
o   Research in context activity: 'Modelling.earth: Develop a website to promote PhD research' (2023)

Other PhD and Advanced MSc Courses

o   Introduction to R for statistical analysis, Wageningen University (2017)
o   The Art of Modelling, Wageningen University (2017)
o   Geostatistics, Wageningen University (2017)
o   Machine learning for spatial data, Wageningen University (2018)

Oral Presentations

o   *Model Assessment and Validation of Ammonia Emissions from Agriculture at High Spatial and Temporal Resolution over Germany.* EGU 2018, 8-13 April 2018, Vienna, Austria
o   *Modelling Atmospheric Ammonia using Agricultural Emissions with Improved Spatial Variability and Temporal Dynamics.* INI 2021, 30 May-3 June 2021, Online
o   *Impact of interannual weather variation on ammonia emission in Germany: a multi-year (2014 - 2018) analysis.* ITM 2021, 18-22 October 2021, Online
o   *Improve Spatial Variability and Temporal Dynamics of Ammonia Emission from Agriculture. LOTOS-EUROS Workshop (2018/ 2019/ 2020/ 2021)*, January 2018, 2019, 2020, 2021

SENSE coordinator PhD education

Dr. ir. Peter Vermeulen